Advances
in Clinical and Experimental Medicine

WROCLAW
MEDICAL UNIVERSITY

Advances
in Clinical and Experimental
Medicine

Editorial Policy

Contents

Research letters

Electrochemotherapy of melanoma:
What we know and what is unexplored?

Anna Choromańska[A,D–F], Urszula Szwedowicz[B,C]

Department of Molecular and Cellular Biology, Faculty of Pharmacy, Wroclaw Medical University, Poland

A – research concept and design; B – collection and/or assembly of data; C – data analysis and interpretation;
D – writing the article; E – critical revision of the article; F – final approval of the article

Abstract

The cell membrane can be permeabilized when subjected to calibrated short electric pulses. This membrane alteration can be reversible, leaving cell viability unaffected. This set of events is called electroporation (EP). It is now used in clinical applications to introduce hydrophilic drugs into the cytoplasm. One of the EP applications is electrochemotherapy (ECT), in which EP is used for the selective delivery of drugs administered to treat cancer. The combination of EP with chemotherapy allows local cancer treatment, lowering the drug dose and reducing the side effects of systemic chemotherapy. Nowadays, bleomycin-based ECT (BLM-ECT) is a safe treatment for cutaneous tumors and skin metastases with established standard operating procedures. Additionally, there is emerging evidence that BLM-ECT may be particularly effective in combination with immunotherapies, acting synergistically and producing enhanced systemic anti-tumor effects. Still, to make it the first-choice therapy in patients with metastatic melanoma, further studies are needed to establish the relative effectiveness of ECT. Analyzing the EP phenomenon and the objective complexity of the associated effects at the cell level, we came across a problem that has not yet been investigated in increasing the therapeutic effectiveness of ECT. The profile and kinetics of extracellular vesicles (EVs) released from cells subjected to EP have not been analyzed. The exact nature of these EVs is unknown.

Key words: melanoma, electroporation, electrochemotherapy, extracellular vesicles

Introduction

The cell membrane is a natural barrier that determines the control of the transport of molecules to the cell. Its permeability is an essential factor determining the effectiveness of therapy. Under the influence of a strong electric field, the lipid molecules in the cell membrane change their organization, and electroporation (EP) occurs. Transient hydrophilic pores are formed, constituting an additional pathway of transport of macromolecules through the cell membrane (Fig. 1).
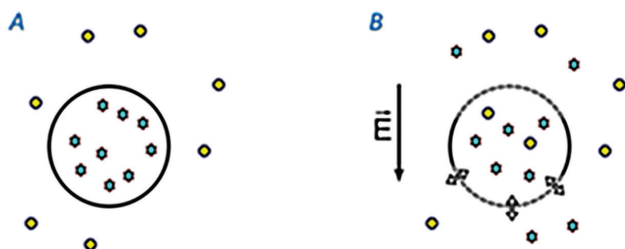
Fig. 1. A. Cell membrane not subjected to the electroporation (EP) procedure. The drug surrounds the cell; B. Cell membrane after the EP procedure. The resulting pores are a way of drug transport to the cell

Currently, EP is used as a standard in in vitro cell culture as the purest available gene transfection method.[1] Electroporation can also be used in gene therapy and in vivo immunogenotherapy. One of the EP applications is electrochemotherapy (ECT), in which EP is used for the selective delivery of drugs administered to treat cancer. The combination of EP with chemotherapy (CT) significantly reduces the need for surgical intervention, allows local treatment of cancer, lowers the drug dose, and reduces the side effects of systemic chemotherapy.[2] Effectiveness of this method is also increased due to the occurrence of the so-called vascular lock after applying an electrical pulse. It reduces the blood flow through the tumor and therefore causes a more extended stay of the drug in the tumor cells. In addition, the blood vessels are damaged, resulting in decreased blood flow within the tumor and the activation of the immune system.[3]

When bleomycin was used with EP, its cytotoxicity index increased 1000 times.[4] The first clinical tests on using ECT were carried out in the 1990s. The squamous cell carcinomas of the head and neck were treated with intravenous injection of bleomycin, followed by EP of the nodules.[5] The investigators found a significant reduction in the size of neoplastic lesions after treatment. In 2006, the European Standard for Operating Procedures for ECT and Electrogene Therapy (ESOPE) was developed to define standard operating procedures.[6] Several methods of treatment have been proposed to ensure the patient's safety and obtain optimal treatment results concerning the selection of a chemotherapeutic drug, the way of drug delivery (intravenous or intratumoral), and the shape of the electrode (plate or needle) and EP parameters.[7] Electrochemotherapy with bleomycin or cisplatin of malignant melanoma tumors results in a marked reduction of tumor size. No local

or general adverse effects are observed during treatment – only temporary redness and accumulation of serum in the treated areas.[6] Electrochemotherapy is used today in clinical practice to treat cutaneous and subcutaneous tumors, especially melanoma tumors.[8,9] The procedure is applicable all over the body surface, with high response rates across various tumor subtypes. In addition, the treatment can be performed with local anesthesia if a patient has a few smaller lesions.[10] New electrodes have been developed to access deep-seated and surgically challenging tumors in different ways.[11]

The effectiveness of systemic and adjuvant therapies has significantly progressed recently. However, more effective therapeutic options for the treatment of melanoma are still being sought. Bleomycin-based ECT (BLM-ECT) is currently considered a safe and effective form of treatment of skin tumors and their metastases. This method has been included in international clinical guidelines. The European Society for Medical Oncology recommendations on managing locoregional melanoma[12] cited the study by Kunte et al. That recently published cohort study found that 78% (306 patients) had a complete or partial response and 58% (229 patients) presented a complete response to BLM-ECT.[13] Currently, clinicians most often choose BLM-ECT treatment for palliative therapy. However, due to the proven effectiveness of BLM-ECT, it can be considered the method of choice when surgical resection or radiotherapy are contraindicated. Moreover, BLM-ECT can be performed after other forms of treatment and can be repeated in the same area several times.[14] Mozzillo et al. presented a report on the retrospective investigation of 15 patients treated with ipilimumab who also received ECT. Over the study duration, a local objective response was attained in 67% of patients. In addition, a systemic response was observed in 9 patients, resulting in a disease control rate of 60%. Evaluation of circulating T-regulatory cells showed significant contrasts between responders and non-responders. The above study showed that the combination of ipilimumab and ECT benefits patients with advanced melanoma, warranting other investigations and trials.[15] An essential method of treating melanoma with in-transit metastases is systemic therapy, while ECT may be a treatment option for patients who cannot receive therapy with BRAF and MEK inhibitors. However, the treatment method should be carefully balanced so as not to deprive the patient of the chance of long-term survival.[16] Decisions about systemic and adjuvant therapy for melanoma patients should be made on an individual basis, taking into consideration potential toxicities, costs and patient preference. A Preferred Reporting Items for Systematic reviews and Meta-Analyses (PRISMA)-compliant systematic review analysis suggested that patients with metastatic melanoma should be treated by multidisciplinary teams including oncologists, dermatologists and radiation oncologists.[17] In addition, ECT procedures should be performed in centers with appropriate equipment and trained personnel experienced in this method.

Evidence indicates that simultaneous local and systemic therapy modalities may lead to synergistic anti-tumor effects in melanoma. Increased response and overall survival when using ECT combined with immunotherapy have already been noted.[10] Heppt et al. showed the use of ECT combined with a monoclonal antibody against cytotoxic T cell antigen-4 (ipilimumab) or PD-1 (programmed death receptor 1) inhibitor. Thirty-three patients with unresectable or metastatic melanoma participated in the study. Twenty-eight patients received ipilimumab, while 5 were treated with a PD-1 inhibitor. It was observed that ipilimumab combined with ECT was tolerable and showed a high systemic response rate.[18] Also, Campana et al. investigated the effectiveness of ECT in combination with a PD-1 inhibitor (pembrolizumab). They compared patient outcomes after treatments with pembrolizumab, pembrolizumab with ECT, and ECT alone. The combined application of inhibitor and ECT was safe and more effective in preventing further tumor growth than pembrolizumab alone. In addition, the patients treated with pembrolizumab and ECT shared lower disease progression and more prolonged survival than those who received only pembrolizumab. The above study showed that ECT might increase the effect of pembrolizumab when an in situ vaccination against melanoma cells is performed.[19]

An interesting approach to the treatment of metastatic melanoma with EP was presented by Greaney et al.[20] Systemic interleukin (IL)-12 is connected with life-threatening toxicity, but intratumoral delivery of IL-12 via telseplasmid (tavo) electroporation is safe and can induce tumor regression in remote places. The mechanism of these reactions is unknown but is supposed to result from a cellular immune response. Greaney et al. results indicated that this local treatment could induce a systemic T-cell response.[20]

Analyzing the EP phenomenon and the objective complexity of the associated effects at the cell level, we came across a problem that has not yet been investigated in the context of increasing the therapeutic effectiveness of ECT. The profile and kinetics of extracellular vesicles (EVs) released from cells subjected to electroporation have not been investigated. The exact nature of these EVs is unknown. It is also not clear how the profile of the released EVs depends on the pulse duration.

Electroporation of melanoma cells: What about molecules transported outside the cell?

Until recently, it was believed that the role of EVs was to remove unnecessary compounds outside the cell. However, we now know that they have enormous potential. They mediate intercellular communication, enable the transfer of bioactive molecules, and can transfer the charge to individual cells by acting on specific receptors in target cells under physiological and pathophysiological conditions.[21]

The main features of EVs depend on the cell they come from, their state and the requirements of the external environment. The EVs are currently a highly heterogeneous group and can be divided into 3 populations: exosomes, ectosomes and apoptotic bodies.

Both normal and cancer cells release all types of EVs. Since EVs modulate intercellular signaling, protein transport and cell proliferation, EVs of neoplastic origin can induce and stimulate cancer growth when delivered to recipient cells. Melanoma-derived exosomes have increased tumor cell proliferation and contribute to the epithelial–mesenchymal transition and pre-metastatic niche formation.[22] They are also involved in extracellular matrix degradation and activation of integrin signaling. Melanoma-derived exosomes can modulate many immune system functions, counteracting the immune response against melanoma.[23,24] The receptor tyrosine kinase MET has also demonstrated its effect on bone marrow progenitor cells. In this way, it interferes with the differentiation and maturation of antigen-presenting cells, controlling the survival and apoptosis of the effector T cells, cytokine production, and NK cell cytotoxicity.[25] Recent studies have found twice as many ectosomes released in vitro by melanoma cells as normal melanocytes. Melanoma-derived ectosomes show higher levels of tissue factor, which is responsible for the coagulation process associated with carcinogenesis.[26] They can also induce metastasis by transporting metastases or their endogenous activators.[27] It has also been shown that ectosomes can transform fibroblasts into fibroblasts related to cancer and suppress the immune response by EV-associated Fas ligand.[28]

Peinado et al. identified MET-associated signaling proteins transmitted by exosomes derived from highly metastatic melanoma cells. They mediate provasculogenic effects on bone marrow progenitor cells.[29] *MET* oncogene causes neoplastic transformation and stimulation of neoplastic cell proliferation, invasion and metastasis.[30] It has been shown that the co-expression of TYRP2 and MET in exosomes is associated with melanoma progression. Moreover, Peinado et al. showed that the transfer of exosome-derived MET oncoproteins to bone marrow progenitor cells promotes metastasis in vivo.[29]

Our preliminary studies on the A375 human melanoma cell line electroporated using a low-intensity electric field (unpublished data) showed a clear difference in kinetics of calcein released from cells depending on the parameters of reversible EP. The analysis of cell confluence levels measured in parallel with the level of calcein released from cells showed no significant changes, confirming that the EP parameters used did not affect cell viability. It was also observed that a low-intensity electric field causes marked differences in the amount of EVs released from A375 melanoma cells as a function of EP parameters 24 h after its application. According to our studies, various parameters of reversible EP impact the kinetics and profile of released EVs following the application of reversible EP with varying

parameters. Different EP parameters will probably affect the protein profile of EVs released after EP. The above proteins may significantly influence the cells in their environment and influence the process of metastasis.

Conclusions

Currently used ECT protocols for malignant melanoma are based on parameters established by ESOPE, where the process conditions did not consider the extracellular transport following EP. More studies analyzing transport from the cell to the external environment induced by external electromagnetic fields of varying intensity are needed to optimize the therapeutic process using ECT.

ORCID iDs

Anna Choromańska ⬤ https://orcid.org/0000-0001-9997-7783
Urszula Szwedowicz ⬤ https://orcid.org/0000-0001-6406-7616

References

1. Haberl S, Miklavcic D, Sersa G, Frey W, Rubinsky B. Cell membrane electroporation. Part 2: The applications. *IEEE Electr Insul Mag*. 2013;29(1):29–37. doi:10.1109/MEI.2013.6410537
2. Skołucka N, Saczko J, Kotulska M, Kulbacka J, Choromańska A. Electroporation and its application [in Polish]. *Pol Merkur Lek*. 2010;28(168):501–504. PMID:20642114.
3. Sersa G, Cufer T, Paulin SM, Cemazar M, Snoj M. Electrochemotherapy of chest wall breast cancer recurrence. *Cancer Treat Rev*. 2012;38(5):379–386. doi:10.1016/j.ctrv.2011.07.006
4. Mir LM, Tounekti O, Orlowski S. Bleomycin: Revival of an old drug. *Gen Pharmacol Vasc Syst*. 1996;27(5):745–748. doi:10.1016/0306-3623(95)02101-9
5. Belehradek M, Domenge C, Luboinski B, Orlowski S, Belehradek J, Mir LM. Electrochemotherapy, a new antitumor treatment: First clinical phase I–II trial. *Cancer*. 1993;72(12):3694–3700. doi:10.1002/1097-0142(19931215)72:12<3694::AID-CNCR2820721222>3.0.CO;2-2
6. Marty M, Sersa G, Garbay JR, et al. Electrochemotherapy – an easy, highly effective and safe treatment of cutaneous and subcutaneous metastases: Results of ESOPE (European Standard Operating Procedures of Electrochemotherapy) study. *Eur J Cancer Suppl*. 2006;4(11):3–13. doi:10.1016/j.ejcsup.2006.08.002
7. Mir LM, Gehl J, Sersa G, et al. Standard operating procedures of the electrochemotherapy: Instructions for the use of bleomycin or cisplatin administered either systemically or locally and electric pulses delivered by the Cliniporator™ by means of invasive or non-invasive electrodes. *Eur J Cancer Suppl*. 2006;4(11):14–25. doi:10.1016/j.ejcsup.2006.08.003
8. Sersa G, Stabuc B, Cemazar M, Miklavcic D, Rudolf Z. Electrochemotherapy with cisplatin: Clinical experience in malignant melanoma patients. *Clin Cancer Res*. 2000;6(3):863–867. PMID:10741708.
9. Cucu CI, Giurcăneanu C, Popa LG, et al. Electrochemotherapy and other clinical applications of electroporation for the targeted therapy of metastatic melanoma. *Materials (Basel)*. 2021;14(14):3985. doi:10.3390/ma14143985
10. Bastrup FA, Vissing M, Gehl J. Electrochemotherapy for metastatic cutaneous melanoma. *Acta Oncol*. 2022;61(5):531–532. doi:10.1080/0284186X.2022.2057199
11. Campana LG, Edhemovic I, Soden D, et al. Electrochemotherapy: Emerging applications technical advances, new indications, combined approaches, and multi-institutional collaboration. *Eur J Surg Oncol*. 2019;45(2):92–102. doi:10.1016/j.ejso.2018.11.023
12. Michielin O, van Akkooi A, Lorigan P, et al. ESMO consensus conference recommendations on the management of locoregional melanoma: Under the auspices of the ESMO Guidelines Committee. *Ann Oncol*. 2020;31(11):1449–1461. doi:10.1016/j.annonc.2020.07.005
13. Kunte C, Letulé V, Gehl J, et al. Electrochemotherapy in the treatment of metastatic malignant melanoma: A prospective cohort study by InspECT. *Br J Dermatol*. 2017;176(6):1475–1485. doi:10.1111/bjd.15340
14. Wichtowski M, Murawa D. Electrochemotherapy in the treatment of melanoma. *Contemp Oncol (Pozn)*. 2018;22(1):8–13. doi:10.5114/wo.2018.74387
15. Mozzillo N, Simeone E, Benedetto L, et al. Assessing a novel immuno-oncology-based combination therapy: Ipilimumab plus electrochemotherapy. *OncoImmunology*. 2015;4(6):e1008842. doi:10.1080/2162402X.2015.1008842
16. Gallagher M, Chin KY, MacKenzie-Ross A. Bleomycin electrochemotherapy for the management of locally advanced metastatic melanoma: Two notable clinical cases potentially indicating a greater therapeutic role in the era of targeted and immunotherapy. *JPRAS Open*. 2020;26:43–48. doi:10.1016/j.jpra.2020.09.007
17. Ferioli M, Lancellotta V, Perrone AM, et al. Electrochemotherapy of skin metastases from malignant melanoma: A PRISMA-compliant systematic review. *Clin Exp Metastasis*. 2022;39(5):743–755. doi:10.1007/s10585-022-10180-9
18. Heppt MV, Eigentler TK, Kähler KC, et al. Immune checkpoint blockade with concurrent electrochemotherapy in advanced melanoma: A retrospective multicenter analysis. *Cancer Immunol Immunother*. 2016;65(8):951–959. doi:10.1007/s00262-016-1856-z
19. Campana LG, Peric B, Mascherini M, et al. Combination of pembrolizumab with electrochemotherapy in cutaneous metastases from melanoma: A comparative retrospective study from the InspECT and Slovenian Cancer Registry. *Cancers (Basel)*. 2021;13(17):4289. doi:10.3390/cancers13174289
20. Greaney SK, Algazi AP, Tsai KK, et al. Intratumoral plasmid IL12 electroporation therapy in patients with advanced melanoma induces systemic and intratumoral T-cell responses. *Cancer Immunol Res*. 2020;8(2):246–254. doi:10.1158/2326-6066.CIR-19-0359
21. Szwedowicz U, Łapińska Z, Gajewska-Naryniecka A, Choromańska A. Exosomes and other extracellular vesicles with high therapeutic potential: Their applications in oncology, neurology, and dermatology. *Molecules*. 2022;27(4):1303. doi:10.3390/molecules27041303
22. Tucci M, Mannavola F, Passarelli A, Stucci LS, Cives M, Silvestris F. Exosomes in melanoma: A role in tumor progression, metastasis and impaired immune system activity. *Oncotarget*. 2018;9(29):20826–20837. doi:10.18632/oncotarget.24846
23. Cheng YC, Chang YA, Chen YJ, et al. The roles of extracellular vesicles in malignant melanoma. *Cells*. 2021;10(10):2740. doi:10.3390/cells10102740
24. Bychkov ML, Kirichenko AV, Mikhaylova IN, et al. Extracellular vesicles derived from acidified metastatic melanoma cells stimulate growth, migration, and stemness of normal keratinocytes. *Biomedicines*. 2022;10(3):660. doi:10.3390/biomedicines10030660
25. Surman M, Stępień E, Przybyło M. Melanoma-derived extracellular vesicles: Focus on their proteome. *Proteomes*. 2019;7(2):21. doi:10.3390/proteomes7020021
26. Lima L, Oliveira A, Campos L, et al. Malignant transformation in melanocytes is associated with increased production of procoagulant microvesicles. *Thromb Haemost*. 2011;106(10):712–723. doi:10.1160/TH11-03-0143
27. Hatanaka M, Higashi Y, Fukushige T, et al. Cleaved CD147 shed from the surface of malignant melanoma cells activates MMP2 produced by fibroblasts. *Anticancer Res*. 2014;34(12):7091–7096. PMID:25503136.
28. Zhao XP, Wang M, Song Y, et al. Membrane microvesicles as mediators for melanoma-fibroblasts communication: Roles of the VCAM-1/VLA-4 axis and the ERK1/2 signal pathway. *Cancer Lett*. 2015;360(2):125–133. doi:10.1016/j.canlet.2015.01.032
29. Peinado H, Alečković M, Lavotshkin S, et al. Melanoma exosomes educate bone marrow progenitor cells toward a pro-metastatic phenotype through MET. *Nat Med*. 2012;18(6):883–891. doi:10.1038/nm.2753
30. Boccaccio C, Comoglio PM. Invasive growth: A MET-driven genetic programme for cancer and stem cells. *Nat Rev Cancer*. 2006;6(8):637–645. doi:10.1038/nrc1912

What is rural? Keynote speech at the XI EURIPA Forum 2022*

Karen Flegg[1,2,A–F]

[1] Rural Clinical School, Australian National University, Canberra, Australia

[2] World Organization of Family Doctors, Brussels, Belgium

A – research concept and design; B – collection and/or assembly of data; C – data analysis and interpretation;
D – writing the article; E – critical revision of the article; F – final approval of the article

Address for correspondence
Karen Flegg
E-mail: karen.flegg@anu.edu.au

Abstract

Background. In order to consider the question of "what is rural", the author chose to use examples from her journey as a rural family doctor (general practitioner) in Australia.

Objective. To consider the diversity of rural practice settings and medical practice styles in primary care that can all be considered to be rural medical practice. In doing so, to consider the size and population density of Australia, compared to Europe, from where the audience of The European Rural and Isolated Practitioners Association (EURIPA) originates.

Results. In discussing rural locations where the author has practiced, the Modified Monash Model of classifications of rurality, used in Australia, is introduced. It will be shown that rural medical practice varies significantly even in places of similar classifications of rurality. In some towns, the family doctors do procedural work or admit patients to hospital. In other towns and remote communities, an unwell patient may need to be looked after in the primary care clinic for hours before they can be evacuated. These are however all variations of rural practice. Does population or the occupations that workers engage in make any difference to rurality? Does distance from a capital city matter?

Conclusions. Rural medical practice is diverse in location, cultures and work undertaken. Rural medical doctors use different names for themselves such as rural family doctor, rural family physician, rural generalist, rural primary care doctor – we are all rural.

Key words: rural, family medicine, rural medicine, rural doctor

Background

In order to consider the question of "what is rural" and the diversity of rural practice settings, I have chosen to use examples from my own journey as a family doctor (general practitioner), and in particular as a rural general practitioner, in Australia.

The World Organisation of Family Doctors (WONCA) past president, Prof. Michael Kidd, was a guest speaker at the WONCA World Rural Health conference held in Gramado, Brazil in 2014. Professor Kidd asked the question "Why is rural family medicine important?" The answer was simple: half of the world's population live in rural areas, but half of the world's doctors do not. He pointed out that most of our colleagues in other specialties are based in cities or in large regional centers, but it is family doctors who are based in rural communities and provide medical care and advice to that half of the world's population.[1]

The Australian rural situation

It is interesting to compare the size and population density of Australia, where I come from, and Europe, the home of EURIPA.

Australia's area is a total of 7.69 million km^2 compared to Wikipedia's estimate for Europe of 10.18 million km^2.[2,3] Roughly comparable.

The population densities are given by World Population Review as Australia 3.4 persons per km^2 compared to Europe's 72.9 per km^2. Not at all comparable, with Australia only exceeded in the sparseness of population density by Mongolia and Greenland. Iceland is similar to Australia with 4 persons per km^2, and next in Europe are Norway with 15 and Finland with 18 persons per km^2 respectively. Monaco with 19,497 persons per km^2 is Europe's most densely populated country.[4]

The majority of Australians live in major cities (72%), and much of the country is sparsely populated.[5] The population is concentrated around the southeast and east coast and southwest corner of the continent. It's easy to 'go rural' in Australia.

My rural GP journey begins

I was born and raised in Sydney, where I went to Sydney University Medical School. I signed up to the General Practice specialty training program, a postgraduate program for 3 years, mostly spent in community general practice.

"Where do you want to go for your training?", I was asked.

Perhaps it was not wise, but my reply was "about as far from Sydney as possible". I did not dislike my hometown, Sydney; however, I had a desire to try something different to what I had known. Now, some 30 years later, I have tried many contexts of work as a rural GP with some specializations including Aboriginal health, management and teaching.

Where did I go for that first general practice placement? Warialda, 600 km from Sydney, with a population of 1300 but also drawing patients from the surrounding farming community. It is a strong sheep and wheat farming area. As well as work in the general practice clinic, the 2 doctors who supervised me ran a 25 bed hospital and we performed uncomplicated obstetrics, anesthetics and minor surgery. The nearest large hospital was 2.5 h by road ambulance.

Was this rural practice? Even those in my country with narrow definitions of rural practice would agree – definitely rural!

Measures of rurality

Australia uses the Modified Monash Model[6] to define rurality for medical workforce purposes. The model classifies metropolitan, regional, rural, and remote areas according to geographical remoteness, as defined by the Australian Bureau of Statistics (ABS), and town size. In this model, MM1 is a major city and MM7 is very remote. Warialda rates as MM5[6] – small rural town (conf. Table 1 and Fig. 1).

In recent years, I have spent my time in Central Australia (MM6 and MM7[6] – remote and very remote) working in the medical team which serves isolated Aboriginal communities. These communities have a population of between 100 and 1000, and can be 800 km from the nearest large hospital in Alice Springs. The remote health clinics are nurse-led, and nurses see acute patients and are on-call after hours. Doctors generally visit the smaller places for 3 or 4 days in a month.

Retrievals of emergencies and very sick patients are done by the well-known Royal Flying Doctor service, or by road if within 2 h of Alice Springs. To get to work, our doctors travel in small charter airplanes for up to 2 h or drive up to 4 h, often on unsealed roads, in a four-wheel-drive vehicle. In our clinics, there was no obstetrics (except antenatal care and unintentional deliveries), no surgery and no general anesthetics. However, we did have to take care of the very sick in our well fitted out emergency rooms, until retrieval – at least 2 h but often much longer.

Was this rural practice even without procedural work? No arguments – not just rural, but remote or isolated!

Strangely, I do not consider Central Australia to be the most isolated place where I have worked. Every working day, doctors, nurses and Aboriginal health workers in these remote communities have the support of a telephone service manned by experienced colleagues who can advise on the day-to-day issues. Out of hours and for emergencies, it easy to call the Alice Springs Hospital retrieval service – so you always have support.

Another training placement I took was in Eugowra, a small town of 670 people, 350 km from Sydney, but with only 1 doctor – me! In that town, there was a 30-bed

MM1		Metropolitan
MM2		Regional centres
MM3		Large rural towns
MM4		Medium rural towns
MM5		Small rural towns
MM6		Remote communities
MM7		Very remote communities
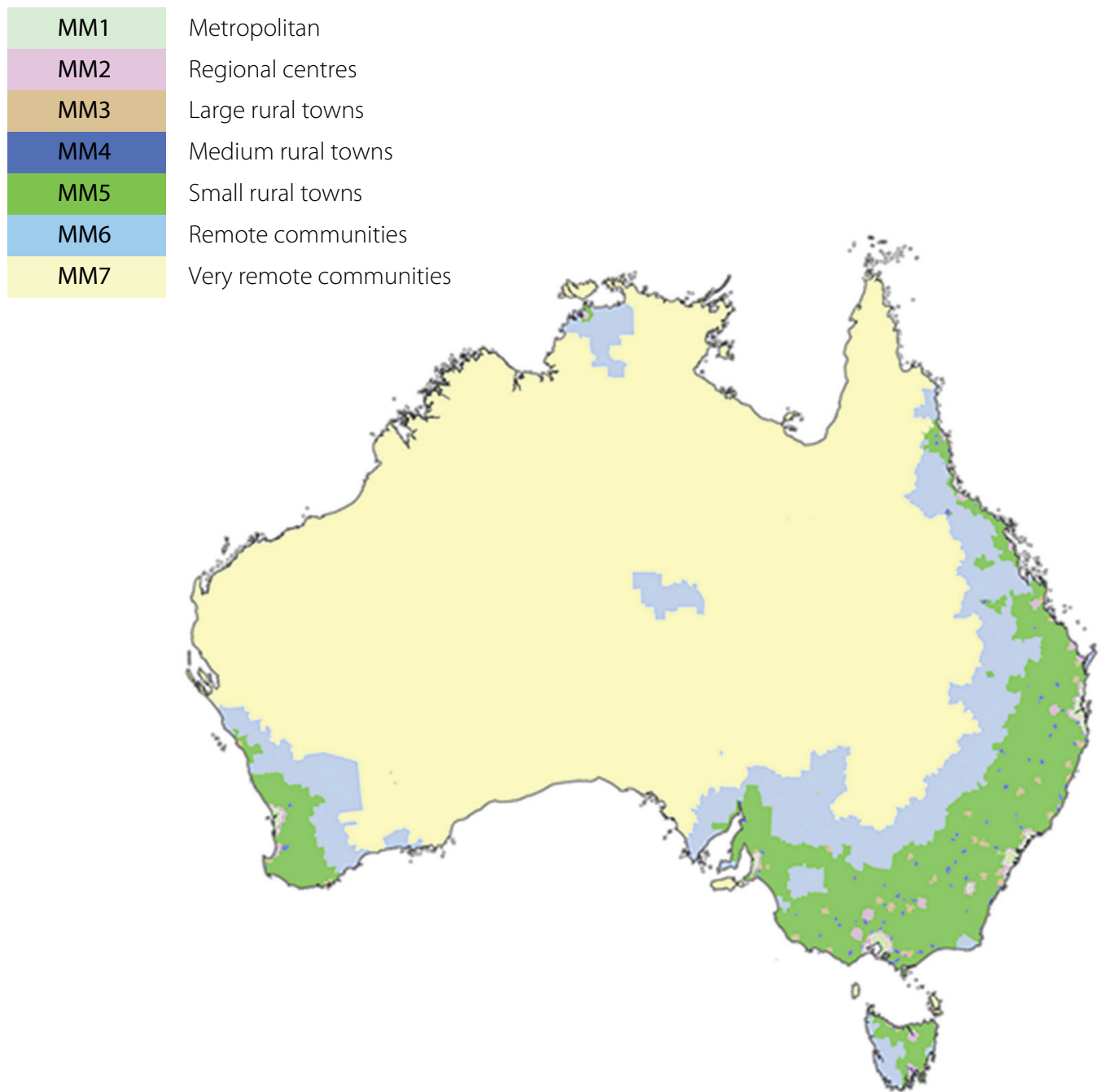
Fig. 1. Modified Monash Categories distribution on map of Australia[6]

Table 1. Modified Monash Categories of remoteness and description[6]

Modified Monash Category (MM)	Description
MM1	**Metropolitan areas:** Major cities accounting for 70% of Australia's population.
MM2	**Regional centres:** Inner and Outer Regional areas that are in, or within a 20-kilometer drive of a town with over 50,000 residents.
MM3	**Large rural towns:** Inner and Outer Regional areas that are in, or within a 15-kilometer drive of a town between 15,000 and 50,000 residents.
MM4	**Medium rural towns:** Inner and Outer Regional areas that are in, or within a 10-kilometer drive of a town with between 5,000 and 15,000 residents.
MM5	**Small rural towns:** All remaining Inner and Outer Regional areas.
MM6	**Remote communities:** Remote mainland areas and islands less than 5 km offshore.
MM7	**Very remote communities:** Very remote areas. Remote island areas more than 5 km offshore.

hospital, mostly aged care beds, but also 5 acute beds to manage. MM5[6] – but no anesthetics, surgery or obstetrics, and with only 1 doctor available. The nearest colleagues were 30 km away and nearest large hospital – 80 km. In case of an emergency, you could call a specialist colleague in the large hospital – or send the patient in our volunteer ambulance[7] staffed by local volunteers, whose day job was as a farmer, a butcher for example.

I felt alone, very alone. With only 80 km to a regional hospital, no one would consider this remote or isolated; however, for me it felt that way.

While researching this topic, I noted Wikipedia[8] provides Indian definitions of rural: a town with a maximum population of 15,000, and 75% of the male working population involved in agriculture and related activities.

I remembered working in Muswellbrook in the wine-growing areas of eastern Australia. It had been a very strong farming community, but by the time I was there, many workers were involved in the mining or power production industries, and its population was just over 15,000. By the Indian definition of male occupation and arguably population, not rural! Yet our 10 doctors did on-call, and worked in our local hospital, admitting patients and performing obstetrics, surgery and anesthetics. I say rural and it ranks as MM4[6] – medium-sized rural town.

My final example is Bungendore, only 38 km from Australia's Parliament House. I had known colleagues who say "How this can be rural?" Until recent years, there was no ambulance in town, so you have to wait up to 1.5 h for an unwell patient to be collected, as you do in remote Central Australia. No procedural work. Rural? I think so, and so does the Modified Monash Model, which rates it as MM5[6] – small rural town.

Rurality is a question of perspective. A farmer will say "real rural isn't living in towns". However, most rural family doctors need to live in their town in order to be available to the patients and their community. The government defines rurality[6] in order to consider statistics on rural health. They look at numbers of primary health care professionals; they consider health spending; they are concerned about death rates being 40 times higher for heart disease and 3 times higher for type II diabetes.

Conclusions

For me, rural has meant diversity of locations, cultures and health problems. Defining rural is challenging within Australia and certainly between countries.

I finish with another reference to the words of Prof. Michael Kidd from 2014. "How we describe who we are differs from place to place. What matters is the common work we do, the vision that we share, the outcomes that we achieve for our patients and their families and for our communities."

We call ourselves rural general practitioners, or rural family physicians, or rural generalists, or rural primary care doctors. We work in diverse settings with diverse people.

We are all rural doctors.

ORCID iDs

Karen Flegg https://orcid.org/0000-0002-0852-4816

References

1. Kidd M. The World of Rural Family Medicine - address to WONCA World Rural Health conference, in Brazil. 2014. https://www.global-familydoctor.com/AboutWonca/PresidentsBlog/TheWorldofRuralFamilyMedicine.aspx. Accessed January 11, 2023.
2. GeoScience Australia. Area of Australia States and Territories. Canberra, Australia: GeoScience Australia; 2004. https://www.ga.gov.au/scientific-topics/national-location-information/dimensions/area-of-australia-states-and-territories. Accessed October 2, 2022.
3. Wikipedia. Europe. 2022. https://en.wikipedia.org/wiki/Europe. Accessed October 2, 2022.
4. World Population Review. Countries by Population Density 2022. 2022. https://worldpopulationreview.com. Accessed October 2, 2022.
5. Australian Institute of Health and Welfare (AIHW), Australian Government. *Rural and Remote Health*. Canberra, Australia: Australian Institute of Health and Welfare (AIHW) & Australian Government; 2022. www.aihw.gov.au/reports/rural-remote-australians/rural-and-remote-health. Accessed October 2, 2022.
6. Australian Government, Department of Health and Aged Care. Modified Monash Model. Canberra, Australia: Australian Government, Department of Health and Aged Care; 2021. https://www.health.gov.au/health-topics/rural-health-workforce/classifications/mmm. Accessed October 2, 2022.
7. Ambulance New South Wales. The Volunteers. Eugowra Volunteer Ambulance Officers. Sydney, Australia: Ambulance New South Wales; 2014. https://www.youtube.com/watch?v=d3FitoXGA10. Accessed October 2, 2022.
8. Wikipedia. Rural area. 2022. https://en.wikipedia.org/wiki/Rural_area. Accessed October 2, 2022.

Systemic immune-inflammation index: A new indicator of predicting 1-, 2-and 3-year disease-free survival of patients with colon cancer

Lu Zhang[1,A–D], Zhong Zhang[1,C], Haochun Guo[1,B], Bin Huang[2,F], Haijun Zhang[1,E,F]

[1] Department of Oncology, Zhongda Hospital, Medical School of Southeast University, Nanjing, China

[2] Comprehensive Cancer Center of Nanjing Drum Tower Hospital, Affiliated Hospital of Nanjing University Medical School & Clinical Cancer Institute of Nanjing University, Clinical College of Nanjing Medical University & Clinical College of Traditional Chinese and Western Medicine, Nanjing University of Chinese Medicine & Medical School of Southeast University, China

A – research concept and design; B – collection and/or assembly of data; C – data analysis and interpretation; D – writing the article; E – critical revision of the article; F – final approval of the article

Address for correspondence
Haijun Zhang
E-mail: haijunzhang@seu.edu.cn

Abstract

Background. The systemic immune-inflammation index (SII) is a useful prognostic indicator for some types of cancer, but it remains to be elucidated if it is similarly useful for colon cancer.

Objectives. This study aims to investigate the prognostic value of preoperative SII in patients with colon cancer undergoing radical surgery.

Materials and methods. The clinical materials of 188 patients with colon cancer who underwent radical surgery from September 1, 2013, to August 31, 2018, in Zhongda Hospital at Southeast University (Nanjing, China) were collected retrospectively. The SII was calculated as platelet count $\times$ neutrophil count / lymphocyte count. All patients enrolled in the study were then assigned into 2 different groups according to the median value of SII for comparison of clinical features between the 2 groups. The survival curve was drawn using the Kaplan–Meier method. Univariate and multivariate analysis were performed using the Cox regression model, analyzing the independent risk factors. The independent factors were analyzed with the R software to construct a nomogram of 1-, 2- and 3-year disease-free survival (DFS) after operation. Lastly, a web-based probability calculator was constructed to dynamically predict the possibility of DFS of patients.

Results. The SII could significantly predict DFS of patients with colon cancer with the median value of 514.13xs. For DFS, multivariate Cox analysis indicated that age, tumor location, pathological N stage, and preoperative SII level were independent risk factors for patients with colon cancer after radical resection ($p < 0.05$). A nomogram and a web-based probability calculator were constructed based on these factors.

Conclusions. The preoperative SII level can predict DFS in patients who received radical surgery with colon cancer. The nomogram constructed based on independent risk factors is helpful in predicting DFS of colon cancer patients in clinical practice.

Key words: prognosis, colon cancer, nomogram, systemic immune-inflammation index

Background

Colorectal cancer is one of the most prevalent malignant tumors of the digestive tract worldwide. According to the World Health Organization (WHO) International Agency for Research on Cancer (IARC) global burden of cancer estimates for 2020, there were over 1.9 million new cases of colorectal cancers (including anal) and 935,000 deaths in 2020, accounting for roughly 1/10 of all cancer cases and deaths.[1] In China, colon cancer ranked 2nd and 5th in terms of new cases and deaths among the top 10 malignancies in 2020.[1] With the advance in treatments in recent years, the 5-year survival rate for colon cancer in China has risen to 57.6%; however, there is still room for improvement.[2] At present, surgery is the most common treatment for resectable colon cancer. However, the postoperative local recurrence and distant metastasis rate are still very high, owing to the anatomical structure of the colon and the characteristics of cancer itself. Local recurrence and distant metastasis are the main causes of decreased survival time and the decline in quality of life.[3] Therefore, to promote good health and prevent mortality, it is critical to assess the recurrence risk and survival time of patients with colon cancer after radical resection. According to previous research, inflammation is vital in various stages of tumor incidence, tissue invasion and metastasis.[4] In recent years, various inflammatory indicators have been presented for predicting tumor prognosis in order to increase the overall survival (OS) rate of patients with cancer, such as platelet-to-lymphocyte ratio (PLR), neutrophil-to-lymphocyte ratio (NLR)[5] and lymphocyte-to-monocyte ratio (LMR).[6] Systemic immune-inflammation index (SII), which is equal to platelet count × neutrophil count / lymphocyte count (P×N/L), could more thoroughly indicate the state of inflammation in the body based on a combination of the aforementioned 3 indicators of platelet, neutrophil and lymphocyte. So far, SII has demonstrated predictive value for prognosis in gastric cancer,[7] bladder cancer[8] and breast cancer.[9] However, its predictive value for the prognosis of colon cancer remains unknown.[10]

Objectives

To this end, this study aimed to investigate the predictive value of preoperative SII level for disease-free survival (DFS) of colon cancer patients undergoing radical surgery, and to construct a nomogram that could be used as a simple prognostication tool in clinical care.

Materials and methods

Patients

From September 1, 2013, to August 31, 2018, patients with colon cancer who were admitted to Zhongda Hospital at Southeast University (Nanjing, China) and received radical surgery were recruited into the study. The inclusion criteria were as follows: 1) radical surgery received; 2) postoperative pathological confirmation of colon cancer; 3) preoperative imaging showing no distant metastasis. Exclusion criteria were as follows: 1) patients who had received neoadjuvant therapy such as radiotherapy, chemotherapy and immunotherapy before surgery; 2) patients with severe cardiopulmonary insufficiency, severe infections, blood system diseases, autoimmune disease, hepatitis, or other tumors before surgery; 3) cases lacking crucial clinical or follow-up data. Finally, a total of 188 eligible cases were included in the study after application of the inclusion and exclusion criteria.

This study retrospectively collected the data of previous cases for anonymous analysis without exposing privacy information of patients, so informed consent could be waived. It was carried out in accordance with the Declaration of Helsinki.

Collection of clinical data

The temperature of all patients was normal 3 days before surgery, without obvious symptoms of local or systemic infection. Venous blood was collected 1 week before surgery, and SII for each patient was calculated using the formula SII = P × N/L. Clinical data (including age, gender, preoperative carcinoembryonic antigen (CEA) level, and preoperative intestinal obstruction) and pathological data (including tumor location, histological type, the maximum diameter, vascular and nerve invasion, the number of dissected lymph nodes, TNM staging, and human epidermal growth factor receptor-2 (HER2) expression) were collected for analysis. Right-sided colon cancer included cecum cancer, ascending colon cancer and right-half transverse colon cancer, while the rest were considered left-sided colon cancer. The follow-up started on the day of surgery (either in hospital or outpatient) and was performed every 3–6 months for the first 2 years, and then every 6 months thereafter. The deadline for follow-up was August 31, 2021. The patient's DFS during follow-up was recorded.

Evaluation criteria

The time from the postoperative period until the first recurrence or death due to recurrence or termination of follow-up was referred to as DFS. Postoperative recurrence was defined as the recurrence of malignant tumors related to the primary focus in all organs after radical resection, including local recurrence and distant metastasis. Local recurrence was understood as recurrence in the pelvic region, whereas distant organ metastasis referred to recurrence outside of the pelvic region. Postoperative recurrence was confirmed with imaging or pathology.

Statistical analyses

The IBM SPSS v. 26.0 software (IBM Corp., Armonk, USA) was used for statistical analysis. The SII scores were divided into a low and a high group according to the median. The χ^2 test or Fisher's exact test were used for comparison between groups. The Kaplan–Meier method was used for survival analysis and the log-rank test were used to compare the differences between the low and high groups. Univariate and multivariate Cox regression model was used to analyze risk factors that impacted the prognosis of patients with colon cancer. Some data regarding preoperative CEA, vascular invasion, nerve invasion, and HER2 expression were missing. In order to avoid the reduction of statistical test efficiency and bias caused by the missing data, multiple interpolation was used to compensate for missing data. Multiple interpolation would generate 5 interpolated datasets, each containing data of 188 patients, without missing items.

These 5 datasets and the original dataset underwent independent Cox analysis to provide 6 survival functions. The 6 survival functions were in good agreement, indicating that the additional data did not cause obvious bias in the results. Therefore, the best-performing dataset was chosen as the final data for analysis. Bilateral probability test was used for all statistics and $p < 0.05$ was considered statistically significant. The nomogram to predict 1-, 2- and 3-year DFS of patients after operation and the web-based probability calculator were constructed with the R software v. 4.1.1 (R Foundation for Statistical Computing, Vienna, Austria). The bootstrap method was used to repeat sampling 1000 times, serving to perform the internal validation of the nomogram. The receiver operating characteristic (ROC) curve and C-index were used to assess the differentiation and accuracy of the predictive model, and a calibration curve was used to evaluate the consistency of the prediction model of the nomogram. The flowchart (Fig. 1) depicts the concept for this study.
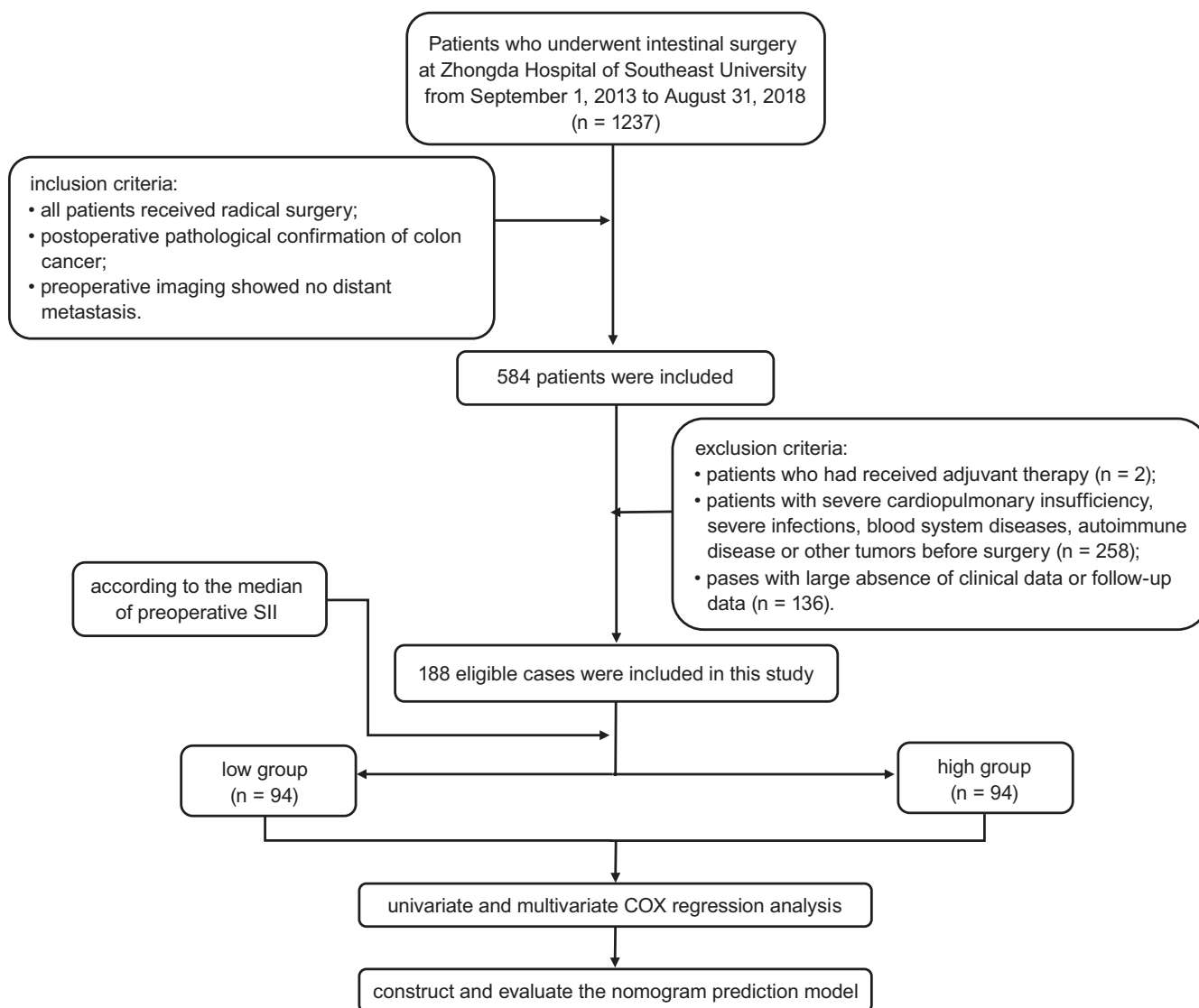
Fig. 1. Flowchart of the study

SII – systemic immune-inflammation index.

Results

General clinical characteristics of the patients

A total of 188 patients were included. There were 117 males and 71 females, whose age ranged from 33 to 92 years, with a median age of 67 years. Preoperative CEA level was ≥5 ng/mL in 93 patients and <5 ng/mL in 81 patients. Preoperative ileus was present in 50 cases. One hundred and seven patients had the tumor in the left colon, while 81 patients had tumors in the right colon. The tumor diameter in 123 patients was ≤5 cm.[11] The number of cases with adenocarcinoma, mucinous adenocarcinoma and other histological types were 148, 9 and 31, respectively. Vascular invasion was observed in the specimens of 65 patients, while 33 patients did not present with invasion. The number of patients with TNM stage I (including T0), stage II and stage III was 9, 93

and 86, respectively. The median follow-up time of all patients was 1294 (206–2766) days, during which 63 patients developed postoperative recurrence, including 11 cases with local recurrence and 52 cases with distant metastasis; 16 patients died. Among the patients with distant metastasis, 36 cases were liver metastasis, while the remaining 16 patients presented with multiple metastasis or single metastasis in other sites. Generally, the postoperative recurrence and mortality rate were 33.5% and 8.5%, respectively. The median value of the preoperative SII was 514.13, ranging from 108.27 to 5596.89. The clinical characteristics of the enrolled patients are presented in Table 1.

Correlation between preoperative SII and clinical variables

The clinical data and characteristics of the patients were compared between the 2 groups. (Table 2). There were

Table 1. Baseline characteristics of patients

Variables	Characteristics	Numbers of patients (n, %)
Gender	male female	117 (62.2) 71 (37.8)
Age [years]	<65 ≥65	76 (40.4) 112 (59.6)
Preoperative CEA [ng/mL]	<5 ≥5 unknown	93 (49.5) 81 (43.1) 14 (7.4)
Preoperative ileus	yes none	50 (26.6) 138 (73.4)
Tumor location	left-sided colon right-sided colon	107 (56.9) 81 (43.1)
Diameter [cm]	≤5 >5	123 (65.4) 65 (34.6)
Histology	adenocarcinoma mucinous adenocarcinoma others	148 (78.7) 9 (4.8) 31 (16.5)
Vascular invasion	yes none unknown	65 (34.6) 121 (64.4) 2 (1.1)
Nerve invasion	yes none unknown	33 (17.6) 152 (80.9) 3 (1.6)
Number of dissected peri-intestinal lymph nodes	<12 ≥12	42 (22.3) 146 (77.7)
HER2 expression	0/1+ 2+/3+ unknown	112 (59.6) 70 (37.2) 6 (3.2)
T stage	1–2 (including Tis) 3 4	14 (7.4) 163 (86.7) 11 (5.9)
N stage	0 1 2	100 (53.2) 59 (31.4) 29 (15.4)
TNM stage	I (including T0) II III	9 (4.8) 93 (49.5) 86 (45.7)

CEA – carcinoembryonic antigen; HER2 – human epidermal growth factor receptor 2.

Table 2. Characteristics of patients from different SII groups

Characteristics	SII		χ^2	p-value
	low group (n = 94)	high group (n = 94)		
Gender (male/female)	61/33	56/38	0.566	0.452
Age (<65/≥65 years)	36/58	40/54	0.353	0.552
Preoperative CEA (<5/≥5 ng/mL)	54/40	48/46	0.772	0.380
Preoperative ileus (yes/no)	20/74	30/64	2.725	0.099
Tumor location (left colon/right colon)	56/38	51/43	0.542	0.461
Diameter (≤5/>5 cm)	71/23	52/42	8.489	**0.004**
Histology (adenocarcinoma/mucinous adenocarcinoma/others)	75/3/16	73/6/15	1.401	0.713
Vascular invasion (yes/no)	27/67	38/56	2.845	0.092
Nerve invasion (yes/no)	15/79	19/75	0.574	0.448
Number of dissected peri-intestinal lymph nodes (<12/≥12)	24/70	18/76	1.104	0.293
HER2 expression (0 and 1+/2+ and 3+)	61/33	54/40	1.097	0.295
T stage (1–2 (including Tis)/3/4)	9/83/2	5/80/9	5.653	0.059
N stage (0/1/2)	53/27/14	47/32/15	0.818	0.664
TNM stage (I (including T0)/II/III)	6/48/40	3/45/46	1.485	0.467

SII – systemic immune-inflammation index; CEA – carcinoembryonic antigen; HER2 – human epidermal growth factor receptor 2. The χ^2 test was used for the comparison between the 2 groups. Values in bold are statistically significant.

statistical differences in tumor diameter in the 2 groups (p < 0.05), while gender, age, preoperative CEA level, intestinal obstruction, tumor location, tumor histology, vessel and nerve invasion, number of dissected peri-intestinal lymph nodes, HER2 expression, and T, N and TNM stage did not differ between the 2 groups (p > 0.05).

Risk factors affecting the prognosis of colon cancer patients receiving radical resection

As shown in Table 3, SII, as well as age, preoperative CEA level, tumor location, vascular and nerve invasion, and N and TNM stage affected the DFS of colon cancer in the 2 groups. Multivariate Cox analysis indicated that

Fig. 2. Survival analysis of SII according to the Kaplan–Meier method

SII – systemic immune-inflammatory index; DFS – disease-free survival.

age, tumor location, pathological N stage, and preoperative SII level were independent risk factors for DFS of patients who received radical resection of colon cancer. The Kaplan–Meier method indicated that there was a statistically significant difference in DFS between the 2 groups (Fig. 2). It revealed that patients in the high-SII group had worse DFS compared with those in the low-SII group.

Nomogram and a web-based probability calculator for prognosis of patients with colon cancer undergoing radical surgery

For DFS, the independent risk factors of DFS according to the results of multivariate analysis, including age, tumor location, pathological N stage, and preoperative SII level, were uploaded into the R software to draw a nomogram (Fig. 3). Bootstrap method was applied for internal validation of the nomogram (B = 1000) and the C-index was 0.717 (95% CI: 0.654–0.779). The ROC curve indicated that the nomogram had a good ability to predict DFS in a 3-year perspective. Furthermore, the calibration curve derived by the nomogram showed that the probability of DFS agreed well with the actual condition. Both curves are shown in Fig. 4. Moreover, a dynamic web-based probability calculator (https://medicalclimbers.shinyapps.io/DynNomapp/) was created to predict the DFS of patients with colon cancer undergoing radical resection according to the nomogram; this web-based probability calculator also made calculation of DFS probability of a single patient easier. As in the example below, it was easy to obtain the DFS probability of a patient by entering the age, tumor location, SII and pathological N stage in the calculator. For example, the 2-year DFS probability of patients who were
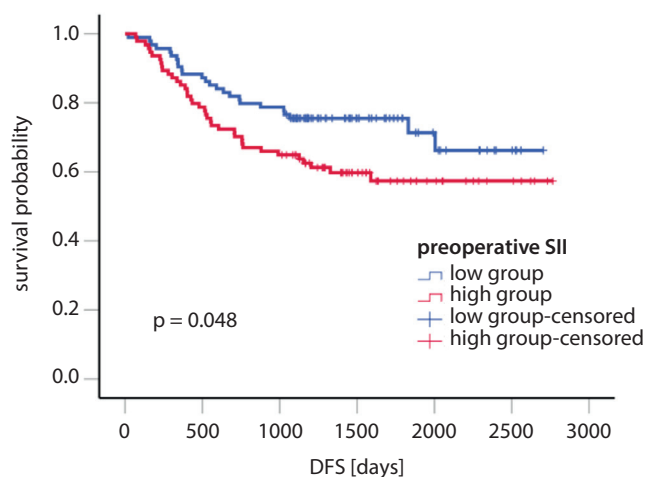
18

L. Zhang et al. SII can predict DFS of colon cancer

Table 3. Univariate and multivariate Cox regression analysis of DFS in patients with colon cancer

Variables	Variables	Univariate analysis		Multivariate analysis	
		HR (95% CI)	p-value	HR (95% CI)	p-value
Age [years]	<65 ≥65	1 (reference) 1.956 (1.131–3.384)	0.016	1 (reference) 2.581 (1.465–4.549)	0.001
Preoperative CEA [ng/mL]	<5 ≥5	1 (reference) 2.049 (1.209–3.472)	0.008	–	–
Tumor location	left colon right colon	1 (reference) 1.849 (1.126–3.037)	0.015	1 (reference) 2.535 (1.509–4.258)	0.000
Vascular invasion	yes none	1 (reference) 1.733 (1.045–2.875)	0.033	–	–
Nerve invasion	yes none	1 (reference) 1.762 (0.968–3.206)	0.064	–	–
N stage	0 1 2	1 (reference) 2.162 (1.202–3.886) 4.442 (2.361–8.358)	0.000	1 (reference) 3.031 (1.648–5.575) 6.222 (3.214–12.045)	0.000
TNM stage	I (including T0) II III	1 (reference) 2.261 (0.304–16.809) 5.690 (0.782–41.378)	0.001	–	–
SII	low group high group	1 (reference) 1.654 (0.998–2.741)	0.051	1 (reference) 1.708 (1.025–2.844)	0.040

DFS – disease-free survival; HR – hazard ratio; 95% CI – 95% confidence interval; CEA – carcinoembryonic antigen; SII – systemic immune-inflammation index.
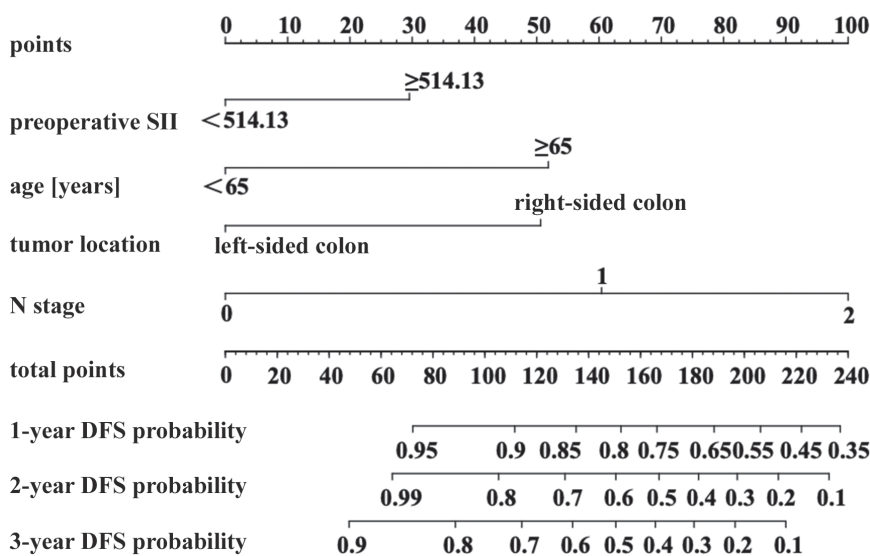
Fig. 3. Nomogram for predicting 1-, 2- and 3-year DFS after radical resection of colon cancer

SII – systemic immune- inflammation index; DFS – disease-free survival.

65 years old or older and had left-sided colon cancer, high preoperative SII and pathological N1 stage was about 65% (95% CI: 50–83%) (Fig. 5).

Discussion

Tumor-associated inflammation plays a vital role in the occurrence and development of tumors, and inflammatory and immune cells are important components of the tumor microenvironment.[12] When tissues are injured or infected, the local immune system activates numerous inflammatory cells, such as neutrophils, lymphocytes, macrophages, etc. which secrete a variety of cytokines to form an inflammatory microenvironment and repair damaged tissues. However, when such inflammatory microenvironment appears in tumor patients, a large number of inflammatory mediators which could alter the internal environment will be released, resulting in a cascade of inflammation-associated reactions. The constant inflammatory microenvironment could lead to the occurrence of tumors, which in turn further aggravate the inflammatory response by tumor formation and development.[13–15] Currently, it is widely believed that tumor-related inflammation suppresses tumor immunity by recruiting regulatory T cells and activating chemokines, leading to tumor progression.[16] Neutrophils inhibit the anti-tumor T response and release pro-angiogenic factors to stimulate the spread of tumor cells, while platelets also secrete a variety of angiogenic factors and tumor growth factors to stimulate the proliferation
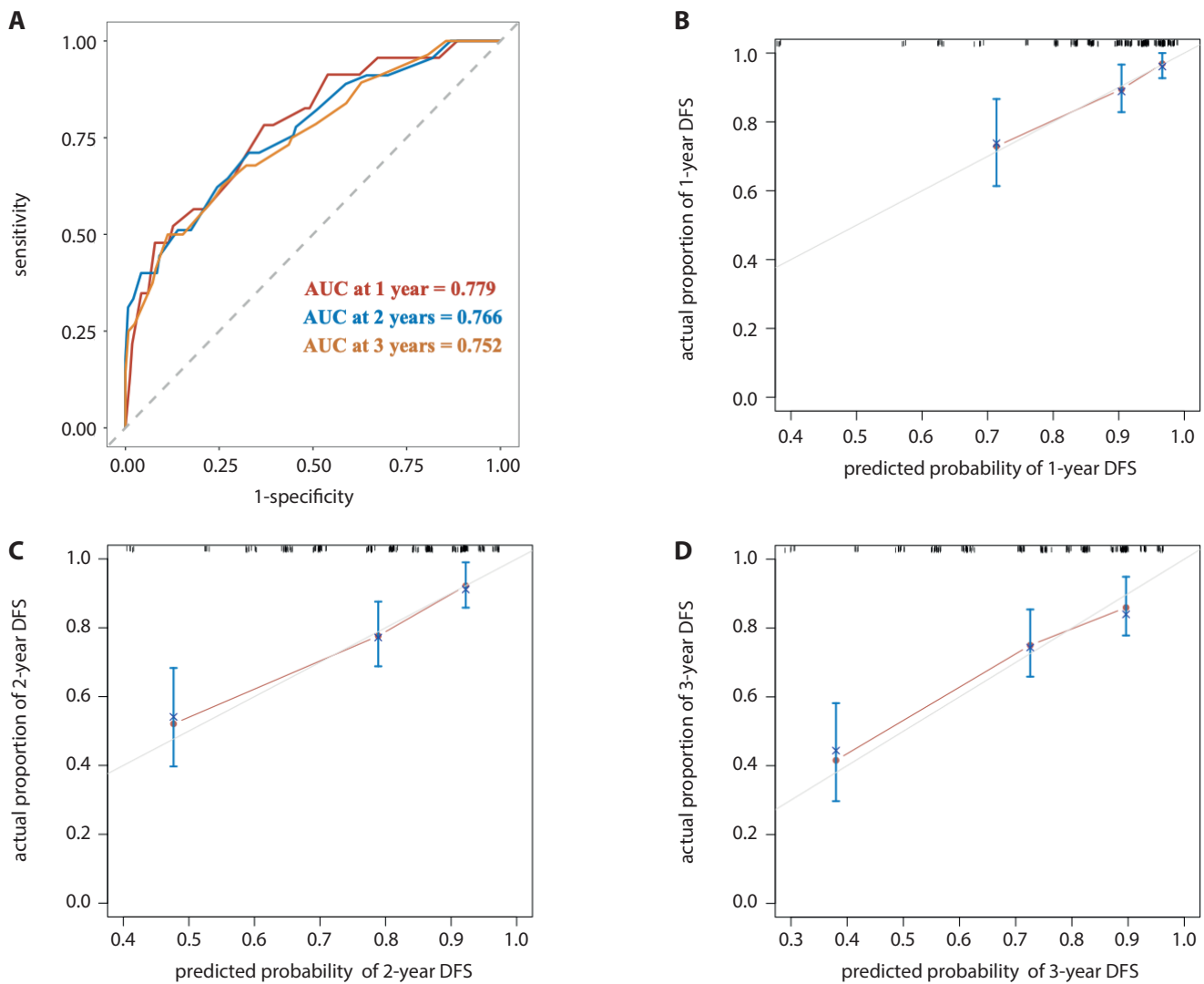
Fig. 4. A. ROC curve of the nomogram for predicting 1-, 2- and 3-year DFS after radical resection of colon cancer; B–D. Calibration curves of nomogram for predicting 1-, 2- and 3-year DFS after radical resection of colon cancer

ROC – receiver operating characteristic; AUC – area under curve; DFS – disease-free survival.

and distant metastasis of cancer cells.[4,17] On the other hand, lymphocytes are involved in anti-tumor immunity, triggering tumor apoptosis and necrosis mechanisms, so the decrease in the number of peripheral lymphocytes represents impaired cellular immunological dysfunction.[18–20]

The blood routine is a low-cost, low-trauma and highly repetitive examination procedure both for patients' admitted to hospitals and in outpatient clinics. Due to this, a series of inflammation-related indicators have been studied more intensively, and some of them have been proven to be useful in the prognosis of colon cancer. Catal et al. found that the preoperative PLR value showed good specificity and sensitivity for predicting lymph node metastasis in patients with colon cancer.[21] The study by Turri et al. indicated that patients with stage I or II colon cancer had worse OS when preoperative NLR was greater than 3 (p = 0.007).[22] Facciorusso et al. proved that LMR could predict OS and time to recurrence (TTR) in patients with colorectal liver metastasis after radiofrequency ablation.[23] Patients with

LMR ≤ 3.96% had a shorter median OS (34 months compared to 38 months, p = 0.007) and TTR (25 months compared to 35 months, p = 0.02) than those with LMR > 3.96%. In this study, SII is based on the comprehensive indicators of neutrophils, platelets and lymphocytes, which might better reflect the relationship between immunity and inflammation. The SII is effective in predicting the prognosis of cancers such as gastric cancer,[14] bladder cancer[9] and others. However, there are few studies regarding SII and colon cancer, and there is a lack of unified conclusion on the threshold value of SII. According to relevant studies, between 40% and 50% of patients with colorectal cancer will experience local tumor recurrence or metastasis, which ultimately leads to death.[24,25] Thus, it is necessary to assess the risk of recurrence of patients with colon cancer and take steps as early as possible in order to improve the survival rate and the quality of life. In recent years, many experts have studied the risk factors for recurrence of colon cancer. Some found that with the increase of age,

Dynamic Nomogram

Age

≥65 ▾

Tumor.location

Left-sided colon ▾

Preoperative.SII

≥514.13 ▾

N.stage

1 ▾

☑ Predicted Survival at this Follow Up:

DFS

21   730   2,766

21   296   571   846   1,121   1,396   1,671   1,946   2,221   2,496   2,766

☑ Alpha blending (transparency)

Predict

Press Quit to exit the application

Quit

Survival plot   Predicted Survival   **Numerical Summary**   Model Summary

```
========================================================================
 DFS Age  Tumor.location  Preoperative.SII N.stage Prediction Lower.bound Upper.bound
------------------------------------------------------------------------
1 730 ≥65 Left-sided colon     ≥514.13          1      0.650       0.500       0.830
------------------------------------------------------------------------
```

Fig. 5. A web-based probability calculator. When a patient was 65 years old or older and had left-sided colon cancer, high preoperative SII and pathological N1 stage, it showed a rough range of probability of 2-year DFS and its 95% confidence interval (95% CI)

the number of lymphocytes in the body decreases, so SII would increase with age, which may lead to a correlation between age and postoperative recurrence rates.[26] Mizuno et al.[27] confirmed that preoperative CEA level was significant for the prognosis of patients with stage II/III colon cancer, while some other investigators[28] pointed out that postoperative CEA, rather than preoperative CEA, could more accurately predict the probability of recurrence and death after operation. This dispute warrants more studies in the future. In addition, Lee et al. found that left colon cancer patients had considerably better DFS and OS compared with those with right colon affected, which might be due to the different biologic characteristics of colon cancer at different location.[29] Saha et al. found that tumor

diameter negatively impacted survival, whereas our study failed to confirm the connection between tumor diameter and prognosis because of the small sample size.[30] Nevertheless, other classic factors, such as pathological N stage,[31] were proven to be related to DFS.

A meta-analysis confirmed that higher preoperative SII level could predict worse DFS of patients with colon cancer, which is in accordance with our study.[4] However, the cutoff value of SII was not standardized in general. In our study, the cutoff value of SII was 514.13, which is similar to the findings presented in other studies, where the cutoff SII ranged from 340 to 667.75.[10,32,33] The varied values of SII do not alter our conclusion; however, the optimal cutoff value still needs to be adjusted according to clinical

practice. Despite the fact that the TNM analysis can predict the prognosis of patients with cancers, its limited accuracy results in heterogeneity of patients with the same stage.[34] Some research has put forward several new TNM staging strategies to predict the prognosis of patients with colorectal cancer.[35–37] Therefore, the nomogram in this study could integrate various clinical information to provide more accurate and individualized prognostic prediction, better than just TNM stage. Furthermore, the nomogram established here is based on independent risk factors that could well predict DFS of patients with colon cancer 1, 2 and 3 years after surgery. To be more exact, we were able to predict the probability of 1-, 2- and 3- DFS of patients with colon cancer based on their clinical characteristics including age, tumor location, preoperative SII, and N stage.

Inflammatory response is not the only factor affecting the prognosis of patients with cancers. Nowadays, more attention has been paid to tumor drug therapies like chemotherapy and immunotherapy, while surgical treatment seems less important. While all cases in this study received radical surgery, the prognosis of patients may be influenced by many factors, including different surgical methods and experience of operators. A meta-analysis of 16 retrospective studies showed that any complication after radical surgery in patients for stage II and III gastric cancer predicted a poor outcome, while the same result was not found in patients with stage I gastric cancer.[38] For functional well-differentiated neuroendocrine tumors (NETs) with liver metastases, surgery is not usually the first choice. However, Citterio et al. demonstrated that resection of the primary tumor might improve the survival in these patients.[39] For pancreatic cancer, radical surgery is still the only curative method, but the choice of surgical method is worth further discussion. The survival benefits of patients with pancreatic head cancer were not significantly improved by extended resection when compared with standard pancreaticoduodenectomy. Conversely, better survival outcomes were achieved by extended resection of pancreatic tail or body cancer.[40] For colon cancer, the choice between open and laparoscopic surgery has always been controversial. Mazaki et al. found that compared with colon cancer patients who underwent open radical surgery, those who received laparoscopic radical surgery had a lower 5-year cumulative local recurrence rate (9.2% compared to 0%, p = 0.007), but the 5-year distant metastasis rate seemed to be higher (9.2% compared to 12.7%, p = 0.49).[41] In summary, future studies should also pay more attention to tumor surgical treatment, such as the timing of surgery, the choice of surgical methods and postoperative complications, so as to provide reference for prolonging the survival of patients.

Limitations

Inevitably, there were some limitations of this study. Firstly, it was a single-center retrospective study with a small sample size and some loss of clinical data, which had selection bias, confounding bias and some other drawbacks. Additionally, the differing surgical experience of the operators could also lead to differences in the postoperative tumor recurrence rate of patients. This nomogram had only been verified internally due to limitations imposed due to COVID-19 pandemic and small sample size. As a result, its reliability was weaker when it was verified in different cohorts. Although our study lacked external validation, the nomogram performed well in terms of discrimination and calibration, and it predicted the probability of disease-free survival 1, 2 and 3 years after radical surgery, which was rarely performed in other studies. Future studies should collect data from other centers for external validation. Finally, factors related to prognosis such as microsatellite instability, KRAS and NRAS[42] mutations, and the question whether to perform postoperative adjuvant therapy were not included in the study. Meanwhile, whether SII has predictive value for patients of all races, regions and types requires more multicenter and larger sample research in the future.

Conclusion

In summary, this study found that SII, as a novel prognostic indicator based on inflammation in recent years, could independently predict the postoperative recurrence of patients with colon cancer. The nomogram based on SII and other independent factors could effectively predict 1-, 2- and 3-year DFS of patients after surgery, providing patients and doctors with more accurate and timely prognostic judgments, which could potentially improve survival rate and quality of life. Moreover, a dynamic web-based probability calculator constructed according to the nomogram made it easier and more convenient to predict the prognosis of patients in clinical work.

ORCID iDs

Lu Zhang https://orcid.org/0000-0003-2065-2287
Zhong Zhang https://orcid.org/0000-0002-5605-4951
Haochun Guo https://orcid.org/0000-0002-6742-6634
Bin Huang https://orcid.org/0000-0002-7738-3455
Haijun Zhang https://orcid.org/0000-0002-4313-3001

References

1. Sung H, Ferlay J, Siegel RL, et al. Global Cancer Statistics 2020: GLOBOCAN estimates of incidence and mortality worldwide for 36 cancers in 185 countries. *CA Cancer J Clin*. 2021;71(3):209–249. doi:10.3322/caac.21660
2. Allemani C, Matsuda T, Di Carlo V, et al. Global surveillance of trends in cancer survival 2000–14 (CONCORD-3): Analysis of individual records for 37 513 025 patients diagnosed with one of 18 cancers from 322 population-based registries in 71 countries. *Lancet*. 2018; 391(10125):1023–1075. doi:10.1016/S0140-6736(17)33326-3
3. National Cancer Center, China, Expert Group of the Development of China Guideline for the Screening, Early Detection and Early Treatment of Colorectal Cancer. China Guideline for the Screening, Early detection and Early Treatment of Colorectal Cancer (2020, Beijing) [in Chinese]. *Zhonghua Zhong Liu Za Zhi*. 2021;43(1):16–38. doi:10.3760/cma.j.cn112152-20210105-00010

4. Yang R, Chang Q, Meng X, Gao N, Wang W. Prognostic value of systemic immune-inflammation index in cancer: A meta-analysis. *J Cancer*. 2018;9(18):3295–3302. doi:10.7150/jca.25691

5. Park BK, Park JW, Han EC, et al. Systemic inflammatory markers as prognostic factors in stage IIA colorectal cancer. *J Surg Oncol*. 2016;114(2):216–221. doi:10.1002/jso.24299

6. Trinh H, Dzul SP, Hyder J, et al. Prognostic value of changes in neutrophil-to-lymphocyte ratio (NLR), platelet-to-lymphocyte ratio (PLR) and lymphocyte-to-monocyte ratio (LMR) for patients with cervical cancer undergoing definitive chemoradiotherapy (dCRT). *Clin Chim Acta*. 2020;510:711–716. doi:10.1016/j.cca.2020.09.008

7. Fu S, Yan J, Tan Y, Liu D. Prognostic value of systemic immune-inflammatory index in survival outcome in gastric cancer: A meta-analysis. *J Gastrointest Oncol*. 2021;12(2):344–354. doi:10.21037/jgo-20-252

8. Zhang Y, Sun Y, Zhang Q. Prognostic value of the systemic immune-inflammation index in patients with breast cancer: A meta-analysis. *Cancer Cell Int*. 2020;20(1):224. doi:10.1186/s12935-020-01308-6

9. Zhang W, Wang R, Ma W, et al. Systemic immune-inflammation index predicts prognosis of bladder cancer patients after radical cystectomy. *Ann Transl Med*. 2019;7(18):431. doi:10.21037/atm.2019.09.02

10. Rimini M, Casadei-Gardini A, Ravaioli A, et al. Could inflammatory indices and metabolic syndrome predict the risk of cancer development? Analysis from the Bagnacavallo Population Study. *J Clin Med*. 2020;9(4):1177. doi:10.3390/jcm9041177

11. Kornprat P, Pollheimer MJ, Lindtner RA, Schlemmer A, Rehak P, Langner C. Value of tumor size as a prognostic variable in colorectal cancer: A critical reappraisal. *Am J Clin Oncol*. 2011;34(1):43–49. doi:10.1097/COC.0b013e3181cae8dd

12. Hanahan D, Weinberg RA. Hallmarks of cancer: The next generation. *Cell*. 2011;144(5):646–674. doi:10.1016/j.cell.2011.02.013

13. Shi H, Jiang Y, Cao H, Zhu H, Chen B, Ji W. Nomogram based on systemic immune-inflammation index to predict overall survival in gastric cancer patients. *Dis Markers*. 2018;2018:1787424. doi:10.1155/2018/1787424

14. Grivennikov SI, Greten FR, Karin M. Immunity, inflammation, and cancer. *Cell*. 2010;140(6):883–899. doi:10.1016/j.cell.2010.01.025

15. Duan R, Nilsson A. Metabolism of sphingolipids in the gut and its relation to inflammation and cancer development. *Prog Lipid Res*. 2009;48(1):62–72. doi:10.1016/j.plipres.2008.04.003

16. Caronni N, Savino B, Bonecchi R. Myeloid cells in cancer-related inflammation. *Immunobiology*. 2015;220(2):249–253. doi:10.1016/j.imbio.2014.10.001

17. Swierczak A, Mouchemore KA, Hamilton JA, Anderson RL. Neutrophils: Important contributors to tumor progression and metastasis. *Cancer Metastasis Rev*. 2015;34(4):735–751. doi:10.1007/s10555-015-9594-9

18. Ivanova OK, Sharapova TN, Romanova EA, Soshnikova NV, Sashchenko LP, Yashin DV. CD3⁺ CD8⁺ NKG2D⁺ T lymphocytes induce apoptosis and necroptosis in HLA-negative cells via FasL–Fas interaction. *J Cell Biochem*. 2017;118(10):3359–3366. doi:10.1002/jcb.25990

19. Dudani S, Marginean H, Tang PA, et al. Neutrophil-to-lymphocyte and platelet-to-lymphocyte ratios as predictive and prognostic markers in patients with locally advanced rectal cancer treated with neoadjuvant chemoradiation. *BMC Cancer*. 2019;19(1):664. doi:10.1186/s12885-019-5892-x

20. Ksienski D, Wai ES, Alex D, et al. Prognostic significance of the neutrophil-to-lymphocyte ratio and platelet-to-lymphocyte ratio for advanced non-small cell lung cancer patients with high PD-L1 tumor expression receiving pembrolizumab. *Transl Lung Cancer Res*. 2021;10(1):355–367. doi:10.21037/tlcr-20-541

21. Catal O, Ozer B, Sit M. Prediction of lymph node metastasis in colon cancer via platelet to lymphocyte ratio and platelet count. *J Coll Physicians Surg Pak*. 2020;30(3):250–253. doi:10.29271/jcpsp.2020.03.250

22. Turri G, Barresi V, Valdegamberi A, et al. Clinical significance of preoperative inflammatory markers in prediction of prognosis in node-negative colon cancer: Correlation between neutrophil-to-lymphocyte ratio and poorly differentiated clusters. *Biomedicines*. 2021;9(1):94. doi:10.3390/biomedicines9010094

23. Facciorusso A, Prete VD, Crucinio N, Serviddio G, Vendemiale G, Muscatiello N. Lymphocyte-to-monocyte ratio predicts survival after radiofrequency ablation for colorectal liver metastases. *World J Gastroenterol*. 2016;22(16):4211–4218. doi:10.3748/wjg.v22.i16.4211

24. Osterman E, Hammarström K, Imam I, Osterlund E, Sjöblom T, Glimelius B. Completeness and accuracy of the registration of recurrences in the Swedish Colorectal Cancer Registry (SCRCR) and an update of recurrence risk in colon cancer. *Acta Oncol*. 2021;60(7):842–849. doi:10.1080/0284186X.2021.1896033

25. Benitez Majano S, Di Girolamo C, Rachet B, et al. Surgical treatment and survival from colorectal cancer in Denmark, England, Norway, and Sweden: A population-based study. *Lancet Oncol*. 2019;20(1):74–87. doi:10.1016/S1470-2045(18)30646-6

26. Macedo Queiroz Mota Castellão Tavares S, de Lima Bravo Junior Jr., Ribeiro Lopes e Silva M. Normal lymphocyte immunophenotype in an elderly population. *Rev Bras Hematol Hemoter*. 2014;36(3):180–183. doi:10.1016/j.bjhh.2014.03.021

27. Mizuno H, Miyake H, Nagai H, et al. Optimal cutoff value of preoperative CEA and CA19-9 for prognostic significance in patients with stage II/III colon cancer. *Langenbecks Arch Surg*. 2021;406(6):1987–1997. doi:10.1007/s00423-021-02236-3

28. Kwaan MR. Postoperative CEA and other non-traditional risk factors for colon cancer recurrence: Findings from Swedish population-based data. *Ann Surg Oncol*. 2020;27(4):971–972. doi:10.1245/s10434-019-08151-8

29. Lee MS, Menter DG, Kopetz S. Right versus left colon cancer biology: Integrating the consensus molecular subtypes. *J Natl Compr Canc Netw*. 2017;15(3):411–419. doi:10.6004/jnccn.2017.0038

30. Saha S, Shaik M, Johnston G, et al. Tumor size predicts long-term survival in colon cancer: An analysis of the National Cancer Data Base. *Am J Surg*. 2015;209(3):570–574. doi:10.1016/j.amjsurg.2014.12.008

31. Osterman E, Mezheyeuski A, Sjöblom T, Glimelius B. Beyond the NCCN risk factors in colon cancer: An evaluation in a Swedish population-based cohort. *Ann Surg Oncol*. 2020;27(4):1036–1045. doi:10.1245/s10434-019-08148-3

32. Chen JH, Zhai ET, Yuan YJ, et al. Systemic immune-inflammation index for predicting prognosis of colorectal cancer. *World J Gastroenterol*. 2017;23(34):6261–6272. doi:10.3748/wjg.v23.i34.6261

33. Tao MY, Wang ZH, Zhang MH, et al. Prognostic value of the systematic immune-inflammation index among patients with operable colon cancer: A retrospective study. *Medicine (Baltimore)*. 2018;97(45):e13156. doi:10.1097/MD.0000000000013156

34. Mo S, Zhou Z, Li Y, et al. Establishment and validation of a novel nomogram incorporating clinicopathological parameters into the TNM staging system to predict prognosis for stage II colorectal cancer. *Cancer Cell Int*. 2020;20(1):285. doi:10.1186/s12935-020-01382-w

35. Ogawa S, Itabashi M, Bamba Y, et al. Stage II colon cancer staging using the number of retrieved lymph nodes may be superior to current TNM staging for prognosis stratification: The Japanese study group for postoperative follow-up of colorectal cancer. *Int J Colorectal Dis*. 2021;36(10):2205–2214. doi:10.1007/s00384-021-03990-y

36. Shinto E, Hida JI, Ike H, et al. A new N staging system for colorectal cancer in the era of extended lymphadenectomy. *Ann Surg Oncol*. 2018;25(13):3891–3897. doi:10.1245/s10434-018-6786-x

37. Arabiki M, Shimada Y, Nakano M, et al. Verification of the Japanese staging system for rectal cancer, focusing on differences with the TNM classification. *Surg Today*. 2020;50(11):1443–1451. doi:10.1007/s00595-020-02024-4

38. Wang S, Xu L, Wang Q, et al. Postoperative complications and prognosis after radical gastrectomy for gastric cancer: A systematic review and meta-analysis of observational studies. *World J Surg Oncol*. 2019;17(1):52. doi:10.1186/s12957-019-1593-9

39. Citterio D, Pusceddu S, Facciorusso A, et al. Primary tumour resection may improve survival in functional well-differentiated neuroendocrine tumours metastatic to the liver. *Eur J Surg Oncol*. 2017;43(2):380–387. doi:10.1016/j.ejso.2016.10.031

40. Cheol Kim S, Hoon Kim Y, Min Park K, Ju Lee Y. Pancreatic cancer surgery: The state of the art. *Curr Drug Targets*. 2012;13(6):764–771. doi:10.2174/138945012800564185

41. Mazaki J, Katsumata K, Tago T, et al. Long-term outcomes of laparoscopic versus open surgery for colon cancer in noncancer-specific hospital: Propensity score analysis. *J Laparoendosc Adv Surg Tech A*. 2021;31(4):433–442. doi:10.1089/lap.2020.0510

42. Dienstmann R, Mason MJ, Sinicrope FA, et al. Prediction of overall survival in stage II and III colon cancer beyond TNM system: A retrospective, pooled biomarker study. *Ann Oncol*. 2017;28(5):1023–1031. doi:10.1093/annonc/mdx052

Polymorphism of *IL-1B* rs16944 (T/C) associated with serum levels of IL-1β affects seizure susceptibility in ischemic stroke patients

*Xiaojun Ma[1,B–D,F], *Liangwei Sun[2,B–D,F], Xiaoli Li[1,A,C,E,F], Yanlu Xu[2,B,C,F], Qingyan Zhang[3,C,E,F]

[1] Department of Geriatrics, Shandong Provincial Third Hospital, Jinan, China
[2] Department of Neurology, Shandong Provincial Third Hospital, Jinan, China
[3] Institute of Scientific Devices, Beihang University, Beijing, China

A – research concept and design; B – collection and/or assembly of data; C – data analysis and interpretation;
D – writing the article; E – critical revision of the article; F – final approval of the article

Address for correspondence
Xiaoli Li
E-mail: lixiaoli20080101@126.com

Abstract

Background. Seizures and the subsequent development of epilepsy after stroke may not only hinder patient's recovery but also increase the risk of complications. Interleukin (IL)-1β has been shown to be acutely upregulated after ischemic stroke and play a role in the recurrence of seizures following the first epileptic seizure in patients suffering an ischemic stroke. Meanwhile, variants of the *IL-1B* gene encoding IL-1β are involved in the stimulation of febrile seizures.

Objectives. To study the potential associations of the 5 polymorphisms of the *IL-1B* gene with seizure susceptibility in ischemic stroke patients, and to explore the possible mechanisms.

Materials and methods. A total of 856 ischemic stroke patients were allocated into the control group (patients without post-stroke seizures) and the case group (patients with post-stroke seizures). The *IL-1B* polymorphisms rs10490571 (T/C), rs114363 (C/T), rs1143623 (G/C), rs16944 (T/C), and rs2853550 (A/G) were detected using TaqMan SNP genotyping assays, and serum IL-1β levels were measured using the enzyme-linked immunosorbent assay (ELISA). Demographic data, clinical characteristics and cerebrovascular disease risk factors at admission were collected. Multivariate analysis was performed to determine independent associations, and IL-1β levels were compared using analysis of variance (ANOVA) followed by a post hoc test.

Results. In 74 patients (8.6%, 74/856), post-stroke seizures occurred within 1 year of stroke onset. The multivariate analysis showed that the rs16944 polymorphism of *IL-1B*, cortical involvement and National Institutes of Health Stroke Scale (NIHSS) score on admission were correlated with post-stroke seizures after adjusting for stroke laterality, thrombolysis, use of statins, and IL-1B rs10490571. The IL-1B rs16944 TT (odds ratio (OR): 1.923, 95% confidence interval (95% CI): 1.257–4.185) and TC genotypes (OR: 1.469, 95% CI: 1.130–2.974) were associated with a significantly increased risk of post-stroke seizures compared to the CC genotype. One-way ANOVA for IL-1β levels demonstrated a tendency for higher levels in TT > TC > CC genotypes (6.41 compared to 4.53 compared to 2.10 pg/mL, respectively).

Conclusions. The *IL-1B* rs16944 polymorphism had an independent association with seizure susceptibility after ischemic stroke. The mechanism might be associated with the regulation of IL-1β levels.

Key words: polymorphism, multivariate analysis, *IL-1B* rs16944 (T/C), post-stroke seizures, IL-1β levels

24

X. Ma et al. Seizure susceptibility in ischemic stroke

Background

Strokes are the 2nd leading cause of preventable deaths around the world and the primary cause of long-term disability.[1] In China, the stroke burden has been increasing over the past 30 years. The age-standardized incidence has risen to 246.8/100,000 person-years, and the age-standardized mortality to 114.8/100,000 person-years.[2] Ischemic stroke, which accounts for 75–80% of all strokes, is the most common cause of seizures among the elderly and is the predominant cause of seizures among the adults.[3–5] Seizures and the subsequent development of epilepsy after stroke may not only hinder patient's recovery but also increase the risk of complications.[6] With demographic changes, the healthcare system is facing a challenge of an increasing number of elderly people with post-stroke seizures. Therefore, the identification and appropriate management of stroke patients with an increased susceptibility for seizures are crucial in stroke care. Interleukin (IL)-1β has been demonstrated to be acutely upregulated after an ischemic stroke and be involved in the recurrence of seizures following the first epileptic seizure in patients with ischemic strokes.[7–9] At the same time, variants of the *IL-1B* gene encoding IL-1β have been shown to be involved in the stimulation of febrile seizures.[10] Additionally, the *IL-1B* polymorphisms rs16944, rs1143623, rs10490571, and rs2853550 were associated with the expression of IL-1β. However, the correlations between these polymorphisms and post-stroke seizures have not been analyzed.

Objectives

In this study, the association of *IL-1B* polymorphisms rs10490571, rs114363, rs16944, rs1143623, and rs2853550 with post-stroke seizures was determined using multivariate analysis. This study aimed to evaluate the potential associations of 5 polymorphisms of the *IL-1B* gene with seizure susceptibility in ischemic stroke patients, and to explore the possible mechanisms.

Materials and methods

Participants

This case-control study was performed at the Shandong Provincial Third Hospital (Jinan, China) between September 2018 and August 2019, and included 856 ischemic stroke patients into the final analysis. Participants meeting the following criteria were included: 1) acute first-ever ischemic stroke definitively diagnosed using magnetic resonance imaging (MRI) or computed tomography (CT); 2) ≥18 years of age at the time of admission; 3) no previous history of seizures; 4) no potentially epileptogenic comorbidities such as cerebral venous thrombosis, cerebral

arteriovenous malformations, intracranial tumors, etc.; 5) complete medical data; and 6) the ability to provide written informed consent. Participants with the following characteristics were excluded: 1) history of antiepileptic drug therapy to prevent seizures or other diseases; 2) primary hemorrhagic stroke or transient ischemic attacks; and 3) lost to follow-up or death before the follow-up. This study received the approval from the Ethical Committee of Shandong Provincial Third Hospital (approval No. SDTH-201813022).

Grouping

All 856 ischemic stroke patients were allocated either into the control group (patients without post-stroke seizures) or the case group (patients with post-stroke seizures), depending on the occurrence of a post-stroke seizure within 1 year of the onset of ischemic stroke. The diagnosis of seizure occurrence was determined using the definition provided by the International League Against Epilepsy (ILAE).

Data collection

We retrospectively collected the demographic data, clinical characteristics and cerebrovascular disease risk factors of participants at admission. The demographic data included sex, age and body mass index (BMI), while cerebrovascular disease risk factors included hypertension, smoking, drinking, diabetes mellitus, coronary heart disease, dyslipidemia, and atrial fibrillation. The clinical characteristics including stroke laterality, cortical involvement, the National Institutes of Health Stroke Scale (NIHSS) score at admission, Trial of ORG 10172 in Acute Stroke Treatment (TOAST) classification (large artery atherosclerosis, cardioembolism, small vessel occlusion, other determined, and undetermined), stroke treatment methods, and duration from stroke onset to admission were collected.

Genotyping and measurement of IL-1β levels

Peripheral blood samples were collected from all participants and DNA was extracted from the blood samples using the phenol-chloroform method. The concentration of DNA was measured using the optical density, and the quality of DNA was assessed according to the 260/280 ratio. TaqMan™ Pre-Designed SNP genotyping assays (Applied Biosystems, Waltham, USA) were used to detect the polymorphisms (C___29921173_20 for rs10490571, C___9546529_30 for rs114363, C___1839943_10 for rs16944, C___1839941_10 for rs1143623, and C___188872117_10 for rs2853550). Haploview software v. 4.2 (Broad Institute, Cambridge, USA) was used to analyze the Hardy–Weinberg equilibrium (HWE), as well as allele and genotype frequencies.

After the blood samples were centrifuged for 10 min at 3000 g, serum IL-1β levels were measured using the Human Interleukin-1β ELISA Kit (Baiaolaibo, Beijing, China).

Statistical analyses

The IBM SPSS v. 22.0 (IBM Corp., Armonk, USA) was used to perform all statistical analyses, and significance was set at a two-sided p-value <0.05. The Shapiro–Wilk test was used to evaluate the normality of continuous data. The Student's t-test was used to compare the means of normally distributed data between the case group and the control group. The Mann–Whitney U test was used to compare the pseudo-medians of non-normally distributed data. The χ^2 test was used to compare the differences in qualitative data between the case and control groups, and the Fisher's exact test was used when 1 or more cells had an expected count of less than 5. To avoid the omission of variables that might be meaningful and to determine independent associations, the multivariate analysis was performed for variables with a two-sided p-value <0.10 in the univariate analysis, using a backward stepwise logistic regression model. The IL-1β levels were compared using analysis of variance (ANOVA) followed by post hoc testing in ischemic stroke patients with different genotypes.

Results

General results

A total of 74 participants (8.6%, 74/856) had post-stroke seizures within 1 year of stroke onset. In the continuous data, NIHSS score at admission was non-normally distributed and was expressed using the median and the 1st and 3rd quartile (Q1, Q3). The NIHSS score at admission was 14 (12, 18) in the case group and 12 (10, 16) in the control group, and its pseudo-median was compared using the Mann–Whitney U test. Other continuous data were normally distributed, and their means were compared using Student's t-tests. According to the results of univariate analysis, stroke laterality, cortical involvement, thrombolysis, use of statins (Table 1), and NIHSS score on admission (Z = 2.013, p = 0.044) were significantly different between the control and case groups. Other variables were not significantly different.

Genotyping results

In 841 participants, these 5 single nucleotide polymorphisms (SNPs) were successfully genotyped. Sequencing was further carried out for the SNPs that were not genotyped successfully. Finally, all 856 participants were successfully genotyped for these 5 SNPs. As shown in Table 2, the genotype frequencies of these 5 SNPs were not significantly different from those predicted using the HWE.

The χ^2 test showed that the genotype frequencies of *IL-1B* rs16944 (degrees of freedom (df) = 2, χ^2 = 8.683, p = 0.013) and rs10490571 (df = 2, Fisher's exact test, p = 0.030) were significantly different between the case and control groups, but rs1143623 (df = 2, χ^2 = 0.261, p = 0.878), rs114363 (df = 2, Fisher's exact test, p = 0.456) and rs2853550 (df = 2, Fisher's exact test, p = 0.698) were not.

Multivariate analysis

The multivariate analysis was conducted for the following variables: cortical involvement, stroke laterality, NIHSS score on admission, thrombolysis, use of statins, *IL-1B* rs16944, and *IL-1B* rs10490571. As demonstrated in Table 3, the *IL-1B* polymorphism rs16944, cortical involvement and NIHSS score on admission were correlated with post-stroke seizures after adjusting for stroke laterality, thrombolysis, use of statins, and *IL-1B* rs10490571. The *IL-1B* rs16944 TT and TC genotypes were associated with a significantly increased risk of post-stroke seizures compared to the CC genotype. Moreover, the odds ratio (OR) of the TT genotype was higher than that of the TC genotype.

IL-1β levels

The IL-1β levels in the case group were higher than that of the control group (Student's t-test, df = 854, t = 2.683, p = 0.008, Fig. 1A). One-way ANOVA for IL-1β levels demonstrated a tendency for higher levels in TT compared to TC and CC genotypes (Fig. 1B, 6.41 compared to 4.53 compared to 2.10 pg/mL, respectively; overall test: F = 10.537, p = 0.007, post hoc results are presented in Table 4).

Discussion

The incidence of post-stroke seizures ranged from 2% to 20% with great variation.[11–13] Post-stroke seizures can lead to additional complications, increased mortality and longer initial hospitalizations, which substantially impact the prognosis and quality of life in stroke patients.[14,15]

Inflammation is extensively involved in the pathophysiology of an ischemic stroke.[16] The expression of pro-inflammatory cytokines, including IL-1β and IL-6, have been found to be significantly upregulated after an acute stroke.[17] Neuroinflammation can result in hyperexcitability, a ground base for seizures.[18,19] In the central nervous system, *IL-1B* is a constitutively expressed gene that can modulate both the expression and activity of ion channels and exert a neurotrophic factor-like activity.[20,21] The levels of inflammatory cytokines in the IL-1β pathway can act as biomarkers for neurologic diseases. The IL-1β can increase neuronal excitability through the activation of its endogenous receptor.[22,23] Following an initial insult to the central nervous system, ongoing inflammation can

Table 1. Univariate analysis results of the differences regarding demographic data, risk factors for cerebrovascular diseases and clinical characteristics between the case group and control group

Variables	All ischemic stroke patients (n = 856)	Case group (n = 74)	Control group (n = 782)	df	Student's t test/χ^2 test	p-value
Demographic data						
Age [years], M ±SD	67.26 ±9.25	68.37 ±9.14	67.15 ±9.26	854	1.096	0.285
Males, n (%)	510 (59.6)	48 (64.9)	462 (59.1)	1	0.940	0.332
BMI [kg/m^2], M ±SD	24.67 ±3.18	25.09 ±3.07	24.63 ±3.19	854	1.228	0.225
Risk factors for cerebrovascular diseases						
Smoking, n (%)	201 (23.5)	21 (28.4)	180 (23.0)	1	1.081	0.298
Alcohol consumption, n (%)	326 (38.1)	25 (33.8)	301 (38.5)	1	0.635	0.425
Diabetes mellitus, n (%)	162 (18.9)	18 (24.3)	144 (18.4)	1	1.539	0.215
Hypertension, n (%)	556 (65.0)	44 (59.5)	512 (65.5)	1	1.074	0.300
Coronary heart disease, n (%)	40 (4.7)	6 (8.1)	34 (4.3)	1	–	0.147*
Dyslipidemia, n (%)	171 (20.0)	19 (25.7)	152 (19.4)	1	1.646	0.200
Atrial fibrillation, n (%)	61 (7.1)	8 (10.8)	53 (6.8)	1	1.474	0.225
Clinical characteristics						
Stroke laterality, n (%)						
Right	418 (48.8)	47 (63.5)	371 (47.4)	1	6.988	0.008
Left	438 (51.2)	27 (36.5)	411 (52.6)			
Cortical involvement, n (%)	199 (23.2)	27 (36.5)	172 (22.0)	1	7.957	0.005
TOAST classification, n (%)						
Large artery atherosclerosis	457 (53.4)	35 (47.3)	422 (54.0)	1	1.207	0.272
Cardioembolism	176 (20.6)	17 (23.0)	159 (20.3)	1	0.289	0.591
Small vessel occlusion	129 (15.1)	8 (10.8)	121 (15.5)	1	1.148	0.284
Other determined	47 (5.5)	2 (2.7)	45 (5.8)	1	–	0.421*
Undetermined	121 (14.1)	12 (16.2)	109 (13.9)	1	0.286	0.592
Stroke treatment, n (%)						
Thrombolysis	79 (9.2)	15 (20.3)	64 (8.2)	1	11.788	0.001
Antiplatelet therapy	600 (70.1)	48 (64.9)	552 (70.6)	1	1.056	0.304
Anticoagulation therapy	255 (29.8)	27 (36.5)	228 (29.2)	1	1.737	0.188
Use of statins	708 (82.7)	55 (74.3)	653 (83.5)	1	3.983	0.046
Duration from stroke onset to admission [h], M ±SD	18.98 ±7.95	19.49 ±7.64	18.93 ±7.98	854	0.600	0.556

M ±SD – mean ± standard deviation; df – degrees of freedom; BMI – body mass index; TOAST – Trial of ORG 101072 in Acute Stroke Treatment; * Fisher's exact test.

change neuronal plasticity through several transcriptionally mediated effects, which have the potential for aberrant and epileptogenic circuits.[24–26] Vezzani et al. reported that IL-1β had proconvulsive effects on limbic seizures in mice induced by electrical stimulation, bicuculine and kainic acid.[27] Šutulović et al. showed that chronic pelvic pain syndrome/chronic prostatitis (CPPS/CP) induced with experimental λ-carrageenan can lead to an increased susceptibility of rats to lindane-induced seizures through the upregulation of IL-6 and IL-1β levels in the thalamus and cerebral cortex.[28]

The mechanisms associated with the proconvulsive effects of IL-1β remain unexplained. Several potential mechanisms refer to IL-1β reducing the seizure threshold through the induction of an intracellular Ca2$^+$ ion surge and resultant modifications on voltage-dependent

ion channels[29]; IL-1β stimulating the production of NO in the brain[30]; IL-1β inducing neuronal hyperexcitability through the activation of the N-methyl-D-aspartate receptor (NMDA-R) and stimulating the chronic release of excitatory neurotransmitters[31]; and IL-1β inhibiting K$^+$ efflux, the recycling of gamma-aminobutyric acid (GABA) receptors, and the uptake of excitatory neurotransmitters by the glial population.[30,32] According to our results, the levels of IL-1β in ischemic stroke patients with post-stroke seizures were significantly higher than in those without post-stroke seizures.

The expression of cytokines can be regulated by polymorphisms within the promoter regions of their genes. Therefore, these promoter polymorphisms can influence the disease susceptibility by mediating the extent of the secretory response of these cytokines.[33,34] The IL-1

Table 2. Results of Hardy–Weinberg equilibrium (HWE) testing in the case and control group

IL-1B polymorphisms		Allele frequency, n		Genotype frequency, n (%)			HWE testing		
							df	χ²	p-value
	–	T	C	TT	TC	CC		–	
rs16944	case group (n = 74)	83	65	23 (31.1)	37 (50.0)	14 (18.9)	2	1.216	0.253
	control group (n = 782)	675	889	165 (21.1)	345 (44.1)	272 (34.8)	2	0.937	0.328
	–	G	C	GG	GC	CC		–	
rs1143623	case group (n = 74)	60	88	12 (16.2)	36 (48.6)	26 (35.1)	2	2.286	0.131
	control group (n = 782)	601	963	113 (14.4)	375 (48.0)	294 (37.6)	2	1.023	0.305
	–	C	T	CC	CT	TT		–	
rs114363	case group (n = 74)	142	6	68 (91.9)	6 (8.1)	0 (0)	2	–	0.547*
	control group (n = 782)	1516	48	734 (93.9)	48 (6.1)	0 (0)	2	–	0.498*
	–	T	C	TT	TC	CC		–	
rs10490571	case group (n = 74)	35	113	5 (6.8)	25 (33.8)	44 (59.5)	2	1.956	0.170
	control group (n = 782)	241	1323	23 (2.9)	195 (24.9)	564 (72.1)	2	1.542	0.203
	–	A	G	AA	AG	GG		–	
rs2853550	case group (n = 74)	16	132	2 (2.7)	12 (16.2)	60 (81.1)	2	–	0.618*
	control group (n = 782)	151	1413	24 (3.1)	103 (13.2)	655 (83.8)	2	0.172	0.674

df – degrees of freedom; * Fisher's exact test.

Table 3. Results of the multivariate analysis of the differences between the case and control group

Variables	Regression coefficient	Standard error	Wald	OR	95% CI	p-value
rs16944	–	–	7.265	–	–	0.029
CC	–	–	–	–	–	Ref = 1
TC	0.512	0.203	6.017	1.469	1.130–2.974	0.038
TT	0.654	0.231	8.786	1.923	1.257–4.185	0.012
rs10490571	–	–	2.685	–	–	0.153
CC	–	–	–	–	–	Ref = 1
TC	0.376	0.128	2.154	1.293	0.714–2.039	0.186
TT	0.395	0.141	2.978	1.327	0.748–2.191	0.132
Cortical involvement	0.428	0.159	5.982	1.354	1.105–2.893	0.041
Stroke laterality	0.297	0.106	1.839	1.277	0.693–2.012	0.214
NIHSS at admission	0.293	0.102	6.326	1.192	1.058–1.705	0.034
Thrombolysis	0.314	0.125	1.548	1.214	0.549–1.692	0.263
Use of statins	0.258	0.116	1.095	1.189	0.457–1.658	0.327

OR – odds ratio; 95% CI – 95% confidence interval; NIHSS – National Institutes of Health Stroke Scale.

Table 4. Post hoc results of the analysis of the interleukin (IL)-1β levels [pg/mL]

(I) Genotypes	(J) Genotypes	Mean difference (I–J)	Standard error	p-value	95% CI	
					lower bound	upper bound
TT	TC	2.03	0.57	0.011	0.91	3.15
	CC	4.32	0.78	0.002	2.79	5.85
TC	TT	−2.03	0.57	0.011	−3.15	−0.91
	CC	2.29	0.64	0.005	1.04	3.54
CC	TT	−4.32	0.78	0.002	−5.85	−2.79
	TC	−2.29	0.64	0.005	−3.54	−1.04

95% CI – 95% confidence interval.
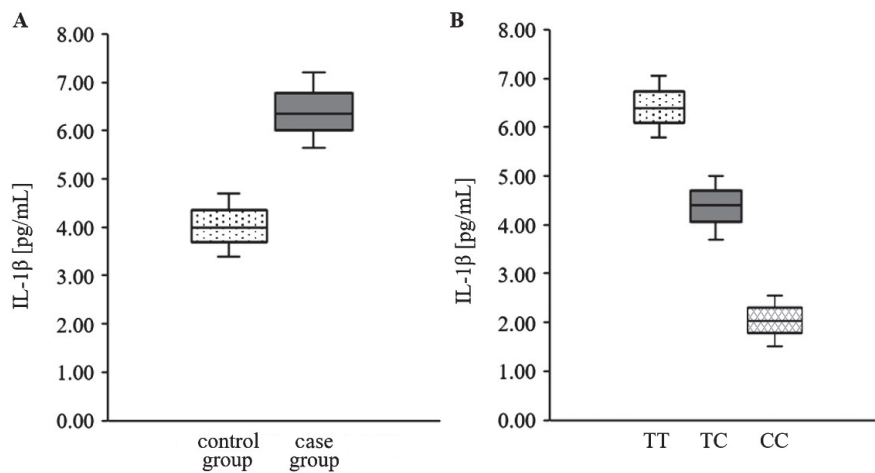
Fig. 1. Interleukin (IL)-1β levels in the case group and control group (A), and in different genotypes (B)

p = 0.008 for the control group compared to the case group; p = 0.011 for TT compared to TC; p = 0.002 for TT compared to CC; p = 0.005 for TC compared to CC.

gene cluster contains *IL-1B*, *IL-1A* and *IL-1RN* which are located on chromosome 2q. The *IL-1B*, encoding IL-1β, is demonstrated to be 7020 base pairs in length and contains numerous polymorphisms. Several SNPs within the promoter region of *IL-1B* have been researched in various infectious and inflammatory diseases.[35] Among them, the *IL-1B* polymorphism rs16944 has been correlated with IL-1β levels among rheumatoid arthritis patients in north India and hence affects disease susceptibility in which the T allele is directly associated with a higher IL-1β expression.[36] The CT genotype of *IL1B* rs16944 has also been shown to be associated with febrile seizure through the upregulation of postictal IL-1β levels in Korean children.[10] The AA genotype of *IL-1B* rs2853550 has been demonstrated to be correlated with a higher level of plasma IL-1β and, thus, an increased risk of ankylosing spondylitis.[37] In addition, the polymorphisms of rs10490571 (T/C) and rs1143623 (G/C) can also affect IL-1β levels in which the TC genotype of rs10490571 and the G allele of rs1143623 are associated with a higher level of IL-1β.[37,38] Therefore, multiple SNPs were included in our study.

According to the multivariate analysis, the *IL-1B* polymorphism rs16944 had an independent association with seizure susceptibility in ischemic stroke patients after adjusting for confounders. The TT and TC genotypes significantly increased the risk of post-stroke seizures compared to CC. We further compared IL-1β levels among different genotypes. The results showed that higher IL-1β levels were noted in TT compared to the TC genotype compared to the CC genotype. Therefore, the mechanism of the polymorphism of *IL-1B* rs16944 in affecting seizure susceptibility in ischemic stroke patients might be associated with the regulation of IL-1β levels.

Limitations

There were 2 main limitations to this study. The first was the small sample size, especially for the case group. Second, the study did not include all the SNPs associated with the expression of IL-1β.

Conclusions

The *IL-1B* polymorphism rs16944 had an independent association with seizure susceptibility in ischemic stroke patients. The mechanism for this might be associated with the regulation of IL-1β levels.

ORCID iDs

Xiaojun Ma   https://orcid.org/0000-0003-4158-4877
Liangwei Sun   https://orcid.org/0000-0003-4158-4877
Xiaoli Li   https://orcid.org/0000-0003-1484-176X
Yanlu Xu   https://orcid.org/0000-0002-0710-5484
Qingyan Zhang   https://orcid.org/0000-0003-0869-5903

References

1. Katan M, Luft A. Global burden of stroke. *Semin Neurol*. 2018;38(2):208–211. doi:10.1055/s-0038-1649503
2. Wang W, Jiang B, Sun H, et al. Prevalence, incidence, and mortality of stroke in China: Results from a nationwide population-based survey of 480 687 adults. *Circulation*. 2017;135(8):759–771. doi:10.1161/CIRCULATIONAHA.116.025250
3. Galovic M, Ferreira-Atuesta C, Abraira L, et al. Seizures and epilepsy after stroke: Epidemiology, biomarkers and management. *Drugs Aging*. 2021;38(4):285–299. doi:10.1007/s40266-021-00837-7
4. Zöllner JP, Schmitt FC, Rosenow F, et al. Seizures and epilepsy in patients with ischaemic stroke. *Neurol Res Pract*. 2021;3(1):63. doi:10.1186/s42466-021-00161-w
5. Balami JS, Chen RL, Grunwald IQ, Buchan AM. Neurological complications of acute ischaemic stroke. *Lancet Neurol*. 2011;10(4):357–371. doi:10.1016/S1474-4422(10)70313-6
6. Kwan J. Stroke: Predicting the risk of poststroke epilepsy: Why and how? *Nat Rev Neurol*. 2010;6(10):532–533. doi:10.1038/nrneurol.2010.140
7. Shen L, Yang J, Tang Y. Predictive values of the SeLECT score and IL-1β for post-stroke epilepsy. *Neuropsychiatr Dis Treat*. 2021;17:2465–2472. doi:10.2147/NDT.S324271
8. Clausen BH, Wirenfeldt M, Høgedal SS, et al. Characterization of the TNF and IL-1 systems in human brain and blood after ischemic stroke. *Acta Neuropathol Commun*. 2020;8(1):81. doi:10.1186/s40478-020-00957-y
9. Zhang Q, Li G, Zhao D, Yang P, Shabier T, Tuerxun T. Association between IL-1β and recurrence after the first epileptic seizure in ischemic stroke patients. *Sci Rep*. 2020;10(1):13505. doi:10.1038/s41598-020-70560-7
10. Choi J, Choi SA, Kim SY, et al. Association analysis of interleukin-1β, interleukin-6, and HMGB1 variants with postictal serum cytokine levels in children with febrile seizure and generalized epilepsy with febrile seizure plus. *J Clin Neurol*. 2019;15(4):555–563. doi:10.3988/jcn.2019.15.4.555

11. Doria JW, Forgacs PB. Incidence, implications, and management of seizures following ischemic and hemorrhagic stroke. *Curr Neurol Neurosci Rep*. 2019;19(7):37. doi:10.1007/s11910-019-0957-4

12. Altman K, Shavit-Stein E, Maggio N. Post stroke seizures and epilepsy: From proteases to maladaptive plasticity. *Front Cell Neurosci*. 2019;13:397. doi:10.3389/fncel.2019.00397

13. Wang JZ, Vyas MV, Saposnik G, Burneo JG. Incidence and management of seizures after ischemic stroke: Systematic review and meta-analysis. *Neurology*. 2017;89(12):1220–1228. doi:10.1212/WNL.0000000000004407

14. Chohan S, Venkatesh P, How C. Long-term complications of stroke and secondary prevention: An overview for primary care physicians. *Singapore Med J*. 2019;60(12):616–620. doi:10.11622/smedj.2019158

15. Castro-Apolo R, Huang JF, Vinan-Vega M, Tatum WO. Outcome and predictive factors in post-stroke seizures: A retrospective case-control study. *Seizure*. 2018;62:11–16. doi:10.1016/j.seizure.2018.09.007

16. Lambertsen KL, Finsen B, Clausen BH. Post-stroke inflammation: Target or tool for therapy? *Acta Neuropathol*. 2019;137(5):693–714. doi:10.1007/s00401-018-1930-z

17. Lambertsen KL, Biber K, Finsen B. Inflammatory cytokines in experimental and human stroke. *J Cereb Blood Flow Metab*. 2012;32(9):1677–1698. doi:10.1038/jcbfm.2012.88

18. Sharma R, Leung WL, Zamani A, O'Brien TJ, Casillas Espinosa PM, Semple BD. Neuroinflammation in post-traumatic epilepsy: Pathophysiology and tractable therapeutic targets. *Brain Sci*. 2019;9(11):318. doi:10.3390/brainsci9110318

19. Wu XF, Li C, Yang G, et al. Scorpion venom heat-resistant peptide attenuates microglia activation and neuroinflammation. *Front Pharmacol*. 2021;12:704715. doi:10.3389/fphar.2021.704715

20. Viviani B, Bartesaghi S, Gardoni F, et al. Interleukin-1beta enhances NMDA receptor-mediated intracellular calcium increase through activation of the Src family of kinases. *J Neurosci*. 2003;23(25):8692–8700. doi:10.1523/JNEUROSCI.23-25-08692.2003

21. Spulber S, Bartfai T, Schultzberg M. IL-1/IL-1ra balance in the brain revisited: Evidence from transgenic mouse models. *Brain Behav Immun*. 2009;23(5):573–579. doi:10.1016/j.bbi.2009.02.015

22. Iori V, Frigerio F, Vezzani A. Modulation of neuronal excitability by immune mediators in epilepsy. *Curr Opin Pharmacol*. 2016;26:118–123. doi:10.1016/j.coph.2015.11.002

23. Song B, Lee SJ, Kim CH. Roles of cytokines in the temporal changes of microglial membrane currents and neuronal excitability and synaptic efficacy in ATP-induced cortical injury model. *Int J Mol Sci*. 2021;22(13):6853. doi:10.3390/ijms22136853

24. Pugazhenthi S, Zhang Y, Bouchard R, Mahaffey G. Induction of an inflammatory loop by interleukin-1β and tumor necrosis factor-α involves NF-kB and STAT-1 in differentiated human neuroprogenitor cells. *PLoS One*. 2013;8(7):e69585. doi:10.1371/journal.pone.0069585

25. del Rey A, Balschun D, Wetzel W, Randolf A, Besedovsky HO. A cytokine network involving brain-borne IL-1β, IL-1ra, IL-18, IL-6, and TNFα operates during long-term potentiation and learning. *Brain Behav Immun*. 2013;33:15–23. doi:10.1016/j.bbi.2013.05.011

26. Yin P, Li Z, Wang YY, et al. Neonatal immune challenge exacerbates seizure-induced hippocampus-dependent memory impairment in adult rats. *Epilepsy Behav*. 2013;27(1):9–17. doi:10.1016/j.yebeh.2012.12.015

27. Vezzani A, Moneta D, Richichi C, et al. Functional role of inflammatory cytokines and antiinflammatory molecules in seizures and epileptogenesis. *Epilepsia*. 2002;43(Suppl 5):30–35. doi:10.1046/j.1528-1157.43.s.5.14.x

28. Šutulović N, Grubač Ž, Šuvakov S, et al. Chronic prostatitis/chronic pelvic pain syndrome increases susceptibility to seizures in rats and alters brain levels of IL-1β and IL-6. *Epilepsy Res*. 2019;153:19–27. doi:10.1016/j.eplepsyres.2019.03.014

29. Xu D, Miller SD, Koh S. Immune mechanisms in epileptogenesis. *Front Cell Neurosci*. 2013;7:195. doi:10.3389/fncel.2013.00195

30. Meini A, Benocci A, Frosini M, et al. Nitric oxide modulation of interleukin-1[beta]-evoked intracellular Ca^{2+} release in human astrocytoma U-373 MG cells and brain striatal slices. *J Neurosci*. 2000;20(24):8980–8986. doi:10.1523/JNEUROSCI.20-24-08980.2000

31. Zhu G, Okada M, Yoshida S, et al. Effects of interleukin-1β on hippocampal glutamate and GABA releases associated with Ca^{2+}-induced Ca^{2+} releasing systems. *Epilepsy Res*. 2006;71(2–3):107–116. doi:10.1016/j.eplepsyres.2006.05.017

32. Hu S, Sheng WS, Ehrlich LC, Peterson PK, Chao CC. Cytokine effects on glutamate uptake by human astrocytes. *Neuroimmunomodulation*. 2000;7(3):153–159. doi:10.1159/000026433

33. Urazova OI, Churina EG, Hasanova RR, Novitskiy VV, Poletika VS. Association between polymorphisms of cytokine genes and secretion of IL-12p70, IL-18, and IL-27 by dendritic cells in patients with pulmonary tuberculosis. *Tuberculosis (Edinb)*. 2019;115:56–62. doi:10.1016/j.tube.2019.02.003

34. Singh M, Mastana S, Singh S, Juneja PK, Kaur T, Singh P. Promoter polymorphisms in IL-6 gene influence pro-inflammatory cytokines for the risk of osteoarthritis. *Cytokine*. 2020;127:154985. doi:10.1016/j.cyto.2020.154985

35. Dinarello CA. Immunological and inflammatory functions of the interleukin-1 family. *Annu Rev Immunol*. 2009;27(1):519–550. doi:10.1146/annurev.immunol.021908.132612

36. Jahid M, Rehan-Ul-Haq, Chawla D, Avasthi R, Ahmed RS. Association of polymorphic variants in *IL1B* gene with secretion of IL-1β protein and inflammatory markers in North Indian rheumatoid arthritis patients. *Gene*. 2018;641:63–67. doi:10.1016/j.gene.2017.10.051

37. Liu W, Yang Z, Yan T, Zhang H, Liu R. Associations of the IL-1B level, IL-1A and IL-1B gene polymorphisms and ankylosing spondylitis risk in a Chinese Han population. *Cytokine*. 2020;126:154918. doi:10.1016/j.cyto.2019.154918

38. Wang J, Shi Y, Wang G, Dong S, Yang D, Zuo X. The association between interleukin-1 polymorphisms and their protein expression in Chinese Han patients with breast cancer. *Mol Genet Genomic Med*. 2019;7(8):e804. doi:10.1002/mgg3.804

High red blood cell distribution width is associated with the mortality of critically ill cancer patients: A propensity-matching study

*Jiahao Zhou[1,A,D], *Linya Feng[1,B], Yan Zhang[1,E], Shuangshuang Huang[2,C], Hao Jiang[3,C], Weijian Wang[1,F]

[1] Department of Anesthesiology, The First Affiliated Hospital of Wenzhou Medical University, China

[2] Yueqing Affiliated Hospital of Wenzhou Medical University, China

[3] Department of Ultrasonography, The First Affiliated Hospital of Wenzhou Medical University, China

A – research concept and design; B – collection and/or assembly of data; C – data analysis and interpretation;
D – writing the article; E – critical revision of the article; F – final approval of the article

Address for correspondence
Weijian Wang
E-mail: wangwj2002@hotmail.com

Conflict of interest
None declared

* Jiahao Zhou and Linya Feng contributed equally to this work.

Abstract

Background. The red blood cell distribution width (RDW) is related to the mortality of patients with malignant tumors, but the relationship between RDW and the prognosis of cancer patients in the intensive care unit (ICU) has not been fully clarified.

Objectives. To investigate the role of RDW in predicting the prognosis of critically ill cancer patients.

Materials and methods. A propensity score matching (PSM) study was conducted using data from adult patients with cancer, admitted to the ICU from the Intensive Care Medical Information Market IV (MIMIC-IV, v. 1.4) database. The correlation between RDW and ICU all-cause mortality was evaluated using a logistic regression model; stratification factors were considered. Additionally, a receiver operating characteristic (ROC) curve analysis was performed to compare the prognostic values of various blood biomarkers.

Results. Overall, 4836 cancer patients were included. The optimal critical RDW value was 15%. The RDW levels were independently correlated with ICU mortality in critically ill cancer patients, with odds ratios (ORs) of 1.56 (1.12–2.18) in the original cohort, 1.64 (1.27–2.12) in the imputation cohort, 1.65 (1.22–2.24) in the matched cohort, and 1.55 (1.19–2.03) in the weighted cohort. The forecasted performance of RDW is better than other blood biomarkers with an area under the ROC curve (AUC) of 0.637 (0.591–0.683).

Conclusions. The RDW has a prognostic value in critically ill cancer patients and a high RDW is independently associated with high mortality.

Key words: cancer, intensive care unit, red blood cell distribution width

32

J. Zhou et al. RDW is a risk factor for critically cancer

Background

Due to high incidence and mortality rates,[1] cancer has become an inevitable burden worldwide. Recently, cancer-related mortality rates have declined due to the advances in the strength of treatments. However, because of cancer-related complications and the side effects of cancer treatments, the number of patients with cancer being admitted to the intensive care unit (ICU) is increasing.[2,3] Approximately 1 in 20 cancer patients are transferred to the ICU within 2 years of their cancer diagnosis.[4] Moreover, nearly 1 in 7 patients in the ICU have malignant tumors.[5] Notably, the mortality rate of cancer patients is 30–77%, and the mortality rate for cancer patients requiring mechanical ventilation in the ICU exceeds 45%.[6]

Although the ICU provides life support and organ protection, it creates a heavy cost burden for treatment. Therefore, studies aimed at identifying effective prognostic indicators to identify a reasonable expectation of survival after treatment are urgently needed.[7]

Red blood cell distribution width (RDW) is a reflection of the volume dispersion of red blood cells, typically expressed as the coefficient of variation in red blood cell volumes. Recently, RDW was reported to be an independent predictor of mortality in cardiovascular disease (CVD)[8] and various types of cancer.[9–12] Additionally, RDW is independently related to mortality in critically ill patients admitted to the ICU due to various etiologies.[13–15] Although the mechanism between the association of RDW and mortality has not been elucidated, it may be involved in oxidative stress and inflammation.[16] However, the relationship between RDW and the prognosis of cancer patients admitted to the ICU is unclear. Therefore, studies evaluating the correlation between RDW and the prognosis of critically ill cancer patients may help in predicting their survival and optimizing the clinical management of these patients. We hypothesized that RDW can predict ICU mortality in critically ill cancer patients.

Objectives

To investigate the role of RDW in predicting the prognosis of critically ill cancer patients.

Materials and methods

Data source

The data were retrieved from the Intensive Care Medical Information Market IV MIMIC-IV v. 1.4,[17] a large, free, public, single-center database (https://mimic.mit.edu/). This database contains clinical information on 53,150 distinct patients admitted to the ICU at the Beth Israel Deaconess Medical Center in Boston, USA, from 2008 to 2019.

The data include demographic characteristics, vital signs, laboratory data, treatment, drug use, and survival information. To protect the patients' privacy, all identifiable patient information was removed. One of the investigators (LF) completed the collaborative institutional training program course required for ethical approval (record ID: 36309108).

Study cohort

Malignancies were identified using the International Classification of Diseases, version 9/10 (ICD-9/10): digestive system (140–159/C00–C26, C48), respiratory system and thoracic cancer (160–165/C30–C39), connective tissue (170–171, 176/C40–C41, C45–C46, C49), genitourinary system (179–189/C51–C68), nervous system (190–192/C47, C69–C72), hematological and lymphatic system (200–208/C81–C96), connective tissue (170–171, 176/C40–C41, C45–C46, C49), other (172–175, 193–195, 2090–2093/C43–C44, C50, C73–C76, C97), and metastatic (196–199, 2097/C77–C80).

The inclusion criteria (Fig. 1) included: 1) age ≥18 years and 2) duration of ICU stay ≥24 h. Patients with hematological tumors or those repeatedly admitted to the ICU were excluded.
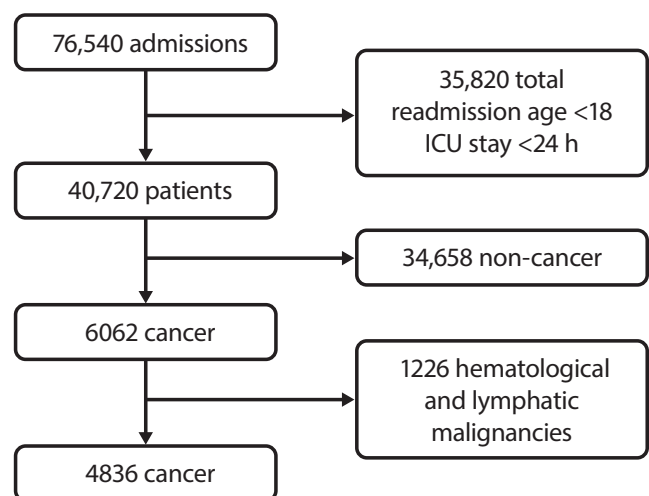
Fig. 1. Flowchart of the inclusion and exclusion of patients. In total, 4836 patients were selected

ICU – intensive care unit.

Data collection

Structured Query Language (SQL) in Navicat Premium (v. 12.0.18; PremiumSoft CyberTech Limited, Hong Kong, China) was applied to extract data from the MIMIC-IV within 24 h of ICU admission for a given patient. For laboratory measurements, the mean values ((maximum+minimum)/2) were selected. Data included demographic information (age, sex, race), type of care unit, type of cancer, comorbidities (congestive heart disease

(CHD), chronic kidney disease (CKD), anemia, atrial fibrillation (AFib), coronary atherosclerotic heart disease (CAD), stroke, chronic obstructive pulmonary disease (COPD), and liver disease), use of mechanical ventilation, vasopressors and continuous renal replacement therapy (CRRT), laboratory data (RDW, red blood cell count (RBC), white blood cell count (WBC), platelet count (PLT), hemoglobin (Hb), blood urea nitrogen (BUN), creatinine, glucose (GLU), neutrophil/lymphocyte ratio (NLR), monocyte/lymphocyte ratio (MLR), and platelet/lymphocyte ratio (PLR)), and scoring systems (sequential organ failure assessment (SOFA) and simplified acute physiology score II (SAPSII)).

The diagnosis of acute respiratory distress syndrome (ARDS), acute kidney injury (AKI) and sepsis was based on the Berlin Definition, Kidney Disease: Improving Global Outcome guidelines[18] and The Third International Consensus Definitions for Sepsis and Septic Shock (Sepsis-3),[19] respectively.

Outcomes

The primary outcome of this study was all-cause mortality in the ICU. The secondary outcome was the length of ICU stay.

Statistical analyses

The random forest model was used to impute missing values and missing data (Fig. 2). After imputation, the largest Youden's index of the receiver operating characteristic (ROC) curves were used to determine the best RDW cutoff value based on ICU mortality. Then, the imputation dataset was stratified by RDW into a high-RDW group and a low-RDW group.

Propensity score matching (PSM) and inverse probability treatment weighting (IPTW)[20] were applied to construct 2 models for controlling confounding factors. The patients were matched using the nearest neighbor algorithm of 1:1 according to propensity scores estimated using the following covariates: sex, age, race, care unit, type of cancer, comorbidities, use of ventilation, vasopressor, CRRT, ARDS, AKI, sepsis, SOFA, and SAPSII.

Baseline characteristics of all cohorts were reported. Continuous variables were represented by median (1st quartile (Q1), 3rd quartile (Q3)), while categorical variables were represented by frequency (percentage). The Kruskal–Wallis test was used to determine the statistical relevance of the study outcomes for continuous variables, while the Fisher's exact test or χ^2 test was used for categorical variables, as appropriate. The standardized mean difference (SMD), difference quotient between 2 means, and pooled standard deviation (SD) were also calculated to assess the balance between the high-RDW group and the low-RDW group.

A univariate logistic regression model was applied to determine the correlation between RDW and ICU mortality. Additionally, to assess the independent effects of RDW on ICU mortality, 2 multivariate logistic regression models were developed. In model I, we only adjusted for demographic information (age, sex and race). In model II, demographic information, type of cancer, comorbidities, use of mechanical ventilation, vasopressors, CRRT, acute diseases (ARDS, AKI and sepsis), and laboratory data (RBC, WBC, PLT, Hb, BUN, creatinine, and GLU) were included. Then, we conducted a sensitivity analysis on the original, imputed, PSM, and IPTW cohorts to evaluate the robustness of the results. The secondary outcome was evaluated by means of multivariate linear regression using model II.

All analyses and figures were carried out using the R v. 4.0.1 (packages: missForest, ggplot2, Matching, tableone, mice, and pROC; R Foundation for Statistical Computing, Vienna, Austria). A bilateral p-value <0.05 was considered statistically significant and a SMD < 0.1 was considered balanced.

Fig. 2. Pattern of missing data in variables of interest

RDW – red blood cell distribution width; RBC – red blood cell; Hb – hemoglobin; PLT – platelet count; WBC – white blood cell count; BUN – blood urea nitrogen; GLU – glucose; NLR – neutrophil–lymphocyte ratio; PLR – platelet–lymphocyte ratio; MLR – monocyte–lymphocyte ratio; SOFA – sequential organ failure assessment; SAPSII – simplified acute physiology score II.

Additional analyses

Stratified analysis was performed on the imputation cohort according to age, sex, race, type of cancer, comorbidities, and scoring system to evaluate the impact of RDW on ICU mortality among the different subgroups. The likelihood ratio test was used to estimate the effects between the stratified factors and RDW.

Finally, the ROC curves were drawn to compare the prognostic values of RDW, NLR, PLR, and MLR. Since the missing values for NLR, MLR and PLR were not imputed, the ROC curves were only drawn using the original dataset.

Results

Characteristics of subjects

We enrolled 4836 subjects who met the inclusion criteria. The baseline patient characteristics of the original cohort are shown in Table 1. The median age of all patients was 67.00 (59.00, 76.00) years, and the median RDW was 14.95% (13.75, 16.70). Among all the patients, malignant tumors of the digestive system were the most common (33.8%), followed by tumors of the respiratory system (22.3%), genitourinary system (16.2%), other tumor sites (6.8%), nervous system (5.9%), and connective tissues (2.0%). Metastatic tumors were present in 2560 (52.9%) patients. The prevalence of AKI and sepsis was 63.8% and 38.3% (3085 and 1851 patients), respectively. During the first 24 h following ICU admission, 1261 patients (26.1%) were placed on mechanical ventilation and 1314 patients (27.2%) required vasopressors. Patients were divided into high-RDW ($\geq$15%) and low-RDW (<15%)

groups consisting of 2483 and 2353 patients, respectively (Table 2). Patients with a high RDW were more likely to have digestive tumors (40.8% compared to 26.3%), distant metastases (60.0% compared to 45.5%), AKI (69.7% compared to 57.6%), and sepsis (46.6% compared to 29.5%), all with a SMD > 0.1. Additionally, patients in the high-RDW group had higher SOFA scores (4.00 (2.00, 6.00) compared to 2.00 (1.00, 4.00) in the low-RDW group) and higher SAPSII scores (40.00 (32.00, 48.00) compared to 34.00 (28.00, 41.00) in the low-RDW group), both with a SMD > 0.1.

Association between RDW and primary outcomes

After matching and weighting, the baseline characteristics of the 2 groups tended to be balanced (Fig. 3). The characteristics of the imputation, matched and weighted cohorts are shown in Table 2. The high-RDW group showed higher ICU mortality (13.9% compared to 5.4%) in comparison to the low-RDW group. In line with these results, the logistic regression analysis showed that high RDW levels were associated with ICU mortality in the IPTW cohort for the unadjusted cohort (1.56 (1.22–2.00), p < 0.001), model I (1.57 (1.23–2.01), p < 0.001) and model II (1.55 (1.19–2.03), p = 0.003) (Table 3). All variables in model II had variance inflation factors <10, which indicates an absence of multicollinearity. The Durbin–Watson test verified the independence of errors (value = 1.958). For evaluating the robustness of the results, a sensitivity analysis was conducted. The same trend was observed in the high-RDW group using model II in the origin cohort (1.56 (1.12–2.18), p = 0.002), imputation cohort (1.64 (1.27–2.12), p < 0.001) and PSM cohort (1.65 (1.22–2.24), p = 0.003) (Table 3).
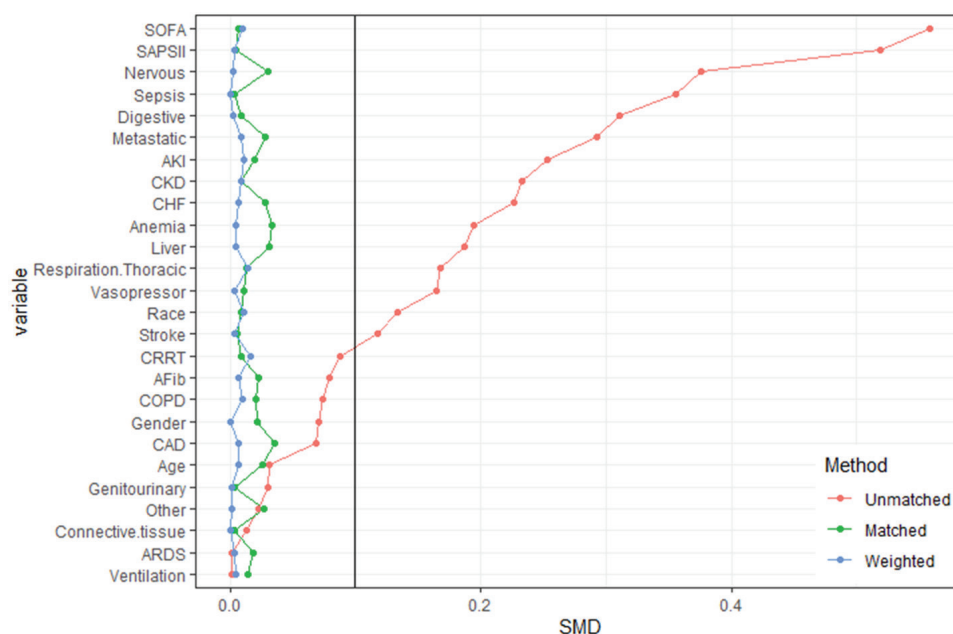
Fig. 3. Balancing the propensity score matching (PSM) model and the inverse probability treatment weighting (IPTW) model

SOFA – sequential organ failure assessment; SAPSII – simplified acute physiology score II; AKI – acute kidney injury; CKD – chronic kidney disease; CHF – congestive heart failure; CRRT – continuous renal replacement therapy; AFib – atrial fibrillation; COPD – chronic obstructive pulmonary disease; CAD – coronary atherosclerotic heart disease; ARDS – acute respiratory distress syndrome; SMD – standardized mean difference.

Table 1. Baseline characteristics of origin of the patient cohort

Variables	Overall	Low-RDW group	High-RDW group	p-value	Test value
Number of patients	4836	2346	2317	–	–
Gender, F (%)	2019 (41.7)	936 (39.9)	998 (43.1)	0.030	4.842[+]
Age	67.00 (59.00, 76.00)	67.00 (59.00, 75.00)	67.00 (59.00, 76.00)	0.209	1.580*
Race (%)					
Black	449 (9.3)	171 (7.3)	252 (10.9)	<0.001	18.185[+]
Other	937 (19.4)	465 (19.8)	441 (19.0)		
White	3450 (71.3)	1710 (72.9)	1624 (70.1)		
ICU mortality (%)	471 (9.7)	127 (5.4)	316 (13.6)	<0.001	–
ICU stay	8.30 (5.30, 13.70)	8.30 (5.50, 13.10)	8.40 (5.30, 14.60)	0.538	3.682*
Type of cancer					
Digestive (%)	1634 (33.8)	617 (26.3)	937 (40.4)	<0.001	104.895[+]
Respiration/thoracic (%)	1077 (22.3)	606 (25.8)	450 (19.4)	<0.001	27.338[+]
Connective tissue (%)	96 (2.0)	49 (2.1)	46 (2.0)	0.884	0.062[+]
Genitourinary (%)	784 (16.2)	393 (16.8)	366 (15.8)	0.399	0.781[+]
Nervous (%)	287 (5.9)	246 (10.5)	36 (1.6)	<0.001	163.687[+]
Other (%)	331 (6.8)	168 (7.2)	144 (6.2)	0.217	1.672[+]
Metastatic (%)	2560 (52.9)	1067 (45.5)	1381 (59.6)	<0.001	93.214[+]
Ventilation (%)	1261 (26.1)	613 (26.1)	623 (26.9)	0.580	0.344[+]
Vasopressor (%)	1314 (27.2)	551 (23.5)	724 (31.2)	<0.001	35.338[+]
CRRT (%)	32 (0.7)	7 (0.3)	22 (0.9)	0.008	7.996[+]
Comorbidities					
AFib (%)	1216 (25.1)	548 (23.4)	622 (26.8)	0.007	7.537[+]
Anemia (%)	945 (19.5)	365 (15.6)	519 (22.4)	<0.001	35.511[+]
CHF (%)	751 (15.5)	266 (11.3)	446 (19.2)	<0.001	56.383[+]
CKD (%)	722 (14.9)	251 (10.7)	434 (18.7)	<0.001	60.009[+]
COPD (%)	878 (18.2)	391 (16.7)	464 (20.0)	0.003	8.785[+]
CAD (%)	833 (17.2)	373 (15.9)	425 (18.3)	0.030	4.906[+]
Liver (%)	443 (9.2)	150 (6.4)	264 (11.4)	<0.001	36.025[+]
Stroke (%)	259 (5.4)	158 (6.7)	95 (4.1)	<0.001	15.770[+]
Sepsis (%)	1851 (38.3)	693 (29.5)	1081 (46.7)	<0.001	144.877[+]
AKI (%)	3085 (63.8)	1353 (57.7)	1619 (69.9)	<0.001	75.094[+]
ARDS (%)	207 (4.3)	101 (4.3)	97 (4.2)	0.898	0.040[+]
Laboratory data					
RDW	14.95 (13.75, 16.70)	13.75 (13.10, 14.35)	16.70 (15.75, 18.10)	<0.001	3496.617*
RBC	3.41 (3.01, 3.92)	3.64 (3.23, 4.12)	3.21 (2.84, 3.66)	<0.001	442.684*
Hb	10.30 (9.00, 11.90)	11.30 (9.90, 12.65)	9.55 (8.41, 10.75)	<0.001	777.953*
PLT	205.00 (141.50, 279.50)	215.00 (158.50, 279.50)	195.50 (128.25, 281.50)	<0.001	40.863*
WBC	10.70 (7.70, 14.46)	11.00 (8.25, 14.50)	10.47 (7.20, 14.60)	<0.001	12.288*
BUN	18.00 (13.00, 25.00)	17.00 (12.50, 22.50)	20.00 (14.00, 28.50)	<0.001	120.939*
Creatinine	0.85 (0.65, 1.20)	0.85 (0.65, 1.10)	0.90 (0.70, 1.30)	<0.001	47.724*
GLU	7.10 (6.10, 8.60)	7.30 (6.20, 8.70)	7.00 (5.90, 8.60)	<0.001	23.358*
NLR	10.00 (5.50, 17.50)	9.80 (5.32, 16.60)	10.40 (5.70, 18.30)	0.075	3.171*
PLR	237.60 (131.20, 399.50)	240.90 (129.40, 400.20)	242.20 (134.73, 403.22)	0.672	0.179*
MLR	0.60 (0.30, 0.90)	0.50 (0.30, 0.90)	0.60 (0.40, 0.90)	0.025	5.005*
SOFA	3.00 (1.00, 5.00)	2.00 (1.00, 4.00)	4.00 (2.00, 6.00)	<0.001	270.736*
SAPSII	36.00 (29.00, 44.00)	34.00 (27.00, 41.00)	39.00 (31.00, 47.00)	<0.001	243.699*

F – female; AFib – atrial fibrillation; CHF – congestive heart failure; CKD – chronic kidney disease; COPD – chronic obstructive pulmonary disease; CAD – coronary atherosclerotic heart disease; CRRT – continuous renal replacement therapy; ICU – intensive care unit; RDW – red blood cell distribution width; AKI – acute kidney injury; ARDS – acute respiratory distress syndrome; RBC – red blood cell count; Hb – hemoglobin; PLT – platelet count; WBC – white blood cell count; BUN – blood urea nitrogen; GLU – glucose; NLR – neutrophil–lymphocyte ratio; PLR – platelet–lymphocyte ratio; MLR – monocyte–lymphocyte ratio; SOFA – sequential organ failure assessment; SAPSII – simplified acute physiology score II. Continuous variables: median (1st quartile (Q1), 3rd quartile (Q3)). Categorical variables: frequency (percentage). * H value for Kruskal–Wallis test; [+] χ^2 value for χ^2 test.

Table 2. Baseline characteristic between unmatched, matched and weighted cohort

Variables	Imputation cohort			PSM cohort			IPTW cohort		
	low-RDW group	high-RDW group	SMD	low-RDW group	high-RDW group	SMD	low-RDW group	high-RDW group	SMD
N	2353	2483	–	1619	1619	–	4835	4851.3	–
Sex, F (%)	940 (39.9)	1079 (43.5)	0.071	662 (40.9)	679 (41.9)	0.021	1983.4 (41.0)	1991.4 (41.0)	0.001
Age	67.00 (58.00, 75.00)	67.00 (59.00, 76.00)	0.031	67.00 (59.00, 76.00)	67.00 (59.00, 76.00)	0.026	67.00 (59.00, 76.00)	67.00 (59.00, 76.00)	0.006
Race (%)									
Black	172 (7.3)	277 (11.2)	0.133	141 (8.7)	137 (8.5)	0.009	464.5 (9.6)	451.8 (9.3)	0.011
Other	468 (19.9)	469 (18.9)		306 (18.9)	306 (18.9)		932.2 (19.3)	931.7 (19.2)	
White	1713 (72.8)	1737 (70.0)		1172 (72.4)	1176 (72.6)		3438.4 (71.1)	3467.7 (71.5)	
ICU mortality (%)	127 (5.4)	344 (13.9)	0.29	102 (6.3)	162 (10.0)	0.136	367.7 (7.6)	553.3 (11.4)	0.13
ICU stay	2.30 (1.60, 4.00)	2.40 (1.70, 4.10)	0.013	2.30 (1.70, 4.00)	2.20 (1.60, 3.90)	0.081	2.40 (1.70, 4.20)	2.30 (1.60, 4.00)	0.041
Types of cancer									
Digestive (%)	620 (26.3)	1014 (40.8)	0.31	535 (33.0)	542 (33.5)	0.009	1622.4 (33.6)	1632.9 (33.7)	0.002
Respiration/thoracic (%)	608 (25.9)	469 (18.9)	0.167	386 (23.8)	377 (23.3)	0.013	1084.2 (22.4)	1116.7 (23.0)	0.014
Connective tissue (%)	49 (2.1)	47 (1.9)	0.014	39 (2.4)	38 (2.3)	0.004	97.4 (2.0)	98.2 (2.0)	0.001
Genitourinary (%)	395 (16.8)	389 (15.7)	0.029	275 (17.0)	273 (16.9)	0.003	784.2 (16.2)	784.0 (16.2)	0.002
Nervous (%)	246 (10.5)	41 (1.7)	0.376	49 (3.0)	41 (2.5)	0.03	287.5 (5.9)	290.8 (6.0)	0.002
Other (%)	168 (7.1)	163 (6.6)	0.023	102 (6.3)	113 (7.0)	0.027	306.7 (6.3)	306.4 (6.3)	0.001
Metastatic (%)	1071 (45.5)	1489 (60.0)	0.293	865 (53.4)	888 (54.8)	0.029	2554.0 (52.8)	2540.0 (52.4)	0.009
Ventilation (%)	613 (26.1)	648 (26.1)	0.001	425 (26.3)	415 (25.6)	0.014	1253.4 (25.9)	1266.9 (26.1)	0.004
Vasopressor (%)	551 (23.4)	763 (30.7)	0.165	417 (25.8)	409 (25.3)	0.011	1313.2 (27.2)	1310.7 (27.0)	0.003
CRRT (%)	7 (0.3)	25 (1.0)	0.088	7 (0.4)	8 (0.5)	0.009	38.7 (0.8)	32.2 (0.7)	0.016
Comorbidities									
AFib (%)	550 (23.4)	666 (26.8)	0.08	415 (25.6)	399 (24.6)	0.023	1212.3 (25.1)	1230.7 (25.4)	0.007
Anemia (%)	367 (15.6)	578 (23.3)	0.195	298 (18.4)	319 (19.7)	0.033	948.8 (19.6)	959.9 (19.8)	0.004
CHF (%)	267 (11.3)	484 (19.5)	0.227	252 (15.6)	236 (14.6)	0.028	757.8 (15.7)	771.5 (15.9)	0.006
CKD (%)	252 (10.7)	470 (18.9)	0.233	229 (14.1)	224 (13.8)	0.009	738.3 (15.3)	725.3 (15.0)	0.009
COPD (%)	393 (16.7)	485 (19.5)	0.074	322 (19.9)	309 (19.1)	0.02	922.8 (19.1)	907.6 (18.7)	0.01
CAD (%)	374 (15.9)	459 (18.5)	0.069	294 (18.2)	272 (16.8)	0.036	849.7 (17.6)	865.3 (17.8)	0.007
Liver (%)	151 (6.4)	292 (11.8)	0.187	137 (8.5)	123 (7.6)	0.032	437.8 (9.1)	445.3 (9.2)	0.004
Stroke (%)	158 (6.7)	101 (4.1)	0.117	82 (5.1)	80 (4.9)	0.006	261.0 (5.4)	258.3 (5.3)	0.003
Sepsis (%)	695 (29.5)	1156 (46.6)	0.356	583 (36.0)	586 (36.2)	0.004	1863.1 (38.5)	1867.3 (38.5)	0.001
AKI (%)	1355 (57.6)	1730 (69.7)	0.253	1033 (63.8)	1018 (62.9)	0.019	3068.6 (63.5)	3104.8 (64.0)	0.011
ARDS (%)	101 (4.3)	106 (4.3)	0.001	67 (4.1)	73 (4.5)	0.018	217.9 (4.5)	214.8 (4.4)	0.004
Laboratory data									
RDW	13.75 (13.10, 14.35)	16.70 (15.75, 18.03)	2.632	67.00 (59.00, 76.00)	67.00 (59.00, 76.00)	2.549	13.85 (13.20, 14.40)	16.50 (15.70, 17.85)	2.522
RBC	3.65 (3.23, 4.12)	3.20 (2.84, 3.66)	0.639	13.85 (13.20, 14.40)	16.45 (15.70, 17.80)	0.414	3.56 (3.13, 4.03)	3.25 (2.90, 3.73)	0.406
Hb	11.30 (9.90, 12.65)	9.50 (8.40, 10.70)	0.911	3.55 (3.14, 4.02)	3.26 (2.90, 3.72)	0.691	11.00 (9.70, 12.45)	9.65 (8.50, 10.90)	0.677
PLT	217.50 (160.00, 280.50)	197.00 (127.00, 281.25)	0.184	11.00 (9.70, 12.40)	9.60 (8.50, 10.85)	0.017	208.50 (148.50, 276.66)	205.00 (137.50, 285.28)	0.042
WBC	11.10 (8.30, 14.45)	10.50 (7.20, 14.30)	0.103	214.00 (150.00, 279.50)	211.50 (143.25, 291.75)	0.128	11.10 (8.15, 14.60)	10.35 (7.20, 14.10)	0.122
Creatinine	0.85 (0.65, 1.15)	1.00 (0.70, 1.43)	0.299	11.10 (8.05, 14.45)	10.30 (7.15, 13.92)	0.08	0.90 (0.70, 1.30)	0.90 (0.65, 1.30)	0.043
BUN	17.00 (12.50, 23.00)	21.50 (14.50, 31.99)	0.438	0.90 (0.70, 1.25)	0.85 (0.65, 1.20)	0.102	18.50 (13.00, 26.00)	20.00 (14.00, 28.50)	0.12

Table 2. Baseline characteristic between unmatched, matched, and weighted cohort – cont.

Variables	Imputation cohort			PSM cohort			IPTW cohort		
	low-RDW group	high-RDW group	SMD	low-RDW group	high-RDW group	SMD	low-RDW group	high-RDW group	SMD
GLU	7.40 (6.30, 8.60)	7.00 (5.90, 8.40)	0.14	18.00 (13.00, 25.00)	19.00 (13.50, 27.50)	0.17	7.40 (6.20, 8.70)	7.00 (6.00, 8.30)	0.169
Scores									
SOFA	2.00 (1.00, 4.00)	4.00 (2.00, 6.00)	0.559	3.00 (1.00, 4.00)	3.00 (1.00, 4.00)	0.007	3.00 (1.00, 5.00)	3.00 (1.00, 5.00)	0.01
SAPSII	34.00 (28.00, 41.00)	40.00 (32.00, 48.00)	0.519	36.00 (30.00, 43.00)	36.00 (30.00, 44.00)	0.005	37.00 (29.00, 45.00)	36.00 (29.00, 45.00)	0.004

F – female; AFib – atrial fibrillation; CHF – congestive heart failure; CKD – chronic kidney disease; COPD – chronic obstructive pulmonary disease; CAD – coronary atherosclerotic heart disease; CRRT – continuous renal replacement therapy; ICU – intensive care unit; RDW – red blood cell distribution width; AKI – acute kidney injury; ARDS – acute respiratory distress syndrome; RBC – red blood cell count; Hb – hemoglobin; PLT – platelet count; WBC – white blood cell count; BUN – blood urea nitrogen; GLU – glucose; SOFA – sequential organ failure assessment; SAPSII – simplified acute physiology score II; SMD – standardized mean difference; PSM – propensity score matching; IPTW – inverse probabilistic treatment weighting. Continuous variables: median (1st quartile (Q1), 3rd quartile (Q3)). Categorical variables: frequency (percentage).

Table 3. The primary outcome and sensitivity analysis. Odds ratio (OR; 95% confidence interval (95% CI)) of the ICU mortality in different models based on RDW grouping

Model		OR	95% CI	p-value
Origin	unadjusted	2.76	2.23–3.43	<0.001
	model I	2.65	2.14–3.30	<0.001
	model II	1.56	1.12–2.18	0.002
Imputation	unadjusted	2.82	2.29–3.50	<0.001
	model I	2.79	2.26–3.46	<0.001
	model II	1.64	1.27–2.12	<0.001
PSM	unadjusted	1.65	1.28–2.15	<0.001
	model I	1.66	1.29–2.16	<0.001
	model II	1.65	1.22–2.24	0.003
IPTW	unadjusted	1.56	1.22–2.00	<0.001
	model I	1.57	1.23–2.01	<0.001
	model II	1.55	1.19–2.03	0.003

Model I adjusted for: age, sex and race. Model II adjusted for: age, sex, race, types of cancer, intervention, ARDS, AKI, sepsis, comorbidities, laboratory parameters (RBC, Hb, PLT, WBC, BUN, creatinine, GLU), SOFA, and SAPSII. AKI – acute kidney injury; ARDS – acute respiratory distress syndrome; RBC – red blood cell count; Hb – hemoglobin; PLT – platelet count; WBC – white blood cell count; BUN – blood urea nitrogen; GLU – glucose; SOFA – sequential organ failure assessment; SAPSII – simplified acute physiology score II; RDW – red blood cell distribution width; ICU – intensive care unit; PSM – propensity score matching; IPTW – inverse probability treatment weighting.

Association between RDW and secondary outcomes

There was no difference in the duration of ICU stays between the high-RDW group and the low-RDW group (2.40 (1.70, 4.10) compared to 2.30 (1.60, 4.00), with a SMD < 0.1). As shown in Table 4, the RDW had no effect on the length of ICU stay for the origin cohort ($R^2 = 0.15$, p = 0.270), imputation cohort ($R^2 = 0.14$, p = 0.140) and PSM cohort ($R^2 = 0.16$, p = 0.050).

Additional analyses

The results of subgroup analysis for the imputation cohort are shown in Fig. 2. Interactions were observed only in subgroups with respect to age (p = 0.014), respiratory and thoracic tumors (p = 0.028), AFib (p = 0.021), CHF (p = 0.026), and no differences were found in associations between RDW and the primary outcomes in the remaining subgroups. In patients with connective tissue tumors, RDW was not related to outcomes. RDW has higher predictive significance in patients with higher SOFA scores, which was the opposite for SAPSII. Additionally, patients with liver disease showed a significantly higher RDW-associated ICU risk of death (3.85 (1.8–9.53)). A high RDW was also associated with prognosis in both men and women. Notably, the relationship between a high RDW and mortality was weaker in older adults (age ≥60 years).

In the 1347 patients without any missing values for RDW, NLR, PLR, and MLR, we calculated the areas under the ROC curve (AUCs) to compare the predictive value of RDW, NLR, PLR, and MLR on ICU mortality (Fig. 4).

Table 4. The secondary outcome evaluated using multivariate linear regression

Model	β	Standard deviation	Adjusted β	Adjusted R²	p-value
Origin cohort	−0.16	0.15	−0.02	0.15	0.270
Imputation cohort	−0.20	0.13	−0.02	0.14	0.140
PSM cohort	−0.28	0.14	−0.03	0.16	0.050

Adjusted for: age, sex, race, types of cancer, intervention, ARDS, AKI, sepsis, comorbidities, laboratory parameters (RBC, Hb, PLT, WBC, BUN, creatinine, GLU), SOFA, andSAPSII. AKI – acute kidney injury; ARDS – acute respiratory distress syndrome; RBC – red blood cell count; Hb – hemoglobin; PLT – platelet count; WBC – white blood cell count; BUN – blood urea nitrogen; GLU – glucose; SOFA – sequential organ failure assessment; SAPSII – simplified acute physiology score II; PSM – propensity score matching.
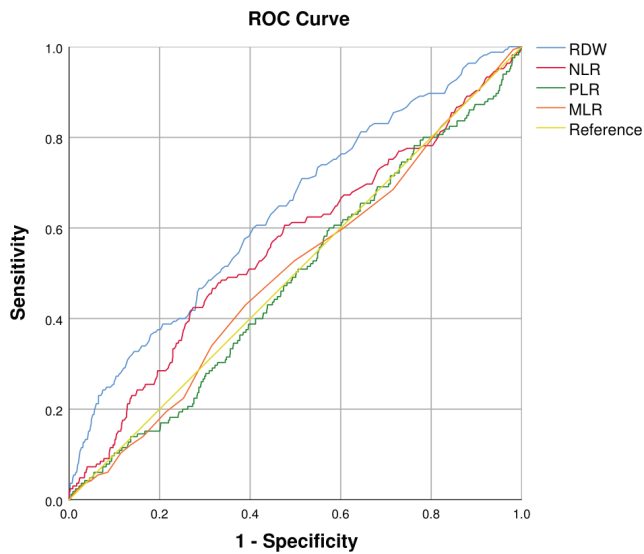
Fig. 4. Receiver operating characteristic (ROC) curve for red blood cell distribution width (RDW), neutrophil/lymphocyte ratio (NLR), platelet/lymphocyte ratio (PLR), monocyte/lymphocyte ratio (MLR), and simplified acute physiology score II (SAPSII) based on the intensive care unit (ICU) mortality

The AUC for RDW, NLR, PLR, and MLR in the context of ICU mortality in critically ill cancer patients were 0.637 (0.591–0.683), p < 0.001; 0.559 (0.510–0.608), p = 0.014; 0.485 (0.438–0.532), p = 0.530; and 0.501 (0.454–0.547), p = 0.982, respectively. The ROC analysis suggested that RDW is superior to NLR, PLR and MLR for predicting the prognosis of critically ill cancer patients.

Discussion

Our results suggest that a higher RDW is related to an increased risk of death in cancer patients admitted to the ICU. However, considering that the effects of blood cell parameters were evaluated, cases involving hematological and lymphatic malignancies were excluded from the final cohort. Importantly, similar trends were observed in the 2 models adjusted for different variables. This suggests that RDW is an independent predictor of the prognosis in critically ill cancer patients. The mean lifespan of a red blood cell is 120 days, and its homeostasis can be affected by many chronic diseases. To exclude bias introduced by chronic

diseases, we conducted subgroup analyses in patients with common comorbidities. A forest plot indicated that there were interactions between AFib and CHF and RDW. This can be explained by the fact that risk factors related to the incidence of AFib and CHF are also the factors associated with increased RDW values, such as endothelial dysfunction, genetic susceptibility, aging, and others.[21,22]

Many studies have confirmed RDW to have prognostic value in various cancers such as gastric,[10] ovarian[11] and lung cancer.[12] For established cancers, there is growing evidence showing that local immune responses and systemic inflammation play a role in tumor progression and the overall survival (OS) rate in patients with cancer.[23] The RDW is also a laboratory indicator for many chronic diseases and thus can be regarded as a nonspecific but outcome-related chronic disease marker.[24] Cancer is often associated with chronic consumption and cachexia.[25]

Besides, plenty of studies have shown RDW to be a good prognostic predictor in ICU patients on account of acute overall inflammation,[26–28] oxidative stress[29] and arterial underfilling.[30] The RDW is a risk factor for a severe prognosis in diseases such as sepsis,[31] acute heart failure,[32] autoimmune diseases, and liver diseases.[33] However, during subgroup analysis, bias caused by comorbidities and acute ICU diseases (sepsis, AKI and ARDS) was not detected.

The exact biological mechanisms between RDW and cancer in ICU patients remain unclear. The underlying mechanism based on the available literature is that an altered myeloid lineage, abnormal iron metabolism and diminished response to erythropoietin[34,35] occurs in the setting of chronic and acute systemic inflammation, leading to reduced erythrocyte survival and an increased entry of premature erythrocytes into the circulation.[36] Therefore, the lower survival in patients with a high RDW might be secondary to inflammation itself. Given the increasing number of cancer patients admitted to the ICU,[2–3] these patients might to some extent be considered as a separate subtype of ICU patients. Additionally, the exact indications for the use of RDW in such a background are unclear, although a high RDW was a risk factor in the vast majority of subgroups (Fig. 5). All in all, the potential mechanisms and indications for the application of RDW in critically ill cancer patients need further exploration.

In addition to RDW, several prognostic parameters based on systemic inflammation have been proposed in cancer

Subgroup	No. of patients	No. of Low-RDW	No. of High-RDW		OR	P for interaction
Overall	4836	2353	2483		1.64 (1.27–2.12)	
Gender						0.526
F	2019	940	1079		2.6 (1.91–3.58)	
M	2817	1413	1404		2.98 (2.25–4.01)	
Age						**0.014**
<60	1353	662	691		3.66 (2.37–5.85)	
≥60	3483	1691	1792		2.6 (2.05–3.32)	
Race						0.854
Black	449	172	277		3.15 (1.55–7.07)	
Other	937	468	469		2.87 (1.86–4.53)	
White	3450	1713	1737		2.76 (2.15–3.58)	
Types of cancer						
Digestive	1634	620	1014		3.14 (2.09–4.87)	0.648
Respiration/Thoracic	1077	608	469		2.08 (1.44–3.02)	**0.028**
Connective tissue	96	49	47		2.8 (0.57–20.26)	0.993
Genitourinary	784	395	389		2.03 (1.17–3.62)	0.222
Nervous	287	246	41		11.25 (2.65–56.76)	0.052
Other	331	168	163		4.82 (1.91–14.74)	0.278
Metastatic	2560	1071	1489		2.28 (1.76–2.98)	0.098
Ventilation						0.238
No	3575	1740	1835		3.18 (2.41–4.24)	
Yes	1261	613	648		2.45 (1.77–3.42)	
Vasopressor						0.563
No	3522	1802	1720		2.79 (2.07–3.8)	
Yes	1314	551	763		2.45 (1.82–3.35)	
Comorbidities						
AFib	1216	550	666		1.91 (1.32–2.82)	**0.021**
Anemia	945	367	578		2.42 (1.49–4.09)	0.500
CHF	751	267	484		1.64 (1–2.78)	**0.026**
CKD	722	252	470		2.2 (1.27–4.03)	0.361
COPD	878	393	485		1.9 (1.23–2.99)	0.054
CAD	833	374	459		2.92 (1.72–5.17)	0.903
Liver	443	151	292		3.85 (1.8–9.53)	0.430
Stroke	259	158	101		2.15 (0.94–5.05)	0.505
Sepsis	1851	695	1156		2.05 (1.56–2.71)	0.145
AKI	3085	1355	1730		2.35 (1.88–2.95)	0.172
ARDS	207	101	106		2.81 (1.31–6.46)	0.987
SOFA						0.551
0–3	2848	1659	1189		1.74 (1.15–2.66)	
≥4	1988	694	1294		2.18 (1.67–2.89)	
SAPSII						0.378
<44	3435	1911	1524		2.07 (1.5–2.88)	
≥44	1401	442	959		1.99 (1.48–2.71)	

Fig. 5. Forest plot of subgroup analysis for the intensive care unit (ICU) mortality. Odds ratios (ORs) and 95% confidence intervals (95% CIs) were acquired using a univariate logistic regression model. The OR of a low-red blood cell distribution width (RDW) group amounted to 1 for the reference value. In the 33 subgroups, the scores were grouped according to the best cutoff value obtained with the largest Youden's index based on ICU mortality

F – female; M – male; AFib – atrial fibrillation; CHF – congestive heart failure; CKD – chronic kidney disease; COPD – chronic obstructive pulmonary disease; CAD – coronary atherosclerotic heart disease; AKI – acute kidney injury; ARDS – acute respiratory distress syndrome; SOFA – sequential organ failure assessment; SAPSII – simplified acute physiology score II.

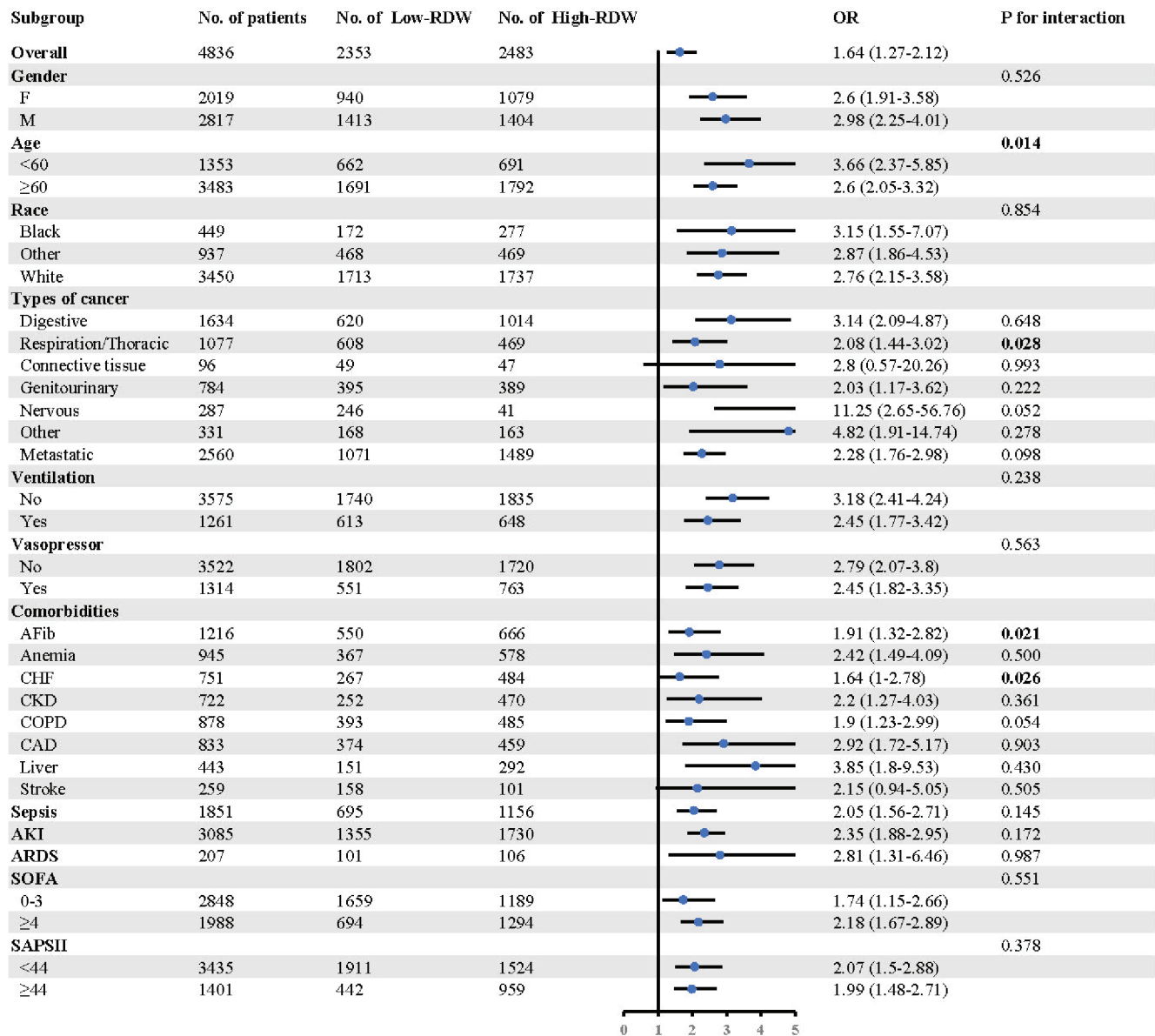patients, including NLR,[37] PLR[38] and MLR.[39] In this study, the performance of RDW was compared to these biochemical indicators. Importantly, the ROC curve analysis suggested that RDW had the best prognostic ability among these indicators.

Limitations

This study had some limitations. First, the data were obtained from the MIMIC-IV database. Although the large sample size was an advantage in this study, the data contained in this database cover a long period (2008–2019). Therefore, some information may be obsolete or missing, such as iron, B12 and other factors necessary for hematopoiesis. This, coupled with chemotherapy that can affect hematopoiesis, may influence the RDW in cancer patients. Second, this was a single-center retrospective study with incomplete numerical records and outliers in the database, which may have led to deviations. Third, we only selected the RDW measurement performed in the first 24 h after the admission to the ICU and did not monitor the dynamic trends in RDW levels. In an environment like the ICU, with numerous operations and treatments, such as blood transfusions, anti-inflammatory drugs, anticoagulant drugs, etc., the measured value of RDW can be greatly affected and should be interpreted carefully.

Conclusions

We showed that a high RDW in critically ill cancer patients is independently associated with ICU mortality. As a simple, inexpensive and routine laboratory index, RDW levels can indicate disease severity to a certain extent in cancer patients transferred to the ICU and guide the monitoring of these patients. However, large multicenter prospective studies are needed to confirm our results. The biological mechanisms underlying why RDW has a statistical significance among various clinical parameters are uncertain. Therefore, it is necessary to further explore the relationship between the dynamic changes of RDW and the prognostic and biological mechanisms to obtain a better clinical interpretation.

ORCID iDs

Jiahao Zhou https://orcid.org/0000-0003-4919-4312
Linya Feng https://orcid.org/0000-0002-6018-0387
Yan Zhang https://orcid.org/0000-0003-4348-815X
Shuangshuang Huang https://orcid.org/0000-0002-7756-6120
Hao Jiang https://orcid.org/0000-0001-7955-1363
Weijian Wang https://orcid.org/0000-0002-4319-2773

References

1. Siegel RL, Miller KD, Jemal A. Cancer statistics, 2020. *CA Cancer J Clin*. 2020;70(1):7–30. doi:10.3322/caac.21590
2. Ostermann M, Ferrando-Vivas P, Gore C, Power S, Harrison D. Characteristics and outcome of cancer patients admitted to the ICU in England, Wales, and Northern Ireland and national trends between 1997 and 2013. *Crit Care Med*. 2017;45(10):1668–1676. doi:10.1097/CCM.0000000000002589
3. Caruso P. Prognostication of critically ill patients with cancer: A long road ahead. *Crit Care Med*. 2017;45(10):1787–1788. doi:10.1097/CCM.0000000000002611
4. Puxty K, McLoone P, Quasim T, Sloan B, Kinsella J, Morrison DS. Risk of critical illness among patients with solid cancers: A population-based observational study. *JAMA Oncol*. 2015;1(8):1078–1085. doi:10.1001/jamaoncol.2015.2855
5. Chen ZQ, Yu XS, Mao LJ, et al. Prognostic value of neutrophil–lymphocyte ratio in critically ill patients with cancer: A propensity score matching study. *Clin Transl Oncol*. 2021;23(1):139–147. doi:10.1007/s12094-020-02405-8
6. Martos-Benítez FD, Soto-García A, Gutiérrez-Noyola A. Clinical characteristics and outcomes of cancer patients requiring intensive care unit admission: A prospective study. *J Cancer Res Clin Oncol*. 2018;144(4):717–723. doi:10.1007/s00432-018-2581-0
7. Shimabukuro-Vornhagen A, Böll B, Kochanek M, Azoulay É, von Bergwelt-Baildon MS. Critical care of patients with cancer. *CA Cancer J Clin*. 2016;66(6):496–517. doi:10.3322/caac.21351
8. Danese E, Lippi G, Montagnana M. Red blood cell distribution width and cardiovascular diseases. *J Thorac Dis*. 2015;7(10):E402–E411. doi:10.3978/j.issn.2072-1439.2015.10.04
9. Goyal H, Hu ZD. Prognostic value of red blood cell distribution width in hepatocellular carcinoma. *Ann Transl Med*. 2017;5(13):271–271. doi:10.21037/atm.2017.06.30
10. Yazici P, Demir U, Bozkurt E, Isil GR, Mihmanli M. The role of red cell distribution width in the prognosis of patients with gastric cancer. *Curr Pharm Des*. 2017;18(1):19–25. doi:10.3233/CBM-160668
11. Li Z, Hong N, Robertson M, Wang C, Jiang G. Preoperative red cell distribution width and neutrophil-to-lymphocyte ratio predict survival in patients with epithelial ovarian cancer. *Sci Rep*. 2017;7(1):43001. doi:10.1038/srep43001
12. Song B, Shi P, Xiao J, et al. Utility of red cell distribution width as a diagnostic and prognostic marker in non-small cell lung cancer. *Sci Rep*. 2020;10(1):15717. doi:10.1038/s41598-020-72585-4
13. Fontana V, Spadaro S, Villois P, et al. Can red blood cell distribution width predict outcome after cardiac arrest? *Minerva Anestesiol*. 2018;84(6):693–702. doi:10.23736/S0375-9393.17.12102-4
14. Fontana V, Bond O, Spadaro S, et al. Red cell distribution width after subarachnoid hemorrhage. *J Neurosurg Anesthesiol*. 2018;30(4):319–327. doi:10.1097/ANA.0000000000000459
15. Fujita B, Franz M, Figulla HR, et al. Red cell distribution width and survival in patients hospitalized on a medical ICU. *Clin Biochem*. 2015;48(16-17):1048–1052. doi:10.1016/j.clinbiochem.2015.07.011
16. Yčas JW. Toward a blood-borne biomarker of chronic hypoxemia: Red cell distribution width and respiratory disease. In: Makowski GS, ed. *Adv Clin Chem*. 2017;82:105–197. doi:10.1016/bs.acc.2017.06.002
17. Johnson A, Bulgarelli L, Pollard T, Horng S, Celi LA, Mark R. MIMIC-IV (version 2.0). PhysioNet; 2022. doi:10.13026/7vcr-e114
18. Khwaja A. KDIGO Clinical Practice Guidelines for Acute Kidney Injury. *Nephron Clin Pract*. 2012;120(4):c179–c184. doi:10.1159/000339789
19. Singer M, Deutschman CS, Seymour CW, et al. The Third International Consensus Definitions for Sepsis and Septic Shock (Sepsis-3). *JAMA*. 2016;315(8):801–810. doi:10.1001/jama.2016.0287
20. Kuss O, Blettner M, Börgermann J. Propensity score: An alternative method of analyzing treatment effects. *Dtsch Arztebl Int*. 2016;113(35–36):597–603. doi:10.3238/arztebl.2016.0597
21. Valenti AC, Vitolo M, Imberti JF, Malavasi VL, Boriani G. Red cell distribution width: A routinely available biomarker with important clinical implications in patients with atrial fibrillation. *Curr Pharm Des*. 2021;27(37):3901–3912. doi:10.2174/1381612827666210211125847
22. Lippi G, Turcato G, Cervellin G, Sanchis-Gomar F. Red blood cell distribution width in heart failure: A narrative review. *World J Cardiol*. 2018;10(2):6–14. doi:10.4330/wjc.v10.i2.6
23. Bottazzi B, Riboli E, Mantovani A. Aging, inflammation and cancer. *Semin Immunol*. 2018;40:74–82. doi:10.1016/j.smim.2018.10.011
24. Zurauskaite G, Meier M, Voegeli A, et al. Biological pathways underlying the association of red cell distribution width and adverse clinical outcome: Results of a prospective cohort study. *PLoS One*. 2018;13(1):e0191280. doi:10.1371/journal.pone.0191280
25. Baracos VE, Martin L, Korc M, Guttridge DC, Fearon KCH. Cancer-associated cachexia. *Nat Rev Dis Primers*. 2018;4(1):17105. doi:10.1038/nrdp.2017.105
26. Jia L, Cui S, Yang J, et al. Red blood cell distribution width predicts long-term mortality in critically ill patients with acute kidney injury: A retrospective database study. *Sci Rep*. 2020;10(1):4563. doi:10.1038/s41598-020-61516-y
27. Liao L, Pinhu L. Red blood cell distribution width as a predictor of 28-day mortality in critically ill patients with alcohol use disorder. *Alcohol Clin Exp Res*. 2020;44(12):2555–2560. doi:10.1111/acer.14483
28. Zhang FX, Li ZL, Zhang ZD, Ma XC. Prognostic value of red blood cell distribution width for severe acute pancreatitis. *World J Gastroenterol*. 2019;25(32):4739–4748. doi:10.3748/wjg.v25.i32.4739
29. Joffre J, Hellman J. Oxidative stress and endothelial dysfunction in sepsis and acute inflammation. *Antioxid Redox Signal*. 2021;35(15):1291–1307. doi:10.1089/ars.2021.0027
30. Bazick HS, Chang D, Mahadevappa K, Gibbons FK, Christopher KB. Red cell distribution width and all-cause mortality in critically ill patients. *Crit Care Med*. 2011;39(8):1913–1921. doi:10.1097/CCM.0b013e31821b85c6
31. Zhao C, Wei Y, Chen D, Jin J, Chen H. Prognostic value of an inflammatory biomarker-based clinical algorithm in septic patients in the emergency department: An observational study. *Int Immunopharmacol*. 2020;80:106145. doi:10.1016/j.intimp.2019.106145
32. Sotiropoulos K, Yerly P, Monney P, et al. Red cell distribution width and mortality in acute heart failure patients with preserved and reduced ejection fraction: Red cell distribution width and acute heart failure. *ESC Heart Fail*. 2016;3(3):198–204. doi:10.1002/ehf2.12091
33. Wei TT, Tang QQ, Qin BD, et al. Elevated red blood cell distribution width is associated with liver function tests in patients with primary hepatocellular carcinoma. *Clin Hemorheol Microcirc*. 2016;64(2):149–155. doi:10.3233/CH-162053
34. Anand IS, Gupta P. Anemia and iron deficiency in heart failure: Current concepts and emerging therapies. *Circulation*. 2018;138(1):80–98. doi:10.1161/CIRCULATIONAHA.118.030099

35. Weiss G, Goodnough LT. Anemia of chronic disease. *N Engl J Med*. 2005;352(10):1011–1023. doi:10.1056/NEJMra041809

36. de Gonzalo-Calvo D, de Luxán-Delgado B, Rodríguez-González S, et al. Interleukin 6, soluble tumor necrosis factor receptor I and red blood cell distribution width as biological markers of functional dependence in an elderly population: A translational approach. *Cytokine*. 2012;58(2):193–198. doi:10.1016/j.cyto.2012.01.005

37. Wang L, Jia J, Lin L, et al. Predictive value of hematological markers of systemic inflammation for managing cervical cancer. *Oncotarget*. 2017;8(27):44824–44832. doi:10.18632/oncotarget.14827

38. Mao M, Wei X, Sheng H, et al. C-reactive protein/albumin and neutrophil/lymphocyte ratios and their combination predict overall survival in patients with gastric cancer. *Oncol Lett*. 2017;14(6):7417–7424. doi:10.3892/ol.2017.7179

39. Huszno J, Kolosza Z. Prognostic value of the neutrophil–lymphocyte, platelet–lymphocyte and monocyte–lymphocyte ratio in breast cancer patients. *Oncol Lett*. 2019;18(6):6275–6283. doi:10.3892/ol.2019.10966

CircHIPK3 promotes bone microvascular endothelial cell proliferation, migration and angiogenesis by targeting miR-7 and KLF4/VEGF signaling in steroid-induced osteonecrosis of the femoral head

Peng Peng[1,2,A,C,D], Wei He[1,C,E], Yi-Xi Zhang[3,B,D], Xiao-Hua Liu[2,A,D], Zhen-Qiu Chen[1,A,D], Ji-Gang Mao[2,A,C–F]

[1] Department of Orthopedic Surgery, The First Affiliated Hospital of Guangzhou University of Chinese Medicine, China

[2] Department of Orthopedic Surgery, Zhuhai Hospital of Integrated Traditional Chinese and Western Medicine, China

[3] Department of Ophthalmology, Zhuhai Hospital of Integrated Traditional Chinese and Western Medicine, China

A – research concept and design; B – collection and/or assembly of data; C – data analysis and interpretation;
D – writing the article; E – critical revision of the article; F – final approval of the article

Address for correspondence
Ji-Gang Mao
E-mail: mjg20200901@126.com

Conflict of interest
None declared

Abstract

Background. Circular RNA homeodomain interacting protein kinase 3 (circHIPK3) has been implicated in facilitating angiogenesis in various conditions. However, its role in steroid-induced osteonecrosis of the femoral head (ONFH) remains unclear.

Objectives. To investigate whether circHIPK3 promotes bone microvascular activity and angiogenesis by targeting miR-7 and Krüppel-like factor 4 (KLF4)/vascular endothelial growth factor (VEGF) signaling in ONFH.

Materials and methods. Fifty patients with steroid-induced ONFH undergoing hip-preserving surgery or total hip arthroplasty were included in this study. The expression of circHIPK3, miR-7 and KLF4 was evaluated using reverse transcription polymerase chain reaction (RT-PCR) in necrotic and healthy samples of the femoral head. Bone microvascular endothelial cells (BMECs) were extracted and cultured with 0.1 mg/mL hydrocortisone to create a hormonally deficient cell model. These BMECs were then transfected with either circHIPK3 overexpressing or silencing plasmids with or without miR-7 mimics. The MTT assays were used to detect cell proliferation. Scratch assays were used to assess the migration ability of the BMECs. The tube formation was carried out using an in vitro Matrigel angiogenesis assay. Annexin V-FITC/PI and terminal deoxynucleotidyl transferase dUTP nick end labeling (TUNEL) assays were used to assess the degree of apoptosis. Western blot assays were carried out to discern KLF4 and VEGF expression. The interactions of circHIPK3, miR-7 and KLF4 were confirmed using luciferase, RNA-binding protein immunoprecipitation (RIP), RNA pull-down, and fluorescence in situ hybridization (FISH) assays.

Results. The circHIPK3 and KLF4 expression was decreased, whereas miR-7 expression was increased in necrotic tissues compared to non-necrotic samples. Both circHIPK3 and KLF4 expression correlated negatively with miR-7. The overexpression of circHIPK3 promoted the proliferative, migratory and angiogenic capabilities of the BMECs, while adding an miR-7 mimic reversed these effects. At the same time, the overexpression of circHIPK3 reduced the apoptosis rate of the BMECs and increased KLF4 and VEGF protein expression, but adding an miR-7 mimic reversed these effects. The FISH, RNA pull-down, RIP, and luciferase assays revealed an interaction between circHIPK3, miR-7 and KLF4.

Conclusions. The circHIPK3 promotes BMEC proliferation, migration and angiogenesis by targeting miR-7 and KLF4/VEGF signaling.

Key words: miR-7, circHIPK3, bone microvascular endothelial cell, osteonecrosis of the femoral head

44

P. Peng et al. CirHIPK3 in steroid-induced ONFH

Background

The hallmark of osteonecrosis of the femoral head (ONFH) is progressive bone cell and bone marrow necrosis, which leads to femoral head necrosis if left untreated.[1] It accounts for approx. 10% of the 250,000 total hip arthroplasties (THAs) performed in the USA each year.[2,3] Osteonecrosis of the femoral head can be either traumatic or nontraumatic. Primary nontraumatic ONFH accounts for 30–50% of all ONFH cases in adults aged 30–60 years in China; it is linked to steroid use.[4] Although clinical steroid use remains closely associated with ONFH progression, the exact mechanism is not clear. Osteonecrosis of the femoral head involves a disruption in bone vascular supply, which is related to endothelial dysfunction, oxidative stress, hyperlipidemia, and coagulopathy.[5–8] Endothelial cells are directly damaged by glucocorticoids, causing vasoconstriction, thrombosis, coagulopathy, and an abnormal fibrinolytic system, all of which culminate in ONFH.[9,10] Femoral head blood circulation needs to be maintained to prevent steroid-induced ONFH.

The current literature suggests that dysfunction of bone microvascular endothelial cells (BMECs) caused by glucocorticoids may lead to altered femoral head microcirculation, so it is an important contributor to glucocorticoid-triggered ONFH.[11] Bone microvascular endothelial cells are distributed in the vascular sinuses and inner bone layers, and play an important role in angiogenesis and vascular homeostasis.[12] Moreover, BMECs regulate cellular apoptosis in relation to angiogenesis.[13] Angiogenic function and vascular integrity have been reported to be inversely related to the levels of apoptosis.[14] Continuous exposure to glucocorticoids results in angiogenesis inhibition, cell apoptosis stimulation and endothelial cell dysfunction.[15] A recent study showed that the angiogenic activity of BMECs was decreased while its apoptotic activity was increased in patients with glucocorticoid-triggered ONFH.[16]

Circular RNAs (circRNAs) are noncoding RNAs in the shape of a covalently closed loop spliced together by covalent bonds at the 3' and 5' ends, which increases their stability, enabling them to resist digestion by RNA exonuclease enzymes.[17] This is in contrast to linear RNA, which has different 5' and 3' ends that mark the stop and start transcription sites. The circRNAs are associated with a variety of disorders, including musculoskeletal,[18] gastrointestinal[19] and cardiovascular diseases,[20] as well as several malignancies.[21] Circular RNA homeodomain interacting protein kinase 3 (circHIPK3) is a ubiquitous circRNA that absorbs microRNAs (miRNAs) in order to regulate cell angiogenesis, migration, proliferation, and apoptosis.[22] The circHIPK3 also participates in many pathophysiological processes, including fibrosis, tumor formation and vascular endothelial damage.[23] The miRNAs are an evolutionarily conserved class of small regulatory noncoding RNAs that have multiple biological functions.[24] Previous studies have demonstrated the ability of circRNAs to sponge miRNAs in order to modulate gene expression.[25] However, data regarding the sponge role of circRNA in the occurrence and progression of steroid-triggered ONFH are scarce, especially with regard to circHIPK3.

The Krüppel-like factors (KLFs) are DNA-bound zinc finger transcription families comprised of 9 specific proteins and 18 KLFs.[26] Several members of the KLF family, such as KLF2, KLF4, KLF5, KLF6, KLF10, and KLF15, are strong angiogenesis promoters in various cellular environments.[27–30] Hale et al. found that KLF4 promotes the angiogenesis by regulating Notch signaling.[31] Both in vitro and in vivo angiogeneses are promoted by vascular endothelial growth factor (VEGF). The KLF4 has been shown to activate VEGF signaling in order to promote angiogenesis in human retinal microvascular endothelial cells.[32]

Objectives

This study was performed to investigate whether circHIPK3 promotes BMEC activity and angiogenesis by targeting miR-7 and KLF4/VEGF signaling in ONFH.

Materials and methods

Study subjects

From April 2020 to April 2021, 50 steroid-induced nontraumatic ONFH patients (37 male, 13 female; mean age: 46.4 ±7.8 years) undergoing hip-preserving surgery or THA at the Department of Orthopedic Surgery in Zhuhai Hospital of Integrated Traditional Chinese and Western Medicine, China, were recruited for this study. All patients were diagnosed using anteroposterior and lateral pelvic radiographs and magnetic resonance imaging. Steroid-induced ONFH was defined by a history of a highest daily dose of 80 mg or a mean daily dose ≥16.6 mg of prednisolone equivalent within 1 year before the development of symptoms or radiological diagnosis in asymptomatic cases. The exclusion criteria were alcohol-induced ONFH, idiopathic ONFH, systemic comorbidities, and a clear history of trauma. The necrotic area of the femoral head was selected as the case group, and the adjacent non-necrotic area was regarded as the control group (Fig. 1). The ethics committee of Zhuhai Hospital of Integrated Traditional Chinese and Western Medicine approved the study (approval No. 20200022). All participants provided informed consent. The study was conducted according to the principles of the Declaration of Helsinki.

Tissue collection

Necrotic and healthy tissue collection was performed based on previous study by Jiang et al.[33] In terms of preserving surgery, marrow core decompression followed by bone
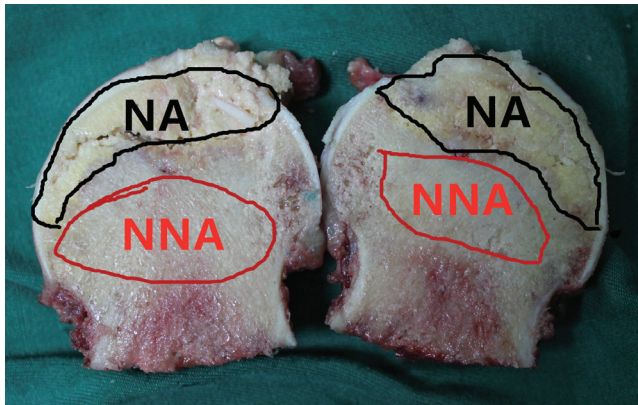
Fig. 1. Representative figures of necrotic area and non-necrotic area in the femoral head

NA – necrotic tissue; NNA – non-necrotic tissue.

grafting was performed. After anesthesia, a longitudinal incision was made on the external side of the femur, 2 cm below the greater trochanter. The position of the guide pin was monitored using a C-arm X-ray machine (Ziehm-9; Ziehm Imaging, Nuremburg, Germany). The guide pin was inserted into the center of the necrotic area beneath the femoral head cartilage through the femoral neck from under the trochanter, and it was screwed into the edge of the lesion area below the head using a decompressor with a tube core. A biopsy device was screwed into the lesion area, and yellowish-white wax-like loose diseased tissue (necrotic tissue) was extracted from the front end of the biopsy device to be used for further study. Non-necrotic tissue as a control was collected at least 3 cm away from the margin of necrotic tissue using the biopsy device. For THA, the femoral head was obtained according to the standard surgical procedure, and necrotic samples and adjacent non-necrotic samples were collected directly (Fig. 1).

Quantitative real-time polymerase chain reaction

TRIzol™ reagent (Invitrogen, Waltham, USA) was used to extract total RNA according to the manufacturer's instructions. The cDNA was synthesized from the extracted RNA using the miScript Reverse Transcription Kit (Qiagen, Valencia, USA). The SYBR™ Green Master Mix (Thermo Fisher Scientific, Waltham, USA) was used to aid the RT-qPCR, with the ABI StepOne Real-time Quantitative PCR System (Applied Biosystems, Foster City, USA) used to carry out the analysis. The polymerase chain reaction (PCR) conditions were as follows: 94°C for 40 min, 60°C for 35 min, 72°C for 30 s, and 90°C for 3 min, for a total of 45 cycles. The internal loading controls were U6 for miR-7 and glyceraldehyde 3-phosphate dehydrogenase (GAPDH) for KLF4 and circHIPK3. Data were analyzed using the $2^{-\Delta\Delta CT}$ method. The primers used were as follows: KLF4 forward 5'-CCCACATGAAGCGACTTCCC-3' and reverse 5'-CAGGTCCAGGAGATCGTTGAA-3'; miR-7

forward 5'-AAAAGAACACGTGGAAGGATAG-3' and reverse 5'-CGCCTAACGTACCGCGAATTT-3'; circH-IPK3 forward 5'-GGGTCGGCCAGTCATGTATC-3' and reverse 5'-ACACAACTGCTTGGCTCTACT-3'; GAPDH forward 5'-TCACCAGGGCTGCTTTTAAC-3' and reverse 5'-GACAAGCTTCCCGTTCTCAG-3'; U6 forward 5'-AACGCTTCACGAATTTGCGT-3' and reverse 5'-CTCGCTTCGGCAGCACA-3'.

Isolation and culture of BMECs and the glucocorticoid damage model

The BMECs were cultured based on the previously published instructions.[33] The subchondral area of the femoral head was used to extract the cancellous bone. Digestible bone fragments were treated with 0.25% trypsin-ethylenediaminetetraacetic acid (EDTA) and 0.2% type I collagenase for 5 min. The reaction was stopped by adding Dulbecco's modified Eagle's medium (DMEM; Gibco, Waltham, USA). The lytic products were filtered using a 70-µmol/L cell filter and centrifuged for 6 min at 1500 rpm. The supernatant was removed, and the cell sediments were exposed to an endothelial cell medium (ECM) (ScienCell Research Laboratories, Carlsbad, USA) containing 100 U/mL penicillin, 100 U/mL streptomycin, 5 mL recombinant human VEGF, and 5% fetal bovine serum (FBS) (Gibco) in 5% CO_2 in a 37°C wet incubator. For cell passage, the medium was removed. The cells were washed using phosphate-buffered saline (PBS) and treated with 0.25% trypsin-EDTA for 5 min. The reaction was ceased using a medium with 10% FBS. The cells were then repeatedly blown using a 1-microliter pipette tip. Cell passage was performed when cell confluence achieved 90%, and the 3rd cell generation was used for the following procedures.

Plasmid and oligonucleotide transfection

A circHIPK3 overexpressing plasmid was created by synthesizing human circHIPK3 cDNA and inserting it into a luciferase-labeled pcDNA3.1 vector (Thermo Fisher Scientific). The BMECs were seeded in a 6-well plate and incubated with serum-free medium (Opti-MEM™; Gibco) at 37°C in humidified 5% CO_2 atmosphere overnight. The overexpression (OE)-circHIPK3, circHIPK3 small interfering RNA (siRNA), miR-7 mimics, and negative controls (NC; GenePharma, Shanghai, China) were used for transfection with the Lipofectamine™ RNAiMAX (Thermo Fisher Scientific) reagent as per manufacturer's protocols.

Examination of cell proliferation and viability

The proliferation of BMECs was assessed using the Cell Counting Kit-8 (CCK-8; Dojindo Laboratories, Kumamoto, Japan) following the manufacturer's instructions. Cells were

incubated in 96-well plates, followed by the addition of 10 μL of the CCK-8 solution and 100 μL of ECM into each well for a 2-hour incubation period. The absorbencies at each time point were measured at 450 nm using an iMark™ Microplate Absorbance Reader (Bio-Rad, Hercules, USA).

Wound healing assay

In the wound healing test, 5×10^5 BMECs were seeded in a 6-well plate for 24 h until 90% cell confluence was achieved. A 10-microliter pipette tip was used to scratch the cell monolayer and draw a gap on the plates. The scratch width was measured at 0 h and 48 h, and the degree of cell migration was calculated as follows: migration area (%) = (A0 – An)/A0 × 100, where A0 represents the area of the initial wound and An represents the remaining area of the wound at the metering point.

Transwell assay

In the transwell assay (8 μm; Corning, New York, USA), the upper chamber was filled with 100 μL of serum-free medium and 5×10^5 BMECs from each treated group. The bottom chamber contained 500 μL of serum with ECM and FBS. The upper chamber was rinsed using PBS and incubated for 12 h at 37°C and in 5% CO_2. The upper chamber cells were then picked up using a cotton swab. The bottom chamber was exposed to 20 min of 4% paraformaldehyde to fix the cells before the addition of 1% crystal violet for 30 min to stain any migratory cells. The cells were then observed under a light microscope (Leica DC 300F; Leica Camera AG, Wetzlar, Germany).

Tube formation assay

A 96-well plate coated with 100 μL BD Matrigel (BD Biosciences, Franklin Lakes, USA) was cured and polymerized for 1 h at 37°C. The transfected BMECs were pretreated with ECM containing FBS for 24 h. Then, 2×10^5 cells per well were seeded onto the Matrigel. After a 6-hour culture period, the tube formation process was visualized microscopically, followed by quantification using ImageJ v. 6.0 software (National Institutes of Health, Bethesda, USA).

Annexin V-FITC and PI assay

First, BMEC apoptosis was detected using an Annexin V-FITC and propidium iodide (PI) Apoptosis Detection Kit (Thermo Fisher Scientific). After transfection, 500 μL of binding buffer was used to resuspend the BMECs. Then, 5 μL PI and 5 μL Annexin V-FITC were added to the suspended cells, followed by a 20-minute darkroom incubation period. The samples were washed on BD FACS™ Lyse Wash Assistant (BD FACSCanto™ II and BD FACSCanto™ 10-Color; BD Biosciences). Cytometry was used to assess the degree of cell apoptosis.

TUNEL assay

The rate of BMEC apoptosis was evaluated using terminal deoxynucleotidyl transferase dUTP nick end labeling (TUNEL) staining with an In Situ Cell Death Detection Kit (Roche, Basel, Switzerland). The cells were fixed with 4% paraformaldehyde for 30 min and then washed with PBS. Next, 0.3% Triton-X 100 in PBS was added and incubated for 5 min. The cells were rinsed 3 times with PBS. Then, the cells were incubated with 50 μL TUNEL Dilution Buffer (Roche-11966006001; Roche) in a 37°C humidified chamber for 1 h. The nuclei were counterstained with 4′,6-diamidino-2-phenylindole (DAPI) for 5 min at room temperature in the dark and later mounted with an anti-fade mounting medium. A fluorescent microscope (Olympus CX23; Olympus Corp., Tokyo, Japan) was used to capture images. Three independent investigators separately quantified the number of apoptotic cells based on the number of TUNEL-positive cells.

Fluorescence in situ hybridization

A fluorescence in situ hybridization (FISH) kit (RiboBio, Guangzhou, China) was used according to the manufacturer's instructions. Briefly, 12-well plates were used to house BMECs seeded onto glass coverslips. Phosphate-buffered saline was then used to rinse the cells before they were fixed for 15 min with 4% paraformaldehyde. Phosphate-buffered saline containing 5 mM $MgCl_2$ was then used to rinse the cells twice. The cells were then rehydrated for 10 min in 2× saline sodium citrate (SSC) and 50% formamide. A solution consisting of 0.5 ng/mL fluorescently labeled circHIPK3 and miR-7 probes, 2.5 mg/mL bovine serum albumin (BSA), 0.25 mg/mL salmon sperm DNA, 2× SSC, 0.25 mg/mL *Escherichia coli* transfer RNA, and 50% formamide was mixed. The cells were incubated in the solution at 37°C. After 3 h, the cells were rinsed twice for 20 min with 2× SSC and 50% formamide at 37°C. Then, they were incubated with 0.5% Triton X-100 solution at 4°C for 5 min. The penultimate detergent contained DAPI. The specimens were analyzed using a Zeiss confocal fluorescence microscope (LSM 510; Carl Zeiss AG, Jena, Germany).

Luciferase reporter assay

Site-directed mutation was used to produce a circHIPK3 mutant. Similarly, by replacing the seed region of the miR-7 binding site, we produced a KLF4 mutant 3′UTR. The firefly luciferase-expressing vector pGL3 (Shanghai Gena Pharmaceutical Co., Ltd., Shanghai, China) was used to clone the mutant sequence. For luciferase activity detection, the BMECs were seeded in 24-well plates at 4×10^4 cells/well 24 h prior to transfection by using Lipofectamine® 2000 (Invitrogen). The cells were collected and lysed 48 h after transfection. The Dual-Luciferase® Reporter Assay System

(Promega, Madison, USA) was used to assess luciferase activity. Luminescence levels were normalized against the β-lactamase gene of the pGL3 luciferase carrier.

RNA-binding protein immunoprecipitation

RNA-binding protein immunoprecipitation (RIP) testing to identify the protein pre-mNRIP1 and the QKI protein was carried out using an RNA-binding protein immunoprecipitation kit (17-700; Merck, Burlington, USA) in compliance with the manufacturer's instructions. The QKI-RNA mixture was then absorbed by the magnetic beads.

RNA pull-down assay

Ultrasound treatments were used on 1×10^7 lysed BMECs. The C-1 magnetic beads (Life Technologies, Carlsbad, USA) were incubated with circHIPK3 probes for 2 h at 25°C to produce a probe-coated magnetic bead. Cell lysates with circHIPK3 probes or oligo probes were incubated overnight at 4°C. After washing with detergent, the bead-bound RNA mixture was eluted and extracted with reverse transcription PCR (RT-PCR) using the RNEasy Mini Kit (Qiagen). The miR-7 pull-down was performed following the same procedure.

Western blot analysis

After transfecting the OE-circHIPK3 and si-circHIPK3 into the BMECs for 24 h, a RIPA lysis buffer (ab156034; Abcam, Cambridge, UK) was used to extract proteins for total protein concentration evaluation with a BCA Detection Kit (Beyotime, Shanghai, China). Protein samples (40 µg) were separated on sodium dodecyl-sulfate polyacrylamide gel electrophoresis (SDS-PAGE) (10% w/v) and transferred electrophoretically to a polyvinylidene fluoride (PVDF) membrane. The cell membranes were blocked with 5% dry skim milk and then incubated overnight at 4°C with the following antibodies: anti-VEGF (1:1000; Abcam), KLF4 (1:1000; Abcam) and β-actin (1:3000; Abcam). The cell membranes were then incubated with their corresponding secondary antibodies. Electrochemiluminescence using Invitrogen reagent was used to analyze the strips. Band intensity was quantified using ImageJ v. 6.0 software.

Statistical analyses

GraphPad Prism v. 8.0 (GraphPad Software, San Diego, USA) was used for data analysis. The Kolmogorov–Smirnov (K–S) test was used to test the distribution (normal or nonnormal) of the variables. The F-test was used to check the homogeneity of variances between groups. Values were presented as mean ± standard deviation (M ±SD) when the data distribution was normal. Otherwise, the values were expressed as median. When the data met normal distribution and homogeneity simultaneously, the Student's t-test was conducted for comparisons between

the 2 groups. One-way analysis of variance (ANOVA) was carried out when 3 or more groups were compared, followed by the Tukey's test for post hoc analysis. When the data did not meet either normal distribution or homogeneity, the Mann–Whitney (M–W) U test was conducted for comparisons between the 2 groups. The Kruskal–Wallis (K–W) test was used when 3 or more groups were compared, followed by the Dunn's test for post hoc analysis. The correlation between 2 genes was examined using the Spearman's correlation test. A value of $p < 0.05$ indicated a statistically significant difference. All the statistical results have been demonstrated in Table 1.

Results

CircHIPK3 expression was downregulated in necrotic tissue in ONFH

The expression of circHIPK3, miR-7 and KLF4 in necrotic and healthy bone samples was assessed using quantitative RT-PCR (qRT-PCR). There was a markedly lower circHIPK3 and KLF4 expression in necrotic tissue compared to nonnecrotic tissue (Fig. 2A,B; circHIPK3: M–W U test, U = 0, $p < 0.001$; KLF4: M–W U test, U = 0, $p < 0.001$). Conversely, miR-7 levels were significantly higher in necrotic tissue compared to healthy tissue (M–W U test, U = 0, $p < 0.001$; Fig. 2C). Further correlation analysis demonstrated that circHIPK3 expression in necrotic tissue was positively correlated with KLF4 levels (Spearman's correlation, r = 0.470, $p < 0.001$; Fig. 2D) but negatively correlated with miR-7 (Spearman's correlation, r = −0.380, p = 0.007; Fig. 2E). In addition, miR-7 expression corresponded inversely with KLF4 (Spearman's correlation, r = −0.462, $p < 0.001$; Fig. 2F).

CircHIPK3 upregulation inhibits apoptosis but augments proliferation of BMECs

We postulated that the BMECs would have reduced migratory and proliferative abilities if circHIPK3 expression was downregulated. Based on this assumption, circHIPK3 siRNA, OE-circHIPK3 and miR-7 mimics were transfected into the BMECs (Fig. 3A). The CCK-8 assay showed that the proliferation of the BMECs transfected with OE-circHIPK3 was significantly enhanced compared with the NC at 72 h (one-way ANOVA followed by the Tukey's test, p = 0.025 compared to negative control (NC)), while the proliferation of the BMECs was significantly suppressed following the transfection with circHIPK3 siRNA (one-way ANOVA followed by the Tukey's test, p = 0.015 compared to NC; Fig. 3C). The transfection of OE-circHIPK3 plus miR-7 yielded similar proliferation rates in contrast to NC (one-way ANOVA followed by the Tukey's test, p = 0.155 compared to NC; Fig. 3C).

To further analyze the impact of circHIPK3 and miR-7 on isolated BMEC growth, the rate of apoptosis was evaluated in the OE-circHIPK3, circHIPK3 siRNA,
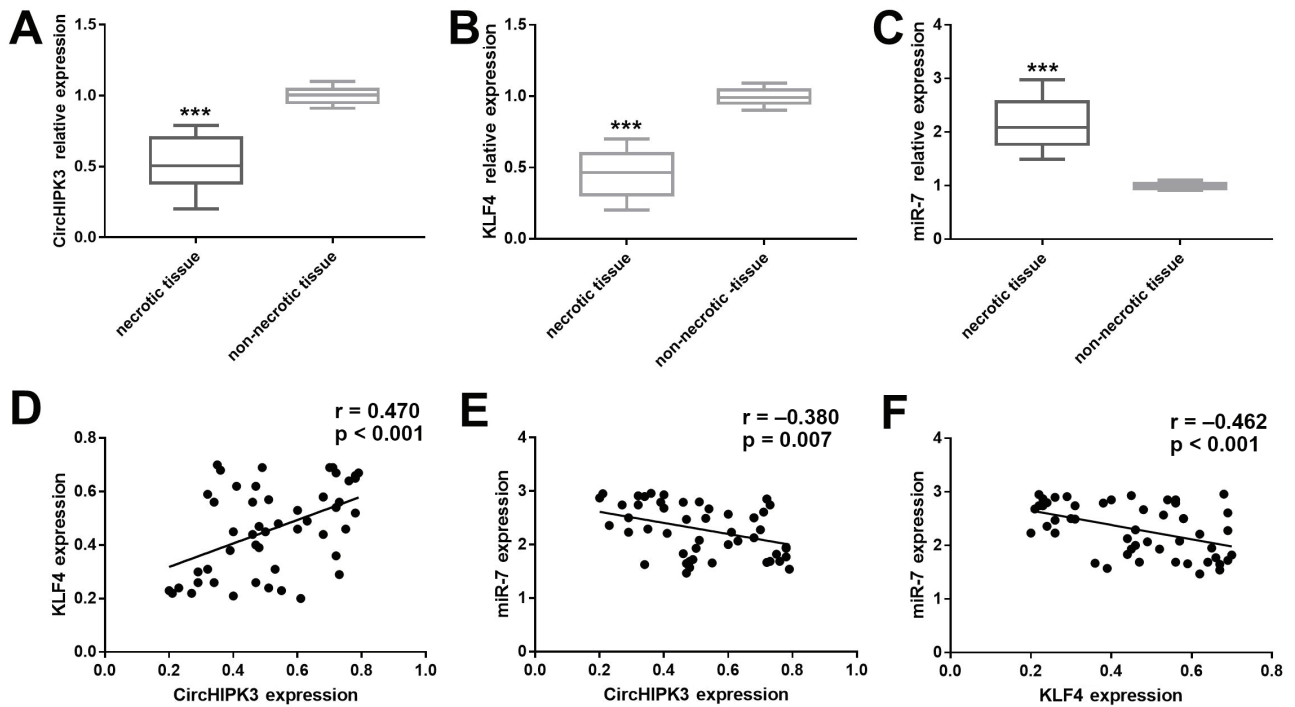
Fig. 2. A. Circular RNA homeodomain-interacting protein kinase 3 (circHIPK3) expression in necrotic and healthy bone samples; B. The Krüppel-like factor 4 (KLF4) expression in necrotic and healthy bone samples; C. The miR-7 expression in necrotic and healthy bone samples. Results were statistically analyzed using the Mann–Whitney U test, ***p < 0.001 compared to non-necrotic tissue; D. Association between KLF4 and circHIPK3 expression in necrotic tissue; E. Association between circHIPK3 and miR-7 expression in necrotic tissue; F. Association between miR-7 and KLF4 expression in necrotic tissue. The results were statistically analyzed using Spearman's correlation

Table 1. Statistical results

Statistical items	Type	Results	p-value
CircHIPK3 expression in necrotic and healthy bone samples	Mann–Whitney U test	U = 0	<0.001
KLF4 expression in necrotic and healthy bone samples	Student's t-test	t = 16.97	<0.001
miR-7 expression in necrotic and healthy bone samples	Mann–Whitney U test	U = 0	<0.001
Association between KLF4 and circHIPK3 expression in necrotic tissue	Pearson's correlation coefficient	r = 0.470	<0.001
Association between circHIPK3 and miR-7 expression in necrotic tissue	Pearson's correlation coefficient	r = −0.380	0.007
Association between miR-7 and KLF4 expression in necrotic tissue	Pearson's correlation coefficient	r = −0.462	<0.001
Wound healing test	Student's t-test	t = 42.35, si-circHIPK3 vs. NC; t = 12.12, OE-circHIPK3 vs. NC	all p < 0.001
Transwell test (48 h)	Student's t-test	t = 57.21, si-circHIPK3 vs. NC; t = 11.27, OE-circHIPK3 vs. NC	all p < 0.001
CircHIPK3 RIP assays	Student's t-test	t = 11.57, input vs. anti-IgG; t = 13.41, anti-AGO2 vs. anti-IgG	all p < 0.001
miR-7 RIP assays	Student's t-test	t = 12.90, input vs. anti-IgG; t = 12.8, anti-AGO2 vs. anti-IgG	all p < 0.001
CircHIPK3 RNA pulldown assays	Student's t-test	t = 22.63, biotin-miR-7 vs. biotin-control	<0.001
miR-7 RNA pulldown assays	Student's t-test	t = 29.51, biotin-circHIPK3 vs. biotin-control	<0.001
Western blot analysis of VEGF (n = 6)	Student's t-test	t = 11.21, si-circHIPK3 vs. NC; t = 14.41, OE-circHIPK3 vs. NC	all p < 0.001
Western blot analysis of KLF4 (n = 6)	Student's t-test	t = 17.23, si-circHIPK3 vs. NC; t = 11.41, OE-circHIPK3 vs. NC	all p < 0.001

circHIPK3 – circular RNA homeodomain interacting protein kinase 3 (circHIPK3); KLF4 – Krüppel-like factor 4; VEGF – vascular endothelial growth factor; RIP – RNA-binding protein immunoprecipitation. IgG – immunoglobulin G; NC – negative control; si – silencing; OE – overexpression.
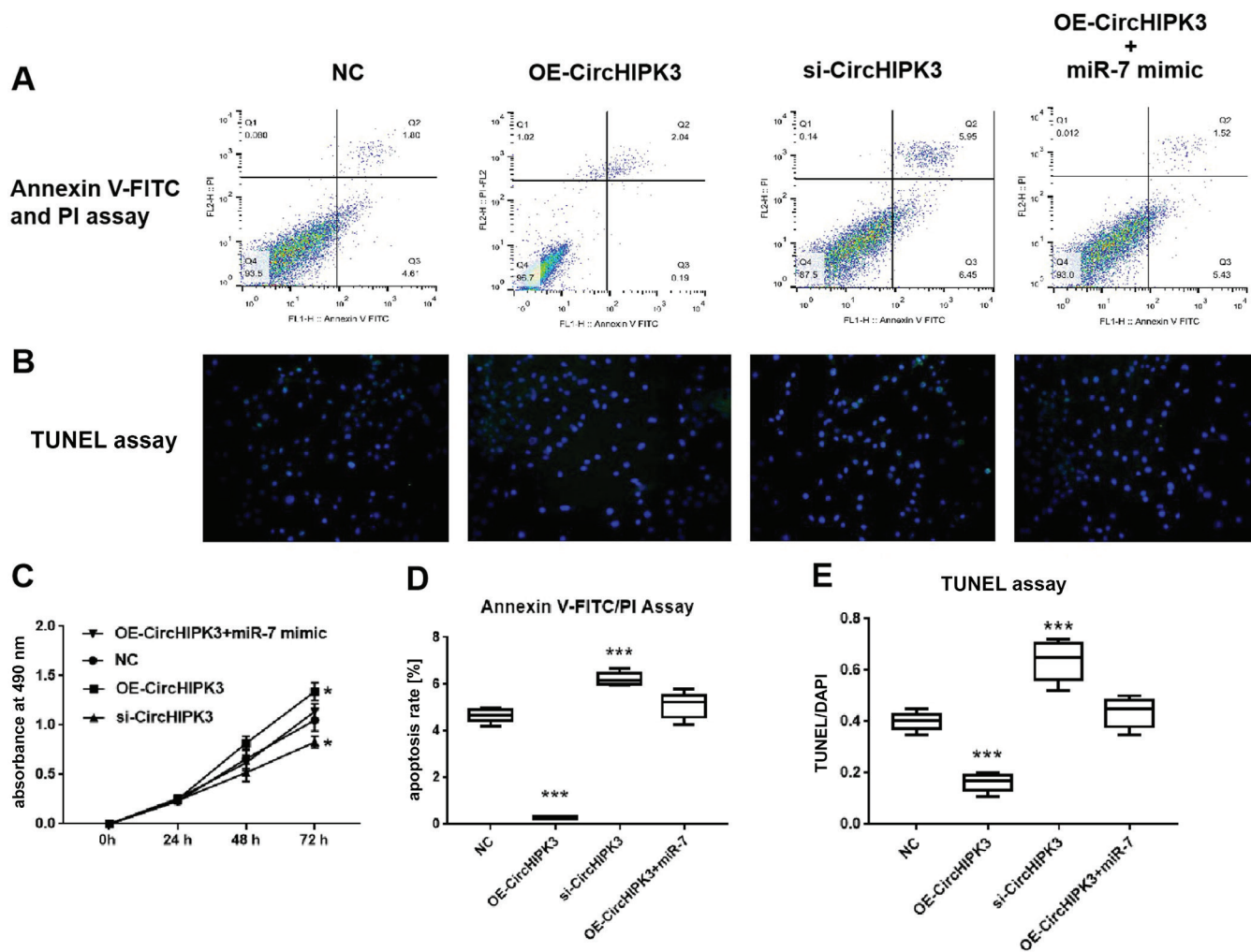
Fig. 3. Evaluation of cell proliferation using MTT, and of cell apoptosis using FACScan flow cytometry and terminal deoxynucleotidyl transferase dUTP nick end labeling (TUNEL) assay. A. Flow cytometry image of bone microvascular endothelial cells (BMECs); B. TUNEL assay for BMECs; C. Degree of cell proliferation from each group from 0 h to 72 h; D. Degree of cell apoptosis using the Annexin V-FITC/PI assay; E. Degree of cell apoptosis using the TUNEL assay. For the MTT and TUNEL assays, the results were statistically analyzed using one-way analysis of variance (ANOVA) followed by the Tukey's test for post hoc analysis, ***$p < 0.001$ compared to NC. For the Annexin V-FITC/PI assay, the results were statistically analyzed using the Kruskal–Wallis test followed by the Dunn's post hoc test, ***$p < 0.001$ compared to negative control (NC)

circHIPK3 – circular RNA homeodomain interacting protein kinase 3; DAPI – 4′,6-diamidino-2-phenylindole; si – silencing; OE – overexpression.

OE-circHIPK3+miR-7 mimic, and NC. According to the results of the Annexin V-FITC, PI and TUNEL assays, the apoptosis rate was markedly decreased upon circHIPK3 upregulation in contrast to NC (apoptosis FITC: K–W test followed by the Dunn's test for post hoc analysis, $p < 0.001$ compared to NC; TUNEL assay: one-way ANOVA followed by the Tukey's test for post hoc analysis, $p < 0.001$ compared to NC; Fig. 3A,B,D,E). When the BMECs were treated with circHIPK3 siRNA, the cell apoptosis rate was markedly increased in contrast to the NC (Fig. 3A,B,D,E; apoptosis FITC: K–W test followed by the Dunn's test for post hoc analysis, $p < 0.001$ compared to NC; TUNEL assay: one-way ANOVA followed by the Tukey's test for post hoc analysis, $p < 0.001$ compared to NC). The cell apoptosis rates were similar between the OE-circHIPK3+miR-7 mimic and NC.

Overexpression of circHIPK3 promotes BMEC migration and angiogenesis

The impact of circHIPK3 upregulation on BMEC tubule formation was observed after 48 h. Accordingly, the total

tubule number and density were significantly increased upon circHIPK3 overexpression compared to NC. Conversely, there was a reduction in density and total tubule number upon circHIPK3 silencing. The OE-circHIPK3 in combination with the miR-7 mimic had similar tubule number and density compared with NC (one-way ANOVA followed by the Tukey's test for post hoc analysis, $p < 0.001$ compared to NC; Fig. 4A,B).

A scratch wound assay allowed us to evaluate the impact of circHIPK3 on BMEC migration. The overexpression of circHIPK3 notably enhanced BMEC motility, as determined by the migration area (Fig. 5A,C; one-way ANOVA followed by the Tukey's test for post hoc analysis, $p < 0.001$ compared to NC), whereas circHIPK3 silencing significantly impaired the motility of BMECs (one-way ANOVA followed by the Tukey's test for post hoc analysis, $p < 0.001$ compared to NC). The OE-circHIPK3+miR-7 mimic group had similar BMEC mobility compared to NC. The promigratory ability of the BMECs influenced by circHIPK3 was further confirmed with the transwell assay, which is another widely used method for evaluating cell
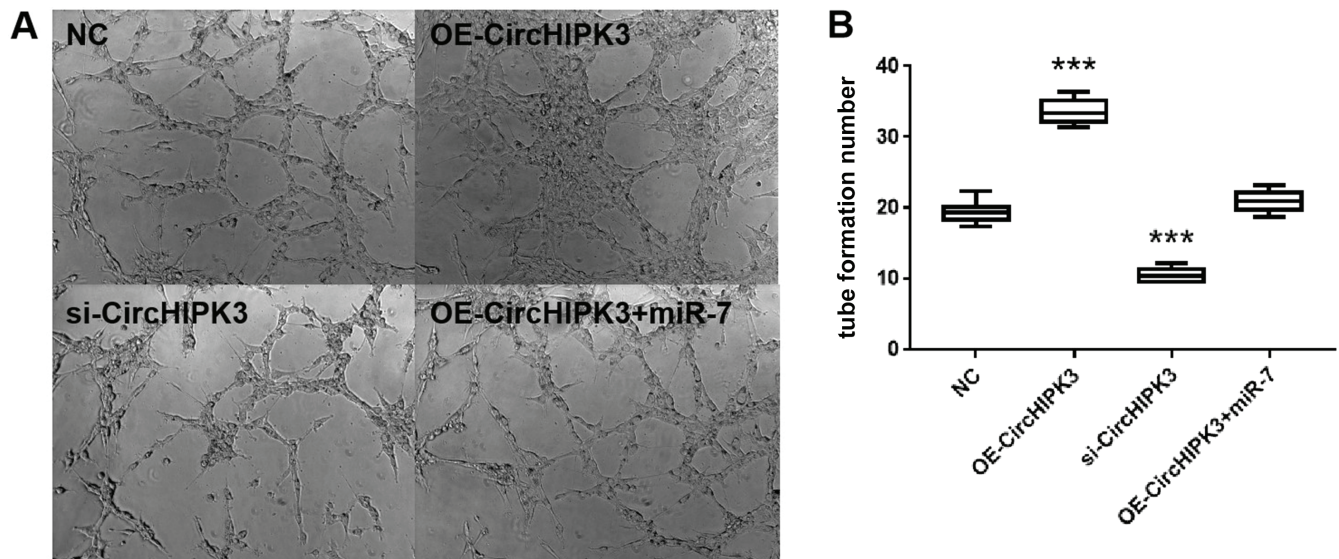
Fig. 4. A. Tube formation assay images of the OE-circHIPK3, circular RNA homeodomain-interacting protein kinase 3 (circHIPK3) siRNA, OE-circHIPK3+miR-7 mimic, and negative control (NC) groups; B. Tube formation numbers of bone microvascular endothelial cells (BMECs) subjected to quantification analysis. The results were statistically analyzed using one-way analysis of variance (ANOVA) followed by the Tukey's test for post hoc analysis, ***$p < 0.001$ compared to NC

si – silencing; OE – overexpression.

migration. There was a higher proportion of migratory cells in the OE-circHIPK3 group compared to NC (K–W test followed by the Dunn's test for post hoc analysis, $p < 0.001$ compared to NC), whereas those of the si-circHIPK3 group exhibited a significantly lower proportion of spreading cells. The OE-circHIPK3+miR-7 mimic and NC groups had similar proportions of migratory cells (the K–W test followed by the Dunn's test for post hoc analysis, $p < 0.001$ compared to NC; Fig. 5B,D).

CircHIPK3 functions to sponge miR-7 expressing KLF4 targets

We carried out bioinformatics analysis (using miRBase (https://www.mirbase.org) and starBase v. 3.0 (https://starbase.sysu.edu.cn/starbase2/)) to predict the likely miRNA target of miR-7 for both KLF4 and circHIPK3. We found that KLF4 was a potential target site for miR-7 (Fig. 6A), with circHIPK3 also possessing an miR-7 target site (Fig. 6B). The luciferase activity assay demonstrated markedly suppressed luciferase activity of KLF4-WT (wild-type) and circHIPK3-WT reporter genes upon miR-7 mimic exposure compared to the simulated NC (Fig. 6C,D) (circHIPK3: K–W test followed by the Dunn's test for post hoc analysis, $p = 0.033$ compared to NC; KLF4: one-way ANOVA followed by the Tukey's test for post hoc analysis, $p = 0.029$ compared to NC). However, the miR-7 mimic had no apparent effect on KLF4-WT and circHIPK3-MUT reporter luciferase activities (Fig. 6C,D). To further discern the relationship between circHIPK3, miR-7 and KLF4 in the BMECs, FISH, RIP and RNA pull-down assays were performed. The RIP test showed that the AGO2 antibody significantly enriched the expression of circHIPK3 and miR-7 in contrast to the control

immunoglobulin G (IgG) antibody (one-way ANOVA followed by the Tukey's test for post hoc analysis, $p < 0.001$ compared to anti-IgG; Fig. 7A,B). In the RNA pull-down test, circHIPK3 was detected in the miR-7 pull-down sphere in contrast to NC (Student's t-test, $p < 0.001$ compared to biotin control; Fig. 7C). The miR-7 was also identified in the miR-7 pull-down particles in contrast to NC (Student's t-test, $p < 0.001$ compared to biotin control; Fig. 7D). The FISH assay colocalized circHIPK3 (red fluorescence) and miR-7 (green fluorescence) in the isolated BMECs (Fig. 7E). These findings suggest that circHIPK3 possesses sponge functions by competing for miR-7 with the potential target of KLF4 in BMECs.

Effect of circHIPK3 on KLF4 and VEGF expression

The likely mechanism of circHIPK3 and miR-7 on potential proteins, including KLF4 and VEGF, was studied. After 48 h, we found that circHIPK3 overexpression further increased KLF4 and VEGF protein expression in contrast to NC. On the other hand, transfection of si-circHIPK3 led to a decreased expression of KLF4 and VEGF (one-way ANOVA followed by the Tukey's test for post hoc analysis, $p < 0.001$ compared to NC). Compared with NC, the expression of these proteins was not significantly different after the co-transfection with the OE-circHIPK3+miR-7 mimic, indicating that miR-7 reduced the impact of circHIPK3 on KLF4 and VEGF expression (one-way ANOVA followed by the Tukey's test for post hoc analysis, $p < 0.001$ compared to NC; Fig. 8A–C). Our findings indicate that KLF4/VEGF signaling activation was promoted by the overexpression of circHIPK3 but suppressed by the overexpression of miR-7.
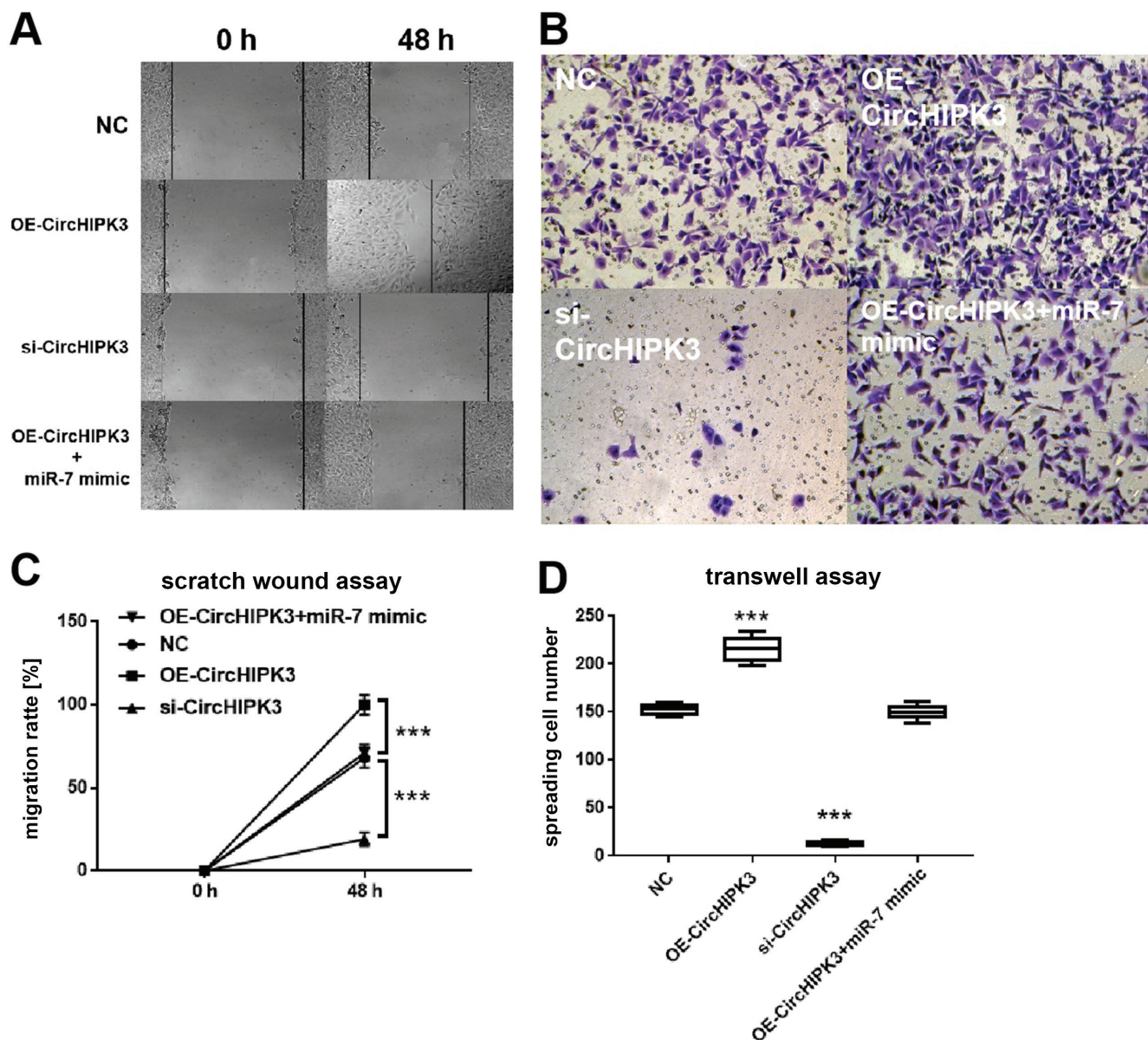
Fig. 5. A. Representative figures of the scratch wound assay at 0 h and 48 h; B. Representative figures of the transwell assay after 48 h; C. The osteonecrosis of the femoral head (ONFH) group bone microvascular endothelial cells (BMECs) had lower migratory abilities (violet-stained) in contrast to the control group; D. Number of migratory cells subjected to quantification analysis. For the scratch wound assay, the results were statistically analyzed using one-way analysis of variance (ANOVA) followed by the Tukey's test for post hoc analysis, ***$p < 0.001$ compared to negative control (NC). For the transwell assay, the results were statistically analyzed using the Kruskal–Wallis test followed by the Dunn's post hoc test, ***$p < 0.001$ compared to NC

si – silencing; OE – overexpression.

Discussion

This study investigated the potential role of circHIPK3 in the progression of steroid-induced ONFH. It is the first study to demonstrate a markedly decreased circHIPK3 expression and a notably raised miR-7 expression in necrotic bone tissue in contrast to healthy bone tissue. Our analyses found that the expression of circHIPK3 was negatively associated with miR-7 expression. Further cell studies showed that circHIPK3 augmentation could promote BMEC proliferation, migration and angiogenesis while also attenuating the degree of cell apoptosis. The addition of miR-7 could counteract these effects. The FISH, RNA

pull-down, RIP, and luciferase assays revealed a relationship between circHIPK3, miR-7 and KLF4. The upregulation of circHIPK3 enhanced the protein expression of KLF4 and VEGF. These results suggest that circHIPK3 promotes BMEC proliferation, migration and angiogenesis by targeting miR-7 and KLF4/VEGF signaling.

Steroid-induced ONFH is often thought to arise in the setting of frequent steroid consumption.[34,35] In recent years, studies on the epigenetics of hormone-induced ONFH have sought to uncover its molecular pathogenesis and to discover likely miRNA, lncRNA and circRNA targets.[36–38] However, detailed reports on the role of circRNA in this disease have yet to be published. The circRNAs
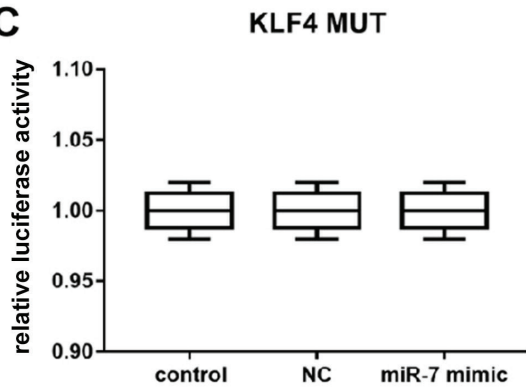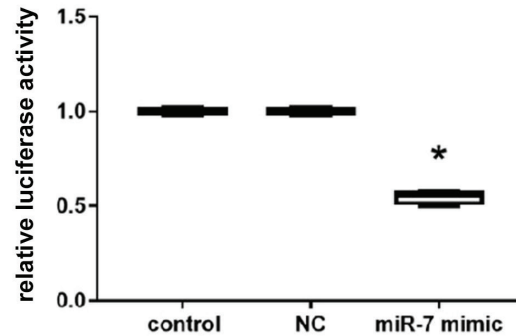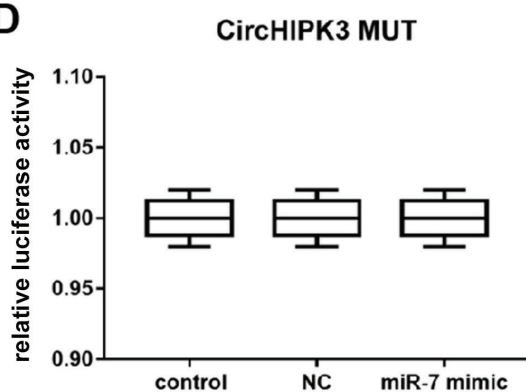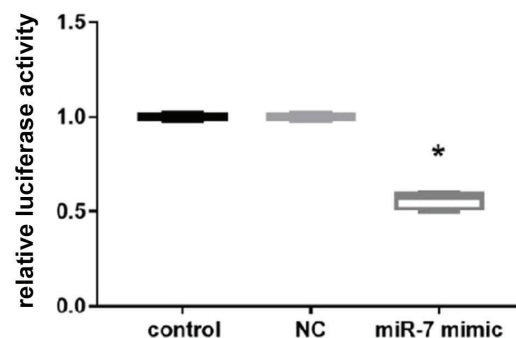
Fig. 6. A. Bioinformatics analysis of matching sequence of miR-7 within 3'-UTR of Krüppel-like factor 4 (KLF4). The KLF4 3'-UTR-MUT is the mutation of the match sequence of 3'-UTR of KLF4 with miR-7 (miRBase); B. Circular RNA homeodomain interacting protein kinase 3 (circHIPK3) and miR-7 (StarBase 3.0) predicted binding sites. The 3'-UTR of circHIPK3 with miR-7; C. Match sequence mutation is denoted as MUT circHIPK3. The miR-7 was found to bind to the 3'-UTR of KLF4 WT instead of MUT CTGF; D. Luciferase activity in bone microvascular endothelial cells (BMECs) co-transfected with miR-7 mimic+circHIPK3 WT, circHIPK3 MUT reporter, or mimic negative control (NC) at 48 h post-transfection. CircHIPK3: the Kruskal–Wallis test followed by the Dunn's test for post hoc analysis, *p = 0.033 compared to NC; KLF4: one-way analysis of variance (ANOVA) followed by the Tukey's test for post hoc analysis, *p = 0.029 compared to NC

represent novel targets due to their relationship with angiogenesis.

In this study, we established the role of circHIPK3 in the regulation of BMEC angiogenesis, highlighting its potential as a therapeutic target in steroid-induced ONFH. The circHIPK3 expression was found to be lower in necrotic bone compared to adjacent non-necrotic bone in ONFH patients. Conversely, miR-7 expression was increased and KLF4 expression was upregulated. A further analysis established that circHIPK3 and miR-7 were inversely correlated. We found that circHIPK3 was localized in the cytoplasm based on FISH studies. The RIP and RNA downregulation experiments suggest that circHIPK3 may affect BMECs through its role on miRNA sponge miR-7.

Angiogenesis is the physiological phenomenon of novel blood vessel formation from existing capillaries.

Angiogenesis serves as a pivotal process during bone repair in ONFH. Many circRNAs have been suggested to regulate angiogenesis in both in vivo and in vitro studies.[39] For example, Ouyang et al. demonstrated that circRNA hsa_circ_0074834 promoted osteogenic and angiogenic coupling of bone marrow mesenchymal stem cells (BMSCs).[40] Zhang et al. discovered that hsa_circRNA_001587 could inhibit angiogenesis of pancreatic cancer cells.[41] Another study indicated that circRNA-001175 is able to inhibit apoptosis while enhancing angiogenesis and proliferation in high glucose-stimulated human umbilical vein endothelial cells.[42] In our study, we found that overexpressing circHIPK3 promoted BMEC angiogenesis, indicating that circHIPK3 may exert positive effects on bone blood supply in ONFH. Previous studies have demonstrated that circHIPK3 could induce cardiac regeneration and promote blood supply in myocardial
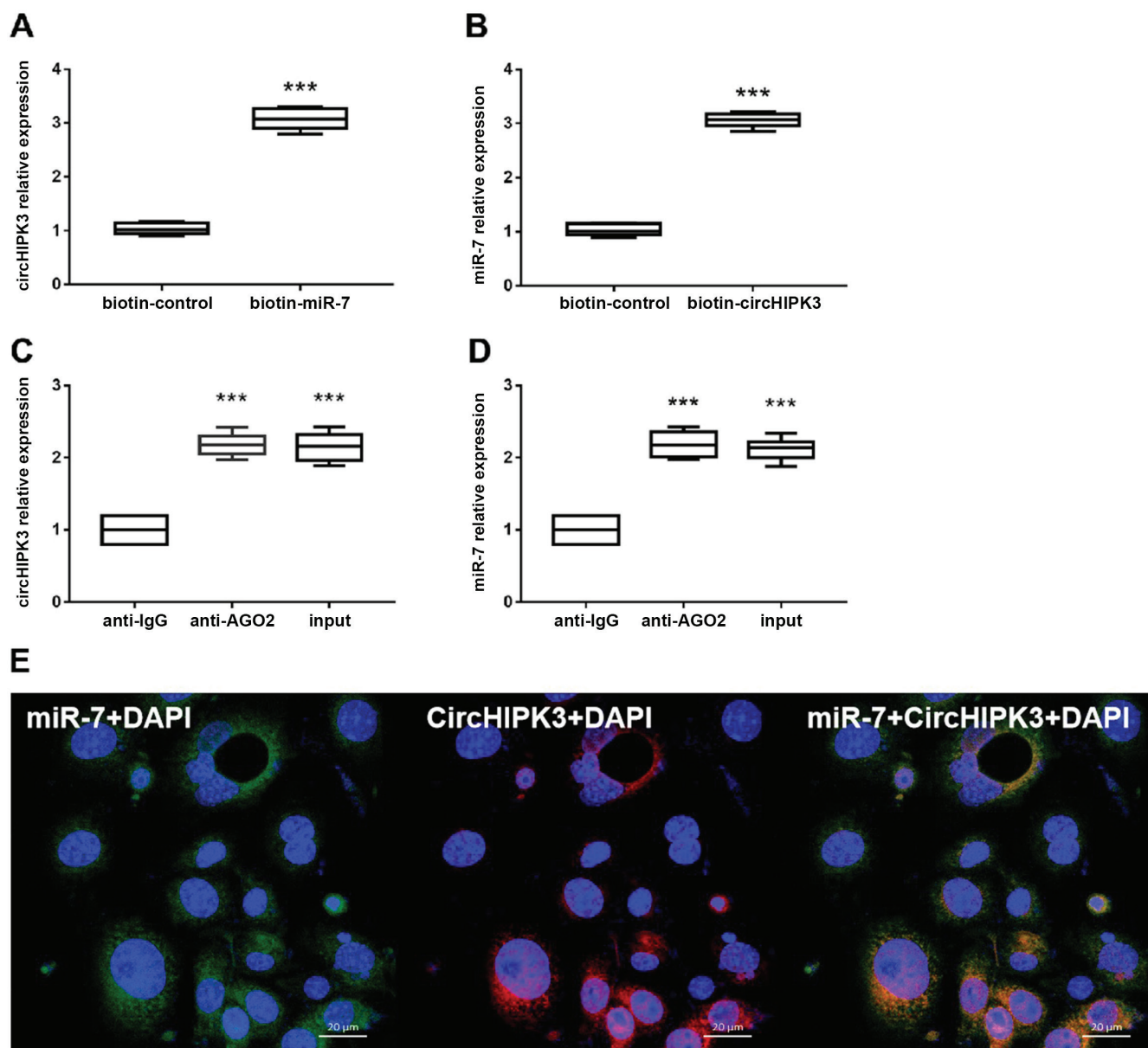
Fig. 7. A. RNA-binding protein immunoprecipitation (RIP) assays demonstrated that circular RNA homeodomain interacting protein kinase 3 (circHIPK3) expression was substantially enriched with AGO2 antibody in contrast to control immunoglobulin G (IgG) antibody; B. RIP assays demonstrated that miR-7 expression was substantially enriched with AGO2 antibody in contrast to control IgG antibody. The results were statistically analyzed using one-way analysis of variance (ANOVA) followed by the Tukey's test for post hoc analysis, ***$p < 0.001$ compared to biotin control; C. Biotin-coupled probe pull-down assay demonstrated evidence of circHIPK3 in the miR-7 pulled-down pellet in contrast to the control group; D. The miR-7 was detected in the biotin-circHIPK3 vector in contrast to the control group. The results were statistically analyzed using the Student's t-test, ***$p < 0.001$ compared to biotin control; E. CircHIPK3 and miR-7 were colocalized in bone microvascular endothelial cells (BMECs) by means of fluorescence in situ hybridization (FISH) through confocal microscope observation. The circHIPK3 was stained red, miR-7 was stained green and nuclei were stained blue (4′,6-diamidino-2-phenylindole (DAPI)); overlapped expression was mixed (scale bar: 20 μm) (***$p < 0.001$ compared to anti-IgG)

infarction. For example, Wang et al. demonstrated an increased VEGF-A activity due to the action of exosomal circHIPK3 derived from hypoxia-induced cardiomyocytes on inhibiting miR-29a activity.[43] Another study showed that the overexpression of circHIPK3 promotes proliferation, migration, tubule-forming ability, and subsequent angiogenesis of coronary endothelial cells.[44] In addition, we found that circHIPK3 enhanced BMEC migration and proliferation while suppressing apoptosis. All these findings indicate that circHIPK3 could act as a stable biomarker that regulates angiogenesis in steroid-induced ONFH.

The circHIPK3 was found to act as an miR-7 sponge, which regulates angiogenesis through its effect on KLF4 expression. In previous studies, KLF4 has been shown to be a pro-angiogenic factor that acts through the VEGF signaling pathway to promote proliferation, migration and duct formation.[45] Therefore, we focused on the KLF4 pathway as a potential target signal pathway. Augmenting circHIPK3 resulted in upregulated KLF4 and VEGF expression. Our study found that circUSP45 regulated VEGF-mediated angiogenesis.
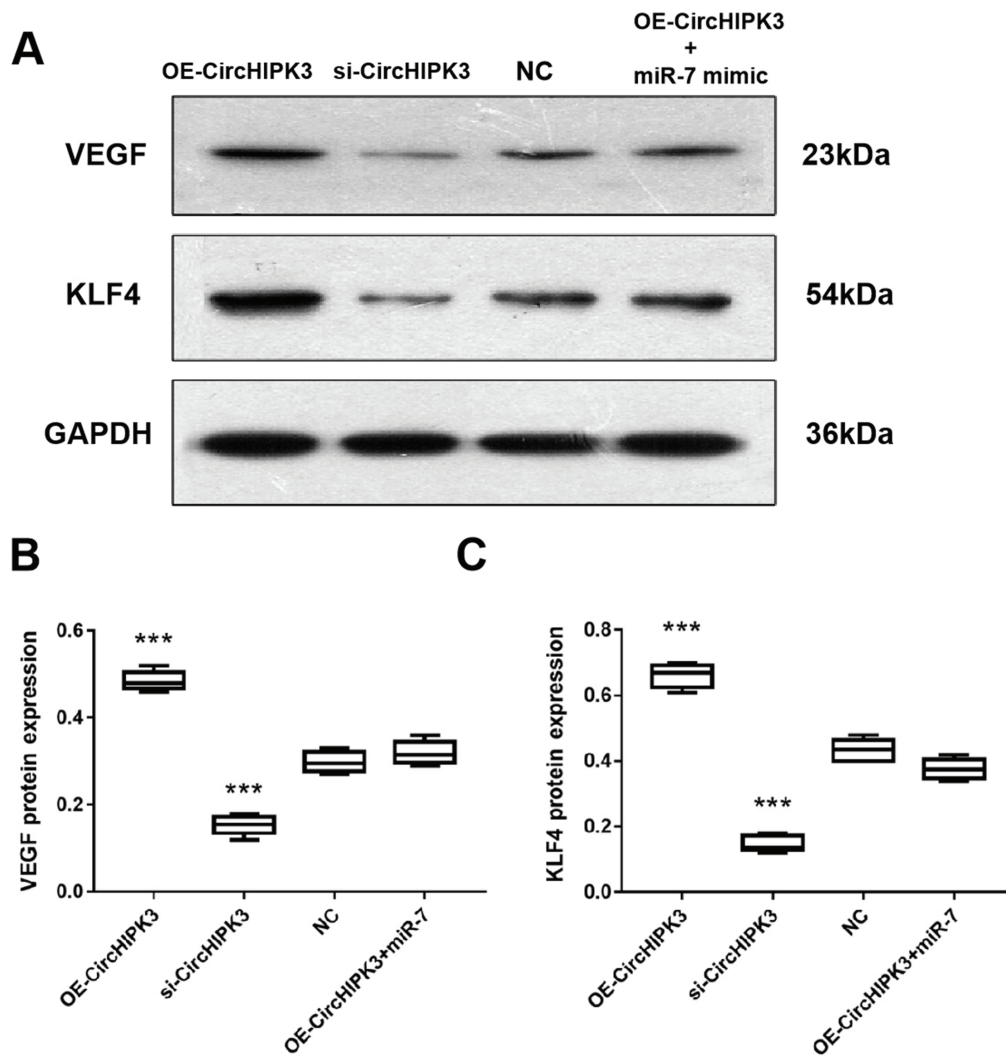
A

B   **C**

Fig. 8. Western blot analysis of vascular endothelial growth factor (VEGF) and Krüppel-like factor 4 (KLF4) followed by transfection after 48 h. A. Representative bands of VEGF and KLF4 proteins; B. VEGF protein expression quantification among various cohorts; C. KLF4 protein expression quantification among various cohorts. The results were statistically analyzed using one-way analysis of variance (ANOVA) followed by the Tukey's test for post hoc analysis, ***$p < 0.001$ compared to negative control (NC)

si – silencing; OE – overexpression.

Limitations

This study has some limitations that should be considered. Although we demonstrated that circHIPK3 increased KLF4 and VEGF signaling by acting as a sponge of miR-7, there may be other yet-to-be-characterized miRNAs that may also be sponged by circHIPK3. More extensive studies on these potential miRNA candidates and their related target proteins and signaling pathways are warranted.

Conclusion

Our study revealed the role of circHIPK3 downregulation in steroid-induced ONFH. The upregulation of circHIPK3 could promote proliferation, migration and angiogenesis through inhibiting apoptosis of isolated BMECs by targeting miR-7 and through activation of KLF4/VEGF signaling. Our study provides a new reference for the diagnosis and treatment of steroid-induced ONFH, but more relevant mechanisms of action and treatment strategies need to be further investigated.

Supplementary materials

The supplementary materials are available at https://doi.org/10.5281/zenodo.7104863. The package contains Supplementary Statistical File 1, presenting the results of the normality and homogeneity tests.

ORCID iDs

Peng Peng ⓘ https://orcid.org/0000-0003-1626-293X
Wei He ⓘ https://orcid.org/0000-0002-8031-3298
Yi-Xi Zhang ⓘ https://orcid.org/0000-0002-1281-1703
Xiao-Hua Liu ⓘ https://orcid.org/0000-0003-4148-0357
Zhen-Qiu Chen ⓘ https://orcid.org/0000-0001-9099-5539
Ji-Gang Mao ⓘ https://orcid.org/0000-0002-8667-2187

References

1. Petek D, Hannouche D, Suva D. Osteonecrosis of the femoral head: Pathophysiology and current concepts of treatment. *EFORT Open Rev*. 2019;4(3):85–97. doi:10.1302/2058-5241.4.180036
2. Desforges JF, Mankin HJ. Nontraumatic necrosis of bone (osteonecrosis). *N Engl J Med*. 1992;326(22):1473–1479. doi:10.1056/NEJM199205283262206
3. Moya-Angeler J. Current concepts on osteonecrosis of the femoral head. *World J Orthop*. 2015;6(8):590. doi:10.5312/wjo.v6.i8.590

4. Cui L, Zhuang Q, Lin J, et al. Multicentric epidemiologic study on six thousand three hundred and ninety five cases of femoral head osteonecrosis in China. *Int Orthop*. 2016;40(2):267–276. doi:10.1007/s00264-015-3061-7

5. Wang GJ, Cui Q, Balian G. The pathogenesis and prevention of steroid-induced osteonecrosis. *Clin Orthop Relat Res*. 2000;370:295–310. doi:10.1097/00003086-200001000-00030

6. Motomura G, Yamamoto T, Miyanishi K, Jingushi S, Iwamoto Y. Combined effects of an anticoagulant and a lipid-lowering agent on the prevention of steroid-induced osteonecrosis in rabbits. *Arthritis Rheum*. 2004;50(10):3387–3391. doi:10.1002/art.20517

7. Kock NB, van Tankeren E, Oyen WJG, Wymenga AB, van Susante JLC. Bone scintigraphy after osteochondral autograft transplantation in the knee: 13 patients followed for 4 years. *Acta Orthop*. 2010;81(2):206–210. doi:10.3109/17453671003587101

8. Ichiseki T. DNA oxidation injury in bone early after steroid administration is involved in the pathogenesis of steroid-induced osteonecrosis. *Rheumatology*. 2005;44(4):456–460. doi:10.1093/rheumatology/keh518

9. Kerachian MA, Harvey EJ, Cournoyer D, Chow TYK, Séguin C. Avascular necrosis of the femoral head: Vascular hypotheses. *Endothelium*. 2006;13(4):237–244. doi:10.1080/10623320600904211

10. Kerachian MA, Cournoyer D, Harvey EJ, et al. New insights into the pathogenesis of glucocorticoid-induced avascular necrosis: Microarray analysis of gene expression in a rat model. *Arthritis Res Ther*. 2010;12(3):R124. doi:10.1186/ar3062

11. Kerachian MA, Séguin C, Harvey EJ. Glucocorticoids in osteonecrosis of the femoral head: A new understanding of the mechanisms of action. *J Steroid Biochem Mol Biol*. 2009;114(3–5):121–128. doi:10.1016/j.jsbmb.2009.02.007

12. Kusumbe AP, Ramasamy SK, Adams RH. Coupling of angiogenesis and osteogenesis by a specific vessel subtype in bone. *Nature*. 2014;507(7492):323–328. doi:10.1038/nature13145

13. Williams TA, Verhovez A, Milan A, Veglio F, Mulatero P. Protective effect of spironolactone on endothelial cell apoptosis. *Endocrinology*. 2006;147(5):2496–2505. doi:10.1210/en.2005-1318

14. O'Connell BJ, Genest J. High-density lipoproteins and endothelial function. *Circulation*. 2001;104(16):1978–1983. doi:10.1161/hc3901.096667

15. Zhang Y, Yin J, Ding H, Zhang C, Gao YS. Vitamin K_2 ameliorates damage of blood vessels by glucocorticoid: A potential mechanism for its protective effects in glucocorticoid-induced osteonecrosis of the femoral head in a rat model. *Int J Biol Sci*. 2016;12(7):776–785. doi:10.7150/ijbs.15248

16. Yu H, Liu P, Zuo W, et al. Decreased angiogenic and increased apoptotic activities of bone microvascular endothelial cells in patients with glucocorticoid-induced osteonecrosis of the femoral head. *BMC Musculoskelet Disord*. 2020;21(1):277. doi:10.1186/s12891-020-03225-1

17. Dou Y, Cha DJ, Franklin JL, et al. Circular RNAs are down-regulated in KRAS mutant colon cancer cells and can be transferred to exosomes. *Sci Rep*. 2016;6(1):37982. doi:10.1038/srep37982

18. Zheng YL, Song G, Guo JB, et al. Interactions among lncRNA/circRNA, miRNA, and mRNA in musculoskeletal degenerative diseases. *Front Cell Dev Biol*. 2021;9:753931. doi:10.3389/fcell.2021.753931

19. Li R, Jiang J, Shi H, Qian H, Zhang X, Xu W. CircRNA: A rising star in gastric cancer. *Cell Mol Life Sci*. 2020;77(9):1661–1680. doi:10.1007/s00018-019-03345-5

20. Altesha M, Ni T, Khan A, Liu K, Zheng X. Circular RNA in cardiovascular disease. *J Cell Physiol*. 2019;234(5):5588–5600. doi:10.1002/jcp.27384

21. Xie Y, Yuan X, Zhou W, et al. The circular RNA HIPK3 (circHIPK3) and its regulation in cancer progression: Review. *Life Sci*. 2020;254:117252. doi:10.1016/j.lfs.2019.117252

22. Fu Y, Sun H. Biogenesis, cellular effects, and biomarker value of circHIPK3. *Cancer Cell Int*. 2021;21(1):256. doi:10.1186/s12935-021-01956-2

23. Zhou J, Wang B, Bin X, et al. CircHIPK3: Key player in pathophysiology and potential diagnostic and therapeutic tool. *Front Med*. 2021;8:615417. doi:10.3389/fmed.2021.615417

24. Saliminejad K, Khorram Khorshid HR, Soleymani Fard S, Ghaffari SH. An overview of microRNAs: Biology, functions, therapeutics, and analysis methods. *J Cell Physiol*. 2019;234(5):5451–5465. doi:10.1002/jcp.27486

25. Du WW, Zhang C, Yang W, Yong T, Awan FM, Yang BB. Identifying and characterizing circRNA-protein interaction. *Theranostics*. 2017;7(17):4183–4191. doi:10.7150/thno.21299

26. Pei J, Grishin NV. A new family of predicted Krüppel-like factor genes and pseudogenes in placental mammals. *PLoS One*. 2013;8(11):e81109. doi:10.1371/journal.pone.0081109

27. Boon RA, Urbich C, Fischer A, et al. Krüppel-like factor 2 improves neovascularization capacity of aged proangiogenic cells. *Eur Heart J*. 2011;32(3):371–377. doi:10.1093/eurheartj/ehq137

28. Nagai R, Suzuki T, Aizawa K, Shindo T, Manabe I. Significance of the transcription factor KLF5 in cardiovascular remodeling. *J Thromb Haemost*. 2005;3(8):1569–1576. doi:10.1111/j.1538-7836.2005.01366.x

29. Yang DHA, Hsu CF, Lin CY, Guo JY, Yu WCY, Chang VHS. Krüppel-like factor 10 upregulates the expression of cyclooxygenase 1 and further modulates angiogenesis in endothelial cell and platelet aggregation in gene-deficient mice. *Int J Biochem Cell Biol*. 2013;45(2):419–428. doi:10.1016/j.biocel.2012.11.007

30. Helbing T, Volkmar F, Goebel U, et al. Krüppel-like factor 15 regulates BMPER in endothelial cells. *Cardiovasc Res*. 2010;85(3):551–559. doi:10.1093/cvr/cvp314

31. Hale AT, Tian H, Anih E, et al. Endothelial Krüppel-like factor 4 regulates angiogenesis and the Notch signaling pathway. *J Biol Chem*. 2014;289(17):12016–12028. doi:10.1074/jbc.M113.530956

32. Wang Y, Yang C, Gu Q, et al. KLF4 promotes angiogenesis by activating VEGF signaling in human retinal microvascular endothelial cells. *PLoS One*. 2015;10(6):e0130341. doi:10.1371/journal.pone.0130341

33. Jiang B, Zhu SH, Zeng JY, Mao Z. Plasma and local expressions of circRNA CDR1as are linked with disease severity in patients with non-traumatic osteonecrosis of femoral head. *J Orthop Surg Res*. 2020;15(1):592. doi:10.1186/s13018-020-02129-z

34. Buckley L, Guyatt G, Fink HA, et al. 2017 American College of Rheumatology Guideline for the Prevention and Treatment of Glucocorticoid-Induced Osteoporosis. *Arthritis Rheum*. 2017;69(8):1521–1537. doi:10.1002/art.40137

35. Fukushima W, Fujioka M, Kubo T, Tamakoshi A, Nagai M, Hirota Y. Nationwide epidemiologic survey of idiopathic osteonecrosis of the femoral head. *Clin Orthop Relat Res*. 2010;468(10):2715–2724. doi:10.1007/s11999-010-1292-x

36. Li Z, Huang C, Yang B, Hu W, Chan MT, Wu WKK. Emerging roles of long non-coding RNAs in osteonecrosis of the femoral head. *Am J Transl Res*. 2020;12(9):5984–5991. PMID:33042474.

37. Wu X, Sun W, Tan M. Noncoding RNAs in steroid-induced osteonecrosis of the femoral head. *BioMed Res Int*. 2019;2019:8140595. doi:10.1155/2019/8140595

38. Yao T, Yin ZS, Huang W, Ding ZF, Cheng C. Microarray profiling of circular RNAs in steroid-associated osteonecrosis of the femoral head: Observational study. *Medicine (Baltimore)*. 2020;99(10):e19465. doi:10.1097/MD.0000000000019465

39. Liu Y, Yang Y, Wang Z, et al. Insights into the regulatory role of circRNA in angiogenesis and clinical implications. *Atherosclerosis*. 2020;298:14–26. doi:10.1016/j.atherosclerosis.2020.02.017

40. Ouyang Z, Tan T, Zhang X, et al. CircRNA hsa_circ_0074834 promotes the osteogenesis-angiogenesis coupling process in bone mesenchymal stem cells (BMSCs) by acting as a ceRNA for miR-942-5p. *Cell Death Dis*. 2019;10(12):932. doi:10.1038/s41419-019-2161-5

41. Zhang X, Tan P, Zhuang Y, Du L. hsa_circRNA_001587 upregulates SLC4A4 expression to inhibit migration, invasion, and angiogenesis of pancreatic cancer cells via binding to microRNA-223. *Am J Physiol Gastrointest Liver Physiol*. 2020;319(6):G703–G717. doi:10.1152/ajpgi.00118.2020

42. Pei X, Ye S, Jin G, Yu Y. Overexpression of circRNA-001175 promotes proliferation and angiogenesis and inhibits apoptosis of the human umbilical vein endothelial cells (HUVECs) induced by high glucose. *Int J Clin Exp Pathol*. 2018;11(1):359–366. PMID:31938119.

43. Wang Y, Zhao R, Shen C, et al. Exosomal circHIPK3 released from hypoxia-induced cardiomyocytes regulates cardiac angiogenesis after myocardial infarction. *Oxid Med Cell Longev*. 2020;2020:8418407. doi:10.1155/2020/8418407

44. Si X, Zheng H, Wei G, et al. CircRNA Hipk3 induces cardiac regeneration after myocardial infarction in mice by binding to Notch1 and miR-133a. *Mol Ther Nucleic Acids*. 2020;21:636–655. doi:10.1016/j.omtn.2020.06.024

45. Wang Y, Yang C, Gu Q, et al. KLF4 promotes angiogenesis by activating VEGF signaling in human retinal microvascular endothelial cells. *PLoS One*. 2015;10(6):e0130341. doi:10.1371/journal.pone.0130341

Toll-like receptor polymorphisms (*TLR2* and *TLR4*) association with the risk of infectious complications in cardiac surgery patients

Agnieszka Żukowska[1,A,D,F], Andrzej Ciechanowicz[2,C,E], Mariusz Kaczmarczyk[2,C,E], Mirosław Brykczyński[4,B,E], Maciej Żukowski[3,A,B,F]

[1] Department of Infection Control, Regional Hospital, Stargard, Poland

[2] Department of Clinical and Molecular Biochemistry, Pomeranian Medical University, Szczecin, Poland

[3] Department of Anesthesiology, Intensive Therapy and Acute Intoxication, Pomeranian Medical University, Szczecin, Poland

[4] Cardiac Surgery Department, Collegium Medicum, University of Zielona Góra, Poland

A – research concept and design; B – collection and/or assembly of data; C – data analysis and interpretation;
D – writing the article; E – critical revision of the article; F – final approval of the article

Abstract

Background. Postoperative infection is a common healthcare-associated problem, and unfortunately, a serious complication in cardiac surgery patients. Toll-like receptors (TLRs) are crucial in activating non-specific immunity mechanisms and integrating elements of the immune system, due to interactions between specific and non-specific responses.

Objectives. In this study, the association of *TLR2* or *TLR4* with the risk of postoperative infections in cardiac surgery patients undergoing a coronary artery bypass grafting (CABG) procedures was investigated.

Materials and methods. Our research was carried out on a cohort of 299 consecutive adult patients with ischemic heart disease (IHD) who underwent a planned CABG procedure. These patients were monitored for the presence of a postoperative infection over a 30-day observation period. All patients were investigated for 2 *TLR2* gene mutations – R753Q (rs5743708) and T16934A (rs4696482), and 2 polymorphisms of the *TLR4* gene – D299G (rs4986790) and T399I (rs4986791). The final stage of the study was an evaluation of the hypothetical association between *TLR2* and *TLR4* gene variances and postoperative infections in patients undergoing CAGB procedures.

Results. The prevalence of infections in the final cohort was 15.3% (46/299). The most common infections were surgical site infections, which were diagnosed in 21 patients (45.6%), bloodstream infections in 15 patients (32.6%) and pneumonia in 10 patients (21.8%). Logistic regression demonstrated that the presence of the AG+GG of D299G (rs4986790) and CT+TT of T399I (rs4986791) variants was related to a higher incidence of infection in patients undergoing CAGB procedures.

Conclusions. To our knowledge, this is the first study of its kind to demonstrate that *TLR2* and *TLR4* mutations affect the risk of post-CABG infections. Being a carrier of the AG+GG of D299G (rs4986790) or CT+TT of T399I (rs4986791), *TLR4* variants constitute a postoperative risk factor for infection in patients undergoing CAGB procedures.

Key words: infection, *TLR4*, *TLR2*, CABG, postoperative

Background

Cardiac surgery carries a high likelihood of postoperative infections due to the invasive nature of the surgery and the subsequent inflammatory response. Postoperative infections can have serious repercussions for the patient and lead to prolonged hospitalization, as well as increased hospitalization costs. A reduction of the prevalence of infections requires not only an augmentation in surgical behavior but also the implementation of a competent epidemiological and microbiological approach.[1,2]

In accordance with current publications, the occurrence of infectious complications after cardiac surgery is between 3.3% and 26.8%.[1–3] The mortality coefficient among cardiac surgery patients with an infection during the postoperative period is approx. 16.8% compared to 2.9% in patients without an infection.[4] A multicenter research study has revealed an infection incidence after open heart surgery using cardiopulmonary bypass (CPB) of approx. 26.8%.[1] Among the most common complications, pneumonia can occur in approx. 57.1% of all postoperative infections.[5] This appears to be a relevant matter, as the mortality in cases of pneumonia associated with mechanical ventilation (ventilator-associated pneumonia (VAP)) reaches 46%. Infectious events occurring postoperatively substantially increase hospitalization costs and prolong hospitalizations. The increased frequency of infections after cardiac surgery procedures is multifactorial. The patient's preoperative condition, underlying diseases and perioperative course are all crucial components in regard to the development of an infection.[3,5,6]

The immune system can identify intruding pathogens through a group of receptors known as pattern-recognition receptors (PRRs). These receptors identify molecular patterns associated with pathogens (pathogen-associated molecular patterns (PAMPS)) and subsequently activate a cascade of signals to generate an immune response. The PRRs are comprised of various groups of molecules such as retinoic acid-inducible gene I (RIG-I-like) receptors, toll-like receptors (TLRs), absent in melanoma-2 (AIM-2)-like receptors (ALRs), Nod-like receptors (NLRs), and others.[7] The presence of TLRs has been confirmed in most immune cells, especially in those responsible for the recognition of pathogens, but also on the surface of neutrophils, eosinophils and lymphocytes. In addition to the cells of the immune system, TLRs are also present on the surface and inside cells that can come into contact with pathogens, such as respiratory epithelial cells, gastrointestinal tract cells, endothelial cells, skin cells, urogenital tract epithelial cells, adipocytes, and myocytes.[8] Ten TLRs with different ligand binding specificities have been identified in humans. The TLRs are key in activating non-specific immune mechanisms and are an important integrating element in the immune system due to interactions between specific and non-specific responses. The binding of PAMPs to TLRs leads to the activation of cells that recognize foreign antigens by inducing the expression of genes responsible for the synthesis of pro-inflammatory cytokines, chemotactic proteins and defensins.[9,10]

For instance, TLR2 has been shown to be associated with an intrinsic response to Gram-positive pathogens through the recognition of bacterial cell wall components, while TLR4 plays an important role in activating a host response against Gram-negative bacteria.[7–9]

A vast amount of research on the relationship between various gene polymorphisms and inflammatory responses associated with infections has been conducted. The discovery of the role genetic variants and gene mutations play in the encoding of immunological response proteins could be used to predict those with an increased risk of postoperative infections and lead to an improvement in perioperative care.

Objectives

The purpose of this research was to estimate whether TLR2 or TLR4 polymorphisms are related to the probability of postoperative infections in cardiac surgery patients who have undergone a coronary artery bypass grafting (CABG) procedure.

Materials and methods

Study group

Our research was carried out on a cohort of 299 consecutive adult patients with ischemic heart disease (IHD) undergoing a planned CABG procedure at the Department of Cardiac Surgery (Pomeranian Medical University, Szczecin, Poland). Exclusion criteria included having previously undergone thoracic surgery, off-pump CABG procedures, the presence of an active infection, valvular operations, and emergency procedures (Fig. 1). The presented research was approved by the Pomeranian Medical University Ethics Committee (approval No. KB-0080/176/09). Informed written consent was obtained from all patients.

Standard operating procedures and antibiotic prophylaxis were performed in all participants. The patients were observed for the presence of a postoperative infection during a 30-day follow-up period. All patients were evaluated for 2 TLR2 gene mutations: R753Q (rs5743708) and T16934A (rs4696482), and 2 polymorphisms of the TLR4 gene: D299G (rs4986790) and T399I (rs4986791).

In addition, clinical data such as New York Heart Association score (NYHA), Canadian Cardiovascular Society score (CCS), logistic EuroSCORE (ESlog), smoking, length of coronary artery disease (CAD), blood loss volume, blood transfusion requirement, serum creatinine level, and length of CBP, as well as demographic data were recorded.
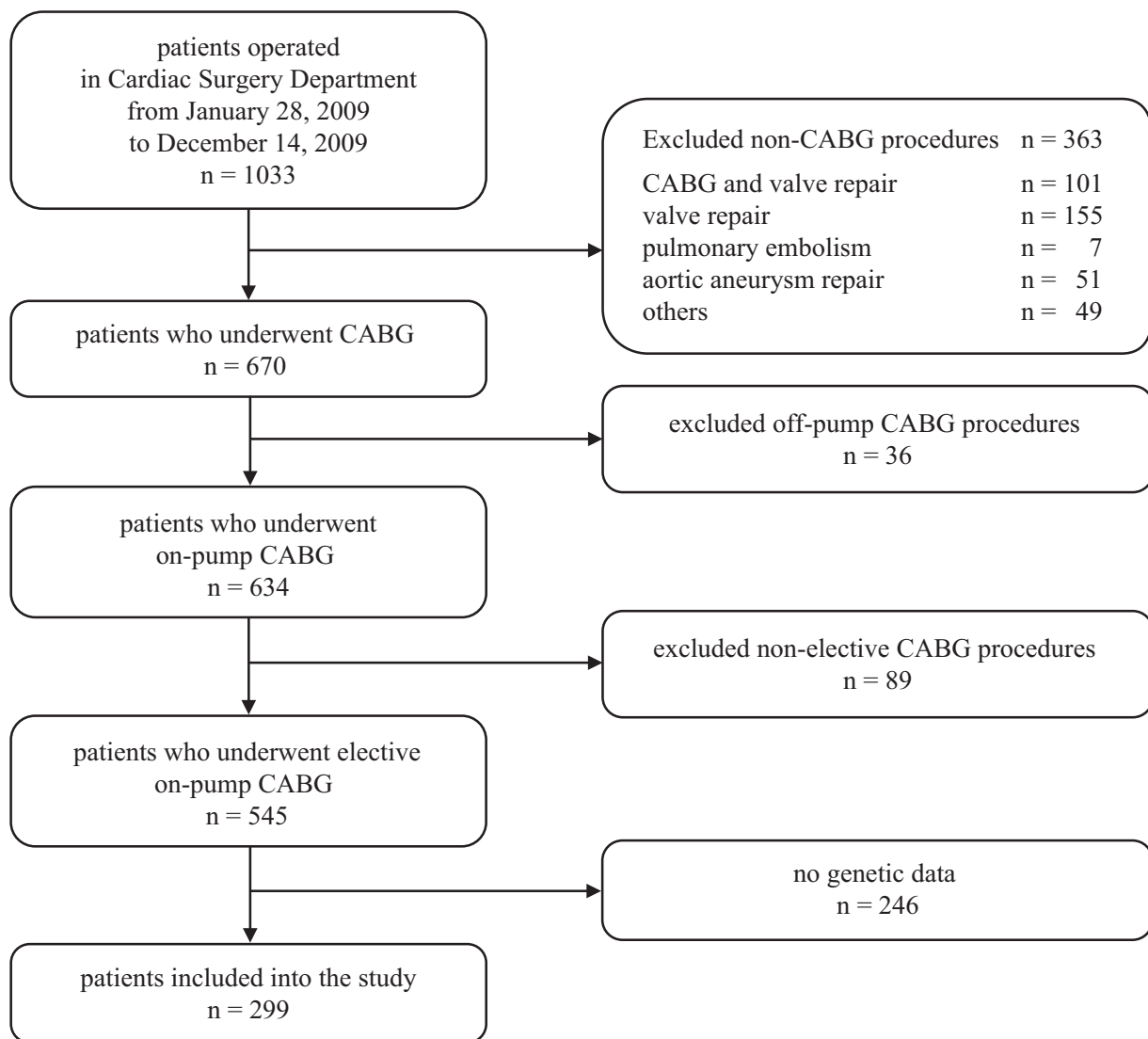
Fig. 1. Study flowchart

CABG – coronary artery bypass grafting.

Criteria for postoperative infection

We identified surgical site infections (SSIs) based on the presence of soreness or vulnerability, regional edema, redness or warmth, and the existence of purulent drainage from the incision site or bacterial growth in wound cultures that appeared at the incision site up to 30 days postoperatively. These criteria are concordant with the European Centre for Disease Prevention and Control (ECDC) definitions. In each case, the wounds were swabbed for microbiological examination. If systemic features of infection, such as fever, chills, hypotension, and elevated C-reactive protein (CRP), white blood cell (WBC) counts or serum procalcitonin (PCT) levels were present, blood cultures were drawn.[11]

According to the ECDC, patients can be diagnosed with pneumonia based on radiological findings of at least 2 chest examinations along with a minimum of 1 of the following: novel or increasing/sustained infiltrates, consolidations or cavitations, as well as an increase in temperature or leukocyte count (<4000 WBC/mm^3 or ≥12,000 WBC/mm^3). The criteria also included individuals with age ≥70 years, presenting with confusion without an identifiable cause, as well as at least 2 of the following: new onset of purulent sputum, change in sputum character, increased respiratory secretions, increased suctioning requirements, new-onset or worsening cough, dyspnea, tachypnea, rales or bronchial tone, worsening gas exchange (e.g., deteriorating oxygenation (e.g., PaO$_2$/FiO$_2$ ≤ 240), increased oxygen demands, or extended (increased) ventilator support. In each case, sputum or bronchoalveolar lavage (BAL) samples were obtained for microbial culture.[12]

Bloodstream infection (BSI) was diagnosed in patients with one of the following findings: pyrexia (>38°C), shivers or low blood pressure, and identified bacterial growth on one or more blood samples, or had the usual commensal bacteria (i.e., co-negative staph., diphtheroids, *Propionibacterium* spp., *Bacillus* spp.) present in more than 1 positive blood culture obtained from different sites.[13]

Genetic analysis

All patients were investigated for 2 well-known functional *TLR2* and *TLR4* gene mutations. During the course of hospitalization, 2 mL-specimens of whole blood were taken from all participants via a typical venipuncture technique. Peripheral blood leukocytes were used for genomic DNA isolation using a Mini Kit QIA DNA (Qiagen, Hilden, Germany). Afterwards, the polymerase chain reaction (PCR)-restriction fragments length polymorphism technique was applied to examine the rs5743708 and rs4696482 of *TLR2* mutations, as well as for rs4986790 and rs4986791 of *TLR4* mutations. All details of the genetic investigation (primers, PCR conditions, amplifications, electrophoresis, and cleaving) were thoroughly described in our previous publication.[14]

The final step of the study was to investigate the hypothetical association between *TLR2* and *TLR4* gene variances and postoperative infections in individuals undergoing CAGB procedures.

Statistical analyses

Compatibility with the Hardy–Weinberg equilibrium model was calculated using a χ^2 test. The composition of individual genotypes with and without postoperative infections was tested using Fisher's exact method. Unpaired and paired Student's t-tests and Mann–Whitney U tests were used to evaluate a correlation among the groups. Adjusted and unadjusted models of multivariate analysis were used to evaluate the connection between TLR polymorphisms and the frequency of post-CABG septic complications. The p-values <0.05 were treated as statistically significant. Odds ratios (ORs) and 95% confidence intervals (95% CIs) were reported when logistic regression analysis was performed. All tests were performed using Statistica v. 8.0 (StatSoft, Inc., Tulsa, USA).

Results

The mean age in the analyzed cohort was 63 years. The study population consisted of 77 (25.7%) females, 42% smokers at the time of admission, and 152 (50.8%) individuals in class 0 of the NYHA scoring. Baseline characteristics were not significantly different between the infected and non-infected groups except for the duration of CAD, CABG, perioperative blood loss volume, and ESlog (Table 1).

The prevalence of infections in the final cohort was 15.3% (46/299). Surgical site infections were the most common, diagnosed in 21 patients (45.6%), followed by bloodstream

Table 1. The baseline characteristics

Variable	Whole group (n = 299)	Non-infected (n = 253)	Infected (n = 46)	p-value
Age [years], M ±SD	63.6 ±9.8	63.2 ±9.9	65.8 ±9.5	0.2837#
Male sex, n (%)	222 (74.2)	187 (73.9)	35 (76.1)	0.8556*
Height [cm], M ±SD	166.9 ±9.1	166.9 ±9.2	166.9 ±8.9	0.8361#
Weight [kg], M ±SD	78.6 ±13.6	78.6 ±13.8	78.5 ±12.3	0.3521#
BMI [kg/m²], M ±SD	28.2 ±4.2	28.2 ±4.1	28.1 ±3.6	0.3011#
NYHA class, n (%)				
0	152 (50.4)	127 (50.2)	25 (54.3)	
I	23 (7.8)	21 (8.3)	2 (4.5)	
II	49 (16.6)	42 (16.6)	7 (15.2)	0.1921*
III	65 (21.8)	57 (22.5)	8 (17.4)	
IV	10 (3.4)	6 (2.4)	4 (8.6)	
CAD [months], M ±SD	60.3 ±112.2	64.9 ±130.5	61.2 ±114.8	0.0001#
Smoking, n (%)	103 (34.4)	90 (35.6)	13 (28.3)	0.2564*
ESlog	6.4 ±7.5	6.2 ±9.8	6.5 ±7.6	0.0064#
CSS class, n (%)				
I	9 (3.7)	8 (3.9)	1 (2.6)	
II	58 (23.9)	50 (24.4)	8 (21.1)	
III	132 (54.3)	109 (53.2)	23 (60.5)	0.8632$
IV	44 (18.1)	38 (18.5)	6 (15.8)	
Costs [PLN]	7969 ±10770	6953 ±7093	13556 ±21181	0.014#
Hospital stay [days]	8.61 ±6.2	8.06 ±5.1	11.65 ±10.2	0.021$
In-hospital mortality, n (%)	8 (2.67)	6 (2.01)	2 (4.34)	0.524*

M ±SD – mean ± standard deviation; CAD – coronary artery disease; BMI – body mass index; CSS – Canadian Cardiovascular Society; NYHA – New York Heart Association; ESlog – logistic EUROScore; * Fisher's exact test; # Mann–Whitney U test; $ χ^2 Pearson's test.

infection in 15 patients (32.6%) and pneumonia in 10 patients (21.8%). The occurrence of infections did not affect hospital mortality, but it significantly extended the hospitalization time (p = 0.021) and significantly increased the overall cost of treatment (p = 0.014) (Table 1). Vacuum-assisted closure (VAC) therapy was not used in any of the cases studied. Of the patients in the study group, 8 died during hospitalization.

Hospital mortality in the study group was 2.67% and did not differ statistically between the groups of patients with and without infections. The univariate analysis showed that older age (p = 0.018), clamping time (p = 0.002), longer duration of CAD (p = 0.001), concentration of creatine kinase-MB (CKMB) >100 during the postoperative period (p = 0.001), increased drainage during the postoperative period (p = 0.001), and a higher NYHA classification score before surgery (p = 0.001) significantly increased the risk of hospital death. Due to the small number of deaths in the study group, it was not possible to demonstrate significance in the multivariate analysis. When analyzing the causes of death, in 2 cases it was possible to unequivocally indicate an infection as the direct cause of death, and in both cases, the patients died of sepsis. Of the remaining 6 cases, 4 suffered a perioperative infarction, while the remaining 2 died of multiple organ failure.

The compositions of genotypes were coherent with the Hardy–Weinberg equilibrium model for all *TLR2* and *TLR4* single-nucleotide polymorphisms (SNPs) in patients with and without infection.

Of the 299 patients, 158 (52.8%) were TA heterozygous with *TLR2* T-16934A (rs4696480) SNPs. The AA variant was identified in 68 cases (22.8%) and the TT variant was identified in 74 cases (24.8%). There were no statistically significant differences among the infected and non-infected groups in relation to SNPs of the T-16934A *TLR2* polymorphisms. Approximately 93% of cases were GG wild-type homozygous for the *TLR2* Arg753Gln (rs5743708). Regarding the *TLR2* Arg753Gln (rs5743708) polymorphism, 21 (7.1%) of the participants were GA heterozygotes, and there were no homozygous patients in the whole study group.

It was also found that in the 299 patients who were investigated for the inherence of *TLR4* D299G SNP (rs4986790), nearly 90% (260/299) were AA homozygous, with the absence of this mutation. The AG polymorphism was observed in 38 individuals (12.7%), whereas the GG variant was observed in only 1 individual. In further evaluations, both AG and GG subgroups were treated as one. In addition, of the 299 patients who were screened for the presence of the *TLR4* T399I SNP (rs4986791), 86.9% of the patients (260/299) were CC homozygous. The CT genotype was seen in 38 cases (12.7%), whereas the TT variant was found in only 1 individual. In further evaluations, both CT and TT subgroups were treated as one. The *TLR4* genotyping showed that the AG+GG variants of D299G (rs4986790) and CT+TT variants of T399I (rs4986791) were more often observed in patients with postoperative infections (Table 2). Logistic regression demonstrated that the presence of the AG+GG variants of D299G (rs4986790) and CT+TT variants of T399I (rs4986791) were related to a higher incidence of infection in patients undergoing CAGB procedures (Table 3).

Table 2. The relationship between analyzed genotypes and postoperative infections

TLR polymorphism	Hardy–Weinberg equilibrium p-value	Infection status, n (%)		p-value*	Total, n (%)
		non-infected	infected		
TLR2 R753Q					
GG (wild-type)		238 (93.0)	41 (95.3)		279 (93.3)
GA	0.549	18 (7.0)	2 (4.7)	0.749	20 (6.7)
AA		0	0		0
Total		256 (100)	43 (100)		299 (100)
TLR2 T16934A					
TA		130 (50.8)	28 (65.2)		158 (52.8)
TT	0.288	64 (25.0)	9 (20.9)	0.184	73 (24.4)
AA		62 (24.2)	6 (13.9)		68 (22.8)
Total		256 (100)	43 (100)		299 (100)
TLR4 D299G					
AA		227 (89.7)	33 (71.7)		260 (86.9)
AG+GG	0.288	26 (10.3)	13 (28.3)	0.003	39 (13.1)
Total		253 (100)	46 (100)		299 (100)
TLR4 T399I					
CC		226 (89.3)	33 (71.7)		259 (86.6)
CT+TT	0.288	27 (10.7)	13 (28.3)	0.003	40 (23.4)
Total		253 (100)	233 (100)		299 (100)

Table 3. Logistic regression

Variable	HR	95% CI	SE	p-value
TLR4 D299G AA variant	3.665	1.655–8.114	0.403	0.001
TLR4 T399I CC variant	3.532	1.601–7.790	0.401	0.002
Blood loss	2.119	1.351–3.581	0.247	0.002

HR – hazard risk; 95% CI – 95% confidence interval; SE – standard error.

Discussion

Postoperative infections are common healthcare-associated problems, and, unfortunately, are serious complications in patients undergoing cardiac surgery. This group of patients differs substantially from patients undergoing surgery in other surgical departments due to the detrimental impact of the cardiopulmonary pump circuit. This leads to a widespread initiation of the innate immune system and subsequently affects the response to pathogens.[15] Previous research has demonstrated a prevalence of postoperative infections ranging from 4.9% to approx. 22% in cardiac surgery wards.[1–3] Gelinjs et al. showed a prevalence of 4.9% in a cohort of 5158 patients.[1] In contrast, Kollef et al. demonstrated a higher prevalence of 21.7%.[3] These variations could be in part due to a discrepancy in the diagnostic criteria used, materials and methods, the inclusion criteria applied, infection control guidelines used, or the types of cardiac surgery interventions performed. This study demonstrated an overall prevalence of hospital-acquired infections (HAI) that was relatively high at 15.3%, which was surprising for the authors. The most likely cause of this phenomenon may be an over-diagnosis of infections by the attending physicians and, consequently, the excess use of antibiotics. Regardless of the infection criteria used, in the case of SSIs, the existence of purulent exudates from the incision site requires subjective assessment. Similarly, in the case of pneumonia, the presence of novel or increasing/sustained infiltrates, consolidations or cavitations was also assessed subjectively. Moreover, the authors were not able to state whether all of the abovementioned criteria were applied in these cases. Our thesis was indirectly confirmed by the fact that there was no need for VAC therapy in patients with surgical site infections. On the other hand, the reported prevalence of hospital-acquired infections is similar to the results of research conducted by van Klarenbosch et al. in 2020,[16] which was reported to be 14.5%. The similarities in both studies can be attributed to several factors such as BMI, ESlog, transfusions requirements, and CPB time. In our study, surgical site infections were the most common and were present in 21 patients (45.6%), followed by bloodstream infection in 15 patients (32.6%), and pneumonia, which was diagnosed in 10 patients (21.8%). The incidence of pneumonia was comparable to other authors' studies.[17,18] The mortality rate observed in our study group did not differ from that reported in other studies, and only slightly exceeded 2%, which was not related to the occurrence or lack of postoperative infections.[19]

In our research, we raised the issue of whether *TLR2* or *TLR4* polymorphisms are related to the occurrence of postoperative infections in cardiac surgery patients undergoing a CABG procedure. Genetic analysis of 2 *TLR2* SNPs (rs4696480 and rs5743708) and 2 *TLR4* SNPs (rs4986790 and rs4986791) led to each of the 4 variants being identified. The allele prevalence of the examined *TLR2* and *TLR4* polymorphisms strongly match the results reported by other authors.[20,21] We were not able to demonstrate any significant disparity in *TLR2* SNPs variants among patients with and without postoperative infections. However, we managed to show a significant correlation between *TLR4* (AG+GG of D299G) and (CT+TT of T399I) SNPs in comparison to wild-type carriers and the incidence of post-CABG infections in cardiac surgery patients. The relationship between carriers of the TLR polymorphisms and the development of infection has been studied in various groups of patients. In a group of 155 acute myeloid leukemia cases, Schnetzke et al. reported a relationship between *TLR4* and *TLR2* polymorphisms and the incidence of sepsis in their study group.[22] Other authors also demonstrated that the Arg753Gln of the *TLR2* mutation was significantly correlated with a greater incidence of pneumonia in a group of patients with acute myeloid leukemia (AML) undergoing a chemotherapy induction protocol. Papadopoulos et al. were able to demonstrate an association between the 2 *TLR4* polymorphisms and the occurrence of serious infections in a cohort of 199 human immunodeficiency virus (HIV)-positive patients.[23] However, other authors failed to establish a significant relationship between *TLR2* and *TLR4* polymorphisms and the occurrence of infections.[24]

In our research, the significant influence of *TLR4* polymorphisms on the predisposition of CABG individuals to postoperative infections could partly be explained by the expression of *TLR4* on enteric epithelium cells, pulmonary epithelial cells and other cells playing the role in recognizing infectious particles and initiating as well as managing a major immune reaction against various groups of pathogens.[25] While *TLR4* primarily identifies Gram-negative bacterial molecules, *TLR2* is able to identify a range of molecules, such as Gram-positive and Gram-negative bacterial components.[26,27] The TLRs play an extremely important role, not only as PRRs, but also through their effect on damage-associated molecular patterns (DAMPs) as well as high-mobility group proteins, heat shock proteins, phospholipids, and others. The SNPs alone are not sufficient to explain the entire genetic component involved

in the development of infections.[26,27] However, the importance of polymorphisms in TLR alleles and the interaction of SNPs in infections requires further investigation.

Limitations of the study

The main limitation of our study is its retrospective nature. Another limitation is the probable over-diagnosis of infections due to the subjective assessment of clinical symptoms and radiological images. Finally, the group of patients was relatively small. However, multivariable evaluation was still possible.

Conclusions

In summary, this research is the first of its kind to demonstrate that *TLR2* and *TLR4* mutations affect the risk of post-CABG infections. The frequency of the various alleles in our study population is in accordance with the current literature. Our study did not show an association between the analyzed SNPs in *TLR2* and susceptibility to infections. Carriers of the AG+GG of D299G (rs4986790) or CT+TT of T399I (rs4986791) *TLR4* variants can contribute to the prevalence of infections during the perioperative period in patients undergoing CAGB procedures.

ORCID iDs

Agnieszka Żukowska https://orcid.org/0000-0001-8918-1247
Andrzej Ciechanowicz https://orcid.org/0000-0002-3804-440X
Mariusz Kaczmarczyk https://orcid.org/0000-0002-0180-644X
Mirosław Brykczyński https://orcid.org/0000-0003-4621-5907
Maciej Żukowski https://orcid.org/0000-0001-5733-0818

References

1. Gelijns AC, Moskowitz AJ, Acker MA, et al. Management practices and major infections after cardiac surgery. *J Am Coll Cardiol*. 2014;64(4): 372–381. doi:10.1016/j.jacc.2014.04.052
2. Massart N, Mansour A, Ross JT, et al. Mortality due to hospital-acquired infection after cardiac surgery. *J Thorac Cardiovasc Surg*. 2022;163(6):2131–2140.e3. doi:10.1016/j.jtcvs.2020.08.094
3. Kollef MH, Sharpless L, Vlasnik J, Pasque C, Murphy D, Fraser VJ. The impact of nosocomial infections on patient outcomes following cardiac surgery. *Chest*. 1997;112(3):666–675. doi:10.1378/chest.112.3.666
4. Cove ME, Spelman DW, MacLaren G. Infectious complications of cardiac surgery: A clinical review. *J Cardiothorac Vasc Anesth*. 2012;26(6): 1094–1100. doi:10.1053/j.jvca.2012.04.021
5. Jiang WL, Hu XP, Hu ZP, et al. Morbidity and mortality of nosocomial infection after cardiovascular surgery: A report of 1606 cases. *Curr Med Sci*. 2018;38(2):329–335. doi:10.1007/s11596-018-1883-4
6. Michalopoulos A, Geroulanos S, Rosmarakis ES, Falagas ME. Frequency, characteristics, and predictors of microbiologically documented nosocomial infections after cardiac surgery. *Eur J Cardiothorac Surg*. 2006;29(4):456–460. doi:10.1016/j.ejcts.2005.12.035
7. Werling D, Jann OC, Offord V, Glass EJ, Coffey TJ. Variation matters: TLR structure and species-specific pathogen recognition. *Trends Immunol*. 2009;30(3):124–130. doi:10.1016/j.it.2008.12.001
8. Akira S, Uematsu S, Takeuchi O. Pathogen recognition and innate immunity. *Cell*. 2006;124(4):783–801. doi:10.1016/j.cell.2006.02.015
9. Takeuchi O, Akira S. Pattern recognition receptors and inflammation. *Cell*. 2010;140(6):805–820. doi:10.1016/j.cell.2010.01.022
10. Aluri J, Cooper MA, Schuettpelz LG. Toll-like receptor signaling in the establishment and function of the immune system. *Cells*. 2021; 10(6):1374. doi:10.3390/cells10061374

11. European Centre for Disease Prevention and Control (ECDC). *Point Prevalence Survey of Healthcare-Associated Infections and Antimicrobial Use in European Acute Care Hospitals: 2011 and 2012*. Solna, Sweden: ECDC Publications Office; 2013. https://www.ecdc.europa.eu/sites/default/files/media/en/publications/Publications/healthcare-associated-infections-antimicrobial-use-PPS.pdf. Accessed August 26, 2022.
12. Horan TC, Gaynes RP, Martone WJ, Jarvis WR, Emori TG. CDC definitions of nosocomial surgical site infections, 1992: A modification of CDC definitions of surgical wound infections. *Infect Control Hosp Epidemiol*. 1992;13(10):606–608. PMID:1334988.
13. European Centre for Disease Prevention and Control (ECDC). *Point Prevalence Survey of Healthcare-Associated Infections and Antimicrobial Use in European Acute Care Hospitals: Protocol Version 5.3: ECDC PPS 2016–2017*. Solna, Sweden: ECDC Publications Office; 2016. https://data.europa.eu/doi/10.2900/374985. Accessed August 26, 2022.
14. Żukowski M, Taryma-Leśniak O, Kaczmarczyk M, et al. Relationship between toll-like receptor 2 R753Q and T16934A polymorphisms and *Staphylococcus aureus* nasal carriage. *Anaesthesiol Intensive Ther*. 2017;49(2):110–115. doi:10.5603/AIT.a2017.0027
15. Wang YC, Wu HY, Luo CY, Lin TW. Cardiopulmonary bypass time predicts early postoperative Enterobacteriaceae bloodstream infection. *Ann Thorac Surg*. 2019;107(5):1333–1341. doi:10.1016/j.athoracsur.2018.11.020
16. van Klarenbosch J, van den Heuvel ER, van Oeveren W, de Vries AJ. Does intraoperative cell salvage reduce postoperative infection rates in cardiac surgery? *J Cardiothorac Vasc Anesth*. 2020;34(6):1457–1463. doi:10.1053/j.jvca.2020.01.023
17. Beckmann A, Funkat AK, Lewandowski J, et al. German Heart Surgery Report 2016: The annual updated registry of the German Society for Thoracic and Cardiovascular Surgery. *Thorac Cardiovasc Surg*. 2017;65(07):505–518. doi:10.1055/s-0037-1606603
18. Jacobs JP, Shahian DM, D'Agostino RS, et al. The Society of Thoracic Surgeons National Database 2017 Annual Report. *Ann Thorac Surg*. 2017;104(6):1774–1781. doi:10.1016/j.athoracsur.2017.10.014
19. Kuliczkowska-Płaksej J, Jończyk M, Jawiarczyk-Przybyłowska A, et al. The frequency of *TLR2* (rs3804099, rs3804100, and rs5743708) and *TLR4* (rs4986790 and rs4986791) polymorphisms in women with polycystic ovary syndrome: Preliminary study. *Gynecol Endocrinol*. 2021;37(11):1027–1034. doi:10.1080/09513590.2021.1952975
20. Pabst S, Yenice V, Lennarz M, et al. Toll-like receptor 2 gene polymorphisms Arg677Trp and Arg753Gln in chronic obstructive pulmonary disease. *Lung*. 2009;187(3):173–178. doi:10.1007/s00408-009-9144-8
21. Schnetzke U, Spies-Weisshart B, Yomade O, et al. Polymorphisms of Toll-like receptors (*TLR2* and *TLR4*) are associated with the risk of infectious complications in acute myeloid leukemia. *Genes Immun*. 2015;16(1):83–88. doi:10.1038/gene.2014.67
22. Papadopoulos AI, Ferwerda B, Antoniadou A, et al. Association of Toll-like receptor 4 Asp299Gly and Thr399Ile polymorphisms with increased infection risk in patients with advanced HIV-1 infection. *Clin Infect Dis*. 2010;51(2):242–247. doi:10.1086/653607
23. Ahmad-Nejad P, Denz C, Zimmer W, et al. The presence of functionally relevant Toll-like receptor polymorphisms does not significantly correlate with development or outcome of sepsis. *Genet Test Mol Biomarkers*. 2011;15(9):645–651. doi:10.1089/gtmb.2010.0258
24. Vogel SN, Awomoyi AA, Rallabhandi P, Medvedev AE. Mutations in *TLR4* signaling that lead to increased susceptibility to infection in humans: An overview. *J Endotoxin Res*. 2005;11(6):333–339. doi:10.1179/096805105X58724
25. Prohinar P, Rallabhandi P, Weiss JP, Gioannini TL. Expression of functional D299G.T399I polymorphic variant of *TLR4* depends more on coexpression of MD-2 than does wild-type *TLR4*. *J Immunol*. 2010;184(8): 4362–4367. doi:10.4049/jimmunol.0903142
26. Tellería-Orriols JJ, García-Salido A, Varillas D, Serrano-González A, Casado-Flores J. TLR2–TLR4/CD14 polymorphisms and predisposition to severe invasive infections by *Neisseria meningitidis* and *Streptococcus pneumoniae*. *Med Intensiv*. 2014;38(6):356–362. doi:10.1016/j.medin.2013.08.006
27. Lee SO, Brown RA, Kang SH, Abdel-Massih RC, Razonable RR. Toll-like receptor 2 polymorphism and Gram-positive bacterial infections after liver transplantation. *Liver Transpl*. 2011;17(9):1081–a1088. doi:10.1002/lt.22327

Fracture risk and fracture prevalence in women from outpatient osteoporosis clinic and subjects from population-based sample: A comparison between GO Study and RAC-OST-POL cohorts

Wojciech Pluskiewicz[1,A,B,D,F], Piotr Adamczyk[2,C,D], Bogna Drozdzowska[3,A,E,F]

[1] Department and Clinic of Internal Diseases, Diabetology and Nephrology, Metabolic Bone Diseases Unit, Faculty of Medical Sciences in Zabrze, Medical University of Silesia in Katowice, Poland

[2] Department of Pediatrics, Faculty of Medical Sciences in Katowice, Medical University of Silesia in Katowice, Poland

[3] Department of Pathomorphology, Faculty of Medical Sciences in Zabrze, Medical University of Silesia in Katowice, Poland

A – research concept and design; B – collection and/or assembly of data; C – data analysis and interpretation;
D – writing the article; E – critical revision of the article; F – final approval of the article

Address for correspondence
Wojciech Pluskiewicz
E-mail: osteolesna@poczta.onet.pl

Abstract

Background. The method of recruiting the study subjects is an important element of the study design. It can have a strong influence on the results. Different recruitment schedules can give a different picture of the studied phenomenon.

Objectives. The aim of the study was to compare bone health in a group of female patients treated for osteoporosis with a population-based sample.

Materials and methods. A cohort of women from GO Study from 1 outpatient osteoporotic clinic (n = 1442, mean age 65.8 ±6.7 years) and population-based female sample of RAC-OST-POL Study (n = 963, mean age 65.8 ±7.5 years) were studied. Mean age did not differ between groups. Mean weight, height and body mass index (BMI) in subjects from GO Study and RAC-OST-POL Study were 69.5 ±13.1 kg, 157.8 ±6.1 cm and 27.9 ±5.1 kg/m², and 74.2 ±13.7 kg, 156.0 ±6.0 cm and 30.5 ±5.4 kg/m², respectively, and differed significantly (p < 0.0001 for each variable). Data on clinical risk factors for osteoporosis and fractures were collected. Bone densitometry at hip was performed using a Prodigy or Lunar DPX device (GE Healthcare, Waukesha, USA). Fracture risk was established using FRAX, Garvan and POL-RISK.

Results. Mean values of T-score for femoral neck in subjects from GO Study and RAC-OST-POL Study were −1.67 ±0.91 and −1.27 ±0.91 and differed significantly (p < 0.0001). In GO Study and RAC-OST-POL Study, there were 518 (35.9%) and 280 (29.1%) subjects with fractures, respectively. The fracture frequency was significantly higher in the GO Study group (p < 0.001). Among clinical risk factors, only rheumatoid arthritis (p < 0.0001) secondary osteoporosis (p < 0.0001) and falls (p < 0.0001) were more frequent in RAC-OST-POL Study. Fracture risk established using FRAX, Garvan and POL-RISK calculators was significantly greater in patients enrolled in the GO Study than in subjects from the RAC-OST-POL population-based sample (p < 0.0001 for each variable).

Conclusions. Differences noted between female patients treated for osteoporosis and population-based sample, especially in regard to fracture risk, reveal a strong influence of recruitment criteria on study results in the field of bone health and osteoporosis.

Key words: bone mineral density, females, clinical risk factors, fracture risk, fracture incidence

Background

The most informative results describing health problems associated with widespread diseases such as osteoporosis can be obtained from representative population samples. However, in daily practice, data gathered according to different inclusion criteria are often presented. It is not clear whether bone health and many specific features such as fracture incidence, the number of clinical risk factors for fractures, and functional status expressed by the number of falls really differ between population-based samples and patients treated for osteoporosis. Such knowledge would be important and helpful for practitioners in daily practice and proper interpretation of a results of their studies. In 2010, a study called RAC-OST-POL was performed.[1] In this study, an epidemiological, population-representative female sample was recruited. This cohort was then studied in regard to various aspects of bone health.[2–12]

More recently, we presented data from a large group of female patients enrolled when attending a single outpatient osteoporosis clinic; this research was published in consecutive papers and identified with the acronym GO Study.[13–15] In recent years, methods for fracture risk assessment were developed,[12,16–18] and fracture risk assessment became an important part of the examination of patients. Nowadays, fracture risk is one of the most important criteria for the initiation of pharmacologic treatment. We consider the comparisons between clinical risk factors and fracture risk in a population-based sample and regular osteoporotic patients to be an important issue.

Objectives

This study aimed to test 2 hypotheses. The 1st is that data describing bone health, e.g., clinical risk factors for fracture, bone mineral density (BMD) and fracture risk, collected in a group of patients treated for osteoporosis, are different from those obtained from a population-based sample. The 2nd hypothesis is related to fracture prevalence in compared cohorts. One may expect the bone status in osteoporosis patients to be worse and these patients to have a higher fracture prevalence than randomly recruited subjects.

Materials and methods

Material

Postmenopausal women from the GO Study were recruited from 1 osteoporosis outpatient clinic in Gliwice in southern Poland. This cohort was previously described in detail.[13] Postmenopausal females were also selected for the RAC-OST-POL Study and recruited according to a population-representative design from the urban area of Racibórz (also southern Poland) and the surrounding rural areas.[1] In both studies, women over 55 years were enrolled. For the current analysis, to obtain reliable comparisons, age-adjusted cohorts were selected. Finally, 1442 women from the original GO Study cohort (including osteoporotic clinic patients) and 963 women from a randomly selected, population-based RAC-OST-POL sample were enrolled in the current study.

In the RAC-OST-POL study, the cohort consisted of women who positively responded to the invitation to participate in the study. The list of invited persons was prepared randomly, based on contact data obtained from the City Hall, and took into account the demographic structure of the population in the region. Health status was not a factor taken into account when recruiting; however, it was assessed during the course of the study. The GO Study included women referred to an osteoporosis outpatient clinic or who presented on their own initiative to this facility. Therefore, they were patients with suspected bone health problems, determined based on their medical or family history. Some participants also reported for an osteoporosis screening or were looking for preventive advice.

Both the GO Study and RAC-OST-POL Study were approved by the Ethics Committee of the Medical University of Silesia, Katowice, Poland. Participants from both studies gave their written consent for enrollment into the study. The study design complied with the Declaration of Helsinki.

Mean weight, height and body mass index (BMI) in subjects from the GO Study and RAC-OST-POL Study were 69.5 ±13.1 kg, 157.8 ±6.1 cm and 27.9 ±5.1 kg/m², and 74.2 ±13.7 kg, 156.0 ±6.0 cm and 30.5 ±5.4 kg/m², respectively, and differed significantly (p < 0.0001 for each variable).

Methods

Data on the clinical aspects influencing bone health (clinical risk factors for fractures, e.g., smoking, secondary osteoporosis, falls, rheumatoid arthritis, and hip fractures in parents) were self-reported by patients in both groups. Study participants also reported previous osteoporotic fractures. The number of falls was established regarding the year prior to data collection. Bone mineral density was measured on the non-dominant femoral neck (FN). Bone status was established using the densitometer device Prodigy (GE Healthcare, Waukesha, USA) in the GO Study and Lunar DPX (GE Healthcare) in the RAC-OST-POL Study. The precision of measurement expressed as the coefficient of variation (CV%) was 1.6% in both studies.[1,13]

Fracture risk (expressed as the probability of experiencing a fracture during a defined period) was established using FRAX™ (www.sheffield.ac.uk), the Garvan calculator (www.frractureriskcalculator.com) and the Polish algorithm POL-RISK (www.fracture-risk.pl) online tools. The FRAX

expresses fracture risk as the probability of a major osteoporotic fracture and a hip fracture in the next 10 years. Garvan presents data for fracture risk for any fracture and hip fractures over a 5- and 10-year period. The POL-RISK algorithm expresses the risk of fracture for any fracture during a 5-year period.

Statistical analyses

Statistical analysis was performed using Statistica software v. 12 (StatSoft Inc., Tulsa, USA). Absolute values and percentages were provided for qualitative variables. The mean values and standard deviations (M ±SD) were used for descriptive statistics of continuous variables. The normality of data distribution was verified using the Shapiro–Wilk test. After checking the test assumptions, the Mann–Whitney U test was applied for the comparisons of continuous variables between the groups. Comparisons of qualitative features such as frequency were performed using the χ^2 test. The significance of the results in all of the statistical analyses was assumed at a $p < 0.05$.

Results

The mean values of T-scores for the FN in subjects from the GO Study and the RAC-OST-POL Study were −1.67 ±0.91 and −1.27 ±0.91, respectively, and differed significantly ($p < 0.0001$). In Table 1, the data on clinical risk factors for fractures are presented. The incidence of smoking, hip fracture and glucocorticoid use did not differ between the compared cohorts, whereas rheumatoid
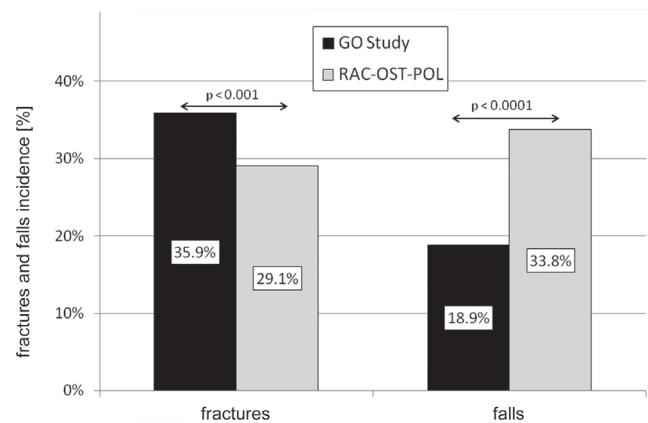

Fig. 1. Incidence of fractures and falls [%] in GO Study and RAC-OST-POL Study cohorts

arthritis and secondary osteoporosis were more frequent in subjects from the RAC-OST-POL Study.

In the GO Study and the RAC-OST-POL Study, there were 518 (35.9%) and 280 (29.1%) subjects who reported previous fractures, respectively. The χ^2 testing showed the fracture frequency to be significantly higher in subjects from the GO Study ($p < 0.001$). The respective total number of fractures (including multiple fractures in the same subjects) were significantly higher in GO Study patients (n = 869) compared to the population-based sample (n = 366, $p < 0.0001$).

Falls were noted more often in subjects from the RAC-OST-POL cohort (n = 326, 33.8%) than in the GO Study (n = 273, 18.9%, $p < 0.0001$). The respective total numbers of falls were 526 and 490, and differed significantly ($p < 0.0001$). The incidences of fractures and falls in both study cohorts are presented in Fig. 1.

Table 1. The incidence of clinical risk factors for fractures [%]

Fracture risk factor	GO Study (n = 1442)	RAC-OST-POL Study (n = 963)	χ^2 statistics	p-value
Smoking	13.4	10.9	3.27	NS
Rheumatoid arthritis	1.5	7.3	51.77	<0.0001
Glucocorticoid use	6.8	5.5	1.64	NS
Hip fractures in parents	5.5	6.7	1.66	NS
Secondary osteoporosis	5.5	25.3	193.98	<0.0001

NS – not significant.

Table 2. Fracture risk assessment established by fracture risk calculators (M ±SD)

Method of fracture risk assessment	GO Study (n = 1442)	RAC-OST-POL Study (n = 963)	Z value	p-value*
FRAX major fractures	7.02 ±4.91	5.85 ±4.03	6.93	<0.0001
FRAX hip fractures	2.35 ±3.80	1.55 ±2.48	8.91	<0.0001
Garvan – 5-year any fractures	12.76 ±12.04	9.85 ±9.16	7.01	<0.0001
Garvan – 5-year hip fractures	5.22 ±10.26	3.23 ±7.20	7.81	<0.0001
Garvan – 10-year any fractures	23.76 ±18.06	18.99 ±14.35	7.06	<0.0001
Garvan – 10-year hip fractures	9.13 ±14.85	5.86 ±10.69	7.57	<0.0001
POL-RISK – 5-year any fractures	13.52 ±9.40	10.96 ±7.21	7.09	<0.0001

M ±SD – mean ± standard deviation. * Mann–Whitney U test.

Data for fracture risk assessment are presented in Table 2. The values of fracture risk established using FRAX, Garvan and POL-RISK were significantly greater in GO Study patients than in patients from the population-based sample ($p < 0.0001$).

Discussion

To our knowledge, the current study is the first of its kind showing a comparison of data on fractures, clinical risk factors for fractures and falls, BMD and fracture risk assessment between female osteoporosis clinic patients and a population-based sample. Some expected and unexpected observations were noted.

First, one might expect that the incidence of fractures would be higher in osteoporosis clinic patients. Patients with prior fractures are obvious candidates for consultation from a physician, post-fracture diagnostic procedures and bone health treatment considerations. The higher fracture incidence in these patients compared to the general population was confirmed in our study and this result might be treated as an expected one.

Second, lower values of BMD expressed by FN T-scores were noted in patients from the GO Study, making it one (perhaps the most important one) of the reasons for the higher fracture incidence. One might expect that the osteoporotic clinic is visited by patients with overall worse bone health.

Third, we found the differences in anthropometric parameters very interesting. Patients from the GO Study cohort had a higher mean height, while the population-representative sample had a higher body weight and BMI. Height has been identified as a factor modifying the risk of fractures in the FRAX[16] and POL-RISK[12] calculators. Contrarily, an excessive body mass reduction, especially during the postmenopausal period, results not only in adipose tissue reduction, but also a lower lean body mass, and may have an adverse effect on bone health.[19] Thus, the higher BMI in the population-based sample from the RAC-OST-POL Study can be regarded as a protective factor in terms of fracture risk.

Fourth, the role of rheumatoid arthritis and secondary osteoporosis on fracture risk seems to be limited, despite these conditions being more frequently reported in the RAC-OST-POL Study sample, as the number of fractures was lower in this cohort. This may also reflect the impact of the data collection method on identifying relevant clinical factors. In the GO Study, complete medical records were available for each patient. Data collection in the population-based RAC-OST-POL Study was performed by filling in a questionnaire during a one-time meeting with the study participant, without verification based on medical records. Thus, the diagnosis of rheumatoid arthritis could have been overinterpreted, e.g., senile joint pain could have been declared as rheumatoid arthritis.

Fifth, the observed higher incidence of falls in the RAC-OST-POL Study sample did not cause an increased number of fractures. One may consider that, despite the poorer functional status in this population, the better bone status was a protective factor against fracture.

In our view, the most valuable point of this study is the fracture risk assessment compared between groups with different enrollment protocols. In recent years, methods of fracture risk assessment have become one of the most important elements of patient's health status evaluation. Such information is especially helpful in making decisions about the implementation of pharmacological therapy. The significantly higher fracture risk shown by all 3 calculators indicates that osteoporosis clinic patients require more attention in terms of therapy, and need treatment more frequently than subjects representing the general population.

It is not easy to summarize the obtained results. Some expected and unexpected observations suggest that the methodology used in subject enrollment and data collection may have significantly influenced the final study results. A population-based cohort had a better bone status with a lower fracture incidence despite more frequent falls, rheumatoid arthritis and secondary osteoporosis. Contrarily, osteoporosis clinic patients displayed a worse bone status and higher fracture incidence. We believe that the main factor influencing the incidence of fractures was bone health, whereas functional status, rheumatoid arthritis and secondary causes of osteoporosis were less significant than expected. Finally, the most important observation concerns the results documenting fracture risk, which indicated that special attention should be paid to osteoporosis clinic patients.

A review of the literature did not reveal many publications comparing the results from outpatient- or hospital-based cohorts with population-based studies for this topic and also in other areas of medical research. The few analyses of this type show that the research results may depend on the analyzed topic. A study assessing the quality of life depending on the method of treatment for intracranial vascular malformations found no differences in the results depending on the method of recruitment used in the study cohort.[20] On the other hand, an analysis of the relationship between psoriasis and metabolic syndrome yielded different results in a population-based sample when compared to hospitalized patients.[21] In the context of this scarce information, our analysis shows a clear difference in the clinical characteristics of patients in an osteoporosis outpatient clinic compared to a population-representative cohort, and sheds new light on osteoporosis research.

Our research strongly support the principle that the study design is a factor that "a priori" modifies the obtained results. Interpretation of the results cannot be carried out without taking into consideration the knowledge of the study design. Even a large sample size in a studied cohort does not allow one to draw conclusions regarding

the entire population unless the study sample has been properly selected. Observed differences between osteoporosis clinic patients and a population-based cohort, especially regarding fracture incidence and bone status, suggest that clinic patients cannot be treated as a representative sample.

Limitations of the study

The presented manuscript is a compilation of data from 2 separate studies. Patients came from different, although geographically close, recruitment areas. The data collection was performed only among female patients.

Conclusions

In conclusion, fracture risk and fracture incidence are higher among women treated in an osteoporosis outpatient clinic compared to the general population. While this is not a surprising observation, it is noteworthy to consider that it did not correlate with a higher incidence of multiple fracture risk factors in the clinic group. Interestingly, the incidence of falls was significantly higher in the population-based sample than among osteoporotic patients.

ORCID iDs

Wojciech Pluskiewicz ⓘ https://orcid.org/0000-0003-1839-6560
Piotr Adamczyk ⓘ https://orcid.org/0000-0001-9557-221X
Bogna Drozdzowska ⓘ https://orcid.org/0000-0002-2287-6842

References

1. Pluskiewicz W, Adamczyk P, Czekajło A, Grzeszczak W, Burak W, Drozdzowska B. Epidemiological data on osteoporosis in women from the RAC-OST-POL study. *J Clin Densitom*. 2012;15(3):308–314. doi:10.1016/j.jocd.2012.01.003
2. Pluskiewicz W, Adamczyk P, Marek B, et al. Adiponectin and resistin in relationship with skeletal status in women from the RAC-OST-POL study. *Endokrynol Pol*. 2012;63(6):427–431. PMID:23338999.
3. Włodarek D, Głąbska D, Kołota A, et al. Calcium intake and osteoporosis: The influence of calcium intake from dairy products on hip bone mineral density and fracture incidence – a population-based study in women over 55 years of age. *Public Health Nutr*. 2014;17(2):383–389. doi:10.1017/S1368980012005307
4. Pluskiewicz W, Adamczyk P, Czekajło A, Grzeszczak W, Drozdzowska B. Influence of education, marital status, occupation, and the place of living on skeletal status, fracture prevalence, and the course and effectiveness of osteoporotic therapy in women in the RAC-OST-POL Study. *J Bone Miner Metab*. 2014;32(1):89–95. doi:10.1007/s00774-013-0471-8
5. Drozdzowska B, Wiktor K, Pluskiewicz W. Functional status and prevalence of falls and fractures in population-based sample of postmenopausal women from the RAC-OST-POL Study. *Int J Clin Pract*. 2013;67(7):673–681. doi:10.1111/ijcp.12118
6. Rokicki W, Drozdzowska B, Czekajło A, et al. Common ophthalmic problems of urban and rural postmenopausal women in a population sample of Raciborz district: A RAC-OST-POL Study. *Ann Agric Environ Med*. 2014;21(1):70–74. PMID:24738500.
7. Pluskiewicz W, Adamczyk P, Czekajło A, Grzeszczak W, Drozdzowska B. High fracture probability predicts fractures in a 4-year follow-up in women from the RAC-OST-POL study. *Osteoporos Int*. 2015;26(12):2811–2820. doi:10.1007/s00198-015-3196-9
8. Pluskiewicz W, Adamczyk P, Czekajło A, Grzeszczak W, Drozdzowska B. Falls in RAC-OST-POL Study: Epidemiological study in postmenopausal women aged over 55 years [in Polish]. *Endokrynol Pol*. 2016;67(2):185–189. doi:10.5603/EP.a2016.0015
9. Głąbska D, Włodarek D, Kołota A, Czekajło A, Drozdzowska B, Pluskiewicz W. Assessment of mineral intake in the diets of Polish postmenopausal women in relation to their BMI – the RAC-OST-POL study: Mineral intake in relation to BMI. *J Health Popul Nutr*. 2016;35(1):23. doi:10.1186/s41043-016-0061-1
10. Rokicki W, Drozdzowska B, Czekajło A, et al. Relationship between visual status and functional status and the risk of falls in women: The RAC-OST-POL study. *Arch Med Sci*. 2016;12(6):1232–1238. doi:10.5114/aoms.2015.55146
11. Bach M, Werner A, Żywiec J, Pluskiewicz W. The study of under- and over-sampling methods' utility in analysis of highly imbalanced data on osteoporosis. *J Inf Sci*. 2017;384:174–190. doi:10.1016/j.ins.2016.09.038
12. Adamczyk P, Werner A, Bach M, et al. Risk factors for fractures identified in the algorithm developed in 5-year follow-up of postmenopausal women from RAC-OST-POL Study. *J Clin Densitom*. 2018;21(2):213–219. doi:10.1016/j.jocd.2017.07.005
13. Pluskiewicz W, Adamczyk P, Drozdzowska B. The significance of height loss in postmenopausal women: The results from GO Study. *Int J Clin Pract*. 2021;75(5):e14009. doi:10.1111/ijcp.14009
14. Pluskiewicz W, Adamczyk P, Drozdzowska B. Low dietary calcium intake does not modify fracture risk but increases fall frequency: The results of GO Study. *Endokrynol Pol*. 2021;72(3):198–201. doi:10.5603/EP.a2021.0021
15. Pluskiewicz W, Adamczyk P, Drozdzowska B. Height loss in postmenopausal women: Do we need more for fracture risk assessment? Results from the GO Study. *Osteoporos Int*. 2021;32(10):2043–2049. doi:10.1007/s00198-021-05941-3
16. Kanis JA, Johnell O, Oden A, Johansson H, McCloskey E. FRAX™ and the assessment of fracture probability in men and women from the UK. *Osteoporos Int*. 2008;19(4):385–397. doi:10.1007/s00198-007-0543-5
17. Nguyen ND, Frost SA, Center JR, Eisman JA, Nguyen TV. Development of a nomogram for individualizing hip fracture risk in men and women. *Osteoporos Int*. 2007;18(8):1109–1117. doi:10.1007/s00198-007-0362-8
18. Nguyen ND, Frost SA, Center JR, Eisman JA, Nguyen TV. Development of prognostic nomograms for individualizing 5-year and 10-year fracture risks. *Osteoporos Int*. 2008;19(10):1431–1444. doi:10.1007/s00198-008-0588-0
19. Hars M, Trombetti A. Body composition assessment in the prediction of osteoporotic fractures. *Curr Opin Rheumatol*. 2017;29(4):394–401. doi:10.1097/BOR.0000000000000406
20. O'Donnell JM, Al-Shahi Salman R, Manuguerra M, Assaad N, Morgan MK. Quality of life and disability 12 months after surgery vs. conservative management for unruptured brain arteriovenous malformations: Scottish population-based and Australian hospital-based studies. *Acta Neurochir (Wien)*. 2018;160(3):559–566. doi:10.1007/s00701-017-3451-2
21. Miller IM, Ellervik C, Zarchi K, et al. The association of metabolic syndrome and psoriasis: A population- and hospital-based cross-sectional study. *J Eur Acad Dermatol Venereol*. 2015;29(3):490–497. doi:10.1111/jdv.12595

Effects of membrane-type PBLs on the expression of TNF-α and IL-2 in pulmonary tissue of SD rats after LPS-induced acute lung injury

Xia Liu[1,A–D], Yang Jiang[1,A–D], Bo Chen[1,B,C], Xiaohua Qiu[1,A,C–F], Songmei He[2,E,F]

[1] Physiological Science Laboratory, Guangdong Medical University, Dongguan, China

[2] Department of Infectious Diseases, Dongguan People's Hospital, China

A – research concept and design; B – collection and/or assembly of data; C – data analysis and interpretation;
D – writing the article; E – critical revision of the article; F – final approval of the article

Address for correspondence
Xiaohua Qiu
E-mail: xiaohua_qiu@163.com

Abstract

Background. As the first target organ, the lungs usually display symptoms of acute lung injury (ALI). Pro-inflammatory cytokines, such as tumor necrosis factor alpha (TNF-α) and interleukin (IL)-2, are crucial in triggering the systemic inflammatory response syndrome and the subsequent cascading effects. Therefore, the inhibition of the release of inflammatory mediators has become an important strategy for the prevention and treatment of ALI.

Objectives. To evaluate the preventive and therapeutic effects of transmembrane peripheral blood leukocytes (PBLs) on lipopolysaccharide (LPS)-induced ALI and its mechanism.

Materials and methods. Sixty Sprague Dawley rats were randomly divided into experimental and control groups. The animal model was established through intravenous injection of LPS. Plasmid PBLs were dissolved in a saline solution and injected into the experimental group of rats in different doses (0.1 mg, 0.2 mg and 0.3 mg per rat) using the in situ injection method. After injecting the PBL solution, the rats were killed after 12 h, 24 h, 36 h, or 48 h. The expression of microRNA (miRNA)-25 and miRNA-223 was detected using the semi-quantitative reverse transcription-polymerase chain reaction (RT-PCR). Tumor necrosis factor alpha and IL-2 levels in bronchoalveolar lavage fluid (BALF) were detected with an enzyme-linked immunosorbent assay (ELISA). The expressions of TNF-α and IL-2 proteins in lung tissue were detected using western blotting.

Results. The expression of miRNA-25 was upregulated in tissues and BALF in a dose- and time-dependent manner, while miRNA-223 was downregulated. The differences were statistically significant compared to the control group (p < 0.05). The TNF-α and IL-2 levels in the BALF of rats in the experimental group were increased in a dose-dependent manner compared to the control group (p < 0.05). In the presence of PBLs, the expressions of TNF-α, IL-2, miRNA, and proteins were inhibited. Thus, PBLs were found to alleviate pulmonary tissue damage.

Conclusions. In summary, PBLs have a protective effect on rats with ALI through the downregulation of TNF-α and IL-2 expression.

Key words: IL-2, TNF-α, LPS, BALF, acute lung injury

Background

When the body is seriously injured, it will induce a systemic inflammatory response syndrome (SIRS) leading to multiple organ dysfunction syndrome (MODS). As the first target organ, the lung usually displays symptoms of acute lung injury (ALI).[1–10] Pro-inflammatory cytokines, such as tumor necrosis factor alpha (TNF-α) and interleukin (IL)-2, are key factors in triggering the SIRS and the subsequent cascading effects. As such, the inhibition of the release of inflammatory mediators has become an important strategy for ALI prevention and treatment.[11–21] It is important to provide identification support for the early diagnosis of ALI as a therapeutic window for targeting in future clinical trials. However, the lack of specific biomarkers for ALI is arguably one of the main obstacles in the diagnosis and successful treatment of this syndrome.[16,17,20,21]

MicroRNAs (miRNAs) are stable and small RNAs that can modulate the regulation of post-transcriptional genes. The expressions of miRNAs used in various tissues and cell types are considered to have cell-type specificity.[3–6] Currently, miRNAs have been reported as potential biomarkers for various types of disease. It has been demonstrated that miRNAs are present in human plasma in a quite stable form which prevents RNase degradation and allows the measurement of tumor-derived miRNAs in serum and plasma.[6,7,13,15] The results and conclusions of these studies generated many potential applications for miRNAs which are considered biomarkers of some diseases. A few publications reported that miRNA-25 may be a potential biomarker for cancer detection and diagnosis.[8–10,12] MiRNA-223 promotes endotoxin-mediated inflammation in endothelial cells and can be released from dendritic cells and subsequently taken up by recipient dendritic cells.[11,12] In summary, the 2 miRNAs investigated in this study were involved in inflammation and considered to be candidates for biomarkers. However, the expression of the above miRNAs in ALI is still unclear and has not been reported. This study aimed to investigate the genetic expression of miRNAs in Sprague Dawley rats with ALI.

Peripheral blood leukocytes (PBLs) have been reported to function as agents in reverse transmission signaling and to affect ALI.[16,17]

Objectives

The objectives of this study were to investigate TNF-α and IL-2 in lung tissues of experimental rats, measure the level of expression of miRNA-25 and miRNA-223, and investigate the influence of PBLs on their expression.

Materials and methods

Animals

Specific pathogen-free (SPF) grade Sprague Dawley rats with an age of 4−5 weeks and a weight between 160 g and 180 g were obtained from Center of Experimental Animal at Guangdong Medical University, China. The animal experiments were conducted in accordance with the Guide for the Care and Use of Laboratory Animals of the National Institutes of Health (NIH).[22] The experiments in this study were approved by the Ethics Committee of Experimental Animal at Guangdong Medical University.

Materials

Lipopolysaccharide (LPS) was purchased from Shanghai Acmec Biochemical Co., Ltd. (Shanghai, China). TRIzol and the reverse transcriptase were obtained from Sinopharm Group (Beijing, China). The miRNAs were purchased from Yeasen Biotechnology Co., Ltd. (Shanghai, China). The anti-agents were obtained from Innochem Co., Ltd. (Beijing, China).

PBLs detection and expression

Seventy rats were selected for the experiments. The PBLs were solubilized in brine followed by a PBL solution injection into the left thigh muscle using an in-situ approach. The rats were divided randomly into 3 groups, based on the amount of PBLs injected (0.1 mg, 0.2 mg and 0.3 mg). Each group consisted of 20 rats. After the injection, the rats were sacrificed at different time intervals. The expression of PBLs in the tissue was detected using the reverse transcription polymerase chain reaction (RT-PCR) method.

Collection of samples

The rats were sacrificed by anesthesia using 2.5% isoflurane inhalation. Samples of lung tissue and bronchoalveolar lavage fluid (BALF) were obtained and centrifuged at 1500 rpm for 15 min at 5°C. The samples were collected in RNase-free tubes and loaded in a fridge at –70°C for future experiments. Tumor necrosis factor alpha and IL-2 levels in BALF were determined and the expressions of proteins were evaluated using western blotting.

cDNA preparation

The tissue samples were disrupted and the lysate was homogenized in an appropriate volume of the buffer solution. The lysate was centrifuged for 3 min at a maximum speed and the supernatant was carefully removed

by pipetting. Then, the tissue samples were transferred to new microtubes and the total miRNAs were isolated from all the specimens using the RNeasy Mini Kit (Qiagen, Hilden, Germany) according to the manufacturer's instructions. The total miRNA levels in BALF were isolated using miRNeasy Serum/Plasma Kit (Qiagen) according to the manufacturer's instructions.

Single-stranded cDNA was prepared in a reverse-transcription reaction by means of TaqMan MicroRNA™ Reverse Transcription Kit (Thermo Fisher Scientific, Waltham, USA) using from 5–10 μg of miRNA according to the manufacturer's protocol.

The measured sequences of cDNA were listed as follows: miRNA-25: 5'-CTTGTCGCAACTGTCGCCGTG-GAGCTC-3' and miRNA-223: 5'-ACGCTGGACTC-CAGCTGGGAGAAATT 3'.

Polymerase chain reaction

The experimental conditions for the PCR experiments were applied as follows: denaturation at 90°C for 6 min with 50 cycles, followed by annealing at 90°C for 10 s and then the extension procedure at 50°C for 10 s.

Gel electrophoresis

The gels were prepared, stained and recorded, and the absorbance of the gel was determined. A sample of miRNA was determined and calculated to normalize for various concentrations and as a control sample to investigate the efficiency of the reaction.

Western blot

The lung tissues of rats were treated with a homogenizer and reagent. The protein concentrations were measured using a dedicated reagent (Kexing Biopharm Co., Ltd., Shanghai, China).

Enzyme-linked immunosorbent assay

The IL-2 and TNF-α levels in BALF were determined using an enzyme-linked immunosorbent assay (ELISA) kit manufactured by Kewei Biology Co., Ltd. (Jiangsu, China). The determination methods followed the manufacturer's instructions.

Statistical analyses

All statistical analyses were conducted using IBM SPSS software v. 24.0 (IBM Corp., Armonk, USA) and R software v. 4.1.0 (R Foundation for Statistical Computing, Vienna, Austria). The Shapiro–Wilk normality test was used to test for the normal distribution of data in each group. If a normal distribution was met, the mean with a 95% confidence interval (95% CI) was used to describe the data. If the data did not conform to a normal distribution, the median (interquartile range (IQR)) was used to describe the data.

The statistical significance of differences in means between the groups was analyzed using analysis of variance (ANOVA) when the data were normally distributed. When the assumption of a normal distribution was not met, the Kruskal–Wallis test was used. The Bartlett's test was used to test for equal variances among groups. If equal variance was met, a post hoc test was performed using the Tukey's test. If not, a post hoc test was performed using the Dunnett's T3 test. The ANOVA linear contrast analysis compares the differences between linear models. In this study, there were contrasts between linear models if the time points were included or when the intervention groups were included as independent variables. A value of $p < 0.05$ indicated that the differences were statistically significant.

Results

The expression of miRNA-25

The in vivo change in miRNA-25 expression was investigated after injecting the membrane-type PBLs into the rats. A control group was also established. We checked the lung tissues and BALF for the expression of miRNA-25 at different time points after the injection of PBLs,. Figures 1,2 present the results of miRNA-25 expression in lung tissue and BALF, respectively. It was found that in BALF, the expression of miRNA-25 was significantly enhanced after PBLs injection in experimental groups, suggesting that the expression of miRNA-25 tends to increase with an increasing amount of time after PBLs stimulation.

Fig. 1. The expression of miRNA-25 in lung tissue of each group at each time point (n = 5 in each group at each time point)

Analysis of variance (ANOVA) at each time point: ** $p < 0.01$; *** $p < 0.001$. The description of the expression values and results of the normal distribution tests are listed in Supplementary Table 1. The ANOVA post hoc analyses for pairwise comparisons are listed in Supplementary Tables 2 and 3.

Fig. 2. The miRNA-25 expression in bronchoalveolar lavage fluid (BALF) in each group at each time point (n = 5 in each group at each time point)

Analysis of variance (ANOVA) at each time point: * $p < 0.05$; ** $p < 0.01$; *** $p < 0.001$. The description of the expression values and results of the normal distribution tests are listed in Supplementary Table 4. The post hoc analyses for pairwise comparisons are listed in Supplementary Tables 5 and 6.

The expression of miRNA-223

The membrane-type PBLs were injected into BALF based on the established experimental approach. Figures 3,4
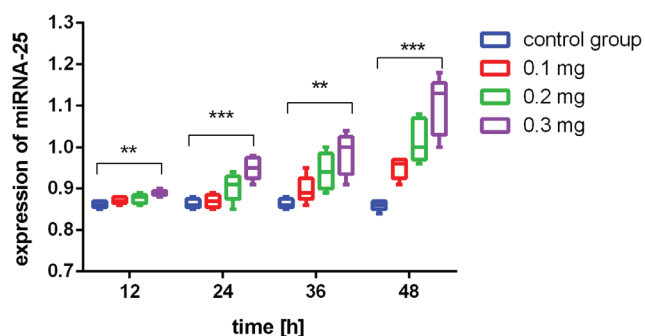

Fig. 3. The miRNA-223 expression in lung tissue in each group at each time point (n = 5 in each group at each time point)

Analysis of variance (ANOVA) at each time point: *** $p < 0.001$. The description of the expression values and results of the normal distribution tests are listed in Supplementary Table 7. The ANOVA post hoc analyses for pairwise comparisons are listed in Supplementary Tables 8 and 9.
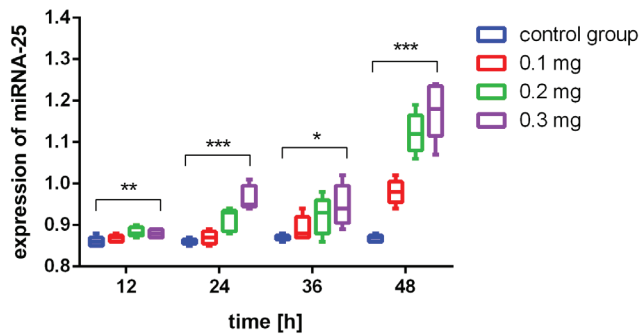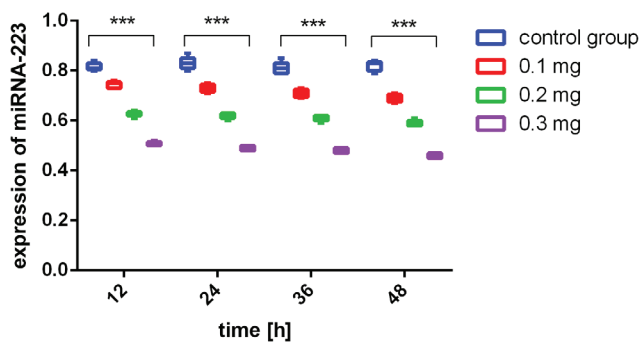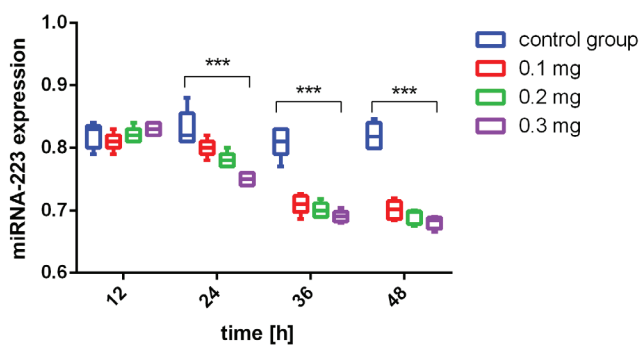

Fig. 4. The miRNA-223 expression in bronchoalveolar lavage fluid (BALF) in each group at each time point (n = 5 in each group at each time point)

Analysis of variance (ANOVA) at each time point: *** $p < 0.001$. The description of the expression values and results of the normal distribution tests are listed in Supplementary Table 10. The ANOVA post hoc analyses for pairwise comparisons are listed in Supplementary Tables 11, 12.

show the results of miRNA-223 expression in lung tissue and BALF, respectively. The miRNA-223 levels were found to be significantly reduced in the experimental groups. Compared to the control group, the expression of miRNA-223 was significantly reduced after prolonged periods following PBL injection.

Pro-inflammatory cytokine production

Figure 5 shows that the levels of TNF-α and IL-2 in BALF were enhanced after PBL injection. Peripheral blood leukocyte stimulation led to a dramatic increase in TNF-α levels. Furthermore, IL-2 levels dramatically rose a dose-dependent profile with statistically significant differences ($p < 0.05$). Similarly, Fig. 6 shows that IL-2 protein levels in lung tissues were both increased. Therefore, it is clear that the administration of higher concentrations of PBLs resulted in higher TNF-α and IL-2 levels ($p < 0.05$).
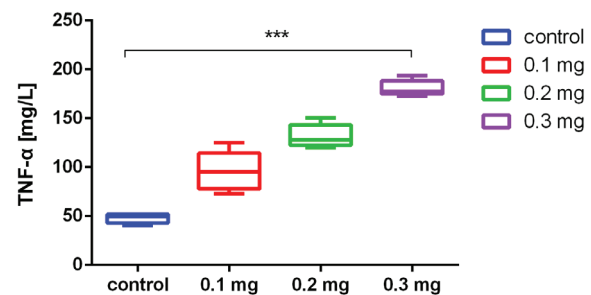
Fig. 5. The expression of tumor necrosis factor alpha (TNF-α) and interleukin (IL)-2 in bronchoalveolar lavage fluid (BALF) after the administration of peripheral blood leukocytes (PBLs) at 48 h

Analysis of variance (ANOVA): *** $p < 0.001$. The description of the expression values and results of the normal distribution tests are listed in Supplementary Tables 13 (TNF-α) and 14 (IL-2). The ANOVA post hoc analyses for pairwise comparisons are listed in Supplementary Tables 15 (TNF-α) and 16 (IL-2).
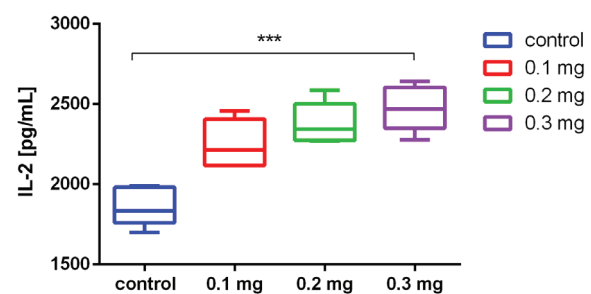
Fig. 6. The expression of tumor necrosis factor alpha (TNF-α) and interleukin (IL)-2 proteins for the control group and experimental groups with different administered doses

*** $p < 0.001$?].

Lung tissue histological examinations

The pathological changes in the lung tissue were detected using hematoxylin and eosin (H&E) staining. Figures 7–10 show that lung injury induced by LPS was reduced in all
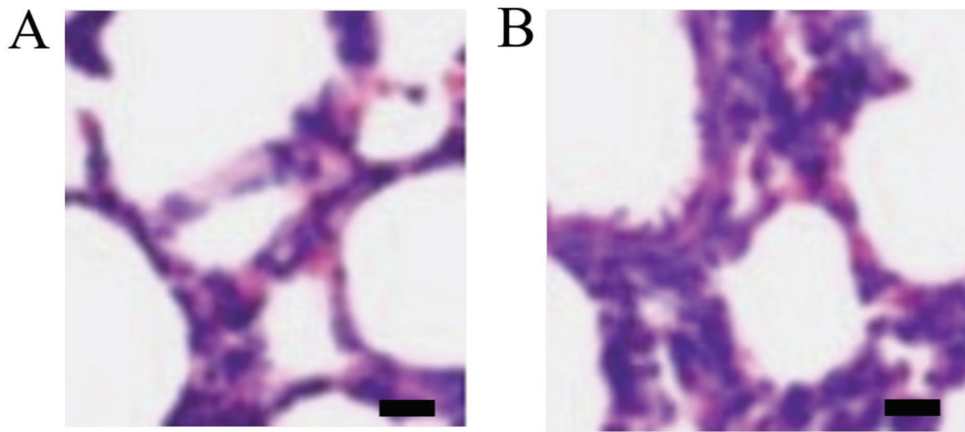
Fig. 7. Images of lung tissue after the administration of peripheral blood leukocytes (PBLs) at 12 h for (A) the control group and (B–D) the experimental groups using a scale bar of 10 μm
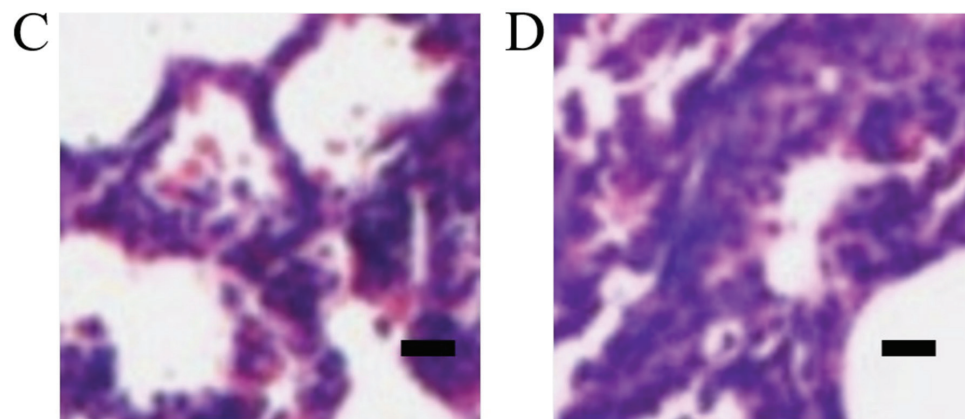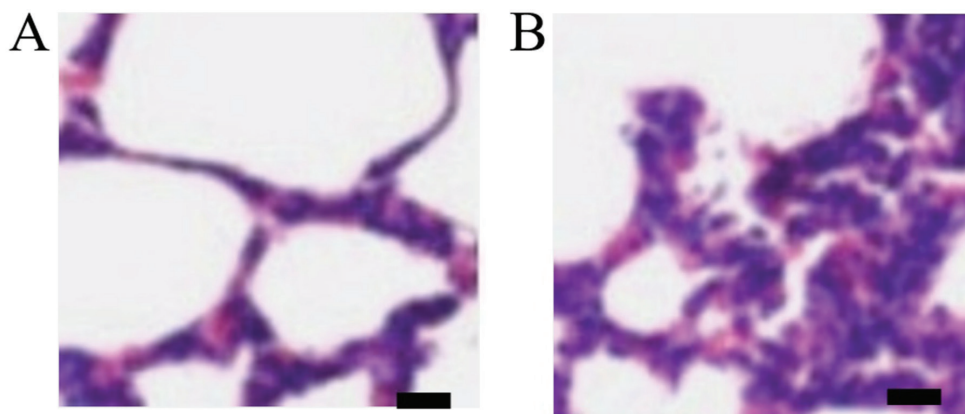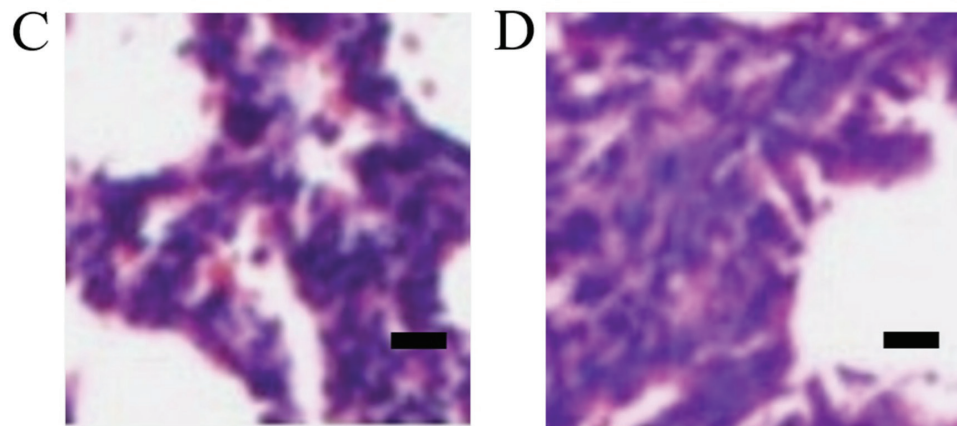
Fig. 8. Images of lung tissue after the administration of peripheral blood leukocytes (PBLs) at 24 h for (A) the control group and (B–D) the experimental groups using a scale bar of 10 μm
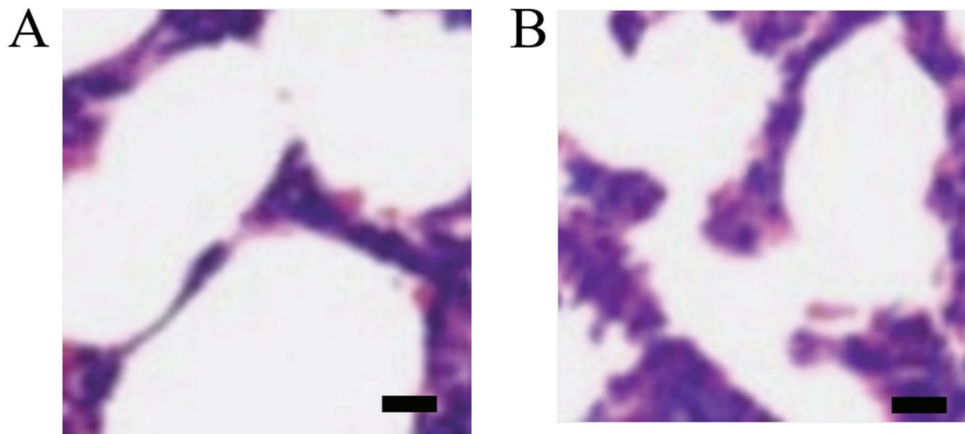
Fig. 9. Images of lung tissue after the administration of peripheral blood leukocytes (PBLs) at 36 h for (A) the control group and (B–D) the experimental groups using a scale bar of 10 μm
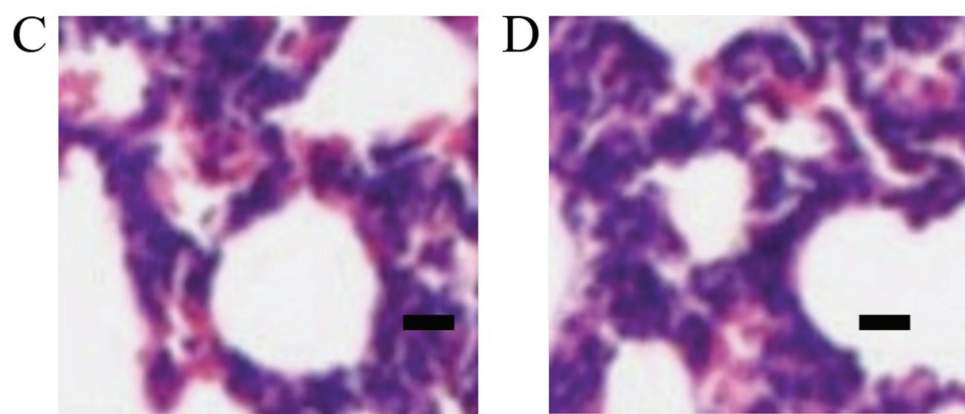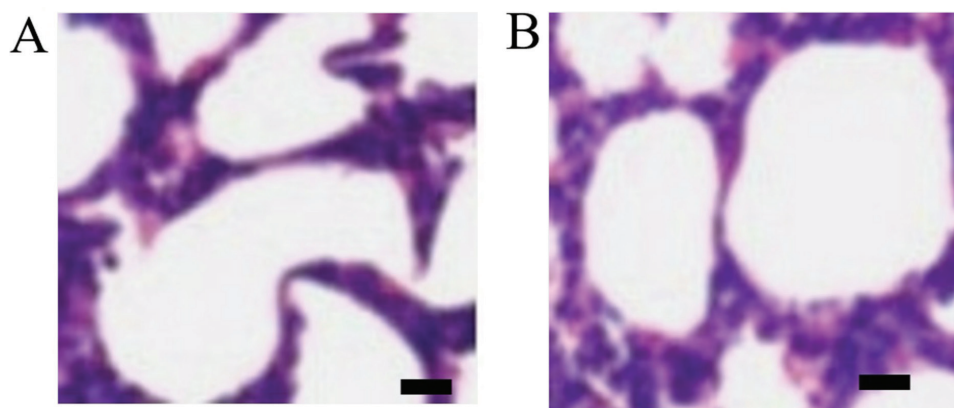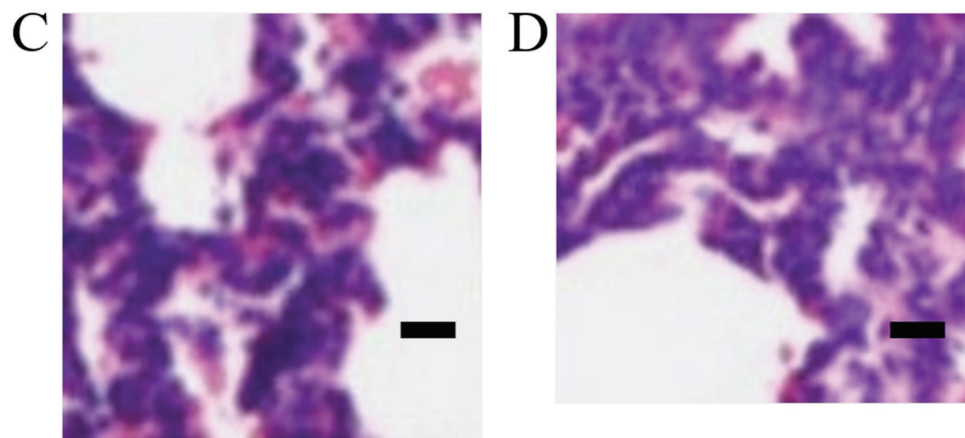
Fig. 10. Images of lung tissue after the administration of peripheral blood leukocytes (PBLs) at 48 h for (A) the control group and (B–D) the experimental groups using a scale bar of 10 μm

experimental groups (the 0.1 mg group, the 0.2 mg group and the 0.3 mg group). As the infiltration of neutrophils increased, thickening of interstitial alveolar regions increased, and structural damage was reduced compared to the results of the control group.

Discussion

Bacterial infection plays a significant role in clinical infections, and endotoxin is its main toxic substance. Lipopolysaccharide can cause ALI. In this experiment, PaO$_2$ decreased significantly after the intravenous injection of LPS. Symptoms such as interstitial pneumonitis, alveolar edema, exudation, bleeding, and granulocyte infiltration were observed in the lung pathology specimens, suggesting that LPS injection led to ALI. After PBL intervention, LPS injury was significantly alleviated, arterial oxygen partial pressures increased, and the wet/dry ratio of lung tissue decreased in the ALI rats. Pathological observation also indicated a reduced pathological reaction and inflammatory injury in lung tissue, which is consistent with previous results of PBLs in ALI.[23–27]

Studies have shown that TNF-α mainly comes from monocytes and macrophages stimulated by LPS.[20,21,23,24] In the process of ALI resulting from various factors, TNF-α functions mainly through the following approaches. First, it induces the production and release of proinflammatory cytokines, such as IL-6 and IL-8 that cause body damage. At the same time, inflammatory signals are further amplified and strengthened by reactivating inflammatory effector cells and releasing more inflammatory factors. Second, it causes direct injury to pulmonary vascular endothelial cells (VECs) and alveolar type II epithelium. Third, it interacts with other cytokines to cause lung injury. Finally, it activates the complement and coagulation systems and promotes the spread of inflammation in lung tissue. The results of this study showed that TNF-α levels in the lung tissue of rats after LPS injection, as well as miRNA-25 and miRNA-223 expressions in a lung homogenate increased significantly. Tumor necrosis factor alpha was mainly expressed in alveolar macrophages. One hour after LPS injury, the positive signal was the strongest. The peak of TNF-α in lung homogenate appeared 1–2 h after injury, which was consistent with the literature reporting a peak time of around 90 min. These results show that the expression of TNF-α precedes protein synthesis, and an intravenous injection of LPS directly produces endotoxemia. Lipopolysaccharide directly stimulates inflammatory effector cells in lung tissue to produce TNF-α. The serum levels of TNF-α in lung homogenate were similar to the dynamic change in TNF-α levels from the same stimulus. Previous studies have indicated that miRNA-25 and miRNA-223 may enhance the inflammatory response by stimulating the release of inflammatory mediators via targeting several negative feedback molecules.[15–20] These results and the results obtained in our study suggest that miRNA-25 and miRNA-223 increase the inflammatory response in LPS-induced ALI.

Some studies have found that IL-2 is mainly mediated by monocytes, macrophages and VECs, which are affected by LPS and other cytokines.[24–26] The main target cells of IL-2 are polymorphonuclear neutrophils (PMNs), which participate in the occurrence and development of ALI by affecting the biological activity of granulocytes. Interleukin 2 induces PMN chemotaxis in interstitial and inflammatory areas, and simultaneously activates PMNs in order to promote its degranulation and production of oxygen-free radical, protease and other media that directly damage lung tissue cells. Moreover, IL-2 increases the penetration of PMNs into the endothelial cell layer and the permeability of the vascular endothelial layer, promoting PMN transmembrane movement. The results obtained in this study confirm that the expression of IL-2 and the level of IL-2 in the homogenate increased significantly after LPS injection. Interleukin 2 was mainly expressed in alveolar macrophages, PMNs and VECs. A positive signal was first observed 2 h after LPS injury, and the strongest signal was recorded 4 h after LPS injury. At the same time, the levels of IL-2 in lung homogenate reached their maximum. The expression of IL-2 preceded its protein expression, which is in accordance with the time sequence of IL-2 expression and transcription. Furthermore, the time of peak TNF-α expression and protein levels was earlier than that of IL-2, suggesting that TNF-α may further stimulate the expression and release of IL-2 by effector cells.

Peripheral blood leukocytes have an antagonistic effect on M receptors. They are widely used in anti-shock and smooth muscle spasmolysis by improving microcirculation. Additional studies have demonstrated that PBLs can antagonize calcium influx and antioxidation, inhibit cell calcium overload and lipid peroxidation in biofilms, and protect tissue cells. Peripheral blood leukocytes can also inhibit the production of shock factors (or inflammatory mediators), such as prostaglandins and leukotrienes. Therefore, PBLs are used to prevent shock and in the prevention and treatment of MODS caused by various reasons, including ALI. The application of PBLs has achieved good therapeutic effects. Since TNF-α, IL-2 and other inflammatory cytokines play an important role in the induction of ALI, this study investigated the mechanisms behind PBLs in the prevention and treatment of ALI by affecting the above inherent functions and factors.

Limitations

The study and conclusions might be limited by the number of selected rats.

Conclusions

In this study, PBLs were found to significantly inhibit TNF-α in ALI tissues induced by LPS. The expression of miRNA-25 and miRNA-223 levels decreased in lung homogenate. The study showed that PBLs inhibit TNF-α

and IL-2 expression to achieve an anti-inflammatory effect, thereby reducing the inflammatory response and inflammatory injury in lung tissue.

Supplementary materials

The Supplementary tables are available at https://doi.org/10.5281/zenodo.6992162. The package contains the following files:

Supplementary Table 1. The miR-25 expression values of lung tissue in each group at each time point and the results of normal distribution tests.

Supplementary Table 2. ANOVA of miR-25 expression values in lung tissue at each time point and post hoc analysis for pairwise comparisons.

Supplementary Table 3. ANOVA of miR-25 expression values of lung tissue in each group and post hoc analysis for pairwise comparisons.

Supplementary Table 4. The miR-25 expression values in BALF in each group at each time point and the results of normal distribution tests.

Supplementary Table 5. ANOVA of miR-25 expression values in BALF at each time point and post hoc analysis for pairwise comparisons.

Supplementary Table 6. ANOVA of miR-25 expression values in BALF in each group and post hoc analysis for pairwise comparisons.

Supplementary Table 7. The miR-223 expression values of lung tissue in each group at each time point and the results of normal distribution tests.

Supplementary Table 8. ANOVA of miR-223 expression values in lung tissue at each time point and post hoc analysis for pairwise comparisons.

Supplementary Table 9. ANOVA of miR-223 expression values of lung tissue in each group and post hoc analysis for pairwise comparisons.

Supplementary Table 10. The miR-223 expression values in BALF in each group at each time point and the results of normal distribution tests.

Supplementary Table 11. ANOVA of miR-223 expression values in BALF at each time point and post hoc analysis for pairwise comparisons.

Supplementary Table 12. ANOVA of miR-223 expression values in BALF in each group and post hoc analysis for pairwise comparisons.

Supplementary Table 13. The TNF-α expression values in BALF at 48 h and the results of normal distribution tests.

Supplementary Table 14. ANOVA of TNF-α expression values in BALF at 48 h and post hoc analysis for pairwise comparisons.

Supplementary Table 15. The IL-2 expression values in BALF at 48 h and the results of normal distribution tests.

Supplementary Table 16. ANOVA of IL-2 expression values in BALF at 48 h and post hoc analysis for pairwise comparisons.

ORCID iDs

Xia Liu   https://orcid.org/0000-0003-3292-4120

References

1. Ye J, Guan M, Lu Y, et al. Protective effects of hesperetin on lipopolysaccharide-induced acute lung injury by targeting MD2. *Eur J Pharmacol*. 2019;852:151–158. doi:10.1016/j.ejphar.2019.02.042
2. Danchuk S, Ylostalo JH, Hossain F, et al. Human multipotent stromal cells attenuate lipopolysaccharide-induced acute lung injury in mice via secretion of tumor necrosis factor-α-induced protein 6. *Stem Cell Res Ther*. 2011;2(3):27. doi:10.1186/scrt68
3. Wang J, Li R, Peng Z, Hu B, Rao X, Li J. [Corrigendum] HMGB1 participates in LPS-induced acute lung injury by activating the AIM2 inflammasome in macrophages and inducing polarization of M1 macrophages via TLR2, TLR4, and RAGE/NF-κB signaling pathways. *Int J Mol Med*. 2020;45(5):1628. doi:10.3892/ijmm.2020.4530
4. Wang B, Gong X, Wan JY, et al. Resolvin D1 protects mice from LPS-induced acute lung injury. *Pulm Pharmacol Ther*. 2011;24(4):434–441. doi:10.1016/j.pupt.2011.04.001
5. Zhang HQ, Wang HD, Lu DX, et al. Berberine inhibits cytosolic phospholipase A2 and protects against LPS-induced lung injury and lethality independent of the alpha2-adrenergic receptor in mice. *Shock*. 2008;29(5):617–622. doi:10.1097/SHK.0b013e318157ea14
6. Wang Q, Kuang H, Su Y, et al. Naturally derived anti-inflammatory compounds from Chinese medicinal plants. *J Ethnopharmacol*. 2013;146(1):9–39. doi:10.1016/j.jep.2012.12.013
7. Yeh CH, Yang JJ, Yang ML, Li YC, Kuan YH. Rutin decreases lipopolysaccharide-induced acute lung injury via inhibition of oxidative stress and the MAPK–NF-κB pathway. *Free Radic Biol Med*. 2014;69:249–257. doi:10.1016/j.freeradbiomed.2014.01.028
8. Niazmand S, Khooshnood E, Derakhshan M. Effects of *Achillea wilhelmsii* on rat's gastric acid output at basal, vagotomized, and vagal-stimulated conditions. *Pharmacogn Mag*. 2010;6(24):282–285. doi:10.4103/0973-1296.71791
9. Khazneh E, Hřibová P, Hošek J, et al. The chemical composition of *Achillea wilhelmsii* C. Koch and its desirable effects on hyperglycemia, inflammatory mediators and hypercholesterolemia as risk factors for cardiometabolic disease. *Molecules*. 2016;21(4):404. doi:10.3390/molecules21040404
10. Nasseri S, Gurusamy M, Jung B, et al. Kinin B1 receptor antagonist BI113823 reduces acute lung injury. *Crit Care Med*. 2015;43(11):e499–e507. doi:10.1097/CCM.0000000000001268
11. Gurusamy M, Nasseri S, Lee H, et al. Kinin B1 receptor antagonist BI113823 reduces allergen-induced airway inflammation and mucus secretion in mice. *Pharmacol Res*. 2016;104:132–139. doi:10.1016/j.phrs.2015.12.017
12. An X, Sun X, Hou Y, et al. Protective effect of oxytocin on LPS-induced acute lung injury in mice. *Sci Rep*. 2019;9(1):2836. doi:10.1038/s41598-019-39349-1
13. Zhang HW, Wang Q, Mei HX, et al. RvD1 ameliorates LPS-induced acute lung injury via the suppression of neutrophil infiltration by reducing CXCL2 expression and release from resident alveolar macrophages. *Int Immunopharmacol*. 2019;76:105877. doi:10.1016/j.intimp.2019.105877
14. Fanelli V, Ranieri VM. Mechanisms and clinical consequences of acute lung injury. *Ann Am Thorac Soc*. 2015;12(Suppl 1):S3–S8. doi:10.1513/AnnalsATS.201407-340MG
15. Chen H, Bai C, Wang X. The value of the lipopolysaccharide-induced acute lung injury model in respiratory medicine. *Expert Rev Respir Med*. 2010;4(6):773–783. doi:10.1586/ers.10.71
16. Chen H, Wu S, Lu R, Zhang YG, Zheng Y, Sun J. Pulmonary permeability assessed by fluorescent-labeled dextran instilled intranasally into mice with LPS-induced acute lung injury. *PLoS One*. 2014;9(7):e101925. doi:10.1371/journal.pone.0101925
17. Yang Y, Li L. Depleting microRNA-146a-3p attenuates lipopolysaccharide-induced acute lung injury via up-regulating SIRT1 and mediating NF-κB pathway. *J Drug Target*. 2021;29(4):420–429. doi:10.1080/1061186X.2020.1850738
18. Grommes J, Soehnlein O. Contribution of neutrophils to acute lung injury. *Mol Med*. 2011;17(3–4):293–307. doi:10.2119/molmed.2010.00138

19. Liou CJ, Huang YL, Huang WC, Yeh KW, Huang TY, Lin CF. Water extract of *Helminthostachys zeylanica* attenuates LPS-induced acute lung injury in mice by modulating NF-κB and MAPK pathways. *J Ethnopharmacol*. 2017;199:30–38. doi:10.1016/j.jep.2017.01.043

20. Blázquez-Prieto J, López-Alonso I, Huidobro C, Albaiceta GM. The emerging role of neutrophils in repair after acute lung injury. *Am J Respir Cell Mol Biol*. 2018;59(3):289–294. doi:10.1165/rcmb.2018-0101PS

21. Aloisi MS, Serraino D, Girardi E, et al. Sexual behaviour of women living with HIV/AIDS naïve for antiretroviral therapy: The ICONA-BEHEPI Study. *AIDS Care*. 2000;12(6):789–795. doi:10.1080/09540120020014336

22. National Research Council (US) Committee for the Update of the Guide for the Care and Use of Laboratory Animals. *Guide for the Care and Use of Laboratory Animals*. 8th ed. Washington, USA: National Academies Press; 2011. doi:10.17226/12910

23. Aziz N, Kim MY, Cho JY. Anti-inflammatory effects of luteolin: A review of in vitro, in vivo, and in silico studies. *J Ethnopharmacol*. 2018;225:342–358. doi:10.1016/j.jep.2018.05.019

24. Li M, Zhao Y, Qi D, He J, Wang D. Tangeretin attenuates lipopolysaccharide-induced acute lung injury through Notch signaling pathway via suppressing Th17 cell response in mice. *Microb Pathog*. 2020;138:103826. doi:10.1016/j.micpath.2019.103826

25. Saadat S, Beheshti F, Askari VR, Hosseini M, Mohamadian Roshan N, Boskabady MH. Aminoguanidine affects systemic and lung inflammation induced by lipopolysaccharide in rats. *Respir Res*. 2019;20(1):96. doi:10.1186/s12931-019-1054-6

26. Yang HH, Duan JX, Liu SK, et al. A COX-2/sEH dual inhibitor PTUPB alleviates lipopolysaccharide-induced acute lung injury in mice by inhibiting NLRP3 inflammasome activation. *Theranostics*. 2020;10(11):4749–4761. doi:10.7150/thno.43108

27. Yeo CD, Rhee CK, Kim IK, et al. Protective effect of pravastatin on lipopolysaccharide-induced acute lung injury during neutropenia recovery in mice. *Exp Lung Res*. 2013;39(2):99–106. doi:10.3109/01902148.2013.763388

Original papers

The role of polymorphonuclear leukocytes in distant organ (lung) oxidative damage of liver ischemia/reperfusion and the protective effect of rutin

Hasan Olmez[1,A], Mustafa Tosun[1,B], Edhem Unver[1,E], Ferda Keskin Cimen[2,B],
Yusuf Kemal Arslan[3,C], Mine Gulaboglu[4,D], Bahadir Suleyman[5,F]

[1] Department of Pulmonary Diseases, Faculty Of Medicine, Erzincan Binali Yildirim University, Turkey

[2] Department of Pathology, Faculty Of Medicine, Erzincan Binali Yildirim University, Turkey

[3] Department of Bioistatistics, Faculty Of Medicine, Erzincan Binali Yildirim University, Turkey

[4] Department of Biochemistry, Faculty of Pharmacy, Atatürk University, Erzurum, Turkey

[5] Department of Pharmacology, Faculty of Medicine, Erzincan Binali Yildirim University, Turkey

A – research concept and design; B – collection and/or assembly of data; C – data analysis and interpretation;
D – writing the article; E – critical revision of the article; F – final approval of the article

Cite as
Olmez H, Tosun M, Unver M, et al. The role of polymorphonuclear leukocytes in distant organ (lung) oxidative damage of liver ischemia/reperfusion and the protective effect of rutin. *Adv Clin Exp Med*. 2023;32(1):81–89. doi:10.17219/acem/152886

DOI
10.17219/acem/152886

Abstract

Background. Ischemia/reperfusion (I/R) can cause damage to distant organs. Rutin is known to have antioxidant and anti-inflammatory properties, and inhibits cytokine and polymorphonuclear leukocyte (PMNL) infiltration. It may prevent the development of reperfusion injury.

Objectives. This study aimed to examine the role of PMNLs in distant organ (lung) injury after a liver I/R procedure, and to evaluate the protective effects of rutin in rats using biochemical and immunohistochemical methods.

Materials and methods. In this study, 18 Wistar albino male rats (255–275 g) were used. Experimental animals were divided into 3 groups: a liver I/R (LIR) group, a 50 mg/kg rutin+liver I/R (RLIR) group and a sham operation (SG) control group. Experimental results obtained from the RLIR group were compared with the LIR and SG groups.

Results. Blood malondialdehyde (MDA) levels in the RLIR and SG groups were significantly lower compared to the LIR group ($p < 0.001$). Blood myeloperoxidase (MPO) activity in the RLIR and SG groups was significantly lower compared to the LIR group ($p < 0.001$). Total glutathione (tGSH) levels in the RLIR and SG groups were significantly higher compared to the LIR group ($p < 0.001$).

Conclusions. Rutin can be used to prevent distant organ (lung) damage due to liver I/R. However, more extensive studies are needed on this issue.

Key words: rutin, distant organ damage (lung), ischemia/reperfusion

82

H. Olmez et al. Protective effect of rutin on lung damage

Background

Ischemia is defined as a condition in which blood flow and the oxygen supply to tissues are reduced or completely obstructed due to various reasons. Reperfusion is the process in which blood flow is restored to the ischemic tissue.[1] Tissue damage caused during the ischemic period increases with reperfusion.

Although ischemia/reperfusion (I/R) injuries have been examined in many tissues and organs, the pathophysiology of I/R injuries has not been fully elucidated. Studies have argued that I/R injuries are complex pathological processes which start with deoxygenation of the tissue, followed by oxidative stress, and result in an inflammatory response involving the activation of polymorphonuclear leukocytes (PMNLs) and the excessive formation of free radicals, which are responsible for the I/R injury. The reperfusion process causes these free radicals formed in the ischemic area to enter the systemic circulation. Activated PMNs are not only present in the primary tissue where the I/R event occurred, but are also transported to other tissues by the circulation, and cause damage to other organs (remote tissues). Activated PMNLs cause increased pulmonary capillary permeability, leading to the passage of PMNLs into the tissue.[2]

In a study by Yu et al., it was stated that an I/R procedure applied to the liver can cause severe inflammatory damage not only in the liver but also in the lung.[3] This information suggests that local I/R injuries may cause systemic damage to distant organs. Moreover, vascular permeability due to activated PMNLs and oxidative stress are the major components in distant organ injury. In the present study, the impact of rutin (3, 3′, 4′, 5, 7-pentahydroxyflavone-3-rhamnoglucoside) on distant organ (lung) damage due to liver I/R was investigated.

Rutin is a P_1 vitamin flavonoid. It is known to have antioxidant and anti-inflammatory properties, and inhibits cytokine and PMNL infiltration.[4,5] Rutin has the potential to bind free oxygen radicals and convert them into more stable non-reactive species, as well as end the free radical chain reaction.[6] Rutin exerts a cleaning effect by inhibiting 1,1-diphenyl-2-picrylhydrazyl (DPPH) radicals.[7] The lipid peroxidation inhibition and superoxide radical-clearing potential of rutin depends on the dose of rutin used.[6] In the inflammation zone, pro-inflammatory cytokines such as tumor necrosis factor alpha (TNF-α), interleukin-1 beta (IL-1β) and interleukin-6 (IL-6) are secreted from pulmonary cells and alveolar macrophages. The secretion of TNF-α, IL-1β, IL-6, and monocyte chemotactic protein (MCP) encourages the production of more effective pro-inflammatory cytokines and chemokines such as macrophage inflammatory protein (MIP), keratinocyte-induced chemokine, cytokine-induced neutrophil chemoattractant (CINC), and macrophage inflammatory protein-2 (MIP-2), which mediates the recruitment of PMNLs, macrophages

and lymphocytes. Studies have shown rutin to suppress TNF-α and IL-1β production, which are known as pro-inflammatory mediators.[9] In umbilical vein endothelial cells (HUVECs) during the acute period induced lipopolysaccharides (LPS), mice with acute liver damage intoxicated with carbon tetrachloride (CCl$_4$), and renal inflammation, rutin was found to reduce TNF-α formation.[10–12] Rutin was shown to reduce leukocyte infiltration of the lung by reducing the expression of pro-inflammatory cytokines. In addition, it has been demonstrated that rutin protects vascular barrier integrity and reduces hyperpermeability.[11] Based on this information, it was hypothesized that rutin may help prevent the development of pulmonary damage in liver I/R procedures.

Objectives

Ischemia/reperfusion causes distant organ damage. Rutin may prevent the development of reperfusion injury. This study aims to examine the role of PMNL in distant organ (lung) injury in liver I/R procedures and the protective effect of rutin in rats using biochemical and immunohistochemical methods.

Material and methods

Animals and chemicals

This experimental study included a total of 18 male albino Wistar rats weighing 255–275 g. The experimental animals were supplied by the Medical Experimental Application and Research Center of Atatürk University (Erzurum, Turkey). The rats were housed in batches and provided with food and water ad libitum, at a temperature of 22°C with 12-hour light/dark cycle until the experiments. The study was conducted at the Atatürk University Experimental Studies and Research Center. Thiopental sodium was supplied by the IE Ulagay (Istanbul, Turkey), and rutin was obtained from Solgar (Leonia, USA).

The animals were divided into 3 groups: liver I/R (LIR) group, 50 mg/kg rutin plus liver I/R (RLIR) group and sham operation control (SG) group, with 6 rats in each.

Ethical standards

This study was approved by the Ethics Committee at the University of Erzincan (approval No. 28.06.2018/148). The experimental procedure was approved by the Erzurum Atatürk University Animal Research Committee. The animal experiments were performed in accordance with the International Guidelines for the Use and Care of Laboratory Animals.

Surgical and pharmacological procedures

All surgical procedures were carried out under general anesthesia using an intraperitoneal injection of 25 mg/kg of thiopental sodium at appropriate intervals, with xylazine sniffing. Rutin was administered at a dose of 50 mg/kg to the rats in the RLIR group by oral lavage 1 h before anesthesia induction, whereas rats in the SG and LIR groups were administered the same amount of distilled water. Following thiopental sodium injection, the animals were kept anesthetized for an appropriate period to perform the surgery. The appropriate anesthesia period for surgical intervention was understood as the period required to immobilize the animals in supine position. After immobilization was confirmed, the anterior abdomen was accessed through a 3.5−4 cm vertical incision and a laparotomy was carried out in all rats.

Rats in the SG group were not subjected to further procedures after the abdominal cavity was closed. Rats in the RLIR and LIR groups were subjected to total hepatic ischemia by clamping the bile duct, portal vein and hepatic artery for 1 h, and then reperfused for 6 h.

At the end of the surgical procedure, all rats were sacrificed using high-dose anesthesia and their lung tissue was removed. Biochemical and histopathological examinations were carried out on the removed lung tissue. Experimental results obtained from the RLIR group were compared to the LIR and SG groups.

Sample preparation

Blood samples collected from the animals to be placed in separation gel were taken in drainage serum tubes. All collected samples were left to incubate at room temperature for 15 min and centrifuged for 15 min at $1500 \times g$ for separation. All samples were kept at −80°C until analysis. Before dissection, all tissue samples were rinsed with a phosphate-buffered saline (PBS) solution, and the lung tissues were then homogenized in a 50 mM ice-cold phosphate buffer at a pH of 7.4, which was suitable for measuring the variables. The obtained homogenates were then subjected to centrifugation at 5000 rpm for 20 min at 4°C. The supernatant portion was separated for analysis of the protein concentrations of myeloperoxidase (MPO), malondialdehyde (MDA) and total intracellular glutathione (tGSH). The protein supernatant levels were determined utilizing the technique described by Bradford.[13] The results were expressed in grams after being divided by the concentration of protein.[5]

MDA, MPO and tGSH analyses

Malondialdehyde levels were determined using the technique described by Ohkawa et al. Briefly, the absorbance of the pink complex formed as a result of the reaction between MDA and thiobarbituric acid (TBA) at a high temperature (95°C) was measured spectrophotometrically

at a wavelength of 532 nm.[14] The MPO-mediated H_2O_2 oxidation reactions containing a 4-aminoantipyrine/phenol solution was used as a substrate to determine MPO enzyme activity.[15] The tGSH analysis in serum and tissue was performed according to the method defined by Sedlak and Lindsay. DTNB (5,5'-dithiobis [2-nitrobenzoic acid]) disulfite is chromogenic in the medium, and DTNB is reduced easily by sulfhydryl groups. The yellow color observed after the reduction of DTNB was read spectrophotometrically at a wavelength of 412 nm.[16]

Histopathology

All tissues were fixed in 10% formaldehyde, dried using ethanol, and then embedded in paraffin blocks. The tissues were cut into 4 mm-thick sections, deparaffinized with xylene, and rehydrated with alcohol and water. Hematoxylin and eosin (H&E) were used to stain the tissue samples, which were then analyzed under a light microscope (Olympus pX53; Olympus Corp., Tokyo, Japan) equipped with a digital camera system (Olympus UTVO. 5XG-3; Olympus Corp.) by the same pathologist, who was blinded to the procedure.

Statistical analyses

Statistical analysis was performed using IBM SPSS Statistics for Windows v. 20 (IBM Corp., Armonk, USA). The results for continuous variables were reported as mean ± standard deviation (M ±SD) for normally distributed variables and as median (interquartile range (IQR), Q1−Q3) for non-normally distributed data. The Shapiro−Wilk test was used to test for normal distribution of continuous variables. One-way analysis of variance (ANOVA) was used to compare continuous variables between groups when the variables were normally distributed. For non-normally distributed variables, the Kruskal−Wallis test was performed. Before ANOVA, the homogeneity of the variances was tested using Levene's test. After ANOVA, a Tukey's honestly significant difference (HSD) test was performed as a post hoc test when the homogeneity assumption was met. Otherwise, a Games−Howell test was used as the post hoc test. Dunn's test was performed as a post hoc test after the Kruskal−Wallis test. A p-value <0.05 was considered statistically significant.

Results

Biochemical results

As shown in Table 1 and Fig. 1, blood MDA levels in the LIR, RLIR and SG groups were 8.1 ±0.9 µmol/g protein, 4.6 ±0.5 µmol/g protein and 1.6 ±0.2 µmol/g protein, respectively. Lung MDA levels were 7.9 ±0.5 µmol/g protein, 2.4 ±0.4 µmol/g protein and 2.0 ±0.4 µmol/g protein, respectively. The total MDA levels in blood and lung

Table 1. Blood and lung MDA, MPO and tGSH levels in SG, LIR and RLIR groups

Tissues	Groups			ANOVA or K–W test results				
	LIR	RLIR	SG	F(2,15) or K–W test statistics	p-value	Post hoc test p-values		
						LIR vs RLIR	LIR vs SG	RLIR vs SG
MDA blood [µmol/g]*	8.1 ±0.9[a,b]	4.6 ±0.5[a]	1.6 ±0.2	180.5*	<0.001	<0.001	<0.001	<0.001
MPO blood [U/g]*	24.0 ±3.6[a,b]	13.2 ±2.5[a]	3.9 ±0.3	96.7*	<0.001	<0.001	<0.001	0.001
tGSH blood [nmol/g]+	1.2 (1.0–1.4)[a,b]	2.7 (2.3–2.9)[a]	7.9 (7.8–8.1)	15.2+	0.001	0.002	<0.001	0.002
MDA lung [µmol/g]**	7.9 ±0.5[a,b]	2.4 ±0.4	2.0 ±0.4	339.3**	<0.001	<0.001	<0.001	0.296
MPO lung [µmol/g]*	18.0 ±3.7[a,b]	3.7 ±0.4	3.3 ±0.3	88.5*	<0.001	0.001	<0.001	0.203
tGSH lung [nmol/g]**	4.6 ±0.4[a,b]	8.9 ±0.7	9.5 ±0.5	139.2**	<0.001	<0.001	<0.001	0.181

MDA – malondialdehyde; MPO – myeloperoxidase; tGSH – total glutathione; LIR – liver ischemia/reperfusion; RLIR – rutin plus liver ischemia/reperfusion; SG – sham operation group. Results were presented as mean ± standard deviation (M ±SD) for normally distributed data, otherwise median and interquartile range (IQR; Q1–Q3) were reported. [a] p < 0.05 when compared with control; [b] p < 0.05 when compared with RLIR; *Games–Howell test was performed as the post hoc test after one-way analysis of variance (ANOVA); **Tukey's honestly significant difference (HSD) test was performed as the post hoc test after one-way ANOVA; + Kruskal–Wallis (K–W) test was used and Dunn's test was performed as post hoc test.

Fig. 1. The malondialdehyde (MDA) levels in blood and lung tissues in LIR, RLIR and SG groups. Horizontal lines: midline of the box – median, the bottom line of the box – 1st quartile (Q1, 25th), the top line of the box – 3rd quartile (Q3, 75th), and whiskers – minimum and maximum observations

LIR – liver ischemia/reperfusion; RLIR – rutin plus liver ischemia/reperfusion; SG – sham operation control group.
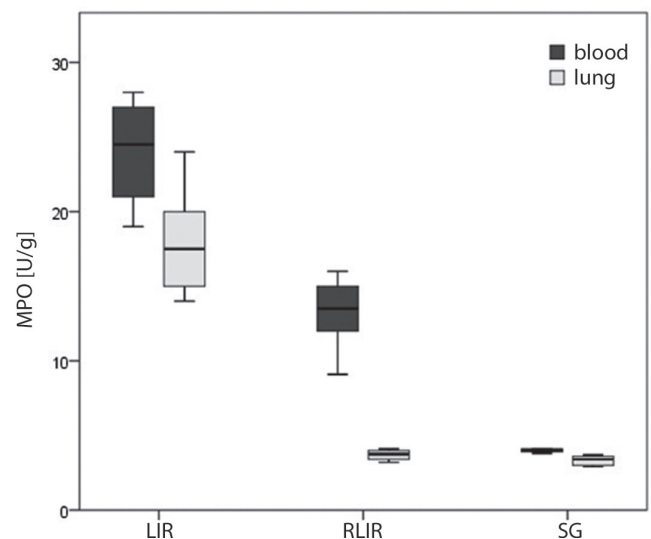
Fig. 2. The myeloperoxidase (MPO) levels in blood and lung tissues in LIR, RLIR and SG groups. Horizontal lines: midline of the box – median, the bottom line of the box – 1st quartile (Q1, 25th), the top line of the box – 3rd quartile (Q3, 75th), and whiskers – minimum and maximum observations

LIR – liver ischemia/reperfusion; RLIR – rutin plus liver ischemia/reperfusion; SG – sham operation control group.

in the RLIR and SG groups were significantly lower compared to the LIR group (p < 0.001, ANOVA, F = 180.5; p < 0.001, ANOVA, F = 339.3, respectively).

As shown in Table 1 and Fig. 2, blood MPO levels in the LIR, RLIR and SG groups were 24.0 ±3.6 µmol/g protein, 13.2 ±2.5 µmol/g protein and 3.9 ±0.3 µmol/g protein,

respectively. Lung MPO levels were 18.0 ±3.7 µmol/g protein, 3.7 ±0.4 µmol/g protein and 3.3 ±0.3 µmol/g protein, respectively. Significantly lower total MPO levels were observed in the RLIR and SG groups compared to the LIR group (p < 0.001, ANOVA, F = 96.7; p < 0.001, ANOVA, F = 88.5, respectively).

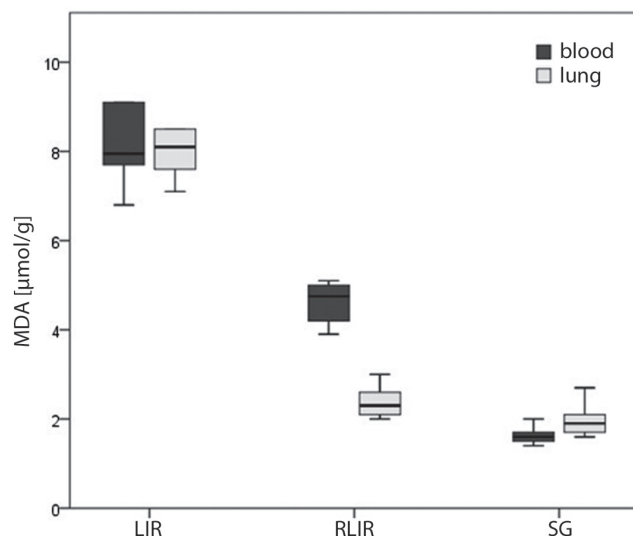**Fig. 3.** The total glutathione (tGSH) levels in blood and lung tissues in LIR, RLIR and SG groups. Horizontal lines: midline of the box – median, the bottom line of the box – 1st quartile (Q1, 25th), the top line of the box – 3rd quartile (Q3, 75th), and whiskers – minimum and maximum observations

LIR – liver ischemia/reperfusion; RLIR – rutin plus liver ischemia/reperfusion; SG – sham operation control group.
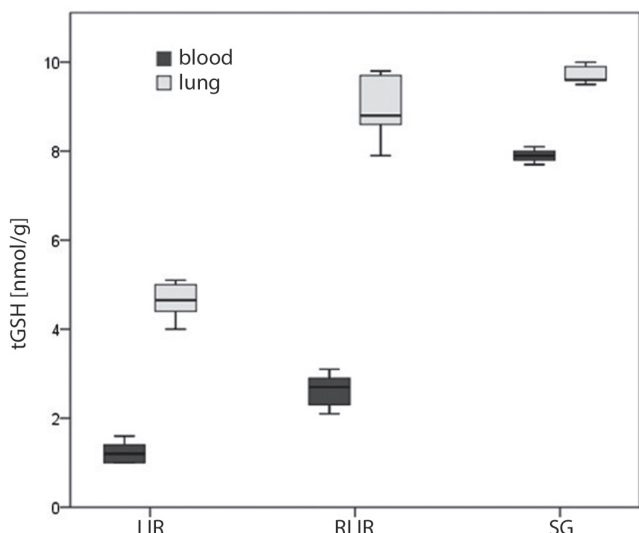
As shown in Table 1 and Fig. 3, tGSH levels in the LIR, RLIR and SG groups were 1.2 ±0.2 nmol/g, 2.6 ±0.4 nmol/g and 8.1 ±0.4 nmol/g in the blood, and 4.6 ±0.4 nmol/g, 8.9 ±0.7 nmol/g and 9.5 ±0.5 nmol/g in the lung, respectively. The total tGSH levels in the RLIR and SG groups were significantly higher compared to the LIR group ($p < 0.001$, Kruskal–Wallis test, $p < 0.001$, ANOVA, F = 139.2, respectively).

Histopathology

On histopathological examination, the alveolar vein, bronchiole structures and pleural mesothelium were identified as normal in pulmonary tissues in the SG group (Fig. 4). However, significant areas of alveolar degeneration, edema and hemorrhage were observed in the pulmonary tissues of the LIR group (Fig. 5). Congestion, PMNL and lymphocytic infiltration were observed in the lung tissues in the LIR group (Fig. 6). In the lung tissue of the RLIR group, the pleural mesothelium, and alveolar, vascular and bronchial structures were identified as normal, which was similar to the observations in the SG group (Fig. 7).

Discussion

Reperfusion is an important surgical treatment for reversing ischemic damage. It has been reported that a considerable amount of free oxygen radicals are formed during re-oxygenation of ischemic tissue. After ischemia, local and systemic damage is initiated by reperfusion via free oxygen radicals and inflammatory mediators. The reperfusion process causes the free radicals formed in the ischemic area to enter the systemic circulation. They then induce direct damage or indirectly exert a stimulating effect on the activation of neutrophils and the production of cytokines. Most of these mediators lead to the migration of neutrophils into tissues by neutrophil–endothelial interactions, and the migrating neutrophils degranulate and damage the tissue. Reperfusion of ischemic tissue leads to a disruption in the endothelium-dependent dilatation

Fig. 4. Microscopic view of normal pleural mesothelium (straight arrow), alveoli (square arrow), blood vessel (striped arrow) and bronchiole (round arrow) structures in lung tissue of the control group (hematoxylin and eosin (H&E) staining, ×100 magnification)
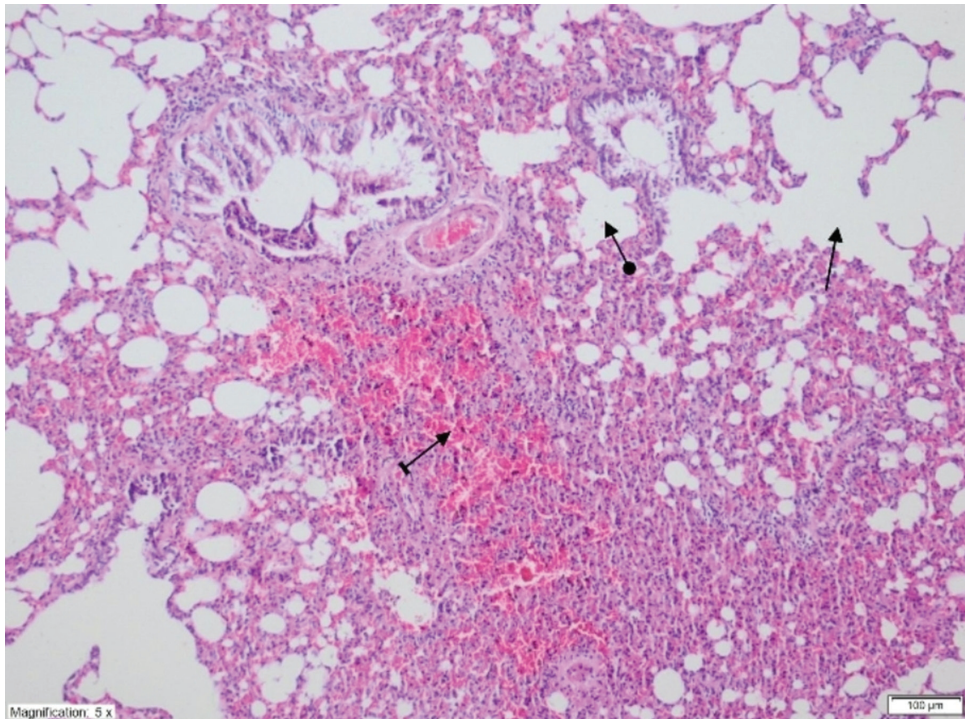
Fig. 5. Histopathological section showing areas of marked hemorrhage (striped arrow), alveolar degeneration (round arrow) and edema (straight arrow) in lung tissue of the LIR group (hematoxylin and eosin (H&E) staining, ×100 magnification)

LIR – liver ischemia/reperfusion.
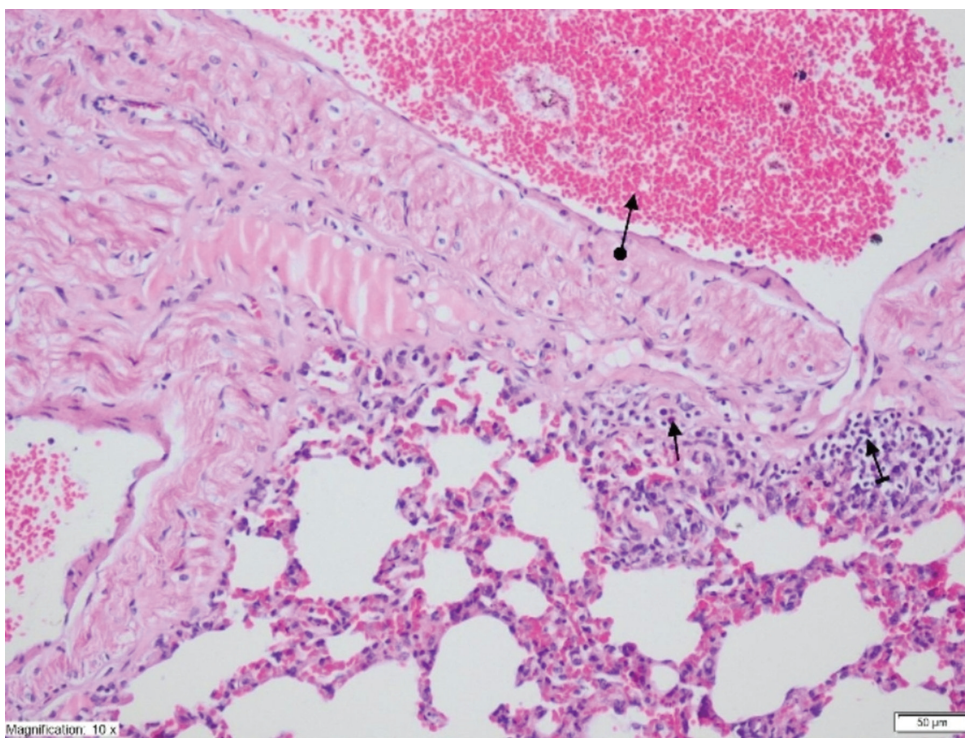
Fig. 6. Histopathological section showing congestion (round arrow), PMNLs (straight arrow) and lymphocytic infiltration (striped arrow) in lung tissue of the LIR group (hematoxylin and eosin (H&E) staining, ×200 magnification)

PMNLs – polymorphonuclear leukocytes; LIR – liver ischemia/ reperfusion.

of arterioles, formation of leucocyte plugs in capillaries, and increased fluid filtration. This in turn causes leakage of plasma proteins out of post-capillary venules and thus disrupts microvascular functions. Restoring blood flow can lead to the development of multisystem organ dysfunction and mortality. This damage is observed especially in myocardial, renal and pulmonary tissues. Animal studies have correlated the degree of reperfusion injury with the degree of PMNL activation.[17]

The PMNLs release various enzymes, such as MPO and free oxygen radicals, which in turn exacerbates the damage.[18] In a recent study by Kumbasar et al., MPO activity was reported to increase in ovarian tissues undergoing I/R.[19] There are numerous studies showing that MDA levels increase in the damaged tissue formed as a result of LIR.[20,21] Under normal physiological conditions, the oxidant–antioxidant balance is maintained in favor of antioxidants. Disruption of this balance leads to tissue damage. This
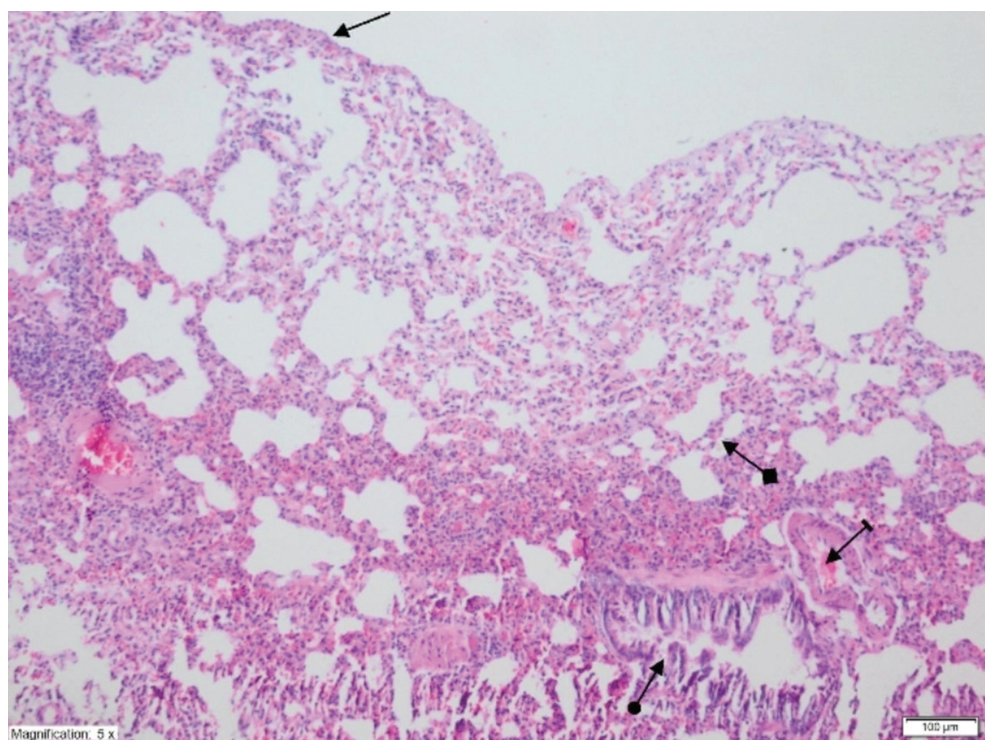
Fig. 7. Histopathological section showing normal pleural mesothelium (straight arrow), alveoli (square arrow), blood vessel (striped arrow), and bronchiole (round arrow) structures similar to the control group (SG) in lung tissue of the RLIR group (hematoxylin and eosin (H&E) staining, ×100 magnification)

RLIR – rutin plus liver ischemia/ reperfusion.
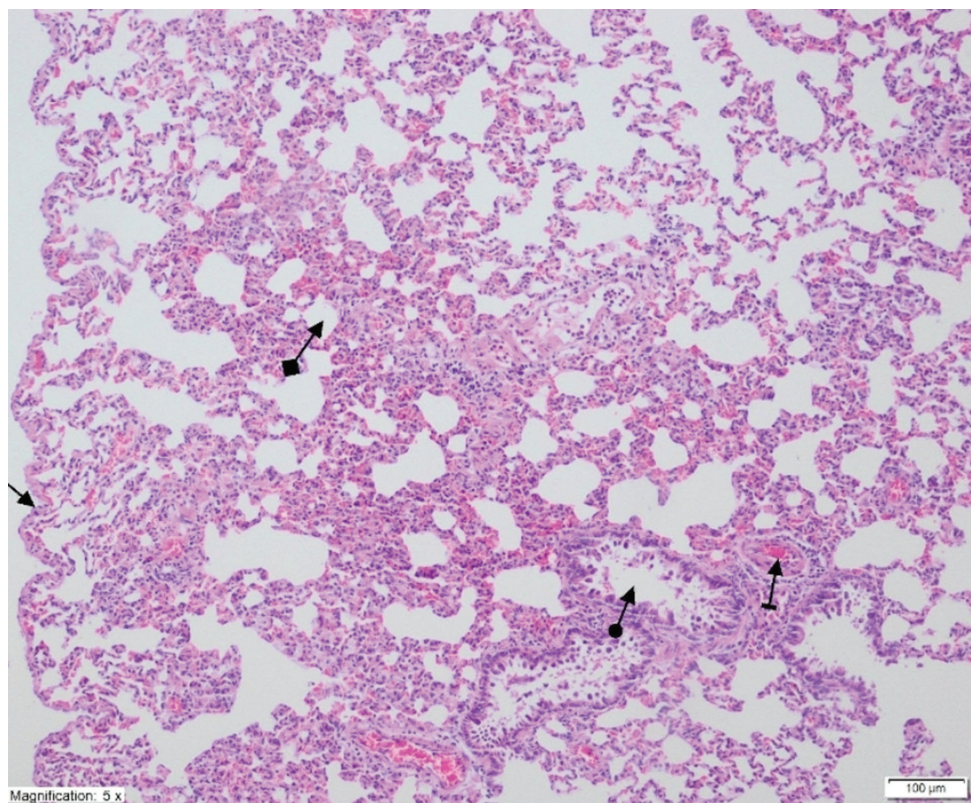
condition is called oxidative stress, and oxidant–antioxidant balance is used to determine whether tissue damage will occur. It has been shown in various I/R injury models that oxidant levels increase, antioxidant levels decrease, and the balance between oxidants and antioxidants changes in favor of oxidants. This demonstrates that enzymatic and non-enzymatic antioxidant mechanisms are continuously working in a controlled manner against oxidant mechanisms in tissues. Total glutathione is one of the critical non-enzymatic endogenous antioxidants that play a role in cellular defense against oxidative damage. It directly reacts with hydrogen peroxide (H_2O_2), hydroxyl ($OH-$), superoxide (O_2-), and alkoxy ($RO\bullet$) radicals in living tissues to protect the cell from the damaging effects of free radicals.[22] High tGSH levels are an important marker of cellular function and viability. Decreased tGSH levels indicate a poor intracellular defense system and are regarded as a damage marker.[23] Oxidation parameters increase during the reperfusion period after ischemia.

Free oxygen radicals are also known as reperfusion mediators. Tok et al. demonstrated that I/R treatment results in decreased tGSH levels and cause serious oxidative damage to rat kidneys; such damage can be reduced with the use of antioxidants.[24] Demiryilmaz et al. reported that tGSH levels decreased and the levels of MDA increased in ovarian tissue treated with I/R.[25] The lungs are a large reservoir of neutrophils, and a significant proportion of I/R injuries occur in the lungs.[26] Fantini et al. emphasized that lung injuries due to reperfusion are characterized by non-hydrostatic pulmonary edema resulting in progressive hypoxemia, pulmonary hypertension, decreased lung compliance, and adult respiratory distress syndrome (ARDS).[27] In addition, humoral mediators produced during reperfusion cause end-organ damage in regions far away from the focus of the I/R, and the lungs are the target organs.[27]

Ischemia/reperfusion injury to the lung can be observed on light microscopy examination of histopathological preparations stained with H&E.[28,29] The accumulation of neutrophils in capillary beds, interstitial edema, thickening of the alveolar septum, and the presence of protein-containing exudates in alveolar air cavities are common. Quantitative injury assessment is possible by examining 10 or 20 different sites under high magnification and counting the PMNLs in slides prepared in the same way.[30]

Various substances, such as superoxide dismutase, allopurinol, catalase, mannitol, vitamin C, pravastatin, alpha-tocopherol, L-carnitine, and pentoxifylline, have been used as treatments. These medications have been shown to be effective in eliminating the negative effects of free oxygen radicals after I/R. These antioxidant substances have shown a protective effect against distant tissue organ damage after I/R, either by decreasing pulmonary microvascular permeability and preventing neutrophil accumulation or by activating the antioxidant system. Dietary antioxidants such as flavonoids found in vegetables, fruit and beverages are known to protect the human body against a range of diseases such as cancer, diabetes, osteoporosis, and cardiovascular and neurodegenerative disorders.[31] Flavonoids in vegetables are used more often due to their better compatibility with the human body and fewer side effects.[32]

Rutin, also known as vitamin P, is a flavonol abundantly found in many foods including apples, vegetables, tea, and wine. The antioxidative, antibacterial, anti-inflammatory, antitumor, anti-ulcer, antidiarrheal, antimutagenic, immunomodulating, and vasodilatory characteristics of rutin have been shown.[33]

In one study, rutin was compared to ascorbic acid (Vc) and butylated hydroxytoluene (BHT), which are commonly used in the pharmaceutical industry. Inhibition of DPPH, which measures rutin antioxidant activity, was found to be higher than that of Vc but similar to that of BHT. The reducing capacity of rutin and the hydroxyl radical (OH) sweeping effect has been found to be similar to that of BHT. The effect of rutin inhibiting lipid peroxidation was greater than that of Vc.[6] Therefore, it is recommended to use antioxidants in combination.[34]

In addition, it has been shown that rutin alleviates I/R injuries that develop in organs such as the heart, brain, liver, kidney, and testes.[35–39] In their study, Adefegha et al. found that rutin has a protective effect against reactive oxygen-mediated oxidative damage due to its anti-inflammatory activity, as seen in rat models of acute inflammation.[40] Studies on LPS-induced acute lung injury (ALI) have shown rutin treatment to not only prevent histopathological changes in lung tissue, and also inhibit the transit of polymorphonuclear granulocytes into bronchoalveolar lavage fluid. The LPS-mediated inflammatory reactions, including increased lipid peroxidation and secretion of pro-inflammatory cytokines, are prevented by rutin treatment in a dose-dependent manner.[5] It has been reported that the decreased activities of antioxidant enzymes such as superoxide dismutase (SOD), glutathione peroxidase (GPx), catalase, and heme oxygenase-1 (HMOX1) in LPS-induced injuries can be reversed by rutin.[5]

Our experimental findings show that the I/R procedure caused significant oxidative damage to liver tissue. It was observed that I/R induced in the liver also caused I/R injuries in distant organs such as the lungs, resulting in hemorrhage, edema, and PMNL infiltration into the lung parenchyma. In our study, the difference in blood and lung MDA levels in the LIR, RLIR and SG groups was statistically significant ($p < 0.001$). The levels of MDA were significantly lower in the lungs compared to the blood in the RLIR group ($p < 0.001$). In the LIR group, MPO activity was higher compared to the RLIR and SG groups ($p < 0.001$). Our experimental results and literature review show that the antioxidant properties of rutin prevent I/R-induced oxidative damage to the lungs caused by PMNL migration in distant organs after I/R injuries to the liver. In our study, tGSH, an important antioxidant in the body, decreased in blood and lungs in the LIR group, increased in the RLIR group and had the highest value in the SG group ($p < 0.001$). Rutin administration significantly prevents the increase of oxidation parameters such as MDA and MPO, and the decrease in tGSH level in rats with distant organ (lung) injury as a result of liver I/R injury ($p < 0.001$).

The results of this study showed that immunohistochemical findings were consistent with our biochemical findings.

Limitations

Many substances have been implicated in the pathogenesis of I/R distant organ damage. However, these items could not be included in our study. In addition, many substances are thought to be useful in I/R injuries. Therefore, there is a need for comprehensive studies including items other than rutin. It is also important to examine the molecular histopathology of the tissues.

Conclusions

Ischemia/reperfusion injuries are complex pathological processes that start with the deoxygenation of tissue, continue with change the oxidant/antioxidant balance in favor of oxidants, and develop with an inflammatory response. In I/R injuries, MDA and MPO levels increase and tGSH levels decrease. The administration of 50 mg/kg of rutin significantly prevented I/R injuries. It was found that rutin also showed antioxidant activity in addition to its known anti-inflammatory activity. The results of this study suggest the possible utilization of rutin in clinical practice to prevent I/R injuries.

ORCID iDs

Mustafa Tosun https://orcid.org/0000-0002-5204-2099
Hasan Olmez https://orcid.org/0000-0003-4153-9953
Edhem Unver https://orcid.org/0000-0002-0322-8102
Ferda Keskin Cimen https://orcid.org/0000-0002-1844-0827
Yusuf Kemal Arslan https://orcid.org/0000-0003-1308-8569
Mine Gulaboglu https://orcid.org/ 0000-0002-3248-1502
Bahadır Suleyman https://orcid.org/0000-0001-5795-3177

References

1. Zimmerman BJ, Granger DN. Reperfusion injury. *Surg Clin North Am*. 1992;72(1):65–83. doi:10.1016/S0039-6109(16)45628-8
2. Bengisun U, Köksoy C, Bengisun JS, Bayraktaroğlu G, Çamur A, Aras N. Ischemia and reperfusion injury: Prevention of pulmonary hypertension and leukosequestration following lower limb ischemia. *Prostaglandins Leukot Essent Fatty Acids*. 1997;56(2):117–120. doi:10.1016/S0952-3278(97)90507-X
3. Yu Z, Tong Y, Zhang R, Ding X, Li Q. Saquinavir ameliorates liver warm ischemia-reperfusion-induced lung injury via HMGB-1- and P38/JNK-mediated TLR-4-dependent signaling pathways. *Mediators Inflamm*. 2017;2017:7083528. doi:10.1155/2017/7083528
4. Ganeshpurkar A, Saluja AK. The pharmacological potential of rutin. *Saudi Pharm J*. 2017;25(2):149–164. doi:10.1016/j.jsps.2016.04.025
5. Yeh CH, Yang JJ, Yang ML, Li YC, Kuan YH. Rutin decreases lipopolysaccharide-induced acute lung injury via inhibition of oxidative stress and the MAPK–NF-κB pathway. *Free Radic Biol Med*. 2014;69:249–257. doi:10.1016/j.freeradbiomed.2014.01.028
6. Yang J, Guo J, Yuan J. In vitro antioxidant properties of rutin. *LWT Food Sci Technol*. 2008;41(6):1060-1066. doi:10.1016/j.lwt.2007.06.010
7. Göktürk Baydar N, Özkan G, Yaşar S. Evaluation of the antiradical and antioxidant potential of grape extracts. *Food Control*. 2007;18(9):1131–1136. doi:10.1016/j.foodcont.2006.06.011
8. Ware LB, Matthay MA. The acute respiratory distress syndrome. *N Engl J Med*. 2000;342(18):1334–1349. doi:10.1056/NEJM200005043421806

9. Taşlı N, Çimen F, Karakurt Y, et al. Protective effects of rutin against methanol induced acute toxic optic neuropathy: An experimental study. *Int J Ophthalmol*. 2018;11(5):780–785. doi:10.18240/ijo.2018.05.10

10. Arjumand W, Seth A, Sultana S. Rutin attenuates cisplatin induced renal inflammation and apoptosis by reducing NFκB, TNF-α and caspase-3 expression in Wistar rats. *Food Chem Toxicol*. 2011;49(9):2013–2021. doi:10.1016/j.fct.2011.05.012

11. Lee W, Ku SK, Bae JS. Barrier protective effects of rutin in LPS-induced inflammation in vitro and in vivo. *Food Chem Toxicol*. 2012;50(9):3048–3055. doi:10.1016/j.fct.2012.06.013

12. Domitrović R, Jakovac H, Vasiljev Marchesi V, et al. Differential hepatoprotective mechanisms of rutin and quercetin in CCl$_4$-intoxicated BALB/cN mice. *Acta Pharmacol Sin*. 2012;33(10):1260–1270. doi:10.1038/aps.2012.62

13. Bradford MM. A rapid and sensitive method for the quantitation of microgram quantities of protein utilizing the principle of protein-dye binding. *Anal Biochem*. 1976;72(1–2):248–254. doi:10.1016/0003-2697(76)90527-3

14. Ohkawa H, Ohishi N, Yagi K. Assay for lipid peroxides in animal tissues by thiobarbituric acid reaction. *Anal Biochem*. 1979;95(2):351–358. doi:10.1016/0003-2697(79)90738-3

15. Bradley PP, Priebat DA, Christensen RD, Rothstein G. Measurement of cutaneous inflammation: Estimation of neutrophil content with an enzyme marker. *J Invest Dermatol*. 1982;78(3):206–209. doi:10.1111/1523-1747.ep12506462

16. Sedlak J, Lindsay RH. Estimation of total, protein-bound, and nonprotein sulfhydryl groups in tissue with Ellman's reagent. *Anal Biochem*. 1968;25:192–205. doi:10.1016/0003-2697(68)90092-4

17. Korthuis RJ, Granger DN. Reactive oxygen metabolites, neutrophils, and the pathogenesis of ischemic-tissue/reperfusion. *Clin Cardiol*. 1993;16(4 Suppl 1):19–26. doi:10.1002/clc.4960161307

18. Dawson TL, Gores GJ, Nieminen AL, Herman B, Lemasters JJ. Mitochondria as a source of reactive oxygen species during reductive stress in rat hepatocytes. *Am J Physiol Cell Physiol*. 1993;264(4 Pt 1):C961–C967. doi:10.1152/ajpcell.1993.264.4.C961

19. Kumbasar S, Yapca OE, Bilen H, et al. The effect of lacidipine on ischemiareperfusion induced oxidative damage in ovaries of female rats. *Biomed Res India*. 2012;23(4):495–500. doi: 10.1007/s00210-018-1524-2

20. Yang S, Chou WP, Pei L. Effects of propofol on renal ischemia/reperfusion injury in rats. *Exp Ther Med*. 2013;6(5):1177–1183. doi:10.3892/etm.2013.1305

21. Chen TH, Yang YC, Wang JC, Wang JJ. Curcumin treatment protects against renal ischemia and reperfusion injury-induced cardiac dysfunction and myocardial injury. *Transplant Proc*. 2013;45(10):3546–3549. doi:10.1016/j.transproceed.2013.09.006

22. Meister A, Anderson ME. Glutathione. *Annu Rev Biochem*. 1983;52(1):711–760. doi:10.1146/annurev.bi.52.070183.003431

23. Santa T. Recent advances in analysis of glutathione in biological samples by high-performance liquid chromatography: A brief overview. *Drug Discov Ther*. 2013;7(5):172–177. doi:10.5582/ddt.2013.v7.5.172

24. Tok A, Sener E, Albayrak A, et al. Effect of mirtazapine on oxidative stress created in rat kidneys by ischemia-reperfusion. *Ren Fail*. 2012;34(1):103–110. doi:10.3109/0886022X.2011.623499

25. Demiryilmaz I, Sener E, Cetin N, Altuner D, Akcay F, Suleyman H. A comparative investigation of biochemical and histopathological effects of thiamine and thiamine pyrophosphate on ischemia-reperfusion induced oxidative damage in rat ovarian tissue. *Arch Pharm Res*. 2013;36(9):1133–1139. doi:10.1007/s12272-013-0173-8

26. Pararajasingam R, Nicholson ML, Bell PRF, Sayers RD. Non-cardiogenic pulmonary oedema in vascular surgery. *Eur J Vasc Endovasc Surg*. 1999;17(2):93–105. doi:10.1053/ejvs.1998.0750

27. Fantini GA, Conte MS. Pulmonary failure following lower torso ischemia: Clinical evidence for a remote effect of reperfusion injury. *Am Surg*. 1995;61(4):316–319. PMID:7893094.

28. Tassiopoulos AK, Carlin RE, Gao Y, et al. Role of nitric oxide and tumor necrosis factor on lung injury caused by ischemia/reperfusion of the lower extremities. *J Vasc Surg*. 1997;26(4):647–656. doi:10.1016/S0741-5214(97)70065-X

29. Wagner FM, Weber AT, Ploetze K, et al. Do vitamins C and E attenuate the effects of reactive oxygen species during pulmonary reperfusion and thereby prevent injury? *Ann Thorac Surg*. 2002;74(3):811–818. doi:10.1016/S0003-4975(02)03666-4

30. Tanahashi Y, Takeyoshi I, Aiba M, Ohwada S, Matsumoto K, Morishita Y. The effects of FK409 on pulmonary ischemia-reperfusion injury in dogs. *Transplant Int*. 1999;12(6):402–407. doi:10.1007/s001470050249

31. Yeung AWK, Tzvetkov NT, El-Tawil OS, Bungău SG, Abdel-Daim MM, Atanasov AG. Antioxidants: Scientific literature landscape analysis. *Oxid Med Cell Longev*. 2019;2019:8278454. doi:10.1155/2019/8278454

32. Abdel-Daim MM, Aly SM, Abo-el-Sooud K, Giorgi M, Ursoniu S. Role of natural products in ameliorating drugs and chemicals toxicity. *Evid Based Complement Alternat Med*. 2016;2016:7879406. doi:10.1155/2016/7879406

33. Singh H, Kaur P, Kaur P, Muthuraman A, Singh G, Kaur M. Investigation of therapeutic potential and molecular mechanism of vitamin P and digoxin in I/R-induced myocardial infarction in rat. *Naunyn-Schmiedeberg's Arch Pharmacol*. 2015;388(5):565–574. doi:10.1007/s00210-015-1103-8

34. Milde J, Elstner EF, Graßmann J. Synergistic inhibition of low-density lipoprotein oxidation by rutin, γ-terpinene, and ascorbic acid. *Phytomedicine*. 2004;11(2–3):105–113. doi:10.1078/0944-7113-00380

35. Jeong JJ, Ha YM, Jin YC, et al. Rutin from *Lonicera japonica* inhibits myocardial ischemia/reperfusion-induced apoptosis in vivo and protects H9c2 cells against hydrogen peroxide-mediated injury via ERK1/2 and PI3K/Akt signals in vitro. *Food Chem Toxicol*. 2009;47(7):1569–1576. doi:10.1016/j.fct.2009.03.044

36. Gupta R, Singh M, Sharma A. Neuroprotective effect of antioxidants on ischaemia and reperfusion-induced cerebral injury. *Pharmacol Res*. 2003;48(2):209–215. doi:10.1016/S1043-6618(03)00102-6

37. Korkmaz A, Kolankaya D. Protective effect of rutin on the ischemia/reperfusion-induced damage in rat kidney. *J Surg Res*. 2010;164(2):309–315. doi:10.1016/j.jss.2009.03.022

38. Acquaviva R, Lanteri R, Li Destri G, et al. Beneficial effects of rutin and L-arginine coadministration in a rat model of liver ischemia-reperfusion injury. *Am J Physiol Gastrointest Liver Physiol*. 2009;296(3):G664–G670. doi:10.1152/ajpgi.90609.2008

39. Akondi BR, Challa SR, Akula A. Protective effects of rutin and naringin in testicular ischemia-reperfusion induced oxidative stress in rats. *J Reprod Infertil*. 2011;12(3):209–214. PMID:23926504. PMCID:PMC3719295.

40. Adefegha SA, Leal DBR, de Oliveira JS, Manzoni AG, Bremm JM. Modulation of reactive oxygen species production, apoptosis and cell cycle in pleural exudate cells of carrageenan-induced acute inflammation in rats by rutin. *Food Funct*. 2017;8(12):4459–4468. doi:10.1039/C7FO01008G

Whole-genome sequencing-based characteristics of *Escherichia coli* Rize-53 isolate from Turkey

Halbay Turumtay[1–3,A–F]

[1] Department of Energy System Engineering, Karadeniz Technical University, Trabzon, Turkey

[2] Environmental Genomics and Systems Biology Division, Lawrence Berkeley National Laboratory, USA

[3] Joint BioEnergy Institute, Emeryville, USA

A – research concept and design; B – collection and/or assembly of data; C – data analysis and interpretation;
D – writing the article; E – critical revision of the article; F – final approval of the article

Address for correspondence
Halbay Turumtay
E-mail: hturumtay@gmail.com

Abstract

Background. Urinary tract infections (UTIs) are one of the most common infectious diseases. Inappropriate and excessive administration of antibiotics has led to the increased antibiotic resistance in the pathogens that cause UTIs. This work focused on identifying genetic determinants of antibiotic resistance in a clinical isolate of UTI-causing *Escherichia coli*.

Objectives. A clinical isolate of *E. coli* resistant to β-lactam, tetracycline and aminoglycoside antibiotics was analyzed using whole-genome sequencing (WGS) to identify genes that contribute to its resistance.

Materials and methods. The clinical isolate was obtained from a urine sample of a UTI patient in Turkey and identified via 16S rDNA sequencing. Antimicrobial susceptibility test was performed for 17 antibiotics using VITEK® 2 and the results were confirmed using minimum inhibitory concentration assay. Whole-genome sequencing of the isolate was performed using Illumina sequencing and analyzed with bioinformatic tools for multilocus sequence typing, replicon types, virulence factors, and antimicrobial resistance genes.

Results. Whole-genome datum was submitted to the National Center for Biotechnology Information (NCBI; accession No. JAKSGM000000000). The isolate was only found to be resistant to piperacillin in the β-lactam class of antibiotics. While the isolate was also resistant to aminoglycoside and tetracycline antibiotics, it was sensitive to other antibiotics tested. Ten antibiotic resistance genes were identified in the genome of the isolate: bla_{OXA-1}, bla_{OXA-2}, $aac(6')$-II, $aac(6')$-Ib-cr, $tetB$, $catB3$, $qacE$, $sitABCD$, $mdfA$, and sul-2. Clonal subtype (ST) and serotype of the isolate were identified as ST2141 and O107/H39, respectively. Plasmid replicon typing was used to identify 5 plasmid types in the genome of *E. coli* Rize-53 (Col(BS512), IncC, IncIA, IncFIB(AP1918), and IncFII(pRSB107)); however, none of the resistance genes were encoded on the plasmid.

Conclusions. Genetic determinants of resistance to tetracycline, β-lactam and aminoglycoside antibiotics were identified using WGS in a uropathogenic *E. coli* from ST2141 lineage and O107:H39 serotype, isolated in Turkey.

Key words: whole-genome sequencing, uropathogenic *Escherichia coli* ST2141, serotype O107:H39, tetracycline resistance (tetB), bla_{OXA-1}/aac6

Background

Extensive antibiotic use to treat urinary tract infections (UTIs) has led to the widespread antibiotic resistance in the pathogens that cause these infections. The primary cause of many UTIs is Gram-negative Enterobacterales, such as uropathogenic *Escherichia coli* (UPEC) and *Klebsiella pneumoniae* spp.[1] Spread of drug-resistant strains of *E. coli* is a serious health concern worldwide, as it leads to more persistent infections and higher mortality rates.[2] *Escherichia coli* is an prevalent human pathogen that is responsible for up to 90% of all community-acquired UTIs.[3]

The production of β-lactamases by uropathogens has led to an increased β-lactam resistance, complicating UTI treatment.[4] The β-lactam antibiotics inhibit peptidoglycan synthesis, though they are ineffective against Enterobacteriaceae that produce extended-spectrum β-lactamases (ESBLs). The resistance to β-lactams means carbapenems need to be used to effectively treat infections caused by ESBL-producing Enterobacteriaceae. The β-lactamases are categorized into 4 classes based on amino acid contents, namely class A, B, C, and D.[5] Class D β-lactamases include oxacillinase (OXA)-type enzymes that hydrolyze cloxacillin and oxacillin faster than benzylpenicillin.[6]

Another class of antibiotics are tetracyclines (TEs), which inhibit protein synthesis in bacteria. The *tet* A–E classes are the most frequently detected TE resistance genes in the Enterobacterales, and they primarily confer resistance via TE efflux or ribosomal protection. Resistance to TE is frequently spread among *E. coli* isolates through horizontal transfer of genes such as *tetA*.[7,8] Consequently, TE resistance has led to a decreased use of these antibiotics in humans. However, TEs are still among the most widely used antibiotics in livestock production globally.[9]

Aminoglycoside antibiotics are used for the single-dose treatment of UTIs.[10] They mainly act by disrupting bacterial protein synthesis through binding to prokaryotic ribosomes via 16S ribosomal RNA (16S rRNA) and disrupting bacterial cell membrane integrity.[11] Aminoglycoside resistance occurs through several mechanisms; however, enzymatic inactivation is the most prevalent in the clinical setting and is carried out by acetyltransferases, nucleotidyltransferases and phosphotransferases, which perform acetylation, adenylation and phosphorylation, respectively. A large number of enzymes that modify aminoglycosides have been described to date, and they are present in nearly all bacteria that present enzymatic resistance to aminoglycosides.[12] Understanding the antimicrobial resistance phenotypes of livestock, wildlife and human pathogens is important for identifying proper treatment plans and addressing the urgent situation of rising antimicrobial resistance.

Objectives

Whole-genome sequencing (WGS) is an important approach to revealing characteristics related to antimicrobial resistance genes in bacteria. This study aimed to perform a whole-genome analysis of one UTI isolate from Turkey in order to characterize resistance genes, multilocus sequence type (MLST) and plasmid profiles.

Materials and methods

Bacterial strain and antimicrobial susceptibility testing

One UTI isolate of *E. coli* was obtained from glycerol stock stored at Recep Tayyip Erdoğan University in Rize, Turkey, and was characterized using standard microbiological procedures and VITEK® 2 (bioMérieux, Marcy-l'Étoile, France). It was further identified using 16S rDNA Sanger dideoxy sequencing and named *E. coli* Rize-53 after the Basic Local Alignment Search Tool (BLAST) analysis on the National Center for Biotechnology Information (NCBI) website. Susceptibility testing was performed using the following antibiotics: piperacillin, piperacillin/tazobactam, ceftazidime, cefepime, aztreonam, imipenem, meropenem, amikacin, gentamicin, netilmicin, tobramycin, ciprofloxacin, levofloxacin, tetracycline, tigecycline, colistin, and trimethoprim/sulfamethoxazole, confirmed with E-test (bioMérieux) in accordance with Clinical and Laboratory Standards Institute guidelines.[13]

Whole-genome sequencing

Given its phenotypic resistance to antibiotics from different groups, such as β-lactams, aminoglycosides and tetracyclines, it was decided to perform WGS in order to identify the resistance gene profile. A bacterial sample was sent to Macrogen Europe (Amsterdam, The Netherlands) for preparation and library construction. The library was sequenced with Illumina sequencing using synthesis technology, and converted into raw data for analysis. Sequence reads were de novo assembled. After the whole-genome was assembled, the location of protein-coding sequences, transfer RNA (tRNA) genes, ribosomal RNA (rRNA) genes, and transfer-messenger RNA (tmRNA) genes were identified and their functions annotated. Prokka software (https://narrative.kbase.us/#catalog/apps/ProkkaAnnotation/annotate_contigs) was used to predict location, while BLAST was used to run the assembled sequences against a nucleotide and protein sequence database in order to identify and predict the function of the coding sequences.

Analysis of genome

The analysis was performed using the website of the Center for Genomic Epidemiology project (https://www.genomicepidemiology.org/). Replicase genes of the plasmids were classified using the PlasmidFinder v. 2.0 online tool (https://cge.food.dtu.dk/services/PlasmidFinder/). The MLST was identified using whole-genome sequences in the MLST database by applying bioinformatics tools available from the Center for Genomic Epidemiology. Serotype of *E. coli* Rize-53 was determined using SerotypeFinder (https://cge.food.dtu.dk/services/SerotypeFinder/) based on the O-(lipopolysaccharide) and H-(flagellar) antigen processing genes.[14] Antimicrobial resistance encoding genes were identified using ResFinder (https://cge.food.dtu.dk/services/ResFinder/) and a cutoff of 80% similarity.

Results

According to the Minimum Inhibitory Concentration (MIC) assay results, only piperacillin resistance (≥ 64) was observed among the β-lactam antibiotics. Moderate resistance was observed in the piperacillin/tazobactam combination, with a decreased MIC value of 16. No resistance to carbapenems was observed. Out of the 4 different aminoglycoside antibiotics, sensitivity was only observed to broad-spectrum gentamicin, while resistance was observed to the other 3 aminoglycosides (Table 1). Of the other antibiotics tested, only tetracycline resistance was observed. A total of 10 resistance genes were identified in the WGS analysis. These were *blaOXA-1* and *blaOXA-2* (β-lactam resistance; piperacillin, piperacillin/tazobactam and cefepime), *aac(6')-II* and *aac(6')-Ib-cr* (aminoglycoside resistance), *tetB* (tetracycline resistance), *catB3* (chloramphenicol resistance), *qacE* (quaternary ammonium compound-resistance protein E), *sitABCD*, *mdfA* (erythromycin and roxithromycin resistance), and *sul2* (sulfonamide resistance).

The whole-genome sequence was 5,430,376 nucleotides in length and was submitted to GenBank (https://www.ncbi.nlm.nih.gov/genbank/; the accession No. JAKSGM000000000). It had coding sequence for a total of 5230 genes, 83 tRNAs, 9 rRNAs, and 1 tmRNA. Clonal subtype (ST) of *E. coli* Rize-53 was determined as ST2141 (*adk*101-*fumC*88-*gyrB*262-*icd*281-*mdh*59-*purA*215-*recA*196). It was then determined that *E. coli* 53-Rize had *wzx* and *fliC* alleles and its serotype was O107/H39. No virulence genes were detected.

A total of 5 plasmids were detected in the genome of *E. coli* Rize-53, which included Col(BS512), IncC, IncFIA, IncFIB(AP1918), and IncFII(pRSB107). While Col(BS512), IncC, IncFIA and IncFII(pRSB107) were 100% similar in replicon typing, IncFIB(AP1918) had nucleotide changes and was found to be 98.39% similar. None of the resistance genes detected with WGS were on these plasmids.

Table 1. Antibiotic resistance profiles and minimum inhibitory concentration (MIC) values

Antimicrobials	MICs	Evaluation	Antibiotic group	Related resistance genes
Piperacillin	64	R	ureidopenicillin	bla$_{OXA-1}$ bla$_{OXA-2}$
Piperacillin/ tazobactam	16	I	ureidopenicillin	
Ceftazidime	0.25	I	third-generation cephalosporin	
Cefepime	0.5	I	fourth-generation cephalosporin	
Aztreonam	≤1	I	monobactam	
Imipenem	≤0.25	S	carbapenem	
Meropenem	≤0.25	S	carbapenem	
Amikacin	≥64	R	aminoglycoside	aac(6')-II aac(6')-Ib-cr
Gentamicin	≤1	S	broad spectrum aminoglycoside	
Netilmicin	≥32	R	aminoglycoside	
Tobramycin	≥16	R	aminoglycoside	
Ciprofloxacin	1	S	fluoroquinolone	–
Levofloxacin	1	S	fluoroquinolone	–
Tetracycline	16	R	tetracycline	tetB
Tigecycline	≤0.5	S	glycylcycline	–
Colistin	≤0.5	S	cyclic polypeptide	–
Trimethoprim/ sulfamethoxazole	≤20	S	sulfonamide	–

R – resistant; S – susceptible; I – intermediate.

Discussion

Escherichia coli isolates are normally found in human flora, though certain strains are the most common cause of UTIs. Antimicrobial therapy is crucial in the treatment of UTIs; however, rising resistance to antimicrobials has made an effective treatment more complicated. Results from a comparative study showed that resistance to trimethoprim-sulfamethoxazole (TMP-SMZ), which is used as a first-line resistance in the treatment of uncomplicated UTIs, did not change significantly over time in UPEC isolates. However, more recently, the increasing resistance to TMP-SMZ has been observed[15]; thus, TMP-SMZ should not be used in empirical therapy.[16] In the case of the *E. coli* Rize-53 isolate analyzed in the study, sensitivity to TMP-SMZ was demonstrated and no genes related to the resistance to this antibiotic were discovered.

Widespread and common use of quinolones and fluoroquinolones in the treatment of UTIs worldwide has led to the increased resistance in UPEC isolates.[17] Moreover, the resistance and level of fluoroquinolones in UPEC isolates reported from different countries are important. In this study, ciprofloxacin and levofloxacin from fluoroquinolones were tested against *E. coli* Rize-53. *Escherichia coli* was found to be sensitive to these fluoroquinolones, and no genes related to the resistance to this antibiotic group were found. Additionally, no tigecycline or colistin resistance genes were found in the genome, which explained the sensitivity to these antibiotics.

Escherichia coli Rize-53 was sensitive to all β-lactams tested, with the exception of piperacillin, and was also sensitive to piperacillin/tazobactam. It was previously demonstrated that carbapenem, piperacillin-tazobactam and amikacin antibiotics were highly effective against *E. coli* isolates identified from UTIs in Canada and the USA between 2010 and 2014 (>95% sensitivity).[18] The main cause of resistance to β-lactams is different types of β-lactamases. According to the WGS data, only 2 OXA genes ($bla_{OXA-1/2}$) are encoded in the *E. coli* Rize-53 genome, which we predict are responsible for piperacillin resistance. Furthermore, WGS data indicated that it was likely the *tetB* gene was the cause of the observed resistance to tetracycline in *E. coli* Rize-53. In an earlier study conducted on urine samples of 121 adult patients from Turkey, the resistance to tetracycline was observed in 82 samples and *tetB* was shown to be the most abundant tetracycline resistance gene.[1] Another study of 268 clinical *E. coli* isolates obtained from urine samples found that 36.8% were resistant to tetracycline.[19] Genetic determinants responsible for tetracycline resistance were not investigated in that study, but it demonstrated that tetracycline resistance is high in UTIs in Turkey.

Escherichia coli Rize-53 is only sensitive to broad-spectrum gentamicin and is resistant to the aminoglycoside antibiotics such as amikacin, netilmicin and tobramycin. Consistent with this phenotype, it has 2 genes,

aac(6')-II and *aac(6')-Ib-cr*, which are likely responsible for this resistance. Aminoglycoside-modifying enzyme genes can coexist in some strains, and combinations such as *aph(3")-Ib/aac(3)-Ia/aac(60)-Ib*, *ant(2")-Ia/aac(6')-Ib*, *aac(3)-Ia/aac(6')-Ib*, *aac(6')-Ib/aph(3")-Ib* and *aac(6')-Ib/aac(3)-IIa*, *aac(3)-IIa/aph(3')-Ia*, *ant(2')-Ia/aph(3')-Ia*, *aac(6')-Ib/aph(3')-Ia* have been identified in clinical isolates of *E. coli*.[20,21] Production of enzymes that alter aminoglycosides is one of the most common mechanisms of resistance to aminoglycosides in *E. coli* isolates. Furthermore, genes encoding aminoglycoside-modifying enzymes are mostly found on plasmids, but here they were identified in the chromosomal genome in *E. coli* Rize-53.

There may be a strong relationship between antibiotic resistance genes and ST in clonal groups. It is important to understand the geographical relationship of this grouping, as this will impact the direction and success of the therapies used. However, there is no detailed data on the STs of *E. coli* identified from Turkey in the literature. Indeed, no whole-genome sequence of *E. coli* from ST2141 type has been submitted to the pathogen watch portal (https://pathogen.watch). Therefore, this work represents the first WGS of ST2141 of *E. coli* from Turkey. Nonetheless, *Escherichia coli* ST2141 was isolated from the domestic duck (*Anas platyrhynchos*) in Bangladesh, though no genome analysis was performed.[22] In the current study, *E. coli* ST2141 was isolated from the urine of a UTI patient. Knowing antimicrobial resistance phenotypes for livestock, wildlife species and humans is important in order to follow changes in antibiotic resistance. In this regard, zoonotic transmission of disease represents a significant threat to human health. However, ST2141 isolated from domestic duck was reported to be *CTX-M15*-positive, whilst this gene could not be detected in the genome of *E. coli* Rize-53, although β-lactamase encoding *OXA-1* and *-2* were detected.

Escherichia coli serotyping is based on O and H antigens. The serotype searching database was based on the O-antigen genes *wzx*, *wzy*, *wzm*, and *wzt* for in silico O typing (comprising more than 188 O antisera) and the flagellin genes *fliC*, *flkA*, *flmA*, *flnA*, and *fllA* for in silico H typing (comprising more than 53 H antisera).[23] Determining the serotype via an in silico WGS approach is more reliable; therefore, this approach was used to identify the serotype of *E. coli* Rize-53 as O107/H39. Although *E. coli* very different *E. coli* serotypes based on O and H antigens have been shown in the literature, it has been determined that the first example of O107/H39 serotype is *E. coli* Rize-53. The O-antigen, an oligosaccharide with many repeats, is an essential component of the lipopolysaccharide on the surface of Gram-negative bacteria and one of the most variable cell constituents. The *E. coli* Rize-53 O107 O-antigen has a close relationship to *E. coli* O117 O-antigens, with only 1 substitution of D-GlcNAc for D-Glc. Furthermore, the O-antigen gene clusters of *E. coli* O107 and O117 share 98.6% overall DNA identity.[24] Flagellin

is the protein subunit of the flagellum, with an average molecular mass of approx. 50 kDa (from 36 to 60 kDa), that carries H-antigen specificity. There are currently 53 H types for *E. coli* flagella named from H1 to H56, and this established distinction between a highly variable central region and more conserved flanking regions was upheld.[25,26]

The Col(BS512) plasmid of *E. coli* Rize-53 was similar to a plasmid of *Shigella boydii* (accession No. NC010656, 2089 bp in length, 100% identity) that does not contain any resistance genes. The IncC plasmid of *E. coli* Rize-53 was also similar to the plasmid pNDM-KN (accession No. JN157804, 162746 bp in length, 100% identity) of *Klebsiella pneumoniae* strain Kp7. However, pNDM-KN, unlike *E. coli* Rize-53 IncC, had genes encoding NDM and AmpC-type β-lactamases.[27] These genes made the Kp7 strain resistant to carbapenems, while *E. coli* Rize-53 was carbapenem-susceptible. The IncFIA (100% identity) and IncFIB(AP1918) (98.38% identity) were similar to *E. coli* K-12 plasmid F (accession No. AP001918, 99159 bp in length) that did not contain any resistance genes.[28] The IncFII(pRSB107) was similar to an uncultured bacterium plasmid pRSB107 (accession No. AJ851089, 120592 bp in length, 100% identity), and harbored several resistance genes such as *aph3* (kanamycin), *strA* and *strB* (streptomycin), *sulII* (sulfonamide), bla_{TEM-1b} (β-lactamase), *mph(A)* (erythromycin and roxithromycin), *dhfR* (trimethoprim), *catA* (chloramphenicol), *tetA*, *tetC*, and *tetR* (tetracycline). The fact that the resistance genes of the *E. coli* Rize-53 isolate are on its genome limits the transmission of these resistance genes to other strains. Limiting transmissibility of these resistance genes is important in terms of preventing their spread.

Limitations

The main limitation of this study was a sample size, as WGS-type studies should be carried out on a whole population and include a variety of bacteria with different resistance patterns. Such efforts require organization at the national level and these limitations will be the focus of subsequent studies.

Conclusions

Antibiotic therapy is important in UTI treatment and there is an increasing resistance of UTIs to routinely applied antibiotics. Identifying the resistance genes encoded in the genome of a pathogen is crucial to understanding the resistance profile and the mechanisms behind the action of these pathogens. In this study, *E. coli* Rize-53 was resistant to the β-lactam piperacillin, the aminoglycosides netilmicin, tobramycin, and amikacin, as well as tetracycline. Resistance genes were identified using WGS, which revealed that piperacillin resistance was due

to the $bla_{OXA1/2}$ genes, while *aac(6')-Il*, *aac(6')-Ib-cr* and *tetB* genes conferred resistance to the aminoglycosides and tetracycline, respectively. However, none of the resistance genes identified in the study were carried by any of the 5 plasmids present in the strain. The genome sequence of *E. coli* Rize-53 demonstrated that this clinical isolate is equipped with important antibiotic resistance genes. Therefore, WGS offers a unique approach to evaluating antibiotic resistance genes across the entire genome of pathogens. This will allow the emerging and serious public health threat posed by such pathogens in both developed and developing countries around the world to be addressed more readily.

ORCID iDs

Halbay Turumtay https://orcid.org/0000-0003-4224-8103

References

1. Çiçek A, Şemen V, Aydoğan Ejder N, et al. Molecular epidemiological analysis of integron gene cassettes and *tetA*/*tetB*/*tetD* gene associations in *Escherichia coli* strains producing extended-spectrum β-lactamase (ESBL) in urine cultures. *Adv Clin Exp Med.* 2022;31(1):71–79. doi:10.17219/acem/142333
2. Rice LB. The clinical consequences of antimicrobial resistance. *Curr Opin Microbiol.* 2009;12(5):476–481. doi:10.1016/j.mib.2009.08.001
3. Jones RN, Kugler KC, Pfaller MA, Winokur PL. Characteristics of pathogens causing urinary tract infections in hospitals in North America: Results from the SENTRY Antimicrobial Surveillance Program, 1997. *Diagn Microbiol Infect Dis.* 1999;35(1):55–63. doi:10.1016/S0732-8893(98)00158-8
4. Khoshnood S, Heidary M, Mirnejad R, Bahramian A, Sedighi M, Mirzaei H. Drug-resistant gram-negative uropathogens: A review. *Biomed Pharmacother.* 2017;94:982–994. doi:10.1016/j.biopha.2017.08.006
5. Bush K, Fisher JF. Epidemiological expansion, structural studies, and clinical challenges of new β-lactamases from gram-negative bacteria. *Annu Rev Microbiol.* 2011;65(1):455–478. doi:10.1146/annurev-micro-090110-102911
6. Bush K, Jacoby GA, Medeiros AA. A functional classification scheme for beta-lactamases and its correlation with molecular structure. *Antimicrob Agents Chemother.* 1995;39(6):1211–1233. doi:10.1128/AAC.39.6.1211
7. Chopra I, Roberts M. Tetracycline antibiotics: Mode of action, applications, molecular biology, and epidemiology of bacterial resistance. *Microbiol Mol Biol Rev.* 2001;65(2):232–260. doi:10.1128/MMBR.65.2.232-260.2001
8. Møller TSB, Overgaard M, Nielsen SS, et al. Relation between tetR and tetA expression in tetracycline resistant *Escherichia coli*. *BMC Microbiol.* 2016;16(1):39. doi:10.1186/s12866-016-0649-z
9. Qadri F, Svennerholm AM, Faruque ASG, Sack RB. Enterotoxigenic *Escherichia coli* in developing countries: Epidemiology, microbiology, clinical features, treatment, and prevention. *Clin Microbiol Rev.* 2005;18(3):465–483. doi:10.1128/CMR.18.3.465-483.2005
10. Wood MJ, Farrell W. Comparison of urinary excretion of tobramycin and gentamicin in adults. *J Infect Dis.* 1976;134(Suppl 1):S133–S138. doi:10.1093/infdis/134.Supplement_1.S133
11. Mingeot-Leclercq MP, Glupczynski Y, Tulkens PM. Aminoglycosides: Activity and resistance. *Antimicrob Agents Chemother.* 1999;43(4):727–737. doi:10.1128/AAC.43.4.727
12. Ramirez MS, Tolmasky ME. Aminoglycoside modifying enzymes. *Drug Resist Updat.* 2010;13(6):151–171. doi:10.1016/j.drup.2010.08.003
13. Cockerill F. *Performance Standards for Antimicrobial Susceptibility Testing.* Wayne, USA: Clinical and Laboratory Standards Institute; 2012. ISBN:978-1-68440-032-4.
14. Joensen KG, Tetzschner AMM, Iguchi A, Aarestrup FM, Scheutz F. Rapid and easy in silico serotyping of *Escherichia coli* using whole genome sequencing (WGS) data. *J Clin Microbiol.* 2015;53(8):2410–2426. doi:10.1128/JCM.00008-15

15. Yamaji R, Rubin J, Thys E, Friedman CR, Riley LW. Persistent pandemic lineages of uropathogenic *Escherichia coli* in a college community from 1999 to 2017. *J Clin Microbiol*. 2018;56(4):e01834-17. doi:10.1128/JCM.01834-17

16. Bartoletti R, Cai T, Wagenlehner FM, Naber K, Bjerklund Johansen TE. Treatment of urinary tract infections and antibiotic stewardship. *Eur Urol Suppl*. 2016;15(4):81–87. doi:10.1016/j.eursup.2016.04.003

17. Walker E, Lyman A, Gupta K, Mahoney MV, Snyder GM, Hirsch EB. Clinical management of an increasing threat: Outpatient urinary tract infections due to multidrug-resistant uropathogens. *Clin Infect Dis*. 2016;63(7):960–965. doi:10.1093/cid/ciw396

18. Lob SH, Nicolle LE, Hoban DJ, Kazmierczak KM, Badal RE, Sahm DF. Susceptibility patterns and ESBL rates of *Escherichia coli* from urinary tract infections in Canada and the United States, SMART 2010–2014. *Diagn Microbiol Infect Dis*. 2016;85(4):459–465. doi:10.1016/j.diagmicrobio.2016.04.022

19. Copur-Cicek A, Ozgumus OB, Saral A, Sandalli C. Antimicrobial resistance patterns and integron carriage of *Escherichia coli* isolates causing community-acquired infections in Turkey. *Ann Lab Med*. 2014;34(2):139–144. doi:10.3343/alm.2014.34.2.139

20. Ojdana D, Sieńko A, Sacha P, et al. Genetic basis of enzymatic resistance of *E. coli* to aminoglycosides. *Adv Med Sci*. 2018;63(1):9–13. doi:10.1016/j.advms.2017.05.004

21. Fernández-Martínez M, Miró E, Ortega A, et al. Molecular identification of aminoglycoside-modifying enzymes in clinical isolates of *Escherichia coli* resistant to amoxicillin/clavulanic acid isolated in Spain. *Int J Antimicrob Agents*. 2015;46(2):157–163. doi:10.1016/j.ijantimicag.2015.03.008

22. Hasan B, Sandegren L, Melhus Å, et al. Antimicrobial drug-resistant *Escherichia coli* in wild birds and free-range poultry, Bangladesh. *Emerg Infect Dis*. 2012;18(12):2055–2058. doi:10.3201/eid1812.120513

23. Jenkins C. Whole-genome sequencing data for serotyping *Escherichia coli*: It's time for a change! *J Clin Microbiol*. 2015;53(8):2402–2403. doi:10.1128/JCM.01448-15

24. Wang Q, Perepelov AV, Feng L, Knirel YA, Li Y, Wang L. Genetic and structural analyses of *Escherichia coli* O107 and O117 O-antigens. *FEMS Immunol Med Microbiol*. 2009;55(1):47–54. doi:10.1111/j.1574-695X.2008.00494.x

25. Chui H, Chan M, Hernandez D, et al. Rapid, sensitive, and specific *Escherichia coli* H antigen typing by matrix-assisted laser desorption ionization–time of flight-based peptide mass fingerprinting. *J Clin Microbiol*. 2015;53(8):2480–2485. doi:10.1128/JCM.00593-15

26. García-Meniño I, Díaz-Jiménez D, García V, et al. Genomic characterization of prevalent mcr-1, mcr-4, and mcr-5 *Escherichia coli* within swine enteric colibacillosis in Spain. *Front Microbiol*. 2019;10:2469. doi:10.3389/fmicb.2019.02469

27. Carattoli A, Villa L, Poirel L, Bonnin RA, Nordmann P. Evolution of IncA/C blaCMY-$_2$-carrying plasmids by acquisition of the blaNDM-$_1$ carbapenemase gene. *Antimicrob Agents Chemother*. 2012;56(2):783–786. doi:10.1128/AAC.05116-11

28. Manwaring NP, Skurray RA, Firth N. Nucleotide sequence of the F plasmid leading region. *Plasmid*. 1999;41(3):219–225. doi:10.1006/plas.1999.1390

Long stress-induced non-coding transcript 5: A promising therapeutic target for cancer treatment

Wei Yang[1,A–F], Xiaoyan Yang[1,B,C], Qing Li[1,B,C], Pu Cao[1,B,C], Liyang Tang[1,B,C], Zhizhong Xie[2,E,F], Xiaoyong Lei[2,E,F]

[1] Institute of Pharmacy and Pharmacology, School of Pharmacy, University of South China, Hengyang, China

[2] The Hunan Provincial Key Laboratory of Tumor Microenvironment Responsive Drug Research, University of South China, Hengyang, China

A – research concept and design; B – collection and/or assembly of data; C – data analysis and interpretation;
D – writing the article; E – critical revision of the article; F – final approval of the article

Abstract

Long non-coding RNAs are RNA molecules with a transcript length of more than 200 nucleotides and without protein-coding ability. They regulate gene expression by interacting with protein, RNA and DNA. Their function is closely related to their subcellular localization, with regulation of gene expression at the epigenetic and transcriptional levels occurring in the nucleus, and at the post-transcriptional and translational levels in the cytoplasm. Long stress-induced non-coding transcript 5 (LSINCT5), which is localized in the nucleus, is overexpressed in many types of cancers such as breast cancer, gastric cancer, ovarian cancer, thyroid cancer, and gastrointestinal cancer. Substantial evidence indicates that there is an obvious connection between cancers and LSINCT5, as it inhibits apoptosis and promotes proliferation, invasion and migration of cancer cells, as well as participates in the pathogenesis and progression of cancer by interacting with DNA, protein and RNA. These findings suggest that LSINCT5 could be a novel biomarker and an emerging therapeutic target in human cancers. In the present study, the structure and corresponding biological function of LSINCT5 were summarized in order to clarify its molecular mechanisms in the progression of various malignant tumors.

Key words: LSINCT5, cancers, lncRNA, molecular mechanisms, tumorigenesis

Introduction

Cancer is caused by dysregulated gene expression that leads to serious illness and death in humans. Less than 2% of all gene sequences in the genome are coding, with mutations in the coding regions leading to the occurrence of most tumors. However, mutations in the non-coding regions of the genome lead to different phenotypes of tumor.[1] Ribonucleic acids (RNAs) are classified as coding RNAs, messenger RNAs (mRNAs) that will be transcribed into protein, and non-coding RNAs (ncRNAs) that are not translated into protein, such as circular RNAs (circRNAs), long non-coding RNAs (lncRNAs) and microRNAs (miR-NAs).[2] Recent studies have demonstrated that ncRNAs, identified using high-throughput sequencing technology, are dysregulated in various types of cancer.

Long non-coding RNAs are RNA molecules with a transcript length between 200 nucleotides (nt) and 100 kilobase (kb) pairs that influence the expression of oncogenes and tumor suppressor genes, with many lncRNAs uniquely expressed in differentiated tissues and specific cancer types.[3] Long non-coding RNA is transcribed by RNA polymerase II, capped, polyadenylated, and spliced. It lacks protein-coding sequences and can exert significant regulatory function.[4] The function of lncRNAs depends on their unique subcellular localization. They can form a functional network comprising DNA, protein and RNA, at the epigenetic and transcriptional levels. They also regulate complex cellular processes such as apoptosis, epigenetic changes, genomic imprinting, alternative splicing, gene expression, chromatin modification, and inflammatory pathologies, at the post-transcriptional level.[5,6] Potential roles of lncRNAs have been demonstrated in both oncogenic and tumor-suppressive pathways, with their dysregulation implicated in various pathophysiological processes, especially tumorigenesis.[7] Indeed, the correlation between lncRNA expression and cancer pathogenesis is one of the most promising areas of research for understanding the underlying pathophysiology of human cancers.[6–9]

Long stress-induced non-coding transcript 5 (LSINCT5) is a 2.6-kb polyadenylated transcript which is potentially transcribed by RNA polymerase III, and is located on 5p15.33.[10] The expression of LSINCT5 is found to be increased in multiple cancers, including breast cancer (BRCA), gastric cancer (GC), ovarian cancer (OC), and bladder cancer (BC).[11–14] Long stress-induced non-coding transcript 5 may be an important regulatory RNA in human cancer cell proliferation, cell cycle, survival, migration, and invasion.[15] Furthermore, a dysregulated expression of LSINCT5 has been linked to cancer progression and unfavorable prognosis in various human tumors.[16] The LSINCT5, which is one of 12 stress-induced lncRNAs (LSINCT1-12), is expressed during stress-induced cell formation and has been reported to promote cancer progression by regulating cell proliferation, metastasis and apoptosis.[17,18] Mechanisms of LSINCT5 include the regulation of mRNA metabolism, interaction with proteins, acting as competitive endogenous RNA (ceRNA), and interacting with miRNA. Many of the cancer types promoting cellular processes with LSINCT5 involvement are listed in Table 1. In this article, various functions of LSINCT5 in different types of cancer have been reviewed and the potential of LSINCT5 as a biomarker and therapeutic target in the treatment of cancer has been discussed.

Objectives

All of the literature related to LSINCT5 was reviewed in order to summarize various functions of LSINCT5 in different types of cancer, with the aim of exploring its potential as a biomarker and potential therapeutic target in the treatment of cancer.

Materials and methods

Relevant literature was retrieved by searching several databases, including GreenMedical, Spis, China National Knowledge Infrastructure, and PubMed, to identify studies published between January 2000 and July 2021. Green-Medical, Spischolar and PubMed databases were searched using 3 separate sets of keywords, namely "LSINCT5 and cancer", "LSINCT5 and tumor" and "LncRNA and cancers". Keywords used to search the China National Knowledge Infrastructure were "LSINCT5 and tumor". Data were extracted from the articles and entered into Microsoft Word (Microsoft Office 2003; Microsoft Corp., Redmond, USA) for analysis. All figures and tables were prepared manually, according to the protocol of the analysis of the studies.

All studies related to LSINCT5 that were conducted in human subjects, including randomized controlled trials, systematic reviews and meta-analyses, were considered. Additionally, only studies published in the English or Chinese were considered. This resulted in 55 articles being included in the systematic literature review.

LSINCT5 in various tumors

LSINCT5 in gastrointestinal cancer

Xu et al. found that LSINCT5 expression was higher in cancerous tissue than in adjacent healthy tissues in GC and colorectal cancer (CRC).[12] The overexpression of LSINCT5 was also associated with clinical progression and development of these gastrointestinal cancers.[12] Indeed, the expression levels of LSINCT5 in GC and CRC were correlated with patient prognosis, whereby higher expression resulted in significantly worse prognoses than for patients with lower expression levels. Furthermore,

Table 1. Functional characterization of long stress-induced non-coding transcript 5 (LSINCT5) in various cancers

Cancer type	Dysregulation	Functional	Related genes	Role	Reference
Gastrointestinal cancer	upregulated	proliferation, migration, invasion, EMT, tumorigenesis	*E2F1, CXCR4, IRX2, IRX4*	oncogene	12, 19
Liver cancer	upregulated	proliferation, migration, invasion, viability, EMT, tumorigenesis	*HMGA2, miR-4516, STAT3, BclxL*	oncogene	21
Pancreatic cancer	upregulated	proliferation, migration, invasion, cell cycle, tumorigenesis	*P21, CyclinB1, CyclinE*	oncogene	22
Breast cancer	upregulated	proliferation, migration, invasion, viability, EMT, tumorigenesis	*GAS5, B2M, miR-30a*	oncogene	11, 26, 27
Lung cancer	upregulated	proliferation, migration, viability, EMT, tumorigenesis	*PI3K, Akt, p-Akt, HMGA2*	oncogene	28–30
Thyroid cancer	upregulated	proliferation, migration, invasion, viability, tumorigenesis	*miR-29c, ITGB1*	oncogene	31, 32
Ovarian cancer	upregulated	proliferation, migration, invasion, viability, tumorigenesis	*CXCR4, CXCL12, SDF-1, PSPC1*	oncogene	11, 13
Osteosarcoma	upregulated	proliferation, migration, invasion, viability, apoptosis, tumorigenesis	*APC, EZH2, CCND1, MYC, SOX9, SOX4, TCF1*	oncogene	10, 16, 36
Glioma	upregulated	proliferation, migration, invasion, viability, apoptosis, tumorigenesis	*miR-451, Rac1, PI3K, AKT, p65, Wnt3a, Wnt5a, β-catenin*	oncogene	34
Bladder cancer	upregulated	proliferation, migration, invasion, viability, EMT, tumorigenesis	*NCYM, β-catenin, GSK3b*	oncogene	25, 42
Esophageal squamous cell carcinoma	upregulated	proliferation, migration, invasion, EMT, senescence, apoptosis, tumorigenesis	*ECM, MAPK, MMP9, N-cadherin, vimentin*	oncogene	23
Endometrial carcinoma	upregulated	proliferation, apoptosis, migration, invasion, cell cycle, tumorigenesis	*HMGA2, Wnt, β-catenin*	oncogene	28
Oral squamous cell carcinoma	upregulated	proliferation, apoptosis, migration, invasion, cell cycle, tumorigenesis	*miR-185-5p, ZNF703, YWHAZ*	oncogene	24

EMT – epithelial–mesenchymal transition.

it was demonstrated that LSINCT5 plays a significant role in GC as an oncogene, as its upregulation significantly promoted tumor cell growth, whereas downregulating had the opposite effect. Therefore, inhibiting the overexpression of LSINCT5 could be an effective way to slow down the progression of GC and CRC (Table 1).

Qi et al. found that LSINCT5 was upregulated in metastatic GC tissues and promoted GC cell migration and invasion.[19] The LSINCT5 had an impact on epithelial–mesenchymal transition (EMT) in GC cells, a process that has been shown to be critically important in the early events of GC tumor cell metastatic dissemination by inducing cell motility. Furthermore, EMT promotes GC cells to acquire invasion potential, and LSINCT5 can change the malignant phenotype by regulating EMT.[19] Therefore, GC cell migration and invasion could be decreased when EMT is inhibited through decreasing the expression of LSINCT5. Transcription factor E2F1 activates LSINCT5 transcription and increases its expression, with E2F1 and LSINCT5 both found to be overexpressed in GC. Consequently, downregulating E2F1 may be a useful strategy to downregulate the expression of LSINCT5. In conclusion, LSINCT5 could be a novel prognostic indicator and a target for gene therapy in GC (Table 1).

LSINCT5 in hepatocellular carcinoma

Hepatocellular carcinoma (HCC) is the most common type of malignant tumor and largely leads to a high occurrence of cancer, with lncRNAs emerging as critical factors for HCC-related gene expression.[20] Li et al. studied the expression pattern and biological function of LSINCT5 in HCC and found it to be upregulated and to predict poor survival through promotion of HCC migration and viability in vivo.[21] They concluded that LSINCT5 might function as a ceRNA of miR-4516.[21] The LSINCT5 stabilizes high mobility group AT-hook protein 2 (HMGA2), which is a master activator of EMT, in order to prevent its degradation.[21] Furthermore, LSINCT5 promotes HCC cells to acquire invasion potential by promoting the progression of EMT. Therefore, the degradation of HMGA2 may stop EMT progression, which could serve as a potential novel therapeutic target for HCC treatment (Table 1).

LSINCT5 in pancreatic cancer

The incidence rate of pancreatic cancer (PC) is increasing year by year globally. Pancreatic cancer leads to the development of a highly malignant tumor with a very poor prognosis. Mei et al. found that the overexpression

100

W. Yang et al. LSINCT5 is a promising target

Table 2. Clinical significance of long stress-induced non-coding transcript 5 (LSINCT5) in various tumors

Cancer type	Associated clinical features	Prognosis	Reference
Gastrointestinal cancer	OS, DFS, DSS, tumor volume, metastasis, TNM stage	poor	12, 19
Liver cancer	OS, DFS, tumor volume, metastasis, TNM stage	poor	21
Pancreatic cancer	OS, DFS, DSS, tumor volume, metastasis	poor	22
Breast cancer	OS, DFS, tumor volume, lymph node metastasis	poor	11, 26, 27
Lung cancer	OS, tumor size, TNM stage, metastasis	poor	28–30
Thyroid cancer	OS, DFS, tumor volume, metastasis	poor	31, 32
Ovarian cancer	OS, tumor size, TNM stage, lymphatic metastasis	poor	11, 13
Osteosarcoma	OS, DFS, tumor volume, tumor size, lymphatic metastasis, TNM stage	poor	10, 16, 35
Glioma	OS, DFS, tumor volume, tumor size, lymphatic metastasis, TNM stage	poor	34
Bladder cancer	OS, DFS, tumor volume, tumor size, lymphatic metastasis, TNM stage	poor	25, 42
Esophageal squamous cell carcinoma	OS, tumor size, TNM stage, lymph node metastasis, tumor size	poor	23
Endometrial carcinoma	OS, DFS, tumor volume, tumor size, lymphatic metastasis, TNM stage	poor	28
Oral squamous cell carcinoma	OS, DFS, DSS, RFS, tumor volume, tumor size, lymphatic metastasis, TNM stage	poor	24

DFS – disease-free survival; DSS – disease-specific survival; RFS – recurrence-free survival; OS – overall survival; TNM – tumor-node-metastasis.

of LSINCT5 was widespread in PC cells and could promote their proliferation and cell cycle progression, inducing adenocarcinoma cell cycle transformation from G1 to S phase.[22] Furthermore, LSINCT5 could regulate the expression level of key cell cycle factors such as mRNA and protein in PC cells. It was concluded that LSINCT5 serves as an oncogene in the progression of pancreatic adenocarcinoma, and its overexpression indicates a poor prognosis for PC patients. Therefore, decreasing the expression of LSINCT5 could have a therapeutic effect in the treatment of PC (Table 1).

LSINCT5 in esophageal squamous cell carcinoma

Esophageal cancer is one of the most common and deadliest cancers in China; its 2 main types are esophageal squamous cell carcinoma (ESCC) and esophageal adenocarcinoma (EA).[23] The LSINCT5 was shown to be significantly overexpressed in ESCC cell lines, with next-generation RNA-sequencing indicating that 138 genes were upregulated and 227 were downregulated in LSINCT5-knockdown ESCC cells in vitro.[23] This demonstrated the great impact of LSINCT5 on gene expression as proliferation, migration, invasion, and EMT were suppressed in these cells.[23] Also, LSINCT5 was upregulated in ESCC tissues, which correlated with tumor size, tumor-node-metastasis (TNM) stage and lymph node metastasis.[23] Consequently, LSINCT5 could cause disorders in gene expression which further contribute to the progression of ESCC. This provides additional insight into esophageal cancer carcinogenesis and strong evidence to suggest that LSINCT5 may be a viable chemotherapeutic target for prevention of gene expression disorders in the treatment of esophageal cancer (Table 1).

LSINCT5 in oral squamous cell carcinoma

Oral squamous cell carcinoma (OSCC) is a type of cancer in which 5-year survival is lower than 50%, and which has a close relationship with smoking and drinking. Wang et al. analyzed the role of LSINCT5 in OSCC progression, as well as the molecular mechanisms it adopts.[24] They found that LSINCT5 was overexpressed in OSCC specimens and influenced malignant progression through the miR-185-5p/zinc finger protein 703 (ZNF703) axis. In this regard, the proliferative and migratory capacities of OSCC were inhibited when LSINCT5 was knocked down. Dual-luciferase reporter assay further verified that miR-185-5p was the target of LSINCT5, as miR-185-5p displayed anti-cancer properties on malignant phenotypes of OSCC through the downregulation by LSINCT.[24] Furthermore, the mechanism of the action of miR-185-5p in OSCC cells was shown through the downregulation of the oncogenic gene *ZNF703*.[24] Additionally, survival analysis showed that OSCC patients expressing low levels of LSINCT5 had much longer overall survival in comparison to those expressing high levels of LSINCT5. As such, LSINCT5 was suggested as a prognostic factor for OSCC. In summary, miR-185-5p and *ZNF703* could be targeted to influence the expression of LSINCT5 in OSCC cells. Upregulating the expression of miR-185-5p could downregulate the expression of LSINCT5, which could be a therapeutic strategy for OSCC patients (Table 1).

LSINCT5 in bladder cancer

Bladder cancer is one of the most common malignant tumors of the urinary system. Zhu et al. found that LSINCT5 was specifically upregulated in BC and its overexpression was significantly associated with tumor size, TNM stage and metastasis.[25] Moreover, a significant upregulation

of LSINCT5 was found to be a characteristic change in BC and indicated poor prognosis.[25] Competitive RNA pull-down confirmed the interaction of LSINCT5 with *NCYM*, which is a de novo evolved gene product that acts as an oncogenic factor in cancer.[25] As such, the LSINCT5/*NCYM* axis could promote the progression of BC through the activation of the wingless-related integration site (Wnt)/β-catenin signaling pathway and by promoting EMT.[25] In summary, LSINCT5 was found to contribute to the oncogenic potential of BC, and LSINCT5/*NCYM*/Wnt/β-catenin may be a potential chemotherapeutic target for BC treatment (Table 1).

LSINCT5 in breast cancer

Breast cancer is one of the most common malignancies that leads to the death of women globally. Long non-coding RNAs play crucial roles in the key biological processes of both normal and malignant breast cells, with early studies implicating LSINCT5 in BRCA cell proliferation and migration.[11,26] Silva et al.[11], Zhang et al.[26] and Liang et al.[27] found that LSINCT5 was overexpressed in BRCA and positively correlated with its progression. Indeed, the level of LSINCT5 in metastatic tissues was higher than in nonmetastatic tissues, and these higher levels were indicative of a poor prognosis. Therefore, LSINCT5 could be a biomarker for the progression of BRCA. The LSINCT5 is a molecular sponge for miR-30a in BRCA cells, as a knockdown of LSINCT5 suppressed cell motility by regulating miR-30a in MCF-7 cells.[26] Additionally, LSINCT5 knockdown inhibited BRCA cell proliferation, invasion, EMT, and motility, by inactivating the β-catenin/TCF4/c-Myc pathway in vivo (Table 1).[26] Therefore, the knockdown of LSINCT5 may be a promising way of inhibiting the progression of BRCA.

LSINCT5 in ovarian cancer

Ovarian cancer is one of the most serious malignant tumors among women worldwide. Epithelial ovarian cancer (EOC) is characterized by frequent implantation and metastases in the abdominopelvic cavity.[13] The expression of LSINCT5 in OC tissues and cell lines was significantly increased and its expression in metastatic OC tissues was higher than in nonmetastatic tissues. Furthermore, LSINCT5 levels were positively correlated with the pathological grade of OC, and the increased expression of LSINCT5 was related to poor prognosis. At the same time, the downregulation of LSINCT5 significantly suppressed the C-X-C motif chemokine ligand-12 (CXCL12)/C-X-C chemokine receptor 4 (CXCR4) signaling axis and inhibited the proliferation, migration and invasion of OC cells.[11,13] High expression of LSINCT5 was associated with the presence of lymphatic metastases and the advanced International Federation of Gynecology and Obstetrics (FIGO) stage, but was not associated

with patient age, histological subtype, histological grade, or residual tumor diameter.[11] As such, LSINCT5 could be used as a biomarker for the progression of OC (Table 1).

LSINCT5 in endometrial carcinoma

Endometrial carcinoma (EC) is one of the most common gynecologic malignancies in women, ranking 6th in morbidity and 3rd in mortality worldwide. Jiang et al. found that the amount of LSINCT5 in EC tissues was significantly higher than in healthy controls.[28] The LSINCT5 could promote cell proliferation, migration and invasion of EC cells, as silencing it caused cell cycle arrest and apoptosis.[28] Mechanistically, LSINCT5 may suppress the degradation of HMGA2 to stabilize the protein in EC cells, which could promote EMT by activating the Wnt/β-catenin signaling pathway. Therefore, EC cells acquire the potential for proliferation, migration and invasion, increasing the level of HMGA2 protein through LSINCT5. In turn, this would contribute to the progression of EC (Table 1).

LSINCT5 in lung cancer

Lung cancer is the main cause of cancer deaths globally, of which non-small cell lung cancer (NSCLC) has a dramatically low 5-year survival and accounts for nearly 85% of all lung cancers. Tian et al. found that LSINCT5 may be an important gene regulator in NSCLC as its overexpression predicted poor prognosis for NSCLC patients.[29] The overexpression of LSINCT5 has been shown to markedly increase the viability of NSCLC cells and tumor growth, potentially through its interaction with HMGA2.[29] The LSINCT5 physically interacts with HMGA2 to prevent its proteasome-mediated degradation.[29] Additionally, LSINCT5 promotes the expression and activity of protein kinase B (Akt) in PC9 cells, and can promote the resistance to epidermal growth factor receptor/tyrosine kinase inhibitors (EGFR/TKIs) in lung cancer cells.[28] This means that HMGA2 could promote EMT of lung cancer cells by increasing the activity of Akt proteins. Furthermore, Chen et al. found that the expression of LSINCT5 in NSCLC tissues was higher in erlotinib-resistant cells.[30] Therefore, LSINCT5 may be a target for inhibiting the expression and activity of Akt, and a target for promoting cell sensitivity to erlotinib. The LSINCT5 was also found to be closely related to tumorigenesis and chemoresistance in NSCLC (Table 1).

LSINCT5 in thyroid cancer

Papillary thyroid carcinoma (PTC) is a type of thyroid cancer and is the most common malignant endocrine tumor. Kuang et al. found that LSINCT5 was overexpressed in PTC and that LSINCT5 knockdown decreased cellular proliferation and migration of TPC-1 and KAT-5 cell lines.[31] Bioinformatic predictions, dual luciferase reporter gene and receptor interacting protein detection found that

miR-29c was a target for LSINCT5 binding.[31] Furthermore, the co-transfection with miR-29c inhibited the effect of LSINCT5 on proliferation and metastasis and inhibited the effect of upregulation of integrin subunit beta 1 (ITGB1) by LSINCT5.[31] LSINCT5 serves as an oncogene that promotes proliferation and metastasis of PTC via miR-29c/ITGB1 axis.[32] Therefore, LSINCT5 is closely associated with the progression of PTC (Table 1). Hence, targeting LSINCT5 may slow down the progression of PTC.

LSINCT5 in glioma

Gliomas are a type of aggressive brain tumor that cause brain cancer-related death.[33] Liu et al. showed that LSINCT5 promoted cell viability, migration and invasion, but inhibited the apoptosis of glioma GL15 cells.[34] The LSINCT5 exerted its influence as a molecular sponge for miR-451,[34] which it regulated to promote the growth and metastasis of the cells. Furthermore, the overexpression of miR-451 suppressed the growth and metastasis of glioma GL15 cells through regulation of Rac family small GTPase 1 (Rac1).[34] This LSINCT5/miR-451/Rac1 axis affected the phosphatidylinositol 3-kinase (PI3K)/Akt, Wnt/β-catenin and nuclear factor-jB pathways to promote the progression of glioma.[34] Therefore, breaking the LSINCT5/miR-451/Rac1 axis is a promising way to stop the progression of glioma. In summary, LSINCT5 contributes to the oncogenic potential of glioma, and the LSINCT5/miR-451/Rac1 axis may be a potential therapeutic target (Table 1).

LSINCT5 in osteosarcoma

Liao et al. found that LSINCT5 was identified as an upregulated lncRNA in osteosarcoma (OS), and its overexpression decreased the survival rate of OS patients.[35] Proliferation, invasion, migration ability, and the number of cell membrane penetrations of OS cells were decreased after LSINCT5 knockdown. In addition, LSINCT5 was found to inhibit the transcription of the tumor suppressor gene adenomatosis adenomatous polyposis coli (*APC*) by recruiting enhancer of zeste 2 polycomb repressive complex 2 subunit (EZH2).[10] Therefore, the invasion, metastasis and growth of OS cells could be promoted by the inhibition of *APC*. In conclusion, LSINCT5 promotes the invasion, metastasis and growth of OS cells through *APC*. Both of these pathways may prove to be promising targets in the treatment of OS (Table 1).

Mechanisms of LSINCT5 in cancer

Interaction between LSINCT5 and proteins

Many lncRNAs interact with proteins, such as the transcriptional and cell cycle regulator HMGA2, to exert their functions. The HMGA2 has attracted much attention due to its extensive carcinogenic effects, and LSINCT5 has been shown to interact with it to regulate gene expression. This interaction was found to increase the abundance of HMGA2 protein, but had no influence on HMGA2 mRNA levels in NSCLC and EC cells.[28,29] The overexpression of LSINCT5 prevented proteasome-mediated degradation of HMGA2 proteins by suppressing their ubiquitination in NSCLC cells. Furthermore, HMGA2 promoted EMT and increased the rate of cell proliferation, which, in turn, increased the metastatic and invasive potential of tumor cells. Therefore, cancer cell proliferation, metastasis, invasion, EMT, and tumor angiogenesis are promoted when LSINCT5 increases the level of HMGA2 proteins in NSCLC and EC cells.

Interaction between LSINCT5 and RNA

The LSINCT5 has been shown to interact with miRNA and mRNA to exert its influence on the progression of cancer (Fig. 1). Many miRNAs serve as tumor suppressor genes in cancer cells. For example, *miR-185-5p* is a tumor suppressor gene in OSCC, *miR-30a* is a tumor suppressor gene in BRCA cells, *miR-451* is a tumor suppressor gene in glioma cells, *miR-20a-5p* is a tumor suppressor gene in OS cells, *miR-4516* is a tumor suppressor gene in HCC cells, and *miR-29c* is a tumor suppressor gene in PTC. The LSINCT5 could be acting as the ceRNA of these miRNAs to inhibit their tumor-suppressing function. Therefore, cancer cell proliferation, metastasis, invasion, and tumor angiogenesis will be promoted when the tumor-suppressing function of these miRNAs is inhibited by LSINCT5 in OSCC, glioma, OS, HCC, PTC, and BRCA cells. Moreover, v-myc avian myelocytomatosis viral oncogene neuroblastoma derived homolog (NYCM) could activate the Wnt/β-catenin signaling pathway in order to promote EMT in BC progression.[25] The LSINCT5 binds NYCM to activate the Wnt/β-catenin signaling pathway. The proliferation, metastasis and invasion of BC cells is then promoted by EMT. In addition, CXCR4 and CXCL12 are 2 forms of mRNA in OC cells and LSINCT5 is found to promote the progression of OC by increasing the expression of both mRNA forms.

Interaction between LSINCT5 and DNA

Decreased expression of LSINCT5 influences the expression of multiple genes (Fig. 1). Both iroquois homeobox 4 (*IRX4*) and *IRX2* were shown to be regulated by LSINCT5 and to promote gastrointestinal tumor progression. Moreover, nuclear paraspeckle assembly transcript 1 (*NEAT1*), paraspeckle component 1 (*PSPC1*), epiplakin 1 (*EPPK1*), actin-related protein 2 (*ACTR2*), and *CXCR4* showed a twofold change in LSINCT5 knockdown of BRCA cells. In addition, 138 genes were upregulated and 227 genes

were downregulated in LSINCT5 knockdown of ESCC cell lines in vitro.[23] This suggested that LSINCT5 exerted its influence on ESCC cell lines by interacting with 365 differentially expressed genes that enriched a dozen signaling pathways, further contributing to tumorigenesis and tumor progression in these cells. In conclusion, LSINCT5 has been demonstrated to interact with multiple genes in order to promote tumorigenesis and progression of different cancers.

Interaction between LSINCT5 and EMT

Regulating EMT by LSINCT5 is a common mechanism in different cancers, including GC, BRCA, BC, ESCC, and HCC. The transformation from epithelium to stromal cells during EMT is a central differentiation process that exerts a great impact on cancer initiation and progression, as well as metastasis and tumor angiogenesis. A key to the EMT process in cancer cells is the regulation of the expression of a number of factors by LSINCT5, including E-cadherin, N-cadherin, vimentin, matrix metalloproteinase 2 (MMP-2), and MMP-9. Moreover, HMGA2 is regulated by LSINCT5 and is known to facilitate EMT by inhibiting E-cadherin. As such, HMGA2 could be an important activator during EMT development in different cancers, with LSINCT5 being an important regulator. Therefore, targeting LSINCT5 to stop EMT could exert chemotherapeutic effect on different cancers.

Clinical significance of LSINCT5

LSINCT5 as a biomarker for cancer diagnosis

Early detection of cancer directly contributes to the effect of cancer treatment, and LSINCT5 plays an important role in this process. The overexpression of LSINCT5 was confirmed in EC and PTC, with levels much higher than in adjacent tissues at the early stages of disease. Indeed, higher levels of LSINCT5 in endometrial tissue and thyroid tissue highlighted its potential diagnostic value. However, many types of lncRNA were shown to be overexpressed in adjacent tissues. Therefore, LSINCT5 does not have high specificity or sufficient sensitivity in EC or PTC. Mechanistically, the LSINCT5/HMGA2/Wnt/β-catenin and LSINCT5/miR-29c/ITGB1 axes promote the proliferation, metastasis and invasion of EC and PTC cells. Fortunately, the LSINCT5/HMGA2/Wnt/β-catenin and LSINCT5/miR-29c/ITGB1 axes have higher specificity and greater sensitivity than LSINCT5 alone as a biomarker for the diagnosis of EC and PTC. In summary, LSINCT5 represents a promising diagnostic biomarker detectable in EC and PTC (Table 2).

LSINCT5 as a biomarker for cancer prognosis

The expression of LSINCT5 may also be used to predict cancer prognosis, as different expression levels indicate varying prognoses in a number of cancers. In patients with OSCC, GC or CRC, higher expression levels of LSINCT5 always predicted a significantly worse prognosis, with lower disease-free survival and shorter overall survival. Therefore, LSINCT5 could be an independent prognostic factor for OSCC, GC and CRC patients. Higher expression of LSINCT5 was found to promote OSCC, GC and CRC cells to acquire more invasive ability. Moreover, a higher expression of LSINCT5 was found to promote more lymph node metastases and distant metastases of OSCC, GC and CRC cells. As a result, a higher expression of LSINCT5 deteriorates the progression of OSCC, GC and CRC patients by strengthening the proliferative and migratory capacities of OSCC, GC and CRC cells. In summary, a high expression of LSINCT5 predicts unfavorable prognosis and poor outcome for OSCC, GC and CRC patients, and has a good prognostic value in these patients (Table 2).
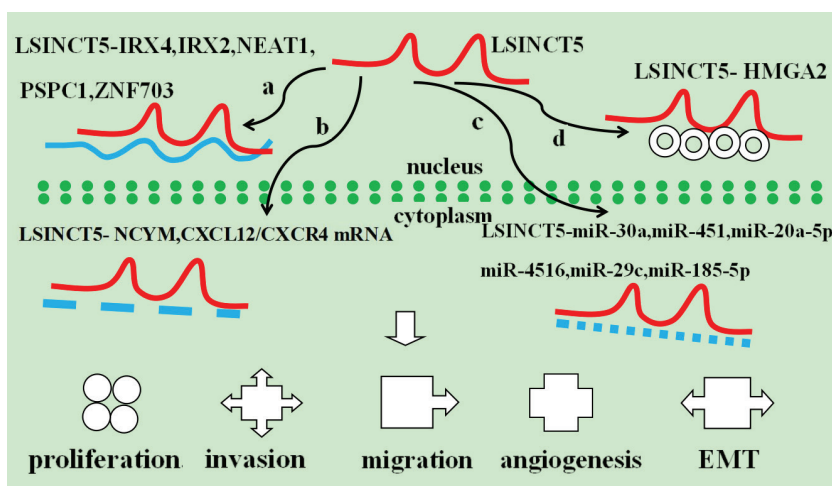
Fig. 1. Graphical representation of interactions between long stress-induced non-coding transcript 5 (LSINCT5) and DNA, RNA, and protein targets – and their role in the multistep development of cancers.
A. The LSINCT5 is shown to interact with iroquois homeobox 4 (IRX4), IRX2, nuclear paraspeckle assembly transcript 1 (NEAT1), paraspeckle component 1 (PSPC1), and zinc finger protein 703 (ZNF703);
B. The LSINCT5 is shown to interact with NCYM, C-X-C motif chemokine ligand-12 (CXCL12)/C-X-C chemokine receptor 4 (CXCR4) and mRNAs;
C. The LSINCT5 is shown to interact with miR-30a, miR-451, miR-20a-5p, miR-4516, miR-29c, miR-185-5p, and other miRNAs;
D. The LSINCT5 is shown to interact with high-mobility group AT-hook protein 2 (HMGA2) protein targets.
The LSINCT5 plays an important role in cancer cell proliferation, metastasis, invasion, epithelial–mesenchymal transition (EMT), and tumor angiogenesis

104

W. Yang et al. LSINCT5 is a promising target

LSINCT5 as a target for cancer treatment

The LSINCT5 is overexpressed in NSCLC, BC, BRCA, glioma, OC, and HCC. Likewise, cancer cell proliferation, metastasis, invasion, EMT, and tumor angiogenesis are inhibited when the expression of LSINCT5 is downregulated. Therefore, LSINCT5 shows promise as a chemotherapeutic target for pharmacological intervention.

Promoting cell proliferation, metastasis, invasion, and EMT of NSCLC was found to be achieved through stabilizing HMGA2 by LSINCT5. Therefore, targeting LSINCT5 to lower its expression level could promote the degradation of HMGA2 as a mean of halting EMT and cancer progression.

Another mechanism by which the overexpression of LSINCT5 was found to promote proliferation, invasion and EMT, was by sponging miR-30a in BRCA cells.[26] The LSINCT5 promoted the progression of BRCA by regulating the Wnt/β-catenin pathway and promoted EMT by activating the Wnt/β-catenin pathway. Therefore, lowering the expression level of LSINCT5 could increase the expression levels of miR-30a, which would suppress proliferation and invasion of BRCA cells and halt EMT. Similar mechanisms have been shown in HCC, BC and glioma, with lower expression levels of LSINCT5 helping to prevent cancer progression. Indeed, lower expression levels of LSINCT5 increased the expression of miR-4516 in HCC cells, which led to a reduction in proliferation and invasion. Similarly, lowering the expression of LSINCT5 suppressed EMT in HCC cells and BC cells. Furthermore, targeting LSINCT5 to lower its expression levels increased the expression of miR-451, which suppressed proliferation and invasion of glioma cells.[34]

Overexpressed LSINCT5 promoted the progression of OC cells through regulation of the CXCL12/CXCR4 signaling axis by increasing the expression of the *CXCR4* gene.[13] Therefore, targeting LSINCT5 to lower its expression level could decrease the expression level of *CXCR4* and lead to suppressed proliferation and invasion of OC cells.

In summary, LSINCT5 is highly expressed in NSCLC, BC, BRCA, glioma, OC, and HCC, and is a promising target for cancer treatment. Targeting LSINCT5 for cancer treatment has some advantages. First, LSINCT5 may be a gene-specific epigenetic regulator and could be targeted to inhibit epigenetic aberrations and stop the process of carcinogenesis. Second, targeting LSINCT5 could result in reduced side effects, as it is a ncRNA. Third, LSINCT5 has been detected in secreted exosomes, which may be used as a safer route for gene delivery. Taken together, the characteristics of LSINCT5 demonstrate its role as a promising target for cancer treatment (Table 2).

Limitations

This systematic review has a number of limitations. First, the precise mechanisms of LSINCT5 in some cancers, such as ESCC and PC, have yet to be fully clarified.

Indeed, the targets of LSINCT5 in these cancers are still unclear. Moreover, evidence of the anti-cancer effect of targeting LSINCT5 is weak, as it has not been proven experimentally and no related articles were found. Furthermore, LSINCT5 has only been linked to 13 types of cancer and its precise mechanisms of action are still unclear. Had there been more data from large trials available, statistical analysis and conclusions would be more persuasive. In addition, there are not enough data and materials available for The Cancer Genome Atlas pan-cancer expression of LSINCT5 to be completed. Therefore, targeting LSINCT5 may provide a novel and effective therapeutic approach for anti-cancer therapies. However, because of the current lack of proper animal and clinical data, it cannot be considered as a definitive target for cancer therapy.

Conclusions

Critical roles for LSINCT5 in tumorigenesis and the mechanisms it adopts are worth exploring, as LSINCT5 is differentially abundant in different cancer types. Indeed, LSINCT5 is closely related to tumorigenesis, metastasis, tumor stage, aggressiveness, invasiveness, poor survival, and other processes through interactions with tumor related DNA, RNA and proteins. Therefore, LSINCT5–DNA, LSINCT5–RNA and LSINCT5–protein interactions are promising approaches for cancer diagnosis and treatment.[43]

The LSINCT5 serves as an oncogene to facilitate tumor cell proliferation, metastasis and invasion, inhibit apoptosis, and induce tumor formation in various types of cancer. It achieves this through regulating gene expression and protein functionality at multiple levels, and its deregulation plays a key role in tumorigenesis.[19,48] Furthermore, LSINCT5 is a novel molecular target in cancer therapy due to its strong predictive and specific expression patterns. In addition, the characterization of LSINCT5 will highlight its potential clinical applications in cancer prevention and diagnosis.

There are several possible approaches for targeting LSINCT5, such as silencing, functional blockage and structure disruption.[51] Targeting LSINCT5 seems to be promising in the fight against cancer and may be available clinically after overcoming certain obstacles.[54] These obstacles include a lack of suitable delivery vehicle, poor cellular uptake and cytotoxicity of antisense oligonucelotides.[52] Furthermore, suitable animal models, significant patient cohorts and clinical experimentation are still required to evaluate the clinical significance of LSINCT5 in cancer progression.

Targeting LSINCT5 as a therapeutic strategy must be based on the identification and functional characterization of LSINCT5. As such, an efficient detection of LSINCT5 and tissue-specific delivery methods are critical to the success of LSINCT5 as a therapeutic target.

The use of the emerging technology, namely clustered regularly interspaced short palindromic repeats (CRISPR)/Cas9 for gene knockout, knock-in and point mutations, may facilitate the development of LSINCT5-based targeted cancer therapy.

This review broadens our understanding of LSINCT5 in the malignant transformation of various cancers and its potential therapeutic application in cancer therapy.[53–55] The LSINCT5 is a potential novel therapeutic target for cancers and a promising and sensitive biomarker for tumor diagnosis and prognosis, as well as personalized cancer treatments. Targeting LSINCT5 may provide a novel and effective therapeutic approach for LSINCT5-based anti-cancer therapies.

ORCID iDs

Wei Yang https://orcid.org/0000-0002-9202-7395
Xiaoyan Yang https://orcid.org/0000-0002-7591-7505
Qing Li https://orcid.org/0000-0002-1194-191X
Pu Cao https://orcid.org/0000-0002-4967-6349
Liyang Tang https://orcid.org/0000-0003-0127-8840
Zhizhong Xie https://orcid.org/0000-0003-3365-0379
Xiaoyong Lei https://orcid.org/0000-0001-9113-452X

References

1. Schmitt AM, Chang HY. Long non-coding RNAs in cancer pathways. *Cancer Cell*. 2016;29(4):452–463. doi:10.1016/j.ccell.2016.03.010
2. Chen QN, Wei CC, Wang ZX, Sun M. Long non-coding RNAs in anti-cancer drug resistance. *Oncotarget*. 2017;8(1):1925–1936. doi:10.18632/oncotarget.12461
3. Iyer MK, Niknafs YS, Malik R, et al. The landscape of long noncoding RNAs in the human transcriptome. *Nat Genet*. 2015;47(3):199–208. doi:10.1038/ng.3192
4. Derrien T, Johnson R, Bussotti G, et al. The GENCODE v7 catalog of human long noncoding RNAs: Analysis of their gene structure, evolution, and expression. *Genome Res*. 2012;22(9):1775–1789. doi:10.1101/gr.132159.111
5. Xing C, Sun SG, Yue ZQ, Bai F. Role of lncRNA LUCAT1 in cancer. *Biomed Pharmacother*. 2021;134:111158. doi:10.1016/j.biopha.2020.111158
6. Bolha L, Ravnik-Glavač M, Glavač D. Long noncoding RNAs as biomarkers in cancer. *Dis Markers*. 2017;2017:7243968. doi:10.1155/2017/7243968
7. Gao YL, Zhao ZS, Zhang MY, Han LJ, Dong YJ, Xu B. Long noncoding RNA PVT1 facilitates cervical cancer progression via negative regulating of miR-424. *Oncol Res*. 2017;25(8):1391–1398. doi:10.3727/096504017X14881559833562
8. Prensner JR, Chinnaiyan AM. The emergence of lncRNAs in cancer biology. *Cancer Discov*. 2011;1(5):391–407. doi:10.1158/2159-8290.CD-11-0209
9. Perez DS, Hoage TR, Pritchett JR, et al. Long, abundantly expressed non-coding transcripts are altered in cancer. *Hum Mol Genet*. 2008;17(5):642–655. doi:10.1093/hmg/ddm336
10. Kong D, Li C, Yang Q, Wei B, Wang L, Peng C. Long noncoding RNA LSINCT5 acts as an oncogene via increasing EZH2-induced inhibition of APC expression in osteosarcoma. *Biochem Biophys Res Commun*. 2018;507(1–4):193–197. doi:10.1016/j.bbrc.2018.11.005
11. Silva JM, Boczek NJ, Berres MW, Ma X, Smith DI. LSINCT5 is over expressed in breast and ovarian cancer and affects cellular proliferation. *RNA Biol*. 2011;8(3):496–505. doi:10.4161/rna.8.3.14800
12. Xu MD, Qi P, Weng WW, et al. Long non-coding RNA LSINCT5 predicts negative prognosis and exhibits oncogenic activity in gastric cancer. *Medicine (Baltimore)*. 2014;93(28):e303. doi:10.1097/MD.0000000000000303
13. Long X, Li L, Zhou Q, et al. Long non-coding RNA LSINCT5 promotes ovarian cancer cell proliferation, migration and invasion by disrupting the CXCL12/CXCR4 signalling axis. *Oncol Lett*. 2018;15(5):7200–7206. doi:10.3892/ol.2018.8241
14. Zhu X, Li Y, Zhao S, Zhao S. LSINCT5 activates Wnt/β-catenin signaling by interacting with NCYM to promote bladder cancer progression. *Biochem Biophys Res Commun*. 2018;502(3):299–306. doi:10.1016/j.bbrc.2018.05.076
15. Meng YB, He X, Huang YF, Wu QN, Zhou YC, Hao DJ. Long noncoding RNA CRNDE promotes multiple myeloma cell growth by suppressing miR-451. *Oncol Res*. 2017;25(7):1207–1214. doi:10.3727/096504017X14886679715637
16. He W, Lu M, Xiao D. LSINCT5 predicts unfavorable prognosis and exerts oncogenic function in osteosarcoma. *Biosci Rep*. 2019;39(5):BSR20190612. doi:10.1042/BSR20190612
17. Silva JM, Perez DS, Pritchett JR, Halling ML, Tang H, Smith DI. Identification of long stress-induced non-coding transcripts that have altered expression in cancer. *Genomics*. 2010;95(6):355–362. doi:10.1016/j.ygeno.2010.02.009
18. Zhang X, Sha M, Yao Y, Da J, Jing D. Increased B-type-natriuretic peptide promotes myocardial cell apoptosis via the B-type-natriuretic peptide/long non-coding RNA LSINCT5/caspase-1/interleukin 1β signaling pathway. *Mol Med Rep*. 2015;12(5):6761–6767. doi:10.3892/mmr.2015.4247
19. Qi P, Lin WR, Zhang M, et al. E2F1 induces LSINCT5 transcriptional activity and promotes gastric cancer progression by affecting the epithelial–mesenchymal transition. *Cancer Manag Res*. 2018;10:2563–2571. doi:10.2147/CMAR.S171652
20. Evans JR, Feng FY, Chinnaiyan AM. The bright side of dark matter: lncRNAs in cancer. *J Clin Invest*. 2016;126(8):2775–2782. doi:10.1172/JCI84421
21. Li O, Li Z, Tang Q, et al. Long stress induced non-coding transcripts 5 (LSINCT5) promotes hepatocellular carcinoma progression through interaction with high-mobility group AT-hook 2 and MiR-4516. *Med Sci Monit*. 2018;24:8510–8523. doi:10.12659/MSM.911179
22. Mei J, Zeng J, Wang Q, Li J, Han Y. Effect of nobiletin on the proliferation of pancreatic cancer cells by long chain non-coding RNA LSINCT5 [in Chinese]. *The Journal of Practical Medicine*. 2020;36(1):49–54. http://www.cnki.com.cn/Article/CJFDTOTAL-SYYZ202001012.htm. Accessed April 14, 2021.
23. Jing L, Lin J, Zhao Y, et al. Long noncoding RNA LSINCT5 is upregulated and promotes the progression of esophageal squamous cell carcinoma. *Eur Rev Med Pharmacol Sci*. 2019;23(12):5195–5205. doi:10.26355/eurrev_201906_18184
24. Wang X, Feng X, Wang H. LncRNA LSINCT5 drives proliferation and migration of oral squamous cell carcinoma through the miRNA-185-5p/ZNF703 axis. *J BUON*. 2021;26(1):124–131. PMID:33721442.
25. Zhu X, Li Y, Zhao S, Zhao S. LSINCT5 activates Wnt/β-catenin signaling by interacting with NCYM to promote bladder cancer progression. *Biochem Biophys Res Commun*. 2018;502(3):299–306. doi:10.1016/j.bbrc.2018.05.076
26. Zhang G, Song W. Long non-coding RNA LSINCT5 inactivates Wnt/β-catenin pathway to regulate MCF-7 cell proliferation and motility through targeting the miR-30a. *Ann Transl Med*. 2020;8(24):1635. doi:10.21037/atm-20-7253
27. Liang B, Zhang L, Lin S, Wang H, Chen X. Expression of lncRNA LSINCT5 in breast cancer and its effects on cell proliferation and metastasis. *Chin Med Biotechnol*. 2020;15(2):199–205. https://mall.cnki.net/magazine/Article/ZYSW202002021.htm. Accessed April 18, 2021.
28. Jiang H, Li Y, Li J, et al. Long noncoding RNA LSINCT5 promotes endometrial carcinoma cell proliferation, cycle, and invasion by promoting the Wnt/β-catenin signaling pathway *via* HMGA2. *Ther Adv Med Oncol*. 2019;11:1758835919874649. doi:10.1177/1758835919874649
29. Tian Y, Zhang N, Chen S, Ma Y, Liu Y. The long non-coding RNA LSINCT5 promotes malignancy in non-small cell lung cancer by stabilizing HMGA2. *Cell Cycle*. 2018;17(10):1188–1198. doi:10.1080/15384101.2018.1467675
30. Chen Y, Liu J, Lu T, Tang J, Li L, Liu F. Effect of long non-coding RNA long stress-induced noncoding transcript 5 on erlotinib resistance to lung cancer cells and the underlying mechanisms. *Zhong Nan Da Xue Xue Bao Yi Xue Ban*. 2020;45(8):886–891. doi:10.11817/j.issn.1672-7347.2020.190705
31. Kuang J, Wei P. Long non-coding RNA LSINCT5 promotes proliferation and metastasis of papillary thyroid cancer by binding to miR-29c [in Chinese]. *J Third Mil Med Univ*. 2018;40(20):1851–1857. https://www.cnki.net/kcms/doi/10.16016/j.1000-5404.201807173.html. Accessed February 28, 2021.

32. Adam S, Hilmi T, Rayyan O, Haziq L. Expression of ITGB1 and E-cadherin regulated by lncLSINCT5 sponging on miR-29c-3p in papillary thyroid cancer cells. *RNA & DISEASE*. 2019;6:e451. https://smartscitech.com/index.php/RD/article/view/451. Accessed April 16, 2021.

33. Li Y, Ma X, Wang Y, Li G. miR-489 inhibits proliferation, cell cycle progression and induces apoptosis of glioma cells via targeting SPIN1-mediated PI3K/AKT pathway. *Biomed Pharmacother*. 2017;93:435–443. doi:10.1016/j.biopha.2017.06.058

34. Liu B, Cao W, Ma H. Knockdown of lncRNA LSINCT5 suppresses growth and metastasis of human glioma cells via up-regulating miR-451. *Artif Cells Nanomed Biotechnol*. 2019;47(1):2507–2515. doi:10.1080/21691401.2019.1626404

35. Shengjie X, Yingchao G, Ying Y, Hongyuan X, Ning Z. The multiple function of long noncoding RNAs in osteosarcoma progression, drug resistance and prognosis. *Biomed Pharmacother*. 2020;127:1–11. doi:10.1016/j.biopha.2020.110141

36. Suenaga Y, Islam SMR, Alagu J, et al. *NCYM*, a Cis-antisense gene of MYCN, encodes a de novo evolved protein that inhibits GSK3β resulting in the stabilization of MYCN in human neuroblastomas. *PLoS Genet*. 2014;10(1):e1003996. doi:10.1371/journal.pgen.1003996

37. Yan X, Zhang D, Wu W, et al. Mesenchymal stem cells promote hepatocarcinogenesis via lncRNA–MUF interaction with ANXA2 and miR-34a. *Cancer Res*. 2017;77(23):6704–6716. doi:10.1158/0008-5472.CAN-17-1915

38. Ma CC, Xiong Z, Zhu GN, et al. Long non-coding RNA ATB promotes glioma malignancy by negatively regulating miR-200a. *J Exp Clin Cancer Res*. 2016;35(1):90. doi:10.1186/s13046-016-0367-2

39. Godlewski J, Bronisz A, Nowicki MO, Chiocca EA, Lawler S. MicroRNA-451: A conditional switch controlling glioma cell proliferation and migration. *Cell Cycle*. 2010;9(14):2742–2748. PMID:20647762.

40. Nan Y, Han L, Zhang A, et al. MiRNA-451 plays a role as tumor suppressor in human glioma cells. *Brain Res*. 2010;1359:14–21. doi:10.1016/j.brainres.2010.08.074

41. Kim Y, Roh S, Lawler S, Friedman A. MiR451 and AMPK mutual antagonism in glioma cell migration and proliferation: A mathematical model. *PLoS One*. 2011;6(12):e28293. doi:10.1371/journal.pone.0028293

42. Nazari M, Nasiri M, Ghaderi A. Evaluation of long stress-induced non-coding transcripts 5 polymorphism in Iranian patients with bladder cancer. *Res Mol Med*. 2016;4(3):17–21. doi:10.18869/acadpub.rmm.4.3.17

43. Rao AKDM, Rajkumar T, Mani S. Perspectives of long non-coding RNAs in cancer. *Mol Biol Rep*. 2017;44(2):203–218. doi:10.1007/s11033-017-4103-6

44. Zhang H, Chen Z, Wang X, Huang Z, He Z, Chen Y. Long non-coding RNA: A new player in cancer. *J Hematol Oncol*. 2013;6(1):37. doi:10.1186/1756-8722-6-37

45. Qiu MT, Hu JW, Yin R, Xu L. Long noncoding RNA: An emerging paradigm of cancer research. *Tumor Biol*. 2013;34(2):613–620. doi:10.1007/s13277-013-0658-6

46. Xu S, Sui S, Zhang J, et al. Downregulation of long noncoding RNA MALAT1 induces epithelial-to-mesenchymal transition via the PI3K-AKT pathway in breast cancer. *Int J Clin Exp Pathol*. 2015;8(5):4881–4891. PMID:26191181.

47. Ji Q, Liu X, Fu X, et al. Resveratrol inhibits invasion and metastasis of colorectal cancer cells via MALAT1 mediated Wnt/β-catenin signal pathway. *PLoS One*. 2013;8(11):e78700. doi:10.1371/journal.pone.0078700

48. Spizzo R, Almeida MI, Colombatti A, Calin GA. Long non-coding RNAs and cancer: A new frontier of translational research? *Oncogene*. 2012;31(43):4577–4587. doi:10.1038/onc.2011.621

49. Gutschner T, Diederichs S. The hallmarks of cancer: A long non-coding RNA point of view. *RNA Biol*. 2012;9(6):703–719. doi:10.4161/rna.20481

50. Rafiee A, Riazi-Rad F, Havaskary M, Nuri F. Long noncoding RNAs: Regulation, function and cancer. *Biotechnol Genet Eng Rev*. 2018;34(2):153–180. doi:10.1080/02648725.2018.1471566

51. Li CH, Chen Y. Targeting long non-coding RNAs in cancers: Progress and prospects. *Int J Biochem Cell Biol*. 2013;45(8):1895–1910. doi:10.1016/j.biocel.2013.05.030

52. Zhang F, Zhang L, Zhang C. Long noncoding RNAs and tumorigenesis: Genetic associations, molecular mechanisms, and therapeutic strategies. *Tumor Biol*. 2016;37(1):163–175. doi:10.1007/s13277-015-4445-4

53. Fu X, Ravindranath L, Tran N, Petrovics G, Srivastava S. Regulation of apoptosis by a prostate-specific and prostate cancer-associated noncoding gene, *PCGEM1*. *DNA Cell Biol*. 2006;25(3):135–141. doi:10.1089/dna.2006.25.135

54. Petrovics G, Zhang W, Makarem M, et al. Elevated expression of *PCGEM1*, a prostate-specific gene with cell growth-promoting function, is associated with high-risk prostate cancer patients. *Oncogene*. 2004;23(2):605–611. doi:10.1038/sj.onc.1207069

55. Srikantan V, Zou Z, Petrovics G, et al. *PCGEM1*, a prostate-specific gene, is overexpressed in prostate cancer. *Proc Natl Acad Sci USA*. 2000;97(22):12216–12221. doi:10.1073/pnas.97.22.12216

Serological proteome analysis identifies crustacean myosin heavy chain type 1 protein and house dust mite Der p 14 as cross-reacting allergens

Antonio Conti[1,A–F], Noor Alqassir[1,B,E,F], Daniela Breda[2,B,C,F], Alan Zanardi[1,B,C,F], *Massimo Alessio[1,A–F], *Samuele E. Burastero[2,A–F]

[1] Proteome Biochemistry, COSR-Centre for Omics Sciences, IRCCS-San Raffaele Hospital, San Raffaele Scientific Institute, Milan, Italy

[2] Laboratory of Cellular and Molecular Allergology, Division of Immunology, Transplantation and Infectious Diseases, San Raffaele Scientific Institute, Milan, Italy

A – research concept and design; B – collection and/or assembly of data; C – data analysis and interpretation;
D – writing the article; E – critical revision of the article; F – final approval of the article

Address for correspondence
Samuele E. Burastero
E-mail: burastero.samuele@hsr.it

Abstract

Background. Allergies to house dust mite (HDM) and to crustaceans are clinically and pathogenically linked. Several homologous allergenic proteins have been identified, among which tropomyosin is the prototype, expressing epitopes endowed with variable levels of immunoglobulin E (IgE) cross-reactivity. Component-resolved diagnosis (CRD) does not allow a thorough characterization of all relevant IgE reactivities to these allergen sources.

Objectives. We studied 1 patient allergic to shrimp with positive skin prick test to HDM and negative scores for IgE to HDM allergen components routinely used in CRD (group 1 and 2 allergens, Der p 23 and tropomyosin).

Materials and methods. In order to identify the allergen(s) involved in IgE reactivity, we used serological proteome analysis (SERPA), which utilizes two-dimensional gel electrophoresis (2DE), immunoblotting and mass spectrometry (MS). The identified allergenic proteins were tested with sera from 20 crustacean-allergic patients and 19 grass-allergic patients serving as controls.

Results. Der p 14 and myosin heavy chain type 1 (MHC1) were identified as the components recognized by patient's IgE in the proteome of *Dermatophagoides pteronyssinus* and *Penaeus monodon*, respectively. The MHC1 protein shows about 30% sequence identity with Der p 14 in specific domains, and cross-reactivity against epitopes shared by the 2 proteins was demonstrated by reduced reactivity to shrimp extract following pre-incubation with Der p 14. Serum IgE from 5 out of 20 patients allergic to crustaceans reacted with MHC1, compared to none among 19 controls (p < 0.05).

Conclusions. We identified MHC1 as a relevant allergic component in the proteome of *Penaeus monodon*, the prototypic allergen source used in diagnosis of allergy to crustaceans. Our data demonstrate MHC1 cross-reactivity between MHC1 and Der p 14 from *Dermatophagoides pteronyssinus*.

Key words: case report, *Dermatophagoides*, proteomics, allergens, immunoglobulin E

Background

Diagnosis of food and inhalant allergies requires the combination of clinical history, physical examination and specific in vitro and in vivo diagnostic tests aimed to identify reactivity of immunoglobulin E (IgE) to the allergen(s) of interest. When used to identify reactivity to individual allergenic components (instead of reactivity to whole allergen extracts), these tests allow component-resolved diagnostics (CRD). Currently, allergens used for CRD are either obtained as purified natural extracts or as recombinant proteins. Commercial availability of individual allergenic components limits the diagnostic opportunities for successful determination of IgE. In fact, patients with verified allergy to a certain allergenic source score negative at CRD analysis when the allergenic component responsible for their IgE reactivity is not included in the molecular allergology-based assays. In such cases, serological proteome analysis (SERPA) combined with protein identification through mass spectrometry (MS) can identify the allergenic protein responsible for IgE reactivity.[1,2]

Here, we report the identification of 1 patient with shrimp allergy and positive skin prick test to house dust mite (HDM) whose serum scored negative for IgE to all HDM allergens routinely used in CRD. Simultaneous IgE reactions to mites and crustaceans is a relatively common occurrence[3] mostly explained by IgE reactivity to tropomyosin.[4] However, several other allergens have been found to be cross-reactive, e.g., arginine kinase, myosin light chain, hemocyanin, and paramyosin.[5] We report the identification of a new mite-shrimp cross-reactive allergen component.

Objectives

This study aimed to characterize using SERPA the allergen component(s) responsible for IgE reactivity to HDM in 1 patient sensitized to shrimp and mites whose IgE scored negative for commercially available *Dermatophagoides* allergen components. The frequency of this reactivity in a group of allergic patients was also evaluated as part of the preliminarily characterization of the clinical relevance of the allergen responsible for the observed cross-reactivity.

Procedures were performed in accordance with the ethical standards of the San Raffaele Ethics Committee (approval ID BIOL-IMMUNO-ALLERGO, date of approval after revision June 12, 2019) and with the Helsinki Declaration of 1975, as revised in 2000 (project ID: BIOL-IMMUNO-ALLERGO, San Raffaele Scientific Institute, Milan, Italy, revised on June 12, 2019).

Materials and methods

A graphical presentation of the study is shown in Fig. 1.

Testing of IgE reactivity

Patients reporting to the allergy clinic of the San Raffaele Scientific Institute (Milan, Italy) are routinely tested using skin prick test with a panel of regionally relevant allergens (conf. Supplementary Materials and Methods). Testing and interpretation of results follows European Academy and Allergy and Clinical Immunology (EAACI) guidelines.[6]

Evaluation of serum IgE reactivity to HDM components was performed in patients scoring positive for IgE to HDM extract, as part of the routine evaluation of patients reporting to our allergy clinic. Patient PT 0321 (a 49-year-old female) had a clinical history of food allergy (generalized urticaria and angioedema) reproducibly correlated with meals containing crustacean-based ingredients. Prick test and IgE to *Dermatophagoides pteronyssinus* scored positive, but she did not report any symptoms compatible with respiratory allergies and respiratory or contact reactions following overt exposure to house dust.

Type of assays used for IgE specific determination are reported in Supplementary Materials and Methods. Frequency of serum IgE reactivity to myosin heavy chain type 1 (MCH1) was studied using western blot in 20 patients allergic to crustacean and in a cohort of 19 patients allergic to grass who served as atopic, non-shrimp allergic controls. Patients allergic to shrimps reported singularly or in various combinations the following symptoms: oral allergy (n = 9), contact urticaria (n = 7), urticaria/angioedema (n = 16), asthma (n = 3), and anaphylaxis (n = 7). Demographic characteristics and profiles of IgE reactivities of patients are shown in Table 1. Two-dimensional electrophoresis (2DE) was performed as described in a study by Conti et al.[2] Details of binding competition assays are reported in Supplementary Materials and Methods.

Mass spectrometry

For protein identification with MS analysis, preparative gels were stained with colloidal blue Coomassie or MS-compatible silver staining, images were acquired and spots of interest were excised from gels, reduced, alkylated, and in-gel digested with bovine trypsin, as described by Conti et al.[2]

Statistical analyses

Patients' characteristics were reported cumulatively as median (interquartile range (IQR)) for continuous variables or proportions (percentage) for categorical variables. Differences between proportions were tested with two-tailed Fisher's exact test. Values of p < 0.05 were considered statistically significant.
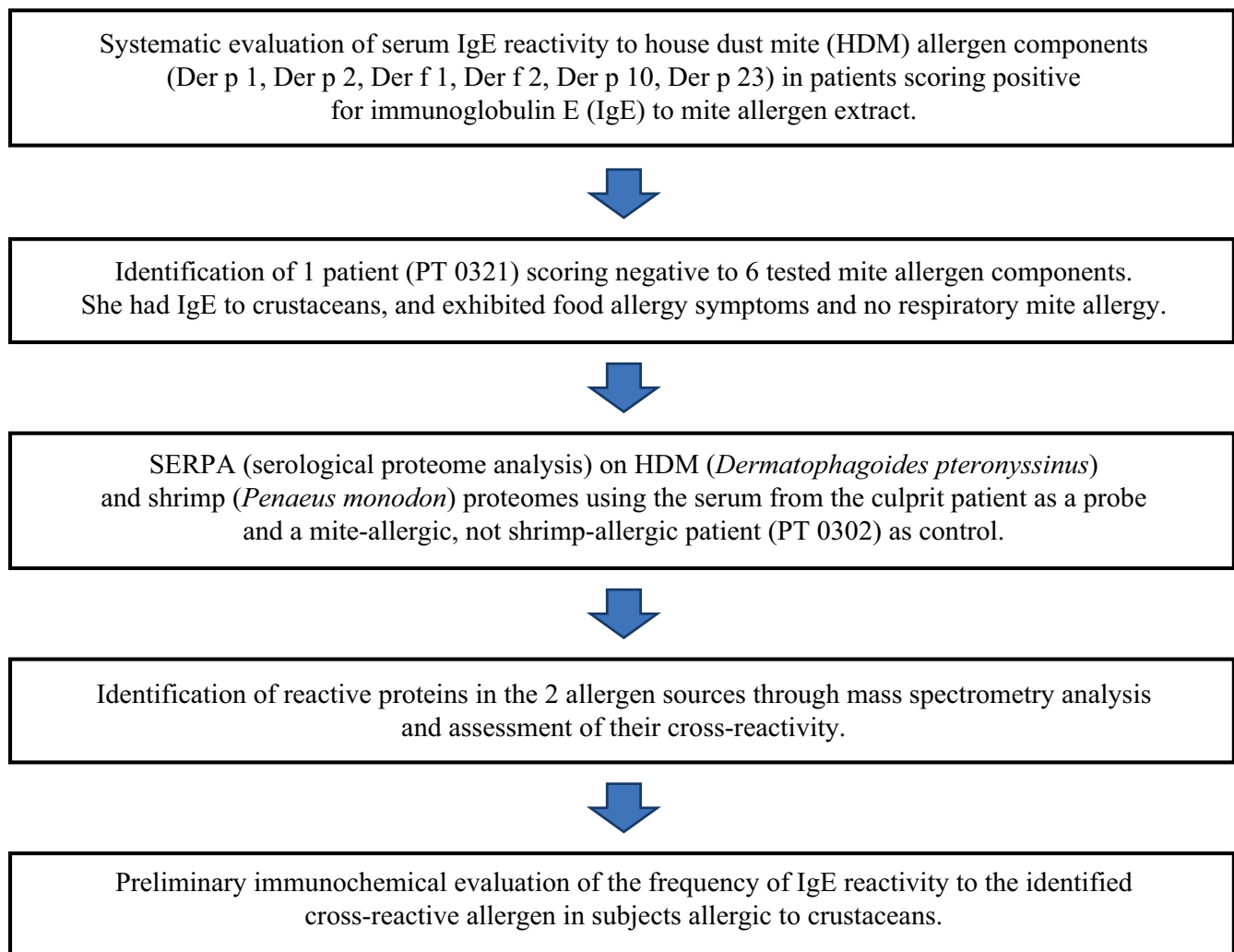
Fig. 1. Graphical presentation of the study

Results

The skin prick test of patient PT 0321 yielded positive results for IgE to HDM allergens *Dermatophagoides pteronyssinus* and *Dermatophagoides farina*, and negative results for all other geographically relevant allergens that were tested (Fagales, pellitory, ragweed, molds, and animal dander). Patient PT 0321's total IgE level was 44 ng/mL (normal value <100 ng/mL), and specific IgE determination with available routine diagnostic tests yielded negative results for reactivity against all HDM allergens (group 1 and 2 allergens, Der p 23, Der p 23 and for mite tropomyosin, i.e., Der p 10). Specific IgE reactivity to other crustaceans (shrimp, lobster and crab extracts) confirmed the results of prick test. Demographic data and IgE reactivity data from all patients are listed in Table 1.

Identification of IgE reactive allergen(s) in HDM and crustacean proteomes

The SERPA analysis of patient PT 0321's serum reactivity to HDM protein extract resulted in the identification of Der p 14 as the major IgE-binding allergen (58 kDa, isoelectric point 5.15 pH; Fig. 2). The SERPA analysis of serum reactivity to shrimp allergen extract allowed for the identification of a 220–240 kDa and 5.44 pH isoelectric point spot compatible with MHC1 (Supplementary Fig. 1). The MS profiles in HDM and shrimp extracts are detailed in Supplementary Tables 1 and 2, respectively. Peptides belonging to Der p 14 allergen identified with MS are shown in Supplementary Fig. 2.

Cross-reactivity between MHC1 and Der p 14

In silico investigation for potential cross reactivity between Der p 14 and MHC1 based on the comparison of the amino acid sequence of the primary structure of the proteins showed some sequence identity in the range of 27–41% in specific domains. For blast protein alignment, amino acid sequence from UniprotKB (https://www.uniprot.org) were Q8N0N0 and K4Q4N8 for Der p 14 and MHC1, respectively. Sequence match analysis was conducted using NIH BLAST website (https://blast.ncbi.nlm.

Table 1. Demographic features and serological immunoglobulin E (IgE) reactivity of allergic patients tested for house dust mite (HDM), grass and crustacean allergens

Patient	Sex	Age [years]	Total IgE [ng/mL]	House dust mite						Grass			Shrimp			
				D. pteronyssinus			D. farinae			Phleum pratense			Penaeus monodon			
				extract [AU/mL]	Der p 1 [AU/mL]	Der p 2 [AU/mL]	extract [AU/mL]	Der f 1 [AU/mL]	Der f 2 [AU/mL]	extract [AU/mL]	Phl p 1 [AU/mL]	Phl p 5 [AU/mL]	extract [AU/mL]	Pen m 1 [AU/mL]	Pen m 2 [AU/mL]	Pen m 4 [AU/mL]
0321	f	49.0	44.0	0.0	0.0	0.0	0.0	0.0	0.0	0.0	0.0	0.0	8.2	0.0	0.0	0.0
0302	f	45.0	63.0	nd	5.8	4.0	nd	4.0	11.9	0.0	0.3	0.0	0.0	0.0	0.0	0.0
grass (n = 19)	10f	30.1	159.9	0.0	0.0	0.0	0.0	0.0	0.0	23.7	22.4	14.3	0.0	0.0	0.0	0.0
lower IQR	–	22.0	105.0	0.0	0.0	0.0	0.0	0.0	0.0	6.5	4.5	4.2	0.0	0.0	0.0	0.0
upper IQR	–	38.0	237.5	0.0	0.0	0.0	0.0	0.0	0.0	20.4	35.1	23.8	0.0	0.0	0.0	0.0
shrimp (n = 20)	5f	28.6	145.9	0.0	0.0	0.0	0.0	0.0	0.0	14.2	19.3	10.1	0.0	0.0	0.0	0.0
lower IQR	–	61	44.0	0.0	0.0	0.0	0.0	0.0	0.0	0.0	0.0	0.0	9.2	0.7	0.0	0.0
upper IQR	–	87.5	280.0	10.1	1.6	13.2	4.3	1.3	9.8	26.5	45.1	18.1	18.6	20.5	0.0	0.0

Der p 1 and Der p 2 – *Dermatophagoides pteronyssinus* allergen p 1 and p 2; Der f 1 and Der f 2 – *Dermatophagoides farinae* allergen f 1 and f 2; Phl p 1 and Phl p 5 – *Phleum pratense* allergen p 1 and p 5; Pen m 1, Pen m 2 and Pen m 4 – *Penaeus monodon* allergen m 1, m 2 and m4; nd – not determined; grass – grass-allergic patients; shrimp – shrimp-allergic patients; AU – arbitrary units; IQR – interquartile range.

nih.gov/Blast.cgi). Results are provided in Supplementary Fig. 3.

Binding competition with Der p 14 demonstrated the substantial reduction of IgE signal binding to MCH1 (~40% reduction at 0.38 µg MCH1 and ~55% reduction at 0.76 µg MCH1, compared to non-preincubated serum). Data were generated in replicates due to Der p 14 reagent limitation. No reduction was observed in IgE signal at 0.38 µg and ~10% reduction at 0.76 µg with Der f 2 used as a control mite allergen (Supplementary Fig. 4).

Evaluation of IgE reactivity to MHC1 protein in a cohort of patients allergic to crustaceans

Following the identification of the spot compatible with MHC1 by means of SERPA analysis based on PT 0321 serum, we made a preliminary estimation of the frequency of IgE reactivity to this allergen in shrimp-allergic patients with immunoblotting. To this aim, we used sera from 20 shrimp-allergic patients who reported to the outpatient clinic of the San Raffaele Scientific Institute. A positive MHC1 immunoblotting signal was detected in 5 out of the 20 patients of this cohort, and 15 of them scored negative. Notably, among these 5 MHC1-positive patients, 3 (including PT 0321) had coexisting sensitization to HDM. A group of 19 subjects allergic to grass served as controls, being representative of an atopic population with a different sensitization profile. Among these 19 subjects, sera scored positive for this marker 0 times and negative 19 times, respectively (p = 0.047, two-tailed Fisher's exact test).

Discussion

This paper reports the identification of MHC1 as a relevant allergic component in the proteome of *Penaeus monodon*, which is not presently available in the diagnostic armamentarium of CRD. We show IgE reactivity compatible with MHC1 in 5 out of 20 of patients allergic to crustaceans. We also demonstrate cross-reactivity between MHC1 and Der p 14 from the *Dermatophagoides* proteome.

Our results confirm and expand previous studies reporting that tropomyosin, the originally described pan-allergen of invertebrates, is just one among several highly cross-reactive allergens between crustaceans and mites.[5,7] These findings are in agreement with aleady reported observations that HDM was able to inhibit shrimp IgE reactivity, or vice versa, in most shrimp-allergic patients.[8] In patients with this sensitization pattern, the primary sensitization may occur via the respiratory or the gastrointestinal tract, likely depending on the characteristics of allergen exposure (frequency, bioavailability, amount, etc.).
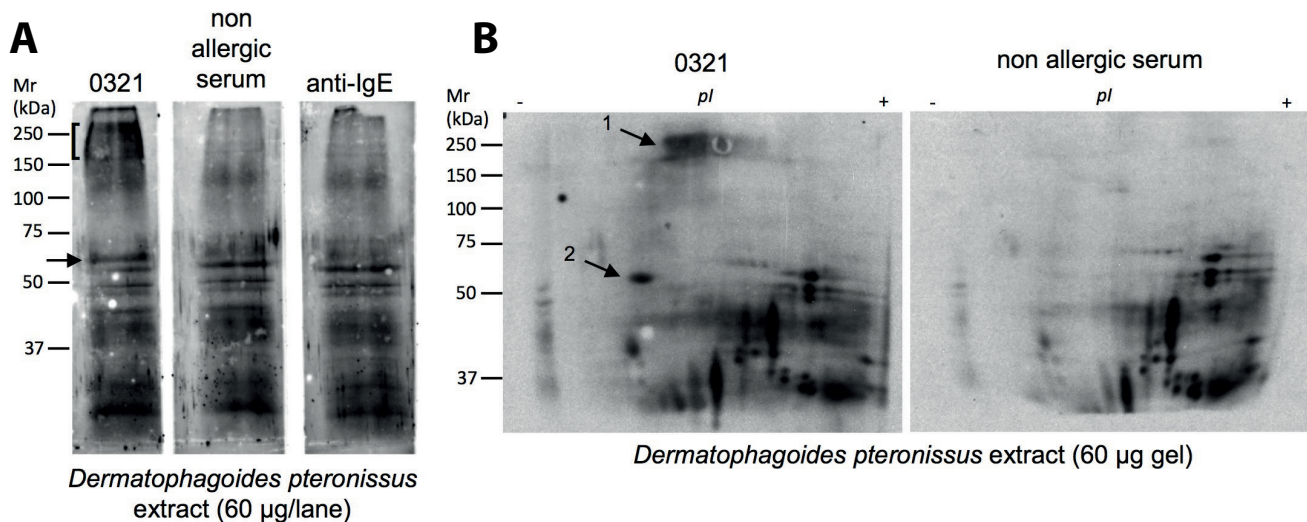
Fig. 2. Reactivity of the serum of patient PT 0321 to *Dermatophagoides pteronyssinus* extract. A. Allergen extract underwent sodium dodecyl-sulfate polyacrylamide gel electrophoresis (SDS-PAGE), and different lanes were probed using western blot for (i) PT 0321 serum, (ii) non-allergic patient serum and (iii) anti-human IgE secondary antibody alone as control; B. Sample extract subject to two-dimensional gel electrophoresis (2DE), and probed using western blot for (i) patients PT 0321's and (ii) non-allergic patient serum. Square bracket and arrows indicate the band or protein spots recognized by patient's 0321 IgE only. Spot 1 and 2 were processed with mass spectrometry (MS) analysis for protein identification

To the best of our knowledge, this is the first time that MCH1 is reported as a mite-shrimp cross-reactive allergen. Although MHC1 from banana shrimp (*Fenneropenaeus merguiensis*) was previously reported as an IgE binding protein, it was not formally classified as a new allergen according to World Health Organization/International Union of Immunology Societies (WHO/IUIS) Allergen Nomenclature subcommittee,[9] and no data on cross-reactivity with other allergens were presented.[10] Shrimp allergy represents an example of coexistence of food and inhalant allergy, as it is the case of allergies triggered by allergen components of the protein families PR-10[11] and LTP.[12] Further work, including cloning of MHC1 or its subunit, is needed to formally characterize this protein as a new allergen.

Limitations

The MCH1 protein was not cloned, either as a whole molecule or as IgE binding subunit(s). The availability of cloned proteins will allow to characterize MHC1 as a new candidate allergen according to the WHO/IUIS, and to study IgE reactivity in a representative population of patients allergic to shrimp.

Conclusions

This paper reports the identification of MHC1 as a relevant allergic component in the proteome of *Penaeus monodon*. Our data highlight MHC1 relevance beyond allergy to crustaceans, as we have found cross-reactivity between MHC1 and Der p 14 from *Dermatophagoides.*

Supplementary Materials and Methods

Detailed description of assays used for IgE specific determination and for binding competition assays are available at doi:10.17632/jbjkntjhkn.1. The package consists of the following files:

Supplementary Table 1. Protein identification using MS in HDM extract.

Supplementary Table 2. Protein identification using MS in shrimp extract.

Supplementary Fig. 1. Identification of IgE reactive allergen(s) from crustacean proteome.

Supplementary Fig. 2. Peptides belonging to Der p 14 allergen identified with MS.

Supplementary Fig. 3. Blast protein sequence alignment between Der p 14 and MCH1.

Supplementary Fig. 4. Competition reactivity test against shrimp extract.

ORCID iDs

Antonio Conti https://orcid.org/0000-0001-9150-5271
Daniela Breda https://orcid.org/0000-0003-2807-0089
Alan Zanardi https://orcid.org/0000-0002-8555-279X
Massimo Alessio https://orcid.org/0000-0002-4133-3472
Samuele E. Burastero https://orcid.org/0000-0001-7302-6381

References

1. Conti A, Burastero GJ, Suli C, et al. Identification by serological proteome analysis of paramyosin as prominent allergen in dust mite allergy. *J Proteomics*. 2017;166:19–26. doi:10.1016/j.jprot.2017.06.024
2. Conti A, Alessio M, Pesca M, et al. Phleum pratense manganese superoxide dismutase identified by proteomic: A new candidate grass allergen. *Ann Allergy Asthma Immunol*. 2014;112(3):261–262.e3. doi:10.1016/j.anai.2013.12.015
3. Wong L, Tham EH, Lee BW. An update on shellfish allergy. *Curr Opin Allergy Clin Immunol*. 2019;19(3):236–242. doi:10.1097/ACI.0000000000000532

4. Wong L, Huang CH, Lee BW. Shellfish and house dust mite allergies: Is the link tropomyosin? *Allergy Asthma Immunol Res*. 2016;8(2):101–106. doi:10.4168/aair.2016.8.2.101

5. Asero R, Pravettoni V, Scala E, Villalta D. House dust mite-shrimp allergen interrelationships. *Curr Allergy Asthma Rep*. 2020;20(4):9. doi:10.1007/s11882-020-0902-2

6. Bousquet J, Heinzerling L, Bachert C, et al. Practical guide to skin prick tests in allergy to aeroallergens: Practical use of skin tests. *Allergy*. 2012;67(1):18–24. doi:10.1111/j.1398-9995.2011.02728.x

7. Asero R, Mistrello G, Amato S, et al. Shrimp allergy in Italian adults: A multicenter study showing a high prevalence of sensitivity to novel high molecular weight allergens. *Int Arch Allergy Immunol*. 2012;157(1): 3–10. doi:10.1159/000324470

8. Sidenius KE, Hallas TE, Poulsen LK, Mosbech H. Allergen cross-reactivity between house-dust mites and other invertebrates. *Allergy*. 2001;56(8):723–733. doi:10.1034/j.1398-9995.2001.056008723.x

9. Pomés A, Davies JM, Gadermaier G, et al. WHO/IUIS Allergen Nomenclature: Providing a common language. *Mol Immunol*. 2018;100:3–13. doi:10.1016/j.molimm.2018.03.003

10. Khanaruksombat S, Srisomsap C, Chokchaichamnankit D, Punyarit P, Phiriyangkul P. Identification of a novel allergen from muscle and various organs in banana shrimp (*Fenneropenaeus merguiensis*). *Ann Allergy Asthma Immunol*. 2014;113(3):301–306. doi:10.1016/j.anai.2014.06.002

11. Biedermann T, Winther L, Till SJ, Panzner P, Knulst A, Valovirta E. Birch pollen allergy in Europe. *Allergy*. 2019;74(7):1237–1248. doi:10.1111/all.13758

12. Wawrzeńczyk A, Żbikowska-Gotz M, Wawrzenczyk A, Bartuzi Z. Sensitisation to lipid transfer proteins in pollen-allergic adults with food allergy. *Adv Dermatol Allergol*. 2020;37(4):508–512. doi:10.5114/ada.2020.98278

Previous chemotherapy can cause PONV

Yesim Cokay Abut[1,A,C–F], Kubra Bolat[1,B], Nurten Yanık[1,B], Abdurrahman Tunay[1,B],
Sevim Baltali[1,C], Veysel Erden[1,E], Gulay Asik Eren[2,E,F]

[1] Department of Anestesiology and Reanimation, University of Health Sciences Istanbul Education and Training Hospital, Turkey

[2] Faculty of Medicine, Near East University, Lefkosa, Cyprus

A – research concept and design; B – collection and/or assembly of data; C – data analysis and interpretation;
D – writing the article; E – critical revision of the article; F – final approval of the article

Address for correspondence
Yesim Cokay Abut
E-mail: yesimabut2000@yahoo.com

Abstract

Background. Although the treatment and mechanisms of postoperative nausea and vomiting (PONV) and chemotherapy-induced nausea and vomiting (CINV) are similar, the interactions between these 2 morbidities require more research.

Objectives. In our prospective observational study, we investigated whether previous chemotherapy has an effect on PONV in breast cancer surgery.

Materials and methods. One hundred and forty-eight female patients with the American Society of Anesthesiologists (ASA) physical status I or II, aged 18–65 years and with a scheduled breast cancer surgery were recruited into the study. After they completed preoperative follow-up questionnaires, anesthesia was induced with propofol (2 mg/kg), remifentanil (1.0 μg/kg) and rocuronium (0.6 mg/kg), and maintained with sevoflurane (1.5–2.0%), 45% oxygen/air mixture and infusion of remifentanil (0.1–0.2 μg/kg/min). After extubation, the intensity of PONV was assessed during the first 2 h and at 2–24 h after surgery. The symptoms of PONV were classified as mild (mild nausea, vomiting once, and nausea caused by an external stimulant (eating, drinking or motion)), moderate (vomiting twice, mild nausea without an external stimulant, and antiemetic medication required once) and severe (vomiting more than twice, severe nausea, antiemetic medication required more than once) by a different researcher. Preoperative interview forms, perioperative anesthetic follow-up forms and postoperative assessment forms were recorded and evaluated by different members of this research group.

Results. Data of 143 patients were analyzed. In the group of patients who received chemotherapy, the prevalence of nausea and vomiting within the postoperative period of 2–24 h significantly increased (p < 0.05).

Conclusions. Previous chemotherapy may be a risk factor for the presence of PONV.

Key words: breast cancer, PONV, CINV

Background

Breast cancer is diagnosed more and more often. According to World Health Organization (WHO), the number of newly diagnosed breast cancer cases amounts to nearly 2 million all over the world. In Turkey in 2018, there were 22,500 new cases of this disease.[1,2]

Postoperative nausea and vomiting (PONV) can cause several problems such as early postoperative aspiration and pneumonia, dehydration, and electrolyte imbalance. Delayed recovery may increase the healthcare costs because of the usage of antiemetics and prolonged hospital stay.[3,4] Gender (female), a history of PONV and/or motion sickness, as well as non-smoking status are well-known patient-related risk factors for PONV. More risk factors have been added by Apfel et al. (use of postoperative opioids) and Koivuranta et al. (length of surgery).[5,6] Other papers report that some types of surgery may be associated with an increased risk of PONV, such as laparoscopic and gynecological operations or cholecystectomy.[3,5–7]

The pathophysiology and treatment of PONV is complex. Such symptoms may occur due to the release of different neurotransmitters (serotonin, dopamine, muscarine, acetylcholine, neurokinin-1, histamine, and opioids) or stimulation of the vestibular-cochlear, glossopharyngeal or vagus nerve.[8] Hesketh indicated that chemotherapy-induced nausea and vomiting (CINV) is observed in approx. 30–90% of patients.[9] Although the treatment methods of PONV and CINV are similar, patients' response to them may be different.[10]

Objectives

In our prospective observational study, we investigated whether previous chemotherapy had the effect on PONV in breast cancer surgery.

Materials and methods

Following the approval from the University of Health Sciences Istanbul Education and Training Hospital Institutional Ethics Committee (approval No. 28.06.2019/1890), signed informed consent was obtained from each patient. The study conforms with the tenets of Declaration of Helsinki of 1964 and its later amendments. One hundred and forty-eight female patients with the American Society of Anesthesiologists (ASA) physical status I or II, aged 18–65 years and with scheduled breast cancer surgery were recruited into the study. Before surgery, all patients were asked about their medical history, and had their Apfel score counted. The exclusion criteria were as follows: 1) a history of drug abuse or known prolongation of the QT interval on electrocardiogram (ECG); 2) obesity (body mass index (BMI) >31 kg/m²); 3) antiemetic use 24 h before the study and presence of hepatic or renal disease; 4) patients who had their last chemotherapy less than 1 month ago; 5) patients with presence of allergy; 6) operation time shorter than 60 min or longer than 120 min; and 7) additional opioid necessity in the postoperative period.

Before the operation, all patients were routinely assessed with basic monitoring (ECG, noninvasive blood pressure (NIBP) measurement and oxygen saturation (SpO_2) probe). Anesthesia was induced with propofol (2 mg/kg), remifentanil (1.0 µg/kg) and rocuronium (0.6 mg/kg), and maintained with sevoflurane (1.5–2.0%), 45% oxygen/air mixture, and the infusion of remifentanil (0.1–0.2 µg/kg/min). In the last 30 min at the end of the operation, meperidine (30 mg) was administered. After extubation, the intensity of PONV was assessed during the first 2 h and at 2–24 h after surgery. Patients who complained of PONV were classified as mild (mild nausea, vomiting once), moderate (vomiting twice or need antiemetic medication once) and severe (vomiting more than twice, severe nausea, antiemetic medication needed more than once) by another anesthesiologist who has not anesthetised the patient. None of the patients were routinely prescribed opioid or antiemetic medication during the postoperative period. Patients who had moderate and severe PONV were given 10 mg of metoclopramide for rescue treatment. Patients who suffered a pain score >4 according to NRSS (numeric rating scale score) were treated with infusion of paracetamol (1 g). If the paracetamol was deemed not enough, an opioid (tramadol or meperidine) was given and patients were excluded from the study. Preoperative interview forms, perioperative anesthetic follow-up forms and postoperative assessment forms were recorded and evaluated by different members of our research group.

Statistical analyses

Statistical analyses were performed using IBM SPSS v. 25.0 software (IBM Corp., Armonk, USA). The conformity of the variables to the normal distribution was examined with histogram graphics and the Kolmogorov–Smirnov test. Parametric values with normal distribution are shown as mean ± standard deviation (M ±SD). Parametric values without normal distribution and nonparametric values are presented as the median and interquartile range (IQR). Categorical variables are expressed as numbers and percentages. Interactions between chemotherapy and demand of additional analgesic were compared with the χ^2 test or the Fisher's exact test according to the number of patients in each group. Values of $p < 0.05$ were deemed statistically significant.

Results

Initially, 148 patients had been enrolled, but 5 were excluded from the study: 1 patient because of delayed surgery and 4 because of missing patient data. Patients' characteristics are presented in Table 1.

Table 1. Characteristics of study population

Variable		n (%) or M ±SD or median (Q1–Q3)
Age		51.90 ±12.51[b]
BMI		28 (25–32)[c]
Apfel score	1	32 (22.37)[a]
	2	81 (56.64)[a]
	3	24 (16.78)[a]
	4	6 (4.19)[a]
Additional disease		85 (59.44)[a]
Additional drug		82 (57.34)[a]
Non-smokers		48 (33.57)[a]
Previous operation		111 (77.62)[a]
PONV 0–2 h	mild	44 (69.84)[a]
	moderate	16 (25.40)[a]
	severe	3 (4.76)[a]
PONV 2–24 h	mild	23 (54.76)[a]
	moderate	14 (33.33)[a]
	severe	5 (11.90)[a]
Previous chemotherapy		51 (35.66)[a]
CINV		35 (68.63)[a]
Additional analgesic		129 (90.21)[a]

[a] n (%); [b] mean ± standard deviation (M ±SD); [c] median (1st quartile – 3rd quartile (Q1–Q3)); BMI – body mass index; CINV – chemotherapy-induced nausea and vomiting; PONV – postoperative nausea and vomiting.

Apfel score distribution was as follows: 1 – 32 patients (22.37%), 2 – 81 patients (56.64%), 3 – 24 patients (16.78%), and 4 – 6 patients (4.19%). The PONV at 0–2 h was mild in 44 patients (69.84%), moderate in 16 (25.40%) and severe in 3 (4.76%), while PONV at 2–24 h was mild in 23 patients (54.76%), moderate in 14 (33.33%) and severe in 5 (11.90%). Fifty-one patients (35.66%) received chemotherapy for at least 1 month. Thity-five patients (68.63%) experienced CINV, while 129 patients demanded additional analgesics. The PONV symptoms at 2–24 h significantly worsened in those who received chemotherapy ($p < 0.05$). There was no significant difference between PONV 0–2 and PONV 2–24 grades in patients with CINV (Table 2).

Discussion

Surgery, chemotherapy, radiotherapy, and various combinations of these are used in breast cancer treatment. Da Silva et al. compared different types of oncologic operations in their retrospective study and reported that the only surgical procedure in which PONV prevalence was significantly higher was mastectomy; however, when they compared the results of Apfel's model, they could not find a difference regarding PONV in different mastectomy cases. Their study included both male and female patients and they used different types of anesthesia (general anesthesia alone or combined with epidural or spinal anesthesia). Also, the treatment with antiemetics and postoperative opioids was dependent of the clinicians' preference, and patient-controlled analgesia was employed in some of the patients.[11] In our prospective study, only female patients were included, and general anesthesia was the dominating type of anesthesia; antiemetics and opioids were used only if necessary.

The expected results for PONV from Apfel's original study were 21%, 39%, 61%, and 79% for grades 1, 2, 3, and 4, respectively. In our study, the Apfel scores were grade 1 for 32 patients (22.37%), grade 2 for 81 patients (56.64%), grade 3 for 24 patients (16.78%), and grade 4 for 6 patients (4.19%).

The association between PONV and CINV has not been fully established. There are studies reporting that hereditary factors may play a role in both PONV and CINV susceptibility and resistance.[12] On the other hand, antiemetic medications which have an effect on CINV are not always protective against PONV.

Janicki and Sugino determined that genetic variations in the *HTR3A* and *HTR3B* genes could increase the risk of PONV, and the *HTR3C* gene polymorphisms could have a predictive role for CINV in patients who receive moderately emetogenic chemotherapy. The main conclusion of that study was that the incidence of CINV was very low after chemotherapy in people who did not experience PONV after surgery.[13] Therefore, in our study, we aimed to investigate whether the reverse situation is also possible.

Oddby-Muhrbeck et al. claimed that CINV is strongly related to PONV, and previous PONV has a predictive role for CINV.[10] However, in their study, chemotherapy was applied after surgery, and in patients who experienced PONV before chemotherapy, supraglottic airway devices were used instead of tracheal intubation.

Our patients were given anesthesia after chemotherapy. In other words, it was investigated whether nausea and

Table 2. Relationship between PONV and chemotherapy

Variable		PONV 0–2 h, n (%)		χ²/p-value	PONV 2–24 h, n (%)		χ²/p-value
		no	yes		no	yes	
Chemotherapy	no	51 (55.43)	41 (44.57)	0.027/0.869[#]	72 (78.26)	20 (21.74)	7.242/0.007[#]
	yes	29 (56.86)	22 (43.14)		29 (56.86)	22 (43.14)	
CINV	no	12 (75)	4 (25)	3.127/0.127[*]	11 (68.75)	5 (31.25)	1.343/0.246[#]
	yes	17 (48.57)	18 (51.43)		18 (51.43)	17 (48.57)	

[#] χ² test; [*] Fisher's exact test; statistically significant p-values are in bold. CINV – chemotherapy-induced nausea and vomiting; PONV – postoperative nausea and vomiting.

vomiting was more common during the postoperative period in patients receiving chemotherapy.

Anesthesia-related pharmacologic risk factors for PONV include inhalation anesthetics, nitrous oxide and usage of postoperative opioids. The effects of volatile anesthetics on PONV demonstrate a dose-dependent manner and particularly appear in the first 2–6 h after surgery.[14] Opioids increase the risk for PONV in a dose- and time-dependent manner.[15] We administered sevoflurane, remifentanil and oxygen/air mix for the maintenance of anesthesia. The incidence of PONV is lower with opioid-free total intravenous anesthesia (TIVA). It is known that propofol and TIVA reduce the PONV risk by approx. 25%.[16] In our study, PONV at 2–24 h was significantly increased in patients who received chemotherapy, and there was no significant difference between PONV 0–2 or PONV 2–24 in those with CINV. We think that we eliminated or minimized the negative effects of anesthetic medications.

We used propofol only in induction of anesthesia, and we reversed the effect of muscle relaxant with neostigmine. We did not apply antiemetic drugs routinely to our patients because of their possible side effects, and infused 1 g of paracetamol intravenously for postoperative analgesia when necessary.

Limitations

We did not compare the Apfel score with PONV and CINV results. When we were planning the methods, we included only female patients, which invalidated the results of Apfel score. Another limitation of our study was the administration of inhalation anesthesia instead of TIVA and/or combination of opioid-free regional anesthesia with TIVA as a part of multimodal analgesia management plan.[17–21] We used inhalation anesthesia because of its cost efficiency and routine preference of our hospital policy.

Conclusion

We concluded that prior chemotherapy may be a risk factor for the occurrence of PONV.

ORCID iDs

Yesim Cokay Abut   https://orcid.org/0000-0001-8763-605X
Kubra Bolat   https://orcid.org/0000-0002-7032-0531
Nurten Yanık   https://orcid.org/0000-0003-1469-7286
Abdurrahman Tunay   https://orcid.org/0000-0001-7118-9312
Sevim Baltali   https://orcid.org/0000-0001-9503-5692
Veysel Erden   https://orcid.org/0000-0002-0039-114X
Gulay Asik Eren   https://orcid.org/0000-0002-5365-3641

References

1. Ferlay J, Colombet M, Soerjomataram I, et al. Cancer incidence and mortality patterns in Europe: Estimates for 40 countries and 25 major cancers in 2018. *Eur J Cancer*. 2018;103:356–387. doi:10.1016/j.ejca.2018.07.005

2. Özmen V, Özmen T, Doğru V. Breast cancer in Turkey: An analysis of 20,000 patients with breast cancer. *Eur J Breast Health*. 2019;15(3):141–146. doi:10.5152/ejbh.2019.4890

3. Gan TJ, Belani KG, Bergese S, et al. Fourth Consensus Guidelines for the Management of Postoperative Nausea and Vomiting. *Anesth Analg*. 2020;131(2):411–448. doi:10.1213/ANE.0000000000004833

4. Miaskowski C. Pharmacologic management of sleep disturbances in noncancer-related pain. *Pain Manag Nurs*. 2009;10(1):3–13. doi:10.1016/j.pmn.2008.05.002

5. Apfel CC, Greim CA, Haubitz I, et al. A risk score to predict the probability of postoperative vomiting in adults. *Acta Anaesthesiol Scand*. 1998;42(5):495–501. doi:10.1111/j.1399-6576.1998.tb05157.x

6. Koivuranta M, Läärä E, Snåre L, Alahuhta S. A survey of postoperative nausea and vomiting. *Anaesthesia*. 1997;52(5):443–449. doi:10.1111/j.1365-2044.1997.117-az0113.x

7. Apfel CC, Läärä E, Koivuranta M, Greim CA, Roewer N. A simplified risk score for predicting postoperative nausea and vomiting. *Anesthesiology*. 1999;91(3):693–700. doi:10.1097/00000542-199909000-00022

8. Gan TJ. Risk factors for postoperative nausea and vomiting. *Anesth Analg*. 2006;102(6):1884–1898. doi:10.1213/01.ANE.0000219597.16143.4D

9. Hesketh PJ. Chemotherapy induced nausea and vomiting. *N Engl J Med*. 2008;358(23):2482–2494. doi:10.1056/NEJMra0706547

10. Oddby-Muhrbeck E, Öbrink E, Eksborg S, Rotstein S, Lönnqvist PA. Is there an association between PONV and chemotherapy-induced nausea and vomiting? *Acta Anaesthesiol Scand*. 2013;57(6):749–753. doi:10.1111/aas.12053

11. da Silva HBG, Sousa AM, Guimarães GMN, Slullitel A, Ashmawi HA. Does previous chemotherapy-induced nausea and vomiting predict postoperative nausea and vomiting? *Acta Anaesthesiol Scand*. 2015;59(9):1145–1153. doi:10.1111/aas.12552

12. Laugsand EA, Fladvad T, Skorpen F, et al. Clinical and genetic factors associated with nausea and vomiting in cancer patients receiving opioids. *Eur J Cancer*. 2011;47(11):1682–1691. doi:10.1016/j.ejca.2011.04.014

13. Janicki PK, Sugino S. Genetic factors associated with pharmacotherapy and background sensitivity to postoperative and chemotherapy-induced nausea and vomiting. *Exp Brain Res*. 2014;232(8):2613–2625. doi:10.1007/s00221-014-3968-z

14. Apfel CC, Kranke P, Katz MH, et al. Volatile anaesthetics may be the main cause of early but not delayed postoperative vomiting: A randomized controlled trial of factorial design. *Br J Anesth*. 2002;88(5):659–668. doi:10.1093/bja/88.5.659

15. Roberts GW, Bekker TB, Carlsen HH, Moffatt CH, Slattery PJ, McClure AF. Postoperative nausea and vomiting are strongly influenced by postoperative opioid use in a dose-related manner. *Anesth Analg*. 2005;101(5):1343–1348. doi:10.1213/01.ANE.0000180204.64588.EC

16. Bhakta P, Ghosh BR, Singh U, et al. Incidence of postoperative nausea and vomiting following gynecological laparoscopy: A comparison of standard anesthetic technique and propofol infusion. *Acta Anaesthesiol Taiwan*. 2016;54(4):108–113. doi:10.1016/j.aat.2016.10.002

17. Bashandy GMN, Abbas DN. Pectoral nerves I and II blocks in multimodal analgesia for breast cancer surgery: A randomized clinical trial. *Reg Anesth Pain Med*. 2015;40(1):68–74. doi:10.1097/AAP.0000000000000163

18. Olanders KJ, Lundgren GAE, Johansson AMG. Betamethasone in prevention of postoperative nausea and vomiting following breast surgery. *J Clin Anesth*. 2014;26(6):461–465. doi:10.1016/j.jclinane.2014.02.006

19. Kim SH, Oh YJ, Park BW, Sim J, Choi YS. Effects of single-dose dexmedetomidine on the quality of recovery after modified radical mastectomy: A randomised controlled trial. *Minerva Anestesiol*. 2013;79(11):1248–1258. PMID:23698545.

20. Chiu C, Aleshi P, Esserman LJ, et al. Improved analgesia and reduced post-operative nausea and vomiting after implementation of an enhanced recovery after surgery (ERAS) pathway for total mastectomy. *BMC Anesthesiol*. 2018;18(1):41. doi:10.1186/s12871-018-0505-9

21. Myles PS, Leslie K, Chan MTV, et al. Avoidance of nitrous oxide for patients undergoing major surgery. *Anesthesiology*. 2007;107(2):221–231. doi:10.1097/01.anes.0000270723.30772.da

Visual pathway function in untreated individuals with major depression

Wojciech Lubiński[1,C–F], Hanna Grabek-Kujawa[1,A–C,E], Maciej Mularczyk[2,C,E],
Jolanta Kucharska-Mazur[3,C,E], Ewa Dańczura[3,C,E], Jerzy Samochowiec[3,C,E]

[1] 2nd Clinic of Ophthalmology, Pomeranian Medical University, Szczecin, Poland

[2] Chair and Department of Human and Clinical Anatomy, Pomeranian Medical University, Szczecin, Poland

[3] Department of Psychiatry, Pomeranian Medical University, Szczecin, Poland

A – research concept and design; B – collection and/or assembly of data; C – data analysis and interpretation;
D – writing the article; E – critical revision of the article; F – final approval of the article

Address for correspondence
Hanna Grabek-Kujawa
E-mail: hgrabek@wp.pl

Abstract

Background. Major depression (MD) is the one of the most debilitating diseases, affecting millions of people all around the world.

Objectives. To establish visual pathway function in untreated individuals with MD.

Materials and methods. In 29 untreated, newly diagnosed, ophthalmologically asymptomatic individuals (58 eyes) with MD (mean age: 47.3 years) and in 29 (58 eyes) of age-, sex- and refractive error-matched healthy controls (mean age: 46.8 years), the following examinations were performed: 1) best corrected distance visual acuity (BCDVA); 2) intraocular pressure (IOP); 3) and 4) biomicroscopy of anterior and posterior segment of eye; 5) macular structure (SD-OCT-Zeiss); and 6) pattern visual evoked potentials (PVEPs) measurements according to the International Society for Clinical Electrophysiology of Vision (ISCEV) standard (ISCEV-standard PVEPs). An analysis of correlation between the parameters of PVEPs and the depression severity (Hamilton Depression Rating Scale (HAMD)) was performed. To estimate the diagnostic power of PVEPs test, a receiver operating characteristics (ROC) curve was used. Data were analyzed with the significance level of p < 0.05.

Results. In the study group and in healthy control, the clinical results and macular structure were normal and not different. In the MD group, in PVEPs test (check size: 1°4′and 0°16′), a significant decrease of amplitudes of P100 (AP100), associated with prolonged P100 peak time (PTP100; check size: 0°16′, p < 0.004) were detected. The most frequent abnormality in PVEPs examination in the MD group was AP100 reduction (in 69% of individuals) detected using stimulation check size 0°16′. The statistically significant positive correlation between PTP100 (check size: 0°16′) and HAMD score was found in severe MD (p = 0.03). The analysis of ROC curve revealed the highest sensitivity of 0.759 and specificity of 1.0 for AP100 (0°16′). The area under the curve (AUC) was 0.841 (p < 0.001).

Conclusions. In individuals with newly diagnosed, ophthalmologically asymptomatic and untreated MD, a dysfunction of visual pathway is present without other signs of ocular pathology. The visual pathway dysfunction measured with ISCEV PVEPs has a potential value to be an objective biomarker of MD.

Key words: major depression, visual pathway function, PVEPs

118

W. Lubiński et al. Visual pathway function in major depression

Background

Major depression (MD) is the one of the most debilitating diseases, affecting millions of people all around the world.[1] It was reported to be one of the 5 leading causes of years lived with disability.[2] Several studies show that visual abnormalities in individuals with MD may occur. Photophobia, perceived dimness, anomalous pre-attentive processing of visual information, and self-reported visual function loss were detected.[3–8] Such patients are also more likely to experience vision problems like blurred vision and watery and strained eyes with surrounding pain and eye floaters. The cause of these complains can be disorders of the retina[9–15] as well as disorders of the brain including visual cortex.[16–18] Visual evoked potentials (VEPs) are visually evoked electrophysiological signals extracted from electroencephalographic activity in the visual cortex, but they depend on functional integrity of central vision at all levels of visual pathway.[19] In the available literature, only a few studies, using various methods, described changes in the PVEPs recordings in individuals with MD.[20–22] In 2 studies, the individuals with MD were medicated with antidepressants, so it was not possible to exclude their influence on PVEPs recordings.[20,21] Only the study by Bubl et al. described visual pathway dysfunction in unmedicated group with MD, and revealed abnormal cortical response, which was less pronounced than the retinal response.[22] It was the reason why we decided to analyze the visual pathway function in an untreated group of individuals with MD.

Objectives

Our aim was to evaluate visual pathway function in unmedicated patients with MD. We wanted to check if commonly performed, standard ISCEV (International Society for Clinical Electrophysiology of Vision) PVEPs recordings are useful in detecting visual pathway dysfunction in individuals with MD.

Materials and methods

Prospective studies were conducted in 2017–2021 in Department of Ophthalmology and Department of Psychiatry at the Pomeranian Medical University in Szczecin, Poland.

In the untreated, ophthalmologically asymptomatic, newly diagnosed 29 individuals (58 eyes) with MD (mean age: 47.3 years, age range: 20–69 years) and in 29 (58 eyes) age-, sex- and refractive error-matched healthy controls (mean age: 46.8 years, age range: 21–65 years), the following examinations were performed: 1) the best corrected distance visual acuity (BCDVA; Snellen Table); 2) intraocular pressure (IOP; Pascal tonometer); 3) and 4) biomicroscopy of anterior and posterior segments of the eye;

5) macular structure (thickness: inner limiting membrane to the retinal pigment epithelium (ILM-RPE) average cube, average retinal nerve fiber layer and average ganglion cell layer (GCL) + inner plexiform layer (IPL; Cirrus HD OCT Model 5000, Carl Zeiss AG, Jena, Germany); and 6) pattern reversal visual evoked potentials measurements (PVEPs according to ISCEV standards)[19] (RetiPort; Roland Consult GmbH, Brandenburg an der Havel, Germany). Stimulus parameters were as follows: black and white reversing checkerboard with 2 check sizes equal to 0°16′ and 1°4′, with the luminance of the white elements of 120 cd/m^2, and the contrast between black and white squares of 97%. Parameters of the recording system were as follows: amplifier range ±100 µV/div; filters 1–100 Hz; sweep time of 300 ms, and artifact rejection threshold of 95%. Two trials of 100 artifact free sweeps for each check size were obtained and averaged off-line. The analysis included the amplitude (A) and the peak time (PT) of the P100 wave (AP100 and PTP100).

Written informed consent was obtained from all participants. Study was approved by the local ethics committee of the Pomeranian Medical University (approval No. KB-0012/107/16 granted on October 17, 2016). The individuals with MD were assessed psychometrically with the Hamilton Depression Rating Scale (HAMD).[23,24] Individuals with MD accompanied by other psychiatric disorders, as well as ocular and systemic diseases with known influence on the retinal function were excluded. The MD individuals with poor focusing ability were also excluded.

Statistical analyses

The average value of the PVEPs parameters from the right and left eye from the MD and the control group were measured for further statistical analysis. Central tendency and dispersion measures of analyzed variables were presented as mean and standard deviation (M ±SD). The assumption of normality was checked using the W Shapiro–Wilk test (Table 1). With reference to the normality tests, the normal ranges were determined based on the values of parameters from the control group. In the case of normal distribution of the variables, the normal range was between −2SD and +2SD; in the absence

Table 1. Results of the W Shapiro–Wilk test checking the assumption of normality of analyzed parameters (n = 58)

Parameter		W test	p-value
Age		0.98	0.314
P100			
1°4′	A	0.96	0.041
	PT	0.95	0.012
0°16′	A	0.97	0.230
	PT	0.92	0.001

A – amplitude; PT – peak time.

of normality, the normal range was between 2.5 and 97.5 percentile. The values of parameters (amplitudes and peak times of the P100 wave with 1°4′ and 0°16′ check sizes) between the 2 groups were compared. To compare the parameters between the groups, the Student's t-test was used in the case of normal distribution (taking into account the homogeneity of variance and Welch's correction) of variables, or the non-parametric Mann–Whitney U test in the case of non-normal distribution. An analysis of the correlation (Spearman's rank correlation test) between the parameters of PVEPs and HAMD scale score was performed. To estimate the diagnostic power of PVEPs test, the receiver operating characteristics (ROC) curves were was used. The results were considered as statistically significant with $p < 0.05$.

Results

In the MD group and the healthy controls, the clinical results were as follow: the BCDVA – 1.0 ±0.1 (both groups), IOP – between normal limits, biomicroscopy of anterior and posterior segment of the eye – normal, and normal macular structure (Table 2). There was no statistically significant difference in the age between the 2 groups (MD: mean age 47.3 years, healthy controls mean age: 46.8 years, Student's t-test; df = 56; p = 0.731). In the MD group, the HAMD mean was equal to 26.4 ±6.6. There was a significant difference in the psychometric measure between the MD and the control group (Mann–Whitney U test; p < 0.001). There was no statistically significant difference in mean age between the 2 groups (Student's t-test; df = 56; p = 0.731). In the MD group, the HAMD score mean was 26.4 ±6.6. There was a significant difference in the psychometric measure between the MD and the control group (Mann–Whitney U test; p < 0.001).

Table 3 presents comparisons of PVEPs parameters such as AP100 and PT100 (check sizes: 0°16′ and 1°4′) between the MD and the control group. In the MD group (Table 3, Fig. 1), a significant decrease of AP100 was achieved (Mann–Whitney U test; p < 0.001 with 1°4′ and Student's t-test; df = 56; p < 0.001 with 0°16′). The significant difference of PTP100 between the MD and the control group was also obtained but only for check size 0°16′ (Mann–Whitney U test; p < 0.004), (Table 3, Fig. 1).

Comparisons of differences between mean A/mean PT of the P100-wave in patients with MD and mean A/PT of the P100-wave in normal subjects showed no statistically significant differences.

The range of normal values for PVEPs parameters was obtained from 58 eyes of 29 healthy controls. On the basis of the PVEPs normal values, the percentage of abnormal results for the analyzed PVEPs parameters in the MD group was estimated (Table 4). The most frequent abnormality in PVEPs examination in the group of MD individuals was the reduction of AP100 (check size: 0°16′) in 69% of them.
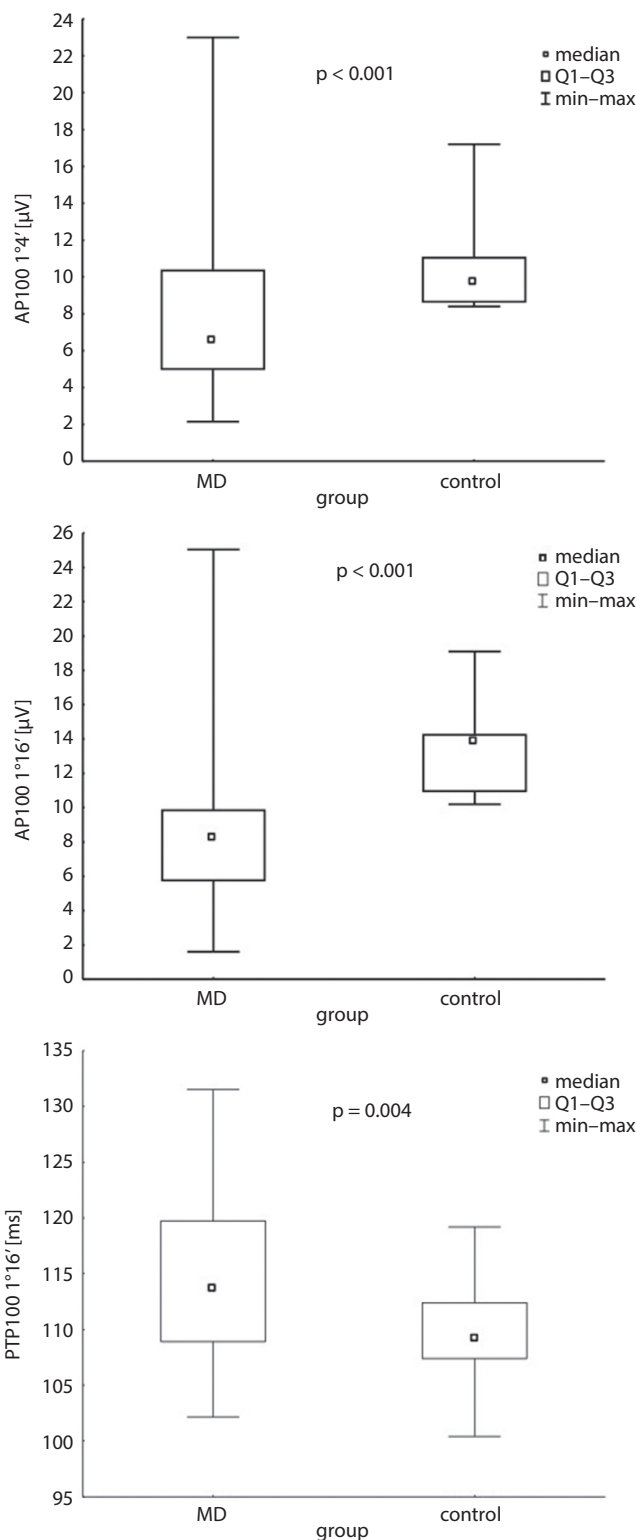
Fig. 1. The values of the AP100 (check sizes: 1°4′ and 0°16′) and PTP100 (check size: 0°16′) between 2 groups. The differences in these parameters between the groups were statistically significant. AP100 and PTP100 are the amplitude (A) and the peak time (PT) of the P100 wave

The HAMD results did not correlated significantly with PVEPs parameters. Correlations between PVEPs parameters as well as the severity of depression were also analyzed, adopting a 2-degree division of MD[25]: mild and moderate (HAMD score 8–23; 11 patients), and severe (score ≥24;

Table 2. Clinical results and macular structure in individuals with MD and healthy controls

Variable	MD group	Control group
BCDVA	1.0 ±0.1	1.0 ±0.1
IOP [mm Hg] (Mann–Whitney U test; p = 0.544)	16.3 ±1.2; (95% CI: 15.8–16.9)	16.1±1.2 (95% CI: 15.07–16.6)
Biomicroscopy of anterior and posterior segment of the eye	normal	normal
Macular structure [μm]		
Cube average thickness (Student's t-test, df = 56; p = 0.786)	279.4 ±13.1 (95% CI: 274.3–285.5)	282.4 ±8.8 (95% CI: 278.4–285.4)
Average retinal nerve fiber layer thickness (Student's t-test; df = 56; p = 0.737)	93.5 ±10.4 (95% CI: 88.0–99.7)	95.0 ±8.2 (95% CI: 91.8–98.8)
Average GCL + IPL thickness (Student's t-test; df = 56; p = 0.703).	81.13 ±7.35 (95% CI: 78.0–84.3)	81.57 ±5.00 (95% CI: 79.4–83.7)

MD – major depression; BCDVA – best corrected distance visual acuity; IOP – intraocular pressure; GCL – ganglion cells layer; IPL – inner plexiform layer; 95% CI – 95% confidence interval.

Table 3. Descriptive statistics of P100-wave of PVEPs (check sizes: 0°16' and 1°4') and results of the comparisons between the groups (n = 29)

Check size	P100	Group	Mean	SD	Median	Min	Max	p-value
1°4'	A	MD	7.87	4.48	6.57	2.15	23.00	<0.001
		control	10.87	2.62	9.70	8.40	17.20	
	PT	MD	109.06	6.40	108.30	97.20	124.30	0.152
		control	106.19	3.50	106.50	99.50	110.10	
0°16'	A	MD	8.90	5.24	8.30	1.60	25.05	<0.004*
		control	13.17	2.70	13.90	10.20	19.10	
	PT	MD	115.40	7.89	113.60	102.15	131.50	0.004
		control	109.71	4.63	109.20	100.40	119.20	

* Student's t-test with Welch's correction; p-value of the F test of variance homogeneity was <0.001. A – amplitude; PT – peak time; SD – standard deviation; PVEP – pattern visual evoked potentials; MD – major depression.

Table 4. Frequency of abnormal PVEPs parameters in individuals with MD (n = 29)

Check size	P100	n	%
1°4'	A	17	58.6
	PT	8	27.6
0°16'	A	20	69.0
	PT	8	27.6

A – amplitude; PT – peak time; PVEP – pattern visual evoked potentials; MD – major depression.

18 patients). The only statistically significant positive correlation between PTP100 (check size: 0°16') and HAMD score was found in severe MD (Spearman's rank correlation coefficient = 0.5; df = 16; p = 0.033).

The ROC analyses for PVEPs parameters were performed to assess the accuracy of the electrophysiological examination of the visual pathway with reference to MD. In the case of AP100 (check size: 1°4'), the cutoff point was 8.3 μV, with sensitivity of 0.690 and specificity of 1.00. The area under the curve (AUC) was 0.775 (p = 0.001). In the case of AP100 (check size: 0°16'), the cutoff point was 9.9 μV, with sensitivity of 0.759 and specificity of 1.00. The AUC was 0.841 (p < 0.001). For the PTP100 (check size: 0°16'), the cutoff point was 115.6 ms, with sensitivity of 0.483 and specificity of 0.897. The AUC was 0.719 (p = 0.001).

Discussion

Results of the present study are consistent with previous PVEPs findings in individuals with MD.[22] A study by Bubl et al. indicated a reduction of the retinal contrast gain on the level of ganglion cells in MD individuals.[26] The decrease in retinal contrast gain was correlated with the reduction of visual evoked potential amplitude.[22] In our study, we did not perform measurements of the contrast gain in the PVEPs. We wanted to check if commonly performed, ISCEV-standard PVEPs recordings (contrast between black and white squares of 97%) are useful in detection of visual pathway dysfunction in individuals with MD. Obtained results in this study strongly suggest that in the untreated, newly diagnosed individuals with MD, visual pathway dysfunction is present without other signs of ocular pathology and can be measured using ISCEV-standard PVEPs recordings (Table 3, Fig. 1,2). The manifestations of detected dysfunction were a reduction of AP100 for used check sizes of stimulation as well as prolonged PTP100 for check size equal to 0°16'.

According to Lam, different sizes of the check stimulus in PVEPs stimulate different part of the retina.[27] The large check stimulus elicits more parafoveal response (magnocellular pathway) but small check sizes stimulate a mainly foveal response (parvocellular pathway). We investigated
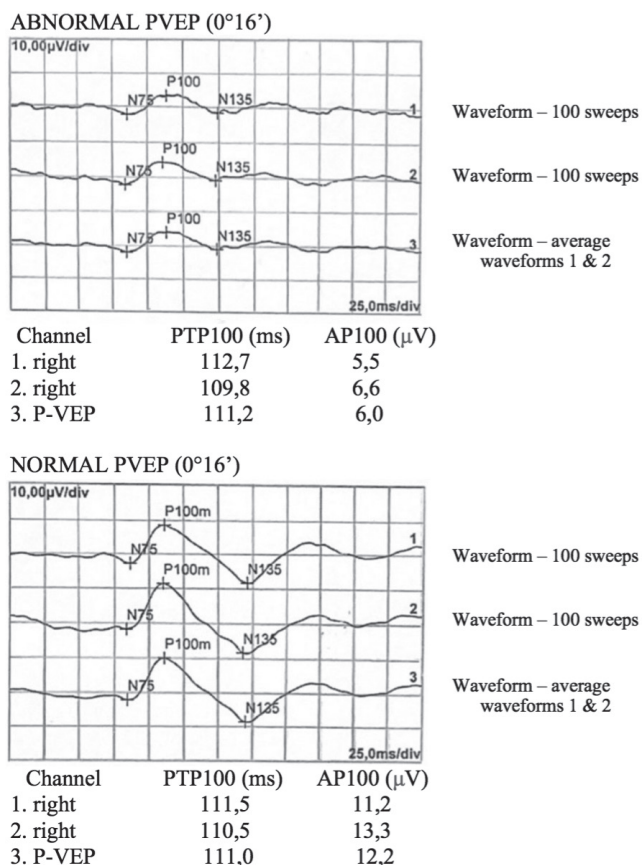
Fig. 2. Abnormal pattern visual evoked potentials (PVEPs; check size: 0°16') with reduced AP100-wave of the major depression (MD) individual (above) in comparison to the normal PVEPs recording (below)

the difference in PVEPs examination between stimulation in the foveal and parafoveal region in patients with MD. Comparative analysis between AP100 and PTP100 after large (1°4') and small (0°16') check stimulation showed no statistically significant differences. This results indicated that in untreated individuals with MD, parvo- and magnocellular pathways are evenly disturbed.

If separated eyes of MD individuals were compared to age- and sex-matched normal values from PVEPs examination of controls (Table 4), the most frequent feature was the reduction of AP100 (check size: 0°16'). The only significant correlation found was between PTP100 (check size: 0°16') and the severe MD measured using HAMD. The lack of correlation between PVEPs parameters in mild and moderate MD suggested that ISCEV-standard PVEPs measurement, contrary to the PVEPs contrast gain, is less useful in estimating MD severity.[22]

The results of the ROC curve analysis show the predictive potential of PVEPs parameters in evaluation of visual pathway dysfunction in individuals with MD. The areas under the ROC curve for AP100 (check sizes: 0°16' and 1°4') and for PTP100 (check size: 0°16') differed significantly from the random model. According to the proposed classification by Hosmer et al., the AUC for AP100 (check size: 0°16') had an excellent predictive value (0.8 < AUC < 0.9) while for AP100 (check size: 1°4') and PTP100 (check

size: 0°16') it was acceptable (0.7 < AUC < 0.8).[28] In our model, in the case of AP100 (check size: 1°4'), at the designated cutoff point, 69% of individuals with MD were correctly classified (sensitivity of 0.69) and 100% were correctly classified as healthy (specificity of 1). For AP100 (check size: 0°16'), at the designated cutoff point, 75.9% (sensitivity of 0.759) of individuals with MD and 100% of healthy individuals were correctly classified (specificity 1). A worse result was obtained for the PTP100 (check size: 0°16'), where 48.3% of MD individuals and 89.7% of healthy individuals were correctly classified at the designated cutoff point.

Despite well-known characteristic symptoms of MD like mood dysregulation and impaired cognitive control, depressive disorder might be associated with the visual complaints not explained in the course of routine ophthalmological examination. There is growing evidence that a dysfunction of dopaminergic system has a significant role in pathogenesis of MD.[29] The ventral tegmental area as well as mesolimbic and mesocortical pathway play important roles in this regard.[30,31] The occipital cortex receives strong dopamine innervation from the mesocortical dopamine system.[32] Moreover, dopamine modulates contrast gain control in the visual pathway in the lateral geniculate body and visual cortex.[33] Dysregulation of dopamine level in MD individuals might be responsible for abnormal retinal contrast response and less pronounced cortical response.[22] There are some studies suggesting influence of the catecholaminergic dysfunction on the PVEPs recording in MD individuals[20,22,34,35] and in another dopamine-related diseases such as Parkinson disease.[36,37] Abnormal PVEPs in our study confirmed previous notions on the connection with the catecholaminergic system changes in MD individuals.

In our study, in the MD individuals, the retinal macular structure was also examined using the OCT test and compared with the controls. We did not find significant changes in the MD group. Our results suggest that due to dysregulation of dopamine level, the visual pathway dysfunction was detected without the presence of structural macular changes. In the past, in individuals with MD, the retinal structure using the OCT test examination was investigated in 5 case-control studies with mixed results.[14,38–42] Jung et al. described decrease of ganglion cell inner plexiform layer thickness in individuals with MD.[12] Kalenderoglu et al. showed significantly reduced GCL, IPL, and global and temporal superior retinal nerve fiber layer (RNFL) thickness in the recurrent-MD individuals compared to the first-episode individuals, and in all MD individuals compared with the controls.[38] This decrease was more severe in individuals with more severe MD. Liu et al. described thinner RNFL in bipolar disorder and MD patients than in healthy people.[42] However, other researchers, like in our study comparing the MD individuals with the healthy controls, found no statistically significant differences in the OCT measures.[39–41]

The feature of abnormal ISCEV-standard PVEPs response has clinical relevance. The PVEPs signal might serve as an objective marker of the major depression and has a potential value in monitoring pharmacological and non-pharmacological treatment trials. The PVEPs test is commonly used in ophthalmology, is easy to perform, minimally invasive and inexpensive in comparison to other techniques like positron emission tomography (PET) or functional magnetic resonance imaging (fMRI). Abnormal PVEPs in patient without diagnosed MD but with ophthalmic MD signs and normal results of other ophthalmological as well as neuroimaging examinations should be an indication for psychiatric consultation. Major depression should be taken into account in differential diagnosis of patients with suspected subclinical visual pathway diseases.

Limitations

A limitation of the present study is the small number of cases, unblinded examination of the MD individuals, as well as possible and not detected poor focusing of the fixation point during the PVEPs test resulting in abnormal results.

Conclusions

The present study results are additional evidence that in patients with MD visual pathway dysfunction is present (as measured based on ISCEV-standard PVEPs). The abnormalities in visual pathway function detected in PVEPs recording have a potential value to be an objective marker of MD. Future studies using the same methodology but with a larger sample size are necessary to confirm such conclusion. The dependence between subjective visual symptoms and severity of visual pathway dysfunction should also be elucidated.

ORCID iDs

Wojciech Lubiński https://orcid.org/0000-0002-3729-9750
Hanna Grabek-Kujawa https://orcid.org/0000-0001-6160-8835
Maciej Mularczyk https://orcid.org/0000-0001-9885-6939
Jolanta Kucharska-Mazur https://orcid.org/0000-0002-8063-3662
Ewa Dańczura https://orcid.org/0000-0002-4161-4055
Jerzy Samochowiec https://orcid.org/0000-0003-1438-583X

References

1. Smith K. Mental health: A world of depression. *Nature*. 2014;515(7526):180–181. doi:10.1038/515180a
2. Vos T, Abajobir AA, Abate KH, et al. Global, regional, and national incidence, prevalence, and years lived with disability for 328 diseases and injuries for 195 countries, 1990–2016: A systematic analysis for the Global Burden of Disease Study 2016. *Lancet*. 2017;390(10100):1211–1259. doi:10.1016/S0140-6736(17)32154-2
3. Anagnostou E, Vikelis M, Tzavellas E, et al. Photophobia in primary headaches, in essential blepharospasm and in major depression. *Int J Neurosci*. 2017;127(8):673–679. doi:10.1080/00207454.2016.1231185
4. Chang Y, Xu J, Shi N, Pang X, Zhang B, Cai Z. Dysfunction of preattentive visual information processing among patients with major depressive disorder. *Biol Psychiatry*. 2011;69(8):742–747. doi:10.1016/j.biopsych.2010.12.024
5. Friberg TR, Borrero G. Diminished perception of ambient light: A symptom of clinical depression? *J Affect Disord*. 2000;61(1–2):113–118. doi:10.1016/S0165-0327(99)00194-9
6. Friberg TR, Bremer RW, Dickinsen M. Diminished perception of light as a symptom of depression: Further studies. *J Affect Disord*. 2008;108(3):235–240. doi:10.1016/j.jad.2007.10.021
7. Qiu X, Yang X, Qiao Z, et al. Impairment in processing visual information at the pre-attentive stage in patients with a major depressive disorder: A visual mismatch negativity study. *Neurosci Lett*. 2011;491(1):53–57. doi:10.1016/j.neulet.2011.01.006
8. Zhang X, Bullard KM, Cotch MF, et al. Association between depression and functional vision loss in persons 20 years of age or older in the United States, NHANES 2005–2008. *JAMA Ophthalmol*. 2013;131(5):573. doi:10.1001/jamaophthalmol.2013.2597
9. Youssef P, Nath S, Chaimowitz GA, Prat SS. Electroretinography in psychiatry: A systematic literature review. *Eur Psychiatry*. 2019;62:97–106. doi:10.1016/j.eurpsy.2019.09.006
10. Schwitzer T, Schwan R, Bubl E, Lalanne L, Angioi-Duprez K, Laprevote V. Looking into the brain through the retinal ganglion cells in psychiatric disorders: A review of evidences. *Prog Neuropsychopharmacol Biol Psychiatry*. 2017;76:155–162. doi:10.1016/j.pnpbp.2017.03.008
11. Lubiński W, Grabek-Kujawa H, Dańczura E, Kucharska-Mazur J, Samochowiec J, Mularczyk M. The influence of escitalopram therapy on macular function in patients with major depression: Preliminary report. *Klinika Oczna*. 2022;124(1):25–30. doi:10.5114/ko.2022.114992
12. Jung KI, Hong SY, Shin DY, Lee NY, Kim TS, Park CK. Attenuated visual function in patients with major depressive disorder. *J Clin Med*. 2020;9(6):1951. doi:10.3390/jcm9061951
13. Cosker E, Moulard M, Baumann C, et al. Complete evaluation of retinal function in major depressive disorder: From central slowdown to hyperactive periphery. *J Affect Disord*. 2021;295:453–462. doi:10.1016/j.jad.2021.08.054
14. Friedel EBN, Tebartz van Elst L, Schmelz C, et al. Replication of reduced pattern electroretinogram amplitudes in depression with improved recording parameters. *Front Med (Lausanne)*. 2021;8:732222. doi:10.3389/fmed.2021.732222
15. Schwitzer T, Le Cam S, Cosker E, et al. Retinal electroretinogram features can detect depression state and treatment response in adults: A machine learning approach. *J Affect Disord*. 2022;306:208–214. doi:10.1016/j.jad.2022.03.025
16. Zeng LL, Shen H, Liu L, et al. Identifying major depression using whole-brain functional connectivity: A multivariate pattern analysis. *Brain*. 2012;135(5):1498–1507. doi:10.1093/brain/aws059
17. Odom JV, Bach M, Brigell M, et al; International Society for Clinical Electrophysiology of Vision. ISCEV standard for clinical visual evoked potentials: 2016 update. *Doc Ophthalmol*. 2016;133(1):1–9. doi:10.1007/s10633-016-9553-y
18. Fotiou F, Fountoulakis KN, Iacovides A, Kaprinis G. Pattern-reversed visual evoked potentials in subtypes of major depression. *Psychiatry Res*. 2003;118(3):259–271. doi:10.1016/S0165-1781(03)00097-0
19. Normann C, Schmitz D, Fürmaier A, Döing C, Bach M. Long-term plasticity of visually evoked potentials in humans is altered in major depression. *Biol Psychiatry*. 2007;62(5):373–380. doi:10.1016/j.biopsych.2006.10.006
20. Bubl E, Kern E, Ebert D, Riedel A, Tebartz van Elst L, Bach M. Retinal dysfunction of contrast processing in major depression also apparent in cortical activity. *Eur Arch Psychiatry Clin Neurosci*. 2015;265(4):343–350. doi:10.1007/s00406-014-0573-x
21. Hamilton M. A rating scale for depression. *J Neurol Neurosurg Psychiatry*. 1960;23(1):56–62. doi:10.1136/jnnp.23.1.56
22. Hamilton M. Development of a rating scale for primary depressive illness. *Br J Soc Clin Psychol*. 1967;6(4):278–296. doi:10.1111/j.2044-8260.1967.tb00530.x
23. Zimmerman M, Martinez JH, Young D, Chelminski I, Dalrymple K. Severity classification on the Hamilton depression rating scale. *J Affect Disord*. 2013;150(2):384–388. doi:10.1016/j.jad.2013.04.028
24. Bubl E, Kern E, Ebert D, Bach M, Tebartz van Elst L. Seeing gray when feeling blue? Depression can be measured in the eye of the diseased. *Biol Psychiatry*. 2010;68(2):205–208. doi:10.1016/j.biopsych.2010.02.009
25. Lam BL. Visual evoked potential. In: Lam BL, ed. *Electrophysiology of Vision: Clinical Testing and Applications*. Boca Raton, USA: Taylor & Francis; 2005:123–125. ISBN:978-0824740689.
26. Hosmer DW, Lemeshow S, Sturdivant RX. *Applied Logistic Regression*. New York, USA: John Wiley & Sons, Inc.; 2013. doi:10.1002/9781118548387

27. Belujon P, Grace AA. Dopamine system dysregulation in major depressive disorders. *Int J Neuropsychopharmacol*. 2017;20(12):1036–1046. doi:10.1093/ijnp/pyx056

28. Chaudhury D, Walsh JJ, Friedman AK, et al. Rapid regulation of depression-related behaviours by control of midbrain dopamine neurons. *Nature*. 2013;493(7433):532–536. doi:10.1038/nature11713

29. Nestler EJ, Carlezon WA. The mesolimbic dopamine reward circuit in depression. *Biol Psychiatry*. 2006;59(12):1151–1159. doi:10.1016/j.biopsych.2005.09.018

30. De Keyser J, Ebinger G, Vauquelin G. Evidence for a widespread dopaminergic innervation of the human cerebral neocortex. *Neurosci Lett*. 1989;104(3):281–285. doi:10.1016/0304-3940(89)90589-2

31. Solomon SG. Chromatic gain controls in visual cortical neurons. *J Neurosci*. 2005;25(19):4779–4792. doi:10.1523/JNEUROSCI.5316-04.2005

32. Vasile RG, Duffy FH, McAnulty G, et al. Abnormal visual evoked response in melancholia. *Biol Psychiatry*. 1989;25(6):785–788. doi:10.1016/0006-3223(89)90250-3

33. Vasile RG, Duffy FH, McAnulty G, Mooney JJ, Bloomingdale K, Schildkraut JJ. Abnormal flash visual evoked response in melancholia: A replication study. *Biol Psychiatry*. 1992;31(4):325–336. doi:10.1016/0006-3223(92)90226-P

34. Ikeda H, Head GM, K. Ellis CJ. Electrophysiological signs of retinal dopamine deficiency in recently diagnosed Parkinson's disease and a follow up study. *Vision Res*. 1994;34(19):2629–2638. doi:10.1016/0042-6989(94)90248-8

35. Langheinrich T, Tebartz van Elst L, Lagrèze WA, Bach M, Lücking CH, Greenlee MW. Visual contrast response functions in Parkinson's disease: Evidence from electroretinograms, visually evoked potentials and psychophysics. *Clin Neurophysiol*. 2000;111(1):66–74. doi:10.1016/S1388-2457(99)00223-0

36. Kalenderoglu A, Çelik M, Sevgi-Karadag A, Egilmez OB. Optic coherence tomography shows inflammation and degeneration in major depressive disorder patients correlated with disease severity. *J Affect Disord*. 2016;204:159–165. doi:10.1016/j.jad.2016.06.039

37. Schönfeldt-Lecuona C, Schmidt A, Kregel T, et al. Retinal changes in patients with major depressive disorder: A controlled optical coherence tomography study. *J Affect Disord*. 2018;227:665–671. doi:10.1016/j.jad.2017.11.077

38. Sonmez I, Kosger F, Aykan U. Retinal nerve fiber layer thickness measurement by spectral-domain optical coherence tomography in patients with major depressive disorder. *Arch Neuropsychiatr*. 2017;54(1):62–66. doi:10.5152/npa.2015.10115

39. Yıldız M, Alim S, Batmaz S, et al. Duration of the depressive episode is correlated with ganglion cell inner plexifrom layer and nasal retinal fiber layer thicknesses: Optical coherence tomography findings in major depression. *Psychiatry Res Neuroimaging*. 2016;251:60–66. doi:10.1016/j.pscychresns.2016.04.011

40. Liu Y, Tong Y, Huang L, Chen J, Yan S, Yang F. Factors related to retinal nerve fiber layer thickness in bipolar disorder patients and major depression patients. *BMC Psychiatry*. 2021;21(1):301. doi:10.1186/s12888-021-03270-7

41. Le TM, Borghi JA, Kujawa AJ, Klein DN, Leung HC. Alterations in visual cortical activation and connectivity with prefrontal cortex during working memory updating in major depressive disorder. *NeuroImage Clin*. 2017;14:43–53. doi:10.1016/j.nicl.2017.01.004

42. Song XM, Hu XW, Li Z, et al. Reduction of higher-order occipital GABA and impaired visual perception in acute major depressive disorder. *Mol Psychiatry*. 2021;26(11):6747–6755. doi:10.1038/s41380-021-01090-5

Identification of cardiac-related serum miRNA in patients with type 2 diabetes mellitus and heart failure: Preliminary report

Monika Wrzosek[1,B,C,E,F], Anna Hojka-Osińska[2,C–F], Dominika Klimczak-Tomaniak[3,A–F], Anna Katarzyna Żarek-Starzewska[3,C,E,F], Wioletta Dyrla[3,A,B,E,F], Magdalena Rostek-Bogacka[3,B,E,F], Maksym Wróblewski[3,B,E,F], Marek Kuch[3,A,C,E,F], Magdalena Kucia[1,4,A,C,E,F]

[1] Laboratory of Regenerative Medicine, Medical University of Warsaw, Poland

[2] International Institute of Molecular and Cell Biology, Warsaw, Poland

[3] Department of Cardiology, Hypertension and Internal Medicine, Medical University of Warsaw, Poland

[4] Stem Cell Institute, James Graham Brown Cancer Center, University of Louisville, USA

A – research concept and design; B – collection and/or assembly of data; C – data analysis and interpretation;
D – writing the article; E – critical revision of the article; F – final approval of the article

Address for correspondence
Dominika Klimczak-Tomaniak
E-mail: dklimczak@wum.edu.pl

Abstract

Background. Diabetic patients present an increased risk for heart failure (HF) independently of the presence of coronary artery disease (CAD) and hypertension. However, little is known about circulatory microRNA (miRNA), an important regulatory RNA in this population.

Objectives. To evaluate serum miRNA profile of patients with diabetes mellitus (DM) and HF and analyze its relationship with pathophysiological pathways involved.

Materials and methods. The accumulation of 179 miRNAs was measured in serum of diabetic patients with HF and compared to the same measurements in healthy control subjects. The miRNAs were assayed using quantitative polymerase chain reaction (qPCR) on the Serum/Plasma Focus microRNA PCR panel (Qiagen) with LightCycler® 96 Real-Time PCR System (Roche). A pairwise comparison of mean relative miRNA accumulation levels was performed to establish those miRNAs that are differently expressed in patients with: 1) HF; 2) HF and chronic coronary syndrome (HF-CAD); and 3) HF without chronic coronary syndrome (HF-nonCAD) compared to healthy controls. To gain insight into these functions of miRNAs, we applied Gene Ontology (GO) enrichment analysis of Biological Processes and Molecular Functions of their predicted targets.

Results. The pairwise comparison revealed that 12 miRNAs were significantly downregulated in HF-CAD patients compared to controls, whereas 4 miRNAs were considerably deregulated in HF-nonCAD patients, with miRNA-15b-5p being downregulated in both groups. The GO analysis revealed that differentially accumulated targets of miRNAs include genes involved in potassium channel function, MAPK kinase activity and DNA transcription regulation, with similar alterations observed in the whole HF group and HF–CAD subgroup as well as a response to stress and apoptosis (in HF group), and genes involved in the development (in HF–CAD group). No oriented specialization of deregulated miRNA targets was observed in the HF–nonCAD subgroup.

Conclusions. We observed a significant downregulation of 13 miRNAs in diabetic HF patients, which was not reported previously either in HF or diabetic patients. Downregulated miRNAs regulate angiogenesis and apoptosis.

Key words: angiogenesis, cytokine, glucocorticoids, lipid, apoptosis

Introduction

Diabetes mellitus (DM) is an independent risk factor for heart failure (HF). Diabetic patients manifest 4 times greater risk for HF and earlier HF onset compared to the general population.[1,2] Myocardial dysfunction in DM has a heterogeneous phenotype and multifactorial origin, as it frequently occurs due to concomitant coronary artery disease (CAD) and hypertension. It may also stem from DM itself, more specifically, a condition termed diabetic cardiomyopathy.[3,4] In vitro and in vivo studies demonstrated that microRNAs (miRNAs) play important roles in the pathogenesis of cardiovascular complications of DM by exerting a direct effect on cardiomyocytes and influencing vascular smooth muscle cells, platelets, as well as processes such as lipid metabolism and inflammation.[5,6] However, little is known about circulating miRNAs in diabetic patients.[7]

Objectives

In this study, we aim to evaluate profiles of circulating miRNAs of diabetic patients with HF diagnosis and the correlation between deregulated miRNAs and pathophysiology of HF in DM.

Materials and methods

Study group

We included 6 adult diabetic patients, in whom HF had been diagnosed according to the European Society of Cardiology Guidelines at least 3 months before the onset of the study.[8] Diabetes was diagnosed according to current guidelines.[9] The control group consisted of 3 healthy age- and sex-matched subjects with no history of cardiovascular disease. The study was approved by the Medical Ethics Committee of the Medical University of Warsaw and was conducted conforming to the tenets of Declaration of Helsinki. All participants provided written informed consent. The exact inclusion and exclusion criteria are described in Supplementary Text S1.

miRNA isolation

Blood samples from 6 patients and 3 healthy donors were centrifuged at 1000 × g for 20 min at 4°C. The serum was stored at −80°C until analyzed. The miRNA was extracted from serum using a commercial column-based system (Micro RNA Concentrator, cat. No. 035-25C; A&A Biotechnology, Gdańsk, Poland), following the manufacturer's instructions. The obtained concentration and quality of miRNA were measured using a NanoDrop Lite spectrophotometer (cat. No. LD-LITE-PR; Thermo Fisher Scientific, Waltham, USA) at 260 nm and a purity analysis based on a 260/280 ratio.

cDNA synthesis and real-time polymerase chain reaction

Briefly, 8 μL of RNA eluate was reverse transcribed in 20-μL reactions using the miRCURY LNA™ Universal RT cDNA Synthesis Kit (cat. No. 339340; Exiqon, Copenhagen, Denmark). The cDNA was diluted 30 times and assayed using real-time polymerase chain reaction (PCR), according to the protocol for the miRCURY LNA™ Universal RT microRNA PCR System (cat. No. 3393306; Exiqon); each microRNA was assayed once using quantitative PCR (qPCR) on the Serum/Plasma Focus microRNA PCR panel (cat. No. 3393325; Qiagen, Hilden, Germany). A no-template control (NTC) of water was purified with the samples and profiled like the samples. The amplification was performed in a LightCycler® 96 Real-Time PCR System (cat. No. 05815916001; Roche, Basel, Switzerland) in 96-well plates. The amplification curves were analyzed using the Roche LC software (Roche), both for the determination of the quantification cycle (Ct; using the second derivative method) and for the melting curve analysis. The amplification efficiency was calculated using algorithms similar to the Lin-RegPCR software (https://medischebiologie.nl/files/). All assays were inspected for distinct melting curves, and the melting temperature was checked to be within known specifications for the assay.

Quantification of miRNA accumulation

The Ct values for all miRNAs and all samples were extracted from the reverse transcription results reports and uploaded into R/Bioconductor environment (https://www.bioconductor.org/), where the analysis was performed. In particular, for data quality control and normalization, the "HTqPCR" package was employed. Two forms of normalization were applied. To compensate for the bias of obtaining Ct values in different runs, normalization to Interplate Calibrator (IPC) UniSp3 (a component of the miRCURY LNA™ Universal RT microRNA PCR System (cat. No. 3393306; Exiqon)) was performed. The second form was normalization to endogenous normalizer. As in serum samples, widely used controls such as snoRNAs or snRNAs are not accumulated on the appropriate level; therefore, we decided to perform normalization to invariant miRNA, and the intra-normalization was performed to hsa-miR-21. As a result, we obtained ΔCt values that are equal to log2-transformed miRNA accumulation levels. Differential miRNA accumulation profiles were performed using fold change calculations based on ΔCt values.

Statistical analyses

First, a heatmap was used to visualize the hierarchical clustering of 179 miRNAs. Second, principal component analysis (PCA) was applied to verify the differences in miRNA profiles between the patients. Subsequently, a pairwise comparison of mean relative miRNA accumulation levels was performed to establish those miRNAs that are differently expressed in patients with: 1) HF; 2) HF and chronic coronary syndrome (HF-CAD); and 3) HF without chronic coronary syndrome (HF-nonCAD) compared to healthy controls. The cutoff values for identifying significantly differentially accumulated miRNAs were adjusted p-value < 0.05 and fold change (FC) >2 or FC < 0.5 (same as $|\log_2 FC| > 1$). To gain insight into these functions of miRNAs, we applied Gene Ontology (GO) enrichment analysis of Biological Processes and Molecular Functions of their predicted targets, selected with TargetScan (https://www.targetscan.org) and miRDB (https://mirdb.org). Data were analyzed with the R Bioconductor environment. A more detailed description is given in Supplementary Text S2.

Results

In total, 6 male patients with DM and HF were included in the preliminary analysis (Table 1). The median age of the patients was 69 years (range: 61–70 years). All patients were in the New York Heart Association (NYHA) class I or II, with median left ventricular ejection fraction (LVEF) equal to 41% (range: 35–50%) and median glycated hemoglobin (HbA1c) equal to 6.9% (6.6–7.5%). The control group consisted of 3 healthy males (age: 66 ±8 years, body mass index (BMI): 28 ±6 kg/m²).

A comprehensive analysis of circulating miRNA profiles revealed that analyzed individuals fall into 4 separate clusters, with all 3 healthy individuals clustered together, as uncovered by hierarchical clustering (Supplementary Fig. 1A,B) and PCA (Supplementary Fig. 1C). We observed a clear shift in HF patients' miRNA levels, with 65 miRNAs (36.3%) being downregulated (Supplementary Fig. 2A). In the case of 13 miRNAs, the downregulation was significant compared to healthy controls (Supplementary Fig. 2B,C). The pairwise comparison revealed that 12 miRNAs are significantly downregulated in HF-CAD patients compared to controls (Fig. 1), whereas 4 miRNAs are considerably deregulated in HF-nonCAD patients (Fig. 1), with miRNA-15b-5p being downregulated in both groups.

The GO analysis revealed that differentially accumulated targets of miRNAs include genes involved in potassium channel function, MAPK kinase activity and DNA transcription regulation, with similar alterations observed in the whole group and HF-CAD subgroup (Supplementary Fig. 3A) as well as genes involved in response to stress and apoptosis (HF), and genes involved in the development (HF-CAD) (Supplementary Fig. 3B). No oriented specializations of deregulated miRNA targets were observed for the HF-nonCAD subgroup. Functional networks of pathways regulated by mRNA targets of significantly altered miRNAs are presented in Fig. 2.

Discussion

This is the first study that investigated serum miRNA profile in HF patients with DM. We identified significant differences in serum miRNA accumulation compared to healthy controls. The pathway analysis revealed that deregulated miRNAs might influence angiogenesis and apoptosis in response to stress in HF patients, as well as cell development, response to glucocorticoids, negative regulation of cytokine production, and membrane lipid metabolism in HF-CAD patients.

MicroRNAs downregulated in HF-CAD patients have been investigated in the preclinical setting. The miR-15 group is implicated in the negative regulation of cardiomyocyte proliferation.[10] The miR-30-b has been shown to repress cyclophilin D-induced necrosis and promote hypoxia-induced apoptosis, similarly to miR-145-5p.[11–13] The miR-143/145 cluster is also involved in inhibiting the phenotype switch of the contractile, mature and differentiated vascular smooth muscle cell type to a dedifferentiated, synthetic and proliferative one.[14] The mir-29b-3p was identified as anti-apoptotic and anti-fibrotic to the myocardium.[15,16] Substantial evidence supports the use of anti-fibrotic miR-29b as a potential therapeutic target against myocardial remodeling, but this application still requires verification in the clinical setting.[17]

Table 1. Characteristics of the study population

Patient number	Sex	Age	EF (%)	CAD	HbA1c (%)	Anti-diabetic medication
1	M	70	50	1	7.5	insulin
2	M	69	35	1	6.6	glimepride, metformin
3	M	80	55	0	6.9	insulin
4	M	54	20	0	7.7	insulin
5	M	68	40	1	6.6	insulin
6	M	61	45	0	–	metformin

CAD – coronary artery disease; EF – ejection fraction; HbA1c – glycated hemoglobin.
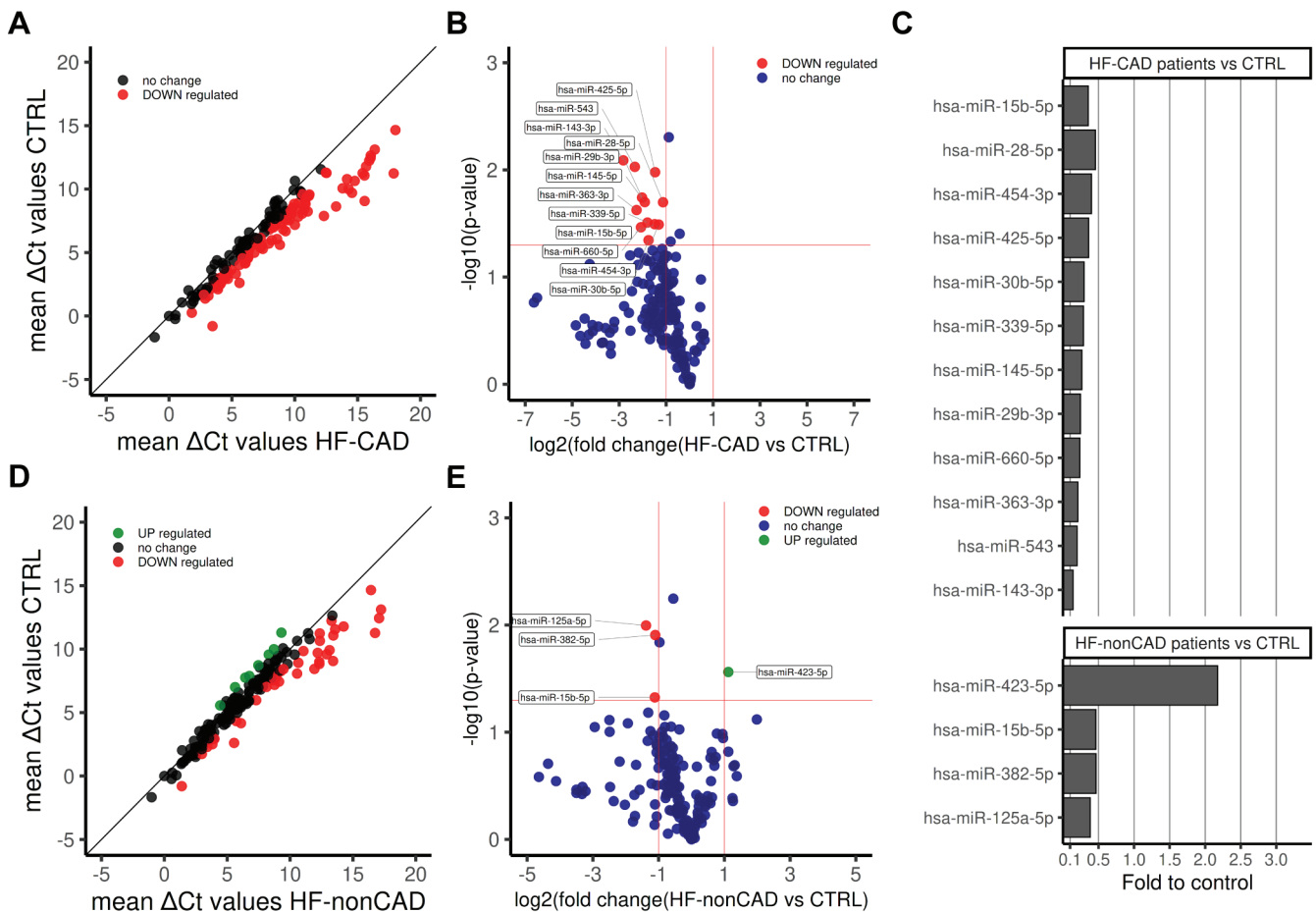
Fig. 1. Distinct microRNA (miRNA) accumulation profiles between healthy controls and heart failure (HF) patients with and without coronary artery disease (CAD). Results are represented as volcano plots to indicate statistical significance of differential accumulation. Blue dots represent miRNAs that are not differentially accumulated. In contrast, red dots represent miRNAs that are significantly differentially accumulated, and red lines represent threshold values (log2(fold change (FC)) < −1, p < 0.05) for discriminating statistically significant miRNAs

In the clinical context, none of the 13 downregulated miRNAs have been reported to be a diagnostic or prognostic biomarker in HF. Still, the higher circulating miR-145-5p expression is associated with a positive response to cardiac resynchronization therapy.[18] According to the recent systematic review, none of the 13 circulating miRNAs, except for the miR-30 family, are deregulated in CAD patients.[19] Similarly, none is deregulated in the case of DM alone.[20] Therefore, we hypothesize that the identified miRNA set is distinctive for HF-CAD patients.

Limitations

In this article, we focused on male patients with HF and CAD. Thus, the results should not be extrapolated to patients with HF without an ischemic component, neither pure diabetic cardiomyopathy nor women.

Conclusions

We observed a significant downregulation of 13 miRNAs in diabetic HF patients, which was not reported previously either in HF or diabetic patients. Downregulated miRNAs regulate angiogenesis and apoptosis. Heart failure in DM is a heterogeneous disease, and these preliminary data should be viewed with caution. Further patient recruitment is ongoing to confirm these results.

Supplementary data

The Supplementary Files are available at https://doi.org/10.5281/zenodo.7295018. The package contains the following files:

Supplementary Text S1. Supplemental methods – study population.

Supplementary Text S2. Supplemental methods – statistical analysis.

Supplementary Fig. 1. Explorative analysis of serum miRNA accumulation profile in heart failure patients.

Supplementary Fig. 2. Profiling of serum miRNA differential accumulation between patients and healthy control individuals.

Supplementary Fig. 3. Gene Ontology (GO) analysis of miRNAs differentially accumulated in heart failure patients.
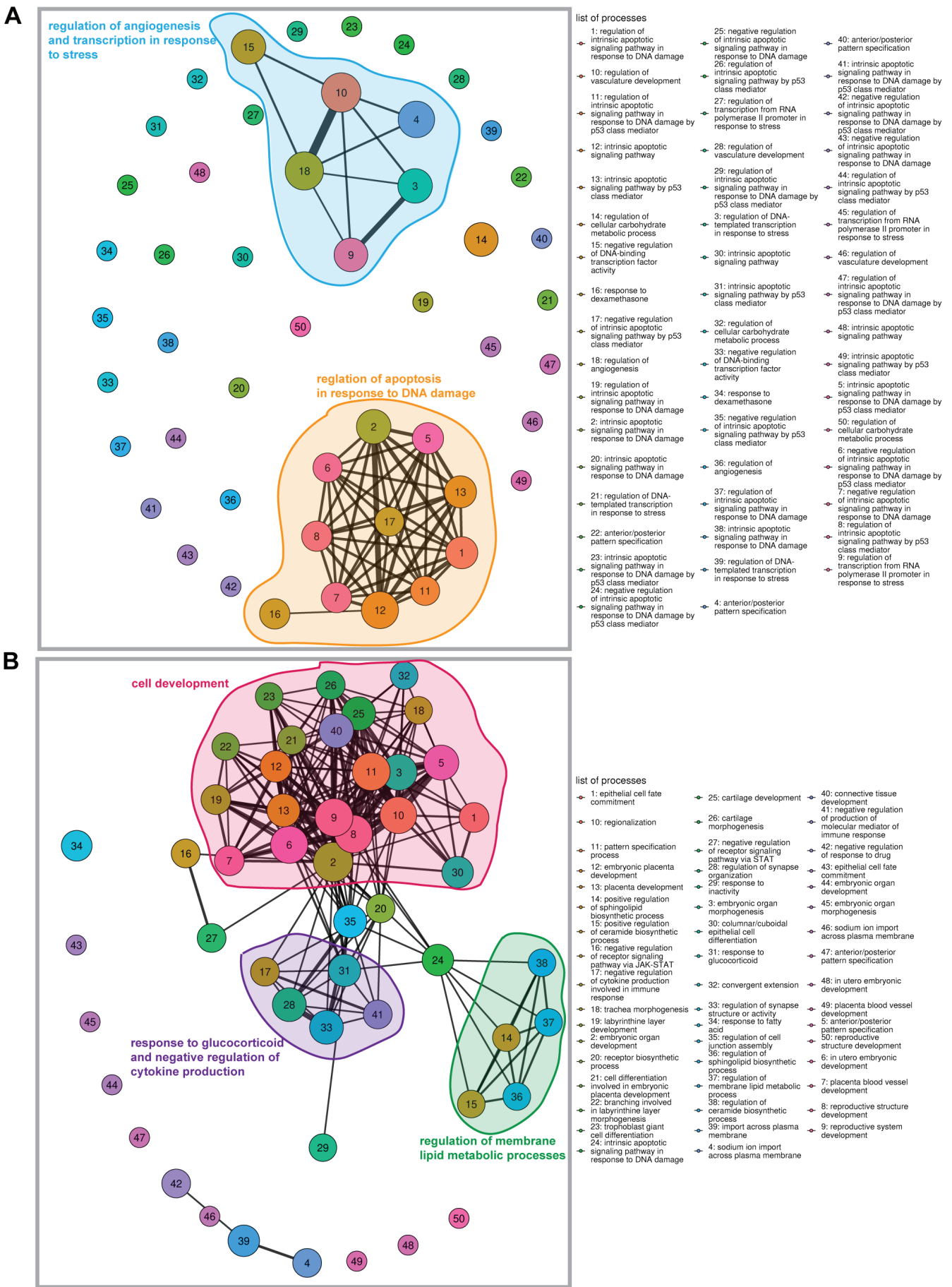
Fig. 2. Functional network analysis of microRNAs (miRNAs) differentially accumulated in heart failure (HF) patients. A. Emapplot representation of interdependence of the pathways regulated by mRNAs that are potential targets of differentially expressed miRNAs in HF patients; B. Emapplot representation of interdependence of the pathways regulated by mRNAs that are potential targets of differentially expressed miRNAs in patients with coronary artery disease (CAD). The networks represent the 50 most significant biological processes, regardless of their p-values. Each node represents the biological process category listed on the right, and the size of the node corresponds to the number of genes enriched in this process. The edge thickness is proportional to the number of shared genes

ORCID iDs

Monika Wrzosek https://orcid.org/0000-0001-9576-0042
Anna Hojka-Osińska https://orcid.org/0000-0003-0539-2122
Dominika Klimczak-Tomaniak
   https://orcid.org/0000-0001-8825-511X
Anna Katarzyna Żarek-Starzewska
   https://orcid.org/0000-0003-1791-4661
Wioletta Dyrla https://orcid.org/0000-0001-5757-8901
Magdalena Rostek-Bogacka https://orcid.org/0000-0001-7853-9274
Maksym Wróblewski https://orcid.org/0000-0001-9056-6398
Marek Kuch https://orcid.org/0000-0001-7622-9758
Magdalena Kucia https://orcid.org/0000-0002-9110-5048

References

1. Teupe C, Rosak C. Diabetic cardiomyopathy and diastolic heart failure: Difficulties with relaxation. *Diabetes Res Clin Pract*. 2012;97(2): 185–194. doi:10.1016/j.diabres.2012.03.008
2. Nichols GA, Gullion CM, Koro CE, Ephross SA, Brown JB. The incidence of congestive heart failure in type 2 diabetes. *Diabetes Care*. 2004;27(8):1879–1884. doi:10.2337/diacare.27.8.1879
3. Rubler S, Dlugash J, Yuceoglu YZ, Kumral T, Branwood AW, Grishman A. New type of cardiomyopathy associated with diabetic glomerulosclerosis. *Am J Cardiol*. 1972;30(6):595–602. doi:10.1016/0002-9149(72)90595-4
4. Seferović PM, Paulus WJ. Clinical diabetic cardiomyopathy: A two-faced disease with restrictive and dilated phenotypes. *Eur Heart J*. 2015;36(27):1718–1727. doi:10.1093/eurheartj/ehv134
5. Xia L, Song M. Role of non-coding RNA in diabetic cardiomyopathy. In: Xiao J, ed. *Non-Coding RNAs in Cardiovascular Diseases. Advances in Experimental Medicine and Biology*; vol. 1229. Singapore: Springer Singapore; 2020:181–195. doi:10.1007/978-981-15-1671-9_10
6. De Rosa S, Arcidiacono B, Chiefari E, Brunetti A, Indolfi C, Foti DP. Type 2 diabetes mellitus and cardiovascular disease: Genetic and epigenetic links. *Front Endocrinol*. 2018;9:2. doi:10.3389/fendo.2018.00002
7. Florijn BW, Valstar GB, Duijs JMGJ, et al. Sex-specific microRNAs in women with diabetes and left ventricular diastolic dysfunction or HFpEF associate with microvascular injury. *Sci Rep*. 2020;10(1):13945. doi:10.1038/s41598-020-70848-8
8. Ponikowski P, Voors AA, Anker SD, et al. 2016 ESC Guidelines for the diagnosis and treatment of acute and chronic heart failure. The Task Force for the diagnosis and treatment of acute and chronic heart failure of the European Society of Cardiology (ESC). Developed with the special contribution of the Heart Failure Association (HFA) of the ESC. *Eur Heart J*. 2016;37(27):2129–2200. doi:10.1093/eurheartj/ehw128
9. American Diabetes Association. Classification and Diagnosis of Diabetes: Standards of Medical Care in Diabetes 2020. *Diabetes Care*. 2020;43(Suppl 1):S14–S31. doi:10.2337/dc20-S002
10. Porrello ER, Johnson BA, Aurora AB, et al. miR-15 family regulates postnatal mitotic arrest of cardiomyocytes. *Circ Res*. 2011;109(6):670–679. doi:10.1161/CIRCRESAHA.111.248880
11. Wang K, An T, Zhou LY, et al. E2F1-regulated miR-30b suppresses cyclophilin D and protects heart from ischemia/reperfusion injury and necrotic cell death. *Cell Death Differ*. 2015;22(5):743–754. doi:10.1038/cdd.2014.165
12. Zhang L, Jia X. Down-regulation of miR-30b-5p protects cardiomyocytes against hypoxia-induced injury by targeting Aven. *Cell Mol Biol Lett*. 2019;24(1):61. doi:10.1186/s11658-019-0187-4
13. Huangfu FT, Tang LQ, Wang HQ, Zhao X, Yang M. MiR-145-5p promotes myocardial cell apoptosis in rats with myocardial infarction through PI3K/Akt signaling pathway. *Eur Rev Med Pharmacol Sci*. 2020;24(24):12904–12911. doi:10.26355/eurrev_202012_24194
14. Feinberg MW, Moore KJ. MicroRNA regulation of atherosclerosis. *Circ Res*. 2016;118(4):703–720. doi:10.1161/CIRCRESAHA.115.306300
15. Cai Y, Li Y. Upregulation of miR-29b-3p protects cardiomyocytes from hypoxia-induced apoptosis by targeting TRAF5. *Cell Mol Biol Lett*. 2019;24(1):27. doi:10.1186/s11658-019-0151-3
16. Xue Y, Fan X, Yang R, Jiao Y, Li Y. miR-29b-3p inhibits post-infarct cardiac fibrosis by targeting FOS. *Biosci Rep*. 2020;40(9):BSR20201227. doi:10.1042/BSR20201227
17. Vegter EL, van der Meer P, de Windt LJ, Pinto YM, Voors AA. MicroRNAs in heart failure: From biomarker to target for therapy. *Eur J Heart Fail*. 2016;18(5):457–468. doi:10.1002/ejhf.495
18. Marfella R, Di Filippo C, Potenza N, et al. Circulating microRNA changes in heart failure patients treated with cardiac resynchronization therapy: Responders vs. non-responders. *Eur J Heart Fail*. 2013;15(11): 1277–1288. doi:10.1093/eurjhf/hft088
19. Kaur J, Young B, Fadel P. Sympathetic overactivity in chronic kidney disease: Consequences and mechanisms. *Int J Mol Sci*. 2017;18(8):1682. doi:10.3390/ijms18081682
20. Vasu S, Kumano K, Darden CM, Rahman I, Lawrence MC, Naziruddin B. MicroRNA signatures as future biomarkers for diagnosis of diabetes states. *Cells*. 2019;8(12):1533. doi:10.3390/cells8121533

Early efficacy and safety of obinutuzumab with chemotherapy in previously untreated patients with follicular lymphoma: A real-world retrospective report of the Polish Lymphoma Research Group

Ewa Paszkiewicz-Kozik[1,A–F], Iwona Hus[2,A,C,E,F], Monika Palka[3,B,F], Małgorzata Dębowska[4,5,A–C,E,F], Agnieszka Końska[2,B,F], Martyna Kotarska[1,B,F], Agata Tyczyńska[6,B,E,F], Monika Joks[7,B,F], Maja Twardosz[8,B,F], Agnieszka Giza[9,B,F], Ewa Wąsik-Szczepanek[10,B,F], Elżbieta Kalicińska[11,B,F], Anna Wiśniewska[12,B,F], Marta Morawska[13,B,F], Barbara Lewicka[14,B,F], Marcin Szymański[1,B,F], Łukasz Targoński[1,B,F], Joanna Romejko-Jarosińska[1,B,F], Joanna Drozd-Sokołowska[15,B,E,F], Edyta Subocz[16,B,F], Ryszard Swoboda[8,B,E,F], Monika Długosz-Danecka[3,B,F], Ewa Lech-Maranda[2,B,F], Jan Walewski[1,A,C–F]

[1] Department of Lymphoid Malignancies, Maria Sklodowska-Curie National Research Institute of Oncology, Warszawa, Poland

[2] Department of Hematology, Institute of Hematology and Transfusion Medicine, Warszawa, Poland

[3] Department of Lymphoid Malignancies, Maria Sklodowska-Curie National Research Institute of Oncology, Kraków, Poland

[4] Department of Mathematical Modeling of Physiological Processes, Nalecz Institute of Biocybernetics and Biomedical Engineering, Polish Academy of Sciences, Warszawa, Poland

[5] Department of Computational Oncology, Maria Sklodowska-Curie National Research Institute of Oncology, Warszawa, Poland

[6] Department of Hematology and Transplantology, Medical University of Gdańsk, Poland

[7] Department of Hematology and Marrow Transplantation, Poznan University of Medical Sciences, Poland

[8] Department of Bone Marrow Transplantation and Oncohematology, Maria Sklodowska-Curie National Research Institute of Oncology, Gliwice, Poland

[9] Department of Hematology, Jagiellonian University Medical College, Kraków, Poland

[10] Department of Hematooncology and Bone Marrow Transplantation, Medical University in Lublin, Poland

[11] Department of Hematology, Wroclaw Medical University, Poland

[12] Department of Oncology and Chemotherapy, Nicolas Copernicus State Hospital, Koszalin, Poland

[13] Department of Hematology, St. John's Cancer Center, Lublin, Poland

[14] Department of Hematology, Ludwik Rydygier Hospital, Kraków, Poland

[15] Department of Hematology, Transplantation and Internal Diseases, Medical University of Warsaw, Poland

[16] Department of Hematology, Warmian-Masurian Cancer Center of the Ministry of the Interior and Administration Hospital, Olsztyn, Poland

A – research concept and design; B – collection and/or assembly of data; C – data analysis and interpretation;
D – writing the article; E – critical revision of the article; F – final approval of the article

Address for correspondence
Ewa Paszkiewicz-Kozik
E-mail: Ewa.Paszkiewicz-Kozik@pib-nio.pl

Abstract

Background. The first-line obinutuzumab-based immunochemotherapy improves the outcome of patients with follicular lymphoma (FL) compared with rituximab-based regimens. However, infusion-related reactions occur in almost half of patients during the 1st obinutuzumab administration.

Objectives. The study aimed to evaluate the early effectiveness and safety of obinutuzumab-based induction regimens in a real-world setting.

Materials and methods. Outcomes of patients diagnosed with FL and treated with obinutuzumab between January 2020 and September 2021 were analyzed.

Results. The study group included 143 treatment-naïve patients with FL. The median age was 52 years (range: 28–89 years); 45.1% of patients had a high-risk disease as assessed using the Follicular Lymphoma International Prognostic Index (FLIPI). Induction chemotherapy included: O-CVP (obinutuzumab, cyclophosphamide, vincristine, prednisolone) in 49.0% of patients, O-CHOP (O-CVP plus doxorubicin) in 28.7% and O-BENDA (obinutuzumab, bendamustine) in 22.4%. Complete response (CR) and partial response (PR) rates were 69.9% and 26.5%, respectively. There was no difference in response rates between different regimens (p = 0.309). Maintenance was started in 115 patients (85.2%). In the 1st cycle, obinutuzumab was administered as a single 1000-milligram infusion in 47.9% of patients, whereas in 52.1%, initial infusions were split

132

E. Paszkiewicz-Kozik et al. Induction obinutuzumab based treatment in FL

over 2 days (100 mg/900 mg). Infusion-related reactions were reported only during the 1st administration of obinutuzumab in 9.1% of patients, with a similar incidence in those receiving the total dose on a single day or split over 2 days (p = 0.458). The most common adverse events were hematological. Five patients died from coronavirus disease 2019 (COVID-19).

Conclusions. The early responses to induction regimens and adverse events profile were similar for every type of induction treatment. The infusion-related reactions were rare and limited to the 1st dose of obinutuzumab.

Key words: follicular lymphoma, chemotherapy, obinutuzumab, induction treatment

Background

Follicular lymphoma (FL) is the 2nd most common type of B-cell non-Hodgkin lymphoma. The median age at diagnosis is 65 years, and the median overall survival is 20 years.[1] There are still controversies about the most efficient first-line treatment for FL and the time when it should be initiated. The watch-and-wait strategy is recommended for advanced FL without symptoms or organ impairment.[2,3]

The standard of care for initial therapy of patients with FL in need of treatment is rituximab with one of the following regimens of chemotherapy: CVP (cyclophosphamide, vincristine and prednisone), CHOP (CVP with doxorubicin) or BENDA (bendamustine), with rituximab with CVP (R-CVP) representing the least toxic and R-BENDA the most active regimen.[3,4]

The type II anti-CD20 antibody, obinutuzumab, when combined with chemotherapy, resulted in prolonged progression-free survival (PFS) compared to rituximab with chemotherapy in a randomized Gallium study, although grade 3 or 4 neutropenia, thrombocytopenia and infusion-related reactions (IRRs) were more frequent.[5,6] Effective measures for reducing incidence of IRRs are generally adopted, including splitting the dose of the 1st infusion, slowing down infusion rates and routine use of pre-medications.[7]

Objectives

The aim of the study was to evaluate the efficacy and adverse events, especially IRRs, following obinutuzumab-based induction therapy in patients with FL in need of treatment.

Materials and methods

The study included patients aged ≥18 years diagnosed with FL in need of treatment. The study was conducted in the Polish Lymphoma Research Group (PLRG) sites (participating health centers). Clinical and laboratory characteristics of the patients were identified retrospectively in electronic records of 14 contributing PLRG

sites. The Independent Ethics Committee of the Maria Sklodowska-Curie National Research Institute of Oncology in Warsaw approved the study (approval No. 84/2021), which was conducted in accordance with the Declaration of Helsinki and Good Clinical Practice Guidelines.

All patients included in the study had a histological diagnosis of FL based on the World Health Organization (WHO) classification.[8] Patients were treated with obinutuzumab in combination with CVP, CHOP or BENDA at the physician's discretion. Obinutuzumab was administrated at a fixed dose of 1000 mg, in up to eight 21-day cycles, in combination with CVP (O-CVP), up to six 21-day cycles with CHOP (O-CHOP), followed by 2 additional cycles of obinutuzumab monotherapy or up to six 28-day cycles in combination with bendamustine (O-BENDA). In the 1st cycle, obinutuzumab was administered on days 1, 8 and 15, then only on the 1st day of every next cycle.[9] However, physicians modify the treatment schedule, e.g., split the 1st dose over 2 days instead of 1 in individual cases. Patients received standard premedication before each infusion. Intravenous infusions of obinutuzumab were administered at the standard recommended infusion rates.[9] Seventeen patients received corticosteroid dose the day before obinutuzumab at 1 participating center.

The response to treatment was evaluated with positron emission tomography/computed tomography (PET/CT) in 81.3% of patients (n = 109/134), and with computed tomography (CT) in 18.7% of patients (n = 25/134), according to response criteria for non-Hodgkin's lymphomas or revised response criteria when PET/CT was available.[10,11] Adverse events (AEs) were described and graded according to the National Cancer Institute Common Terminology Criteria for AEs (NCI-CTCAE v. 5).[12]

Statistical analyses

Descriptive statistics was used to evaluate variables including demographic, pathologic, clinical, laboratory, type of treatment, response to the therapy, and deaths of patients receiving obinutuzumab-based immunochemotherapy regimens. The χ^2 test or the exact Fisher's test was used to compare categorical variables. Survival curves were estimated using the Kaplan–Meier method, and log-rank test was used to compare time-to-event distributions. Statistical analyses were performed using Matlab v. 2021a

(https://www.mathworks.com) and R v. 4.2.0 (R Foundation for Statistical Computing, Vienna, Austria).[13] The χ^2 test, the Fisher's exact test and the Kaplan–Meier method were performed using 'chisq.test', 'fisher.test' and 'survfit' functions from R, whereas figures were plotted using Matlab. Effects were considered statistically significant for $p < 0.05$.

Results

A total of 143 consecutive patients who started treatment after obinutuzumab was made available for use in Poland on January 1, 2020, were included in the analysis. The last analyzed patients began treatment in September 2021. The characteristics of patients are presented in Table 1. According to the Groupe d'Étude des Lymphomes Folliculaires (GELF) criteria, the median tumor burden was 2 (range: 0–7). Four patients with GELF = 0 received treatment on their explicit request.

The O-CVP regimen was used across the analyzed group the most often (49.0%). The majority of patients responded to the induction treatment. Progression of disease (PD) was reported at the end of immunochemotherapy in less than 3% of patients. We did not find differences in response rates between used regimens (Fisher's exact test, $p = 0.309$; Table 2). Clinical and laboratory characteristics of patients treated according to different regimens are presented in Table 1.

The median follow-up was 15 months and the median number of treatment cycles was 6. Maintenance treatment was started in 115 patients (85.2%) at the discretion of treating physicians. We did not find differences between regimens regarding progression-free survival (PFS; log-rank test, $p = 0.327$) and overall survival (OS; log-rank test, $p = 0.897$) (Fig. 1). During the follow-up, 5 patients exhibited disease progression. No lymphoma-related deaths were reported. Five patients died from coronavirus disease 2019 (COVID-19) during the induction therapy of lymphoma.

The 1st obinutuzumab dose was administered as a single infusion on day 1 of the 1st cycle in 68 patients (47.9%) or split in 2 infusions in 74 patients (52.1%), i.e., 100 mg on day 1 and 900 mg on day 2 of the 1st cycle. The majority of patients (n = 136, 95.1%) received all planned infusions in the 1st cycle. Doses were omitted in 7 patients due to COVID-19 (n = 4), neutropenia (n = 2) or pneumonia with neutropenia (n = 1). In 27 patients (19.3%), doses were postponed. In 11 patients, day 8 dose was delayed, and in 20 – day 15 dose. Delays occurred due to grade 3 or 4 neutropenia (n = 18), admission restrictions due to the pandemic (n = 5), infections other than COVID-19 (n = 4), COVID-19 (n = 1), and other reasons (n = 3).

The IRRs were reported during the 1st administration of obinutuzumab only, and occurred in 13 patients (9.1%) (grade 1 or 2 in 11 patients and grade 3 in 2 patients). A similar proportion of patients receiving the 1st infusion on a single day or split over 2 days experienced IRRs – 11.8% and 6.8%, respectively (χ^2 test statistics = 0.551, df = 1, $p = 0.458$). A median duration of the 1st infusion measured in 69 patients was 4 h and 52 min (range: 1.30–9.45).

The most common grade 3 to 4 AEs in patients receiving obinutuzumab-containing regimens was neutropenia (46.1%). Granulocyte-colony stimulating factor (G-CSF) was used in 94 patients (65.7%), including 69 patients (48.2%) who received G-CSF as a primary prophylaxis of neutropenic fever. Grade 3 or 4 thrombocytopenia occurred in 4 patients (2.8%). The COVID-19 infection occurred in 19 patients (13.3%), and other infections (pneumonia, upper respiratory infections, zoster, contagious impetigo) in 6 patients (4.2%). The incidence of AEs was similar across chemotherapy regimens used.

Discussion

Follicular lymphoma patients in this real-world study were younger than FL patients in general population in Poland (median age: 52 years compared to 61 years, respectively),[14] and younger than patients treated in Gallium study (median: age 59 years) that established superiority of obinutuzumab over rituximab (both combined with chemotherapy). Briefly, 45.1% and 36.5% of patients had high-risk FL according to Follicular Lymphoma International Prognostic Index (FLIPI) and PRIMA prognostic index (PRIMA PI) assessment, respectively. These patient characteristics may suggest a preferred choice of obinutuzumab for younger patients with more aggressive disease.

In our study, we focused on evaluation of response and safety. The median follow-up time was 15 months. We presented objective response rate of 96.3%. The limitations of our analysis are retrospective design and small group of patients, but our overall response rate (ORR) is superior to the 88.5% of ORR in the Gallium study.[5]

The choice of chemotherapy regimen combined with the antibody was consistent with the European Society for Medical Oncology (ESMO) guidelines and practice in the particular health center.[3] So far, it is not clear which of the recommended induction chemotherapy regimens is the most effective for FL – CVP, CHOP or bendamustine – but except for Gallium trial, they were analyzed in combination with rituximab. In FOLL05 trial, response rates after induction therapies R-CVP, R-CHOP, R-FM (rituximab, fludarabine, mitoxantron) were similar (88%, 93% and 91%, respectively, $p = 0.247$), but improved PFS of R-CHOP and R-FM over R-CVP were demonstrated.[15] The PLRG4 trial compared R-CVP to R-CHOP followed by rituximab maintenance for the treatment of indolent lymphoma in need of induction therapy (including FL). Overall response rate (ORR) in the R-CVP arm was 97.1%, and in the R-CHOP arm – 94.5% ($p = 0.218$). No differences is PFS or OS were demonstrated.[16]

Table 1. Baseline characteristics of patients with newly diagnosed FL (number and percentages or median (IQR))

Variable		All	O-CVP	O-CHOP	O-BENDA
Number of patients		143	70	41	32
Gender, male		59 (41.3%)	30 (42.9%)	18 (43.9%)	11 (34.4%)
Age (IQR)		52 (41–63)	55 (43–65)	47 (40–58)	52 (41–67)
FL grade (n = 137)	G1	30 (21.9%)	17 (24.6%)	3 (7.7%)	10 (34.5%)
	G2	61 (44.5%)	31 (44.9%)	20 (51.3%)	10 (34.5%)
	G3	46 (33.6%)	21 (30.4%)	16 (41.0%)	9 (31.0%)
ECOG Performance Score (n = 142)	0	42 (29.6%)	22 (31.4%)	15 (37.5%)	5 (15.6%)
	1	77 (54.2%)	33 (47.1%)	19 (47.5%)	25 (78.1%)
	2	20 (14.1%)	13 (18.6%)	5 (12.5%)	2 (6.2%)
	3	3 (2.1%)	2 (2.9%)	1 (2.5%)	0 (0.0%)
Clinical stage	1	1 (0.7%)	1 (1.4%)	0 (0.0%)	0 (0.0%)
	2	12 (8.4%)	6 (8.6%)	3 (7.3%)	3 (9.4%)
	3	34 (23.8%)	21 (30.0%)	6 (14.6%)	7 (21.9%)
	4	96 (67.1%)	42 (60.0%)	32 (78.0%)	22 (68.8%)
B symptoms (n = 141)		63 (44.7%)	34 (49.3%)	18 (45.0%)	11 (34.4%)
Extranodal disease		96 (67.1%)	43 (61.4%)	30 (73.2%)	23 (71.9%)
HGB < 12 g/dL		36 (25.2%)	22 (31.4%)	9 (22.0%)	5 (15.6%)
Elevated LDH		50 (35.0%)	23 (32.9%)	14 (34.1%)	13 (40.6%)
Serum β_2-microglobulin >3 mg/L (n = 99)		35 (35.4%)	21 (38.9%)	9 (31.0%)	5 (31.2%)
Bone marrow involvement (n = 134)		73 (54.5%)	36 (58.1%)	24 (58.5%)	13 (41.9%)
Involvement of at least 3 nodal sites (n = 142)		87 (61.3%)	43 (61.4%)	21 (51.2%)	23 (74.2%)
Organ dysfunction		41 (28.7%)	21 (30.0%)	13 (31.7%)	7 (21.9%)
Exudation		19 (13.3%)	11 (15.7%)	5 (12.2%)	3 (9.4%)
Splenomegaly (n = 142)		20 (14.1%)	10 (14.5%)	8 (19.5%)	2 (6.2%)
FL cells in blood (n = 60)		11 (18.3%)	6 (18.2%)	3 (14.3%)	2 (33.3%)
Bulky disease >7 cm diameter		63 (44.1%)	28 (40.0%)	18 (43.9%)	17 (53.1%)
Lymph nodes >3 cm diameter		73 (51.0%)	38 (54.3%)	21 (51.2%)	14 (43.8%)
GELF criteria (n = 109)	0	4 (3.7%)	1 (1.6%)	2 (5.4%)	1 (11.1%)
	1	23 (21.1%)	13 (20.6%)	8 (21.6%)	2 (22.2%)
	2	37 (33.9%)	24 (38.1%)	11 (29.7%)	2 (22.2%)
	3	22 (20.2%)	14 (22.2%)	6 (16.2%)	2 (22.2%)
	4	12 (11.0%)	6 (9.5%)	5 (13.5%)	1 (11.1%)
	5	8 (7.3%)	4 (6.3%)	4 (10.8%)	0 (0.0%)
	6	1 (0.9%)	1 (1.6%)	0 (0.0%)	0 (0.0%)
	7	2 (1.8%)	0 (0.0%)	1 (2.7%)	1 (11.1%)
FLIPI (n = 142)	low risk	29 (20.4%)	15 (21.4%)	12 (29.3%)	2 (6.5%)
	intermediate risk	49 (34.5%)	24 (34.3%)	12 (29.3%)	13 (41.9%)
	high risk	64 (45.1%)	31 (44.3%)	17 (41.5%)	16 (51.6%)
PRIMA PI (n = 96)	low risk	31 (32.3%)	15 (29.4%)	9 (31.0%)	7 (43.8%)
	intermediate risk	30 (31.2%)	15 (29.4%)	11 (37.9%)	4 (25.0%)
	high risk	35 (36.5%)	21 (41.2%)	9 (31.0%)	5 (31.2%)

Total number of patients (n) = 143, otherwise indicated in brackets. IQR – interquartile range; FL – follicular lymphoma; ECOG – Eastern Cooperative Oncology Group; clinical stage – Ann Arbor clinical stage; HGB – hemoglobin; LDH – lactate dehydrogenase; GELF – Groupe d'Étude des Lymphomes Folliculaires; FLIPI – Follicular Lymphoma International Prognostic Index; IQR – interquartile range; PRIMA PI – PRIMA prognostic index; O-CVP – obinutuzumab, cyclophosphamide, vincristine, prednisolone; O-CHOP – obinutuzumab, cyclophosphamide, doxorubicin, vincristine, prednisolone; O-BENDA – obinutuzumab, bendamustine.

Table 2. Response to induction regimens

Response/induction regimen	O-CVP	O-CHOP	O-BENDA	All regimens
CR	48 (73.8%)	28 (70.0%)	19 (61.3%)	95 (69.9%)
PR	15 (23.1%)	9 (22.5%)	12 (38.7%)	36 (26.5%)
SD	1 (1.5%)	0 (0.0%)	0 (0%)	1 (0.7%)
PD	1 (1.5%)	3 (7.5%)	0 (0%)	4 (2.9%)
Total	65 (100%)	40 (100%)	31 (100%)	136 (100%)
Not evaluated	5	1	1	7

CR – complete response; PR – partial response; SD – stable disease; PD – progression of disease; O-CVP – obinutuzumab, cyclophosphamide, vincristine, prednisolone; O-CHOP – obinutuzumab, cyclophosphamide, doxorubicin, vincristine, prednisolone; O-BENDA – obinutuzumab, bendamustine; p = 0.309 (Fisher's exact test, for CR+PR and SD+PD compared to O-CVP, O-CHOP and O-BENDA).
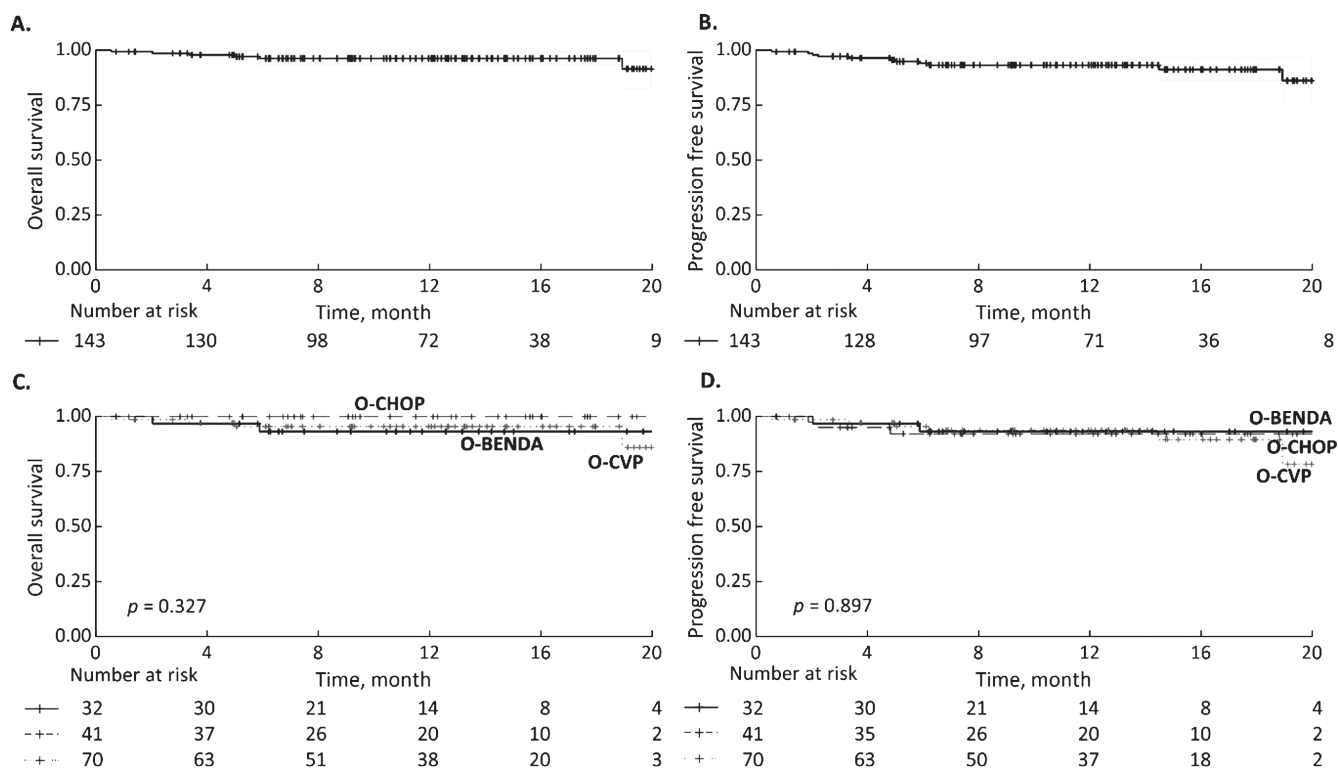

Fig. 1. Overall survival (A) and progression-free survival (B) of patients with newly diagnosed follicular lymphoma treated with obinutuzumab-based regimens. There were no differences in overall survival (C) and progression-free survival (D) between obinutuzumab combined with CHOP, CVP and bendamustine (log-rank test)

O-CVP – obinutuzumab, cyclophosphamide, vincristine, prednisolone; O-CHOP – obinutuzumab, cyclophosphamide, doxorubicin, vincristine, prednisolone; O-BENDA – obinutuzumab, bendamustine.

The Gallium study was not designed to compare differences within chemotherapy groups combined with rituximab or obinutuzumab, but ORR and PFS were superior with obinutuzumab to rituximab, with consistent effects across chemotherapy regimens.[5] In any of these trials, OS difference was demonstrated.

The events of special interest for safety evaluation were IRRs, which usually occur during the 1st administration of obinutuzumab.[9] In a phase IV GAZELLE study, where safety of 90-minute infusion of obinutuzumab from C2 was evaluated in 101 patients,[17] IRRs were observed in the 1st cycle of treatment with a standard infusion duration. A single patient experienced grade >3 IRRs beyond the 1st cycle. In our study, the rate of IRRs was even lower and

they occurred only during the 1st obinutuzumab infusion. We assume that this phenomenon can be associated with the underreporting of adverse events in retrospective studies. The initial dose of obinutuzumab was split in 2 in half of the patients; however, the incidence of IRRs was similar no matter if the dose was split or not. An amendment of the CLL11 study protocol changing the administration of the 1st obinutuzumab infusion to patients with chronic lymphocytic leukemia (CLL) from 1 day to 2 days resulted in a decreasing grade 3 or 4 IRRs to 20%.[18] The practice adapted from the CLL therapy probably does not need to be extended to patients with FL. The occurrence of IRRs in FL and CLL patients beyond the 1st infusion are only occasional; thus, shortened duration of obinutuzumab

infusions starting from the 2nd can be used as a routine, and since October 2021, obinutuzumab is approved for induction treatment of FL.[9,14]

Neutropenia was the most common AE that required therapeutic use of G-CSF and delay of subsequent cycles of treatment. Unfortunately, 5 patients died from COVID-19; there were no other deaths in this group of patients. Therefore, the protection of patients requiring treatment with anti-CD20 antibodies against severe acute respiratory syndrome coronavirus 2 (SARS-CoV-2) is a high priority, with measures including appropriate vaccination and/or pre-exposure treatment with anti-SARS-CoV-2 antibodies, as well as early treatment with anti-viral agents in case the infection occurs.

Conclusions

The first-line treatment of follicular lymphoma patients with obinutuzumab combined with cytotoxic chemotherapy is efficacious and well-tolerated. The response to treatment with 3 different chemotherapy regimens was similar. Low grade and incidence of infusion-related reactions that exclusively occurred in the 1st administration of obinutuzumab support the use of abbreviated 90-minute infusions starting from the 2nd treatment cycle.

ORCID iDs

Ewa Paszkiewicz-Kozik   https://orcid.org/0000-0003-2629-3932
Iwona Hus   https://orcid.org/0000-0002-6096-4093
Monika Palka   https://orcid.org/0000-0002-8558-4214
Małgorzata Dębowska   https://orcid.org/0000-0001-8741-7930
Martyna Kotarska   https://orcid.org/0000-0003-3918-9704
Monika Joks   https://orcid.org/0000-0002-7965-9873
Agnieszka Giza   https://orcid.org/0000-0001-9095-9749
Ewa Wąsik-Szczepanek   https://orcid.org/0000-0002-9715-3745
Elżbieta Kalicińska   https://orcid.org/0000-0002-4797-8001
Marta Morawska   https://orcid.org/0000-0001-6836-2903
Łukasz Targoński   https://orcid.org/0000-0002-6155-8791
Joanna Romejko-Jarosińska   https://orcid.org/0000-0003-4603-1112
Joanna Drozd-Sokołowska   https://orcid.org/0000-0002-4562-6264
Edyta Subocz   https://orcid.org/0000-0001-5225-3921
Ryszard Swoboda   https://orcid.org/0000-0002-5897-3919
Monika Długosz-Danecka   https://orcid.org/0000-0002-8927-4125
Ewa Lech-Marańda   https://orcid.org/0000-0001-9592-0851
Jan Walewski   https://orcid.org/0000-0003-4247-2674

References

1. Mounier M, Bossard N, Remontet L, et al. Changes in dynamics of excess mortality rates and net survival after diagnosis of follicular lymphoma or diffuse large B-cell lymphoma: Comparison between European population-based data (EUROCARE-5). *Lancet Haematol*. 2015;2(11):e481–e491. doi:10.1016/S2352-3026(15)00155-6

2. Freedman A, Jacobsen E. Follicular lymphoma: 2020 update on diagnosis and management. *Am J Hematol*. 2020;95(3):316–327. doi:10.1002/ajh.25696

3. Dreyling M, Ghielmini M, Rule S, et al. Newly diagnosed and relapsed follicular lymphoma: ESMO Clinical Practice Guidelines for diagnosis, treatment and follow-up. *Ann Oncol*. 2021;32(3):298–308. doi:10.1016/j.annonc.2020.11.008

4. Salles G, Seymour JF, Offner F, et al. Rituximab maintenance for 2 years in patients with high tumour burden follicular lymphoma responding to rituximab plus chemotherapy (PRIMA): A phase 3, randomised controlled trial. *Lancet*. 2011;377(9759):42–51. doi:10.1016/S0140-6736(10)62175-7

5. Marcus R, Davies A, Ando K, et al. Obinutuzumab for the first-line treatment of follicular lymphoma. *N Engl J Med*. 2017;377(14):1331–1344. doi:10.1056/NEJMoa1614598

6. Amitai I, Gafter-Gvili A, Shargian-Alon L, Raanani P, Gurion R. Obinutuzumab-related adverse events: A systematic review and meta-analysis. *Hematol Oncol*. 2021;39(2):215–221. doi:10.1002/hon.2828

7. Byrd JC, Flynn JM, Kipps TJ, et al. Randomized phase 2 study of obinutuzumab monotherapy in symptomatic, previously untreated chronic lymphocytic leukemia. *Blood*. 2016;127(1):79–86. doi:10.1182/blood-2015-03-634394

8. Swerdlow SH, Campo E, Pileri SA, et al. The 2016 revision of the World Health Organization classification of lymphoid neoplasms. *Blood*. 2016;127(20):2375–2390. doi:10.1182/blood-2016-01-643569

9. European Medicines Agency (EMA). Gazyvaro. Summary of product characteristics. Updated May 10, 2022. May 2022. https://www.ema.europa.eu/en/medicines/human/EPAR/gazyvaro. Accessed May 7, 2022.

10. Cheson BD, Pfistner B, Juweid ME, et al. Revised response criteria for malignant lymphoma. *J Clin Oncol*. 2007;25(5):579–586. doi:10.1200/JCO.2006.09.2403

11. Cheson BD, Horning SJ, Coiffier B, et al. Report of an international workshop to standardize response criteria for non-Hodgkin's lymphomas. *J Clin Oncol*. 1999;17(4):1244–1244. doi:10.1200/JCO.1999.17.4.1244

12. National Cancer Institute (NCI). Common Terminology Criteria for Adverse Events (CTCAE). April 2021. https://ctep.cancer.gov/protocoldevelopment/electronic_applications/ctc.htm. Accessed May 7, 2022.

13. R Core Team. R: A language and environment for statistical computing. https://www.R-project.org/. Accessed May 2, 2022.

14. Szumera-Ciećkiewicz A, Wojciechowska U, Didkowska J, et al. Population-based epidemiological data of follicular lymphoma in Poland: 15 years of observation. *Sci Rep*. 2020;10(1):14610. doi:10.1038/s41598-020-71579-6

15. Federico M, Luminari S, Dondi A, et al. R-CVP versus R-CHOP versus R-FM for the initial treatment of patients with advanced-stage follicular lymphoma: Results of the FOLL05 trial conducted by the Fondazione Italiana Linfomi. *J Clin Oncol*. 2013;31(12):1506–1513. doi:10.1200/JCO.2012.45.0866

16. Walewski J, Paszkiewicz-Kozik E, Michalski W, et al. First-line R-CVP versus R-CHOP induction immunochemotherapy for indolent lymphoma with rituximab maintenance: A multicentre, phase III randomized study by the Polish Lymphoma Research Group PLRG4. *Br J Haematol*. 2020;188(6):898–906. doi:10.1111/bjh.16264

17. Hübel K, Buchholz TA, Izutsu K, et al. Obinutuzumab can be administered as a 90-minute short-duration infusion (SDI) in patients with previously untreated follicular lymphoma: GAZELLE end of induction analysis. *Hematol Oncol*. 2021;39(S2):hon.30_2880. doi:10.1002/hon.30_2880

18. Goede V, Fischer K, Busch R, et al. Obinutuzumab plus chlorambucil in patients with CLL and coexisting conditions. *N Engl J Med*. 2014;370(12):1101–1110. doi:10.1056/NEJMoa1313984